UNIVERSIDADE DE BRASÍLIA - UnB
INSTITUTO DE GEOCIÊNCIAS - IG
PROGRAMA DE PÓS-GRADUAÇÃO EM GEOLOGIA - PPGG

Caracterização petrológica, geoquímica e geocronológica da unidade Novo Gosto e suas implicações para a evolução do domínio Canindé, Faixa Sergipana, Província Borborema

Tese de Doutorado Nº 170

Luiz Henrique Passos

Brasília - DF
2020

UNIVERSIDADE DE BRASÍLIA - UnB
INSTITUTO DE GEOCIÊNCIAS - IG
PROGRAMA DE PÓS-GRADUAÇÃO EM GEOLOGIA - PPGG

Caracterização petrológica, geoquímica e geocronológica da unidade Novo Gosto e suas implicações para a evolução do domínio Canindé, Faixa Sergipana, Província Borborema

Discente:

Luiz Henrique Passos

Orientador:

Prof. Dr. Reinhardt Adolfo Fuck

Banca Examinadora:

Prof. Dr. Reinhardt Adolfo Fuck (Orientador)

Prof. Dr. Fabricio de Andrade Caxito (IG/UFMG)

Prof. Dr. Lauro Cézar Montefalco de Lira Santos (DGEO/UFPE)

Prof. Dr. Elton Luiz Dantas (IG/UnB)

Brasília - DF

2020

FICHA CATALOGRÁFICA

Passos, Luiz Henrique

PP289c Caracterização petrológica, geoquímica e geocronológica da unidade Novo Gosto e suas implicações para a evolução do domínio Canindé, Faixa Sergipana, Província Borborema / Luiz Henrique Passos; orientador Reinhardt Adolfo Fuck . -- Brasília, 2021.

203 p.

Tese (Doutorado - Doutorado em Geologia) -- Universidade de Brasília, 2021.

1. Unidade Novo Gosto. 2. Domínio Canindé. 3. Faixa Sergipana. I. Fuck , Reinhardt Adolfo, orient. II. Título.

Dedico esta tese de modo incondicional à minha família.

“A ciência compõe-se de erros que, por sua vez, são os passos até a verdade.”

Abert Einstein

AGRADECIMENTOS

Meu agradecimento em especial para a minha mãe e família por ser meu alicerce e fonte de forças para enfrentar as dificuldades que a vida e a pós-graduação impôs ao longo dessa jornada.

Agradeço a meu companheiro Bruno que vivenciou junto comigo todos os altos e baixos, desde o período do mestrado até o momento, e que também sempre me apoiou a não desistir nas adversidades.

Aos meus amigos que estiveram ao meu lado dando apoio nas horas difíceis.

Aos grandes professores que a vida pôs em meu caminho e que fazem de mim o que sou hoje, e que continuo usando de inspiração como profissional, em especial a Cristine que foi um anjo no meu caminho, e Viter, Lucy, Pacheco e Adriane.

Aos professores Farid, Fuck e Pimentel (*in memoriam*), por ter dado uma chance para a orientação de meu trabalho e ter me apoiado até o fim, principalmente o professor Farid que me acompanhou desde a graduação, ao qual sou eternamente grato pelas oportunidades abertas. Também deixo minha gratidão ao professor Tiago Jalowitzki que aceitou ser meu orientador, e mesmo que sem sucesso na tentativa de oficialização, sei que se tivesse conseguido faria o possível para colaborar com o trabalho, e aos demais professores da pós-graduação em geologia da Universidade de Brasília.

E finalmente, ao CAPES pelo investimento direcionado a mim e meu trabalho, durante o período em que fui bolsista de doutorado. O presente trabalho foi realizado com apoio da Coordenação de Aperfeiçoamento de Pessoal de Nível Superior - Brasil (CAPES) - Código de Financiamento 001.

RESUMO

O Domínio Canindé, NW da Faixa Sergipana, no sul da Província Borborema, Brasil, é umaparte importante para entender os eventos pré-colisionais na província, sobretudo no tardi-Toniano. O domínio compreende uma associação de rochas metavulcanossedimentares, intrusões gabróicas, rochas magmáticas bimodais e granitóides sin- a pós-tectônicos. Devido à complexidade litoestratigráfica e geoquímica várias interpretações controversas do ambiente tectônico foram propostas ao longo dos anos. A unidade Novo Gosto é uma unidade litotectônica neoproterozoica composta por rochas metavulcanossedimentares e compreende a unidade mais antiga do domínio Canindé. Os anfibolitos Novo Gosto analisados foram classificados como basaltos toleíticos de alto Fe. Três grupos geoquímicos foram identificados: Grupo 1 é dominantemente mais empobrecido em elementos incompatíveis e tem padrão similar a IAB, com depleção em HFSE (Nb-Ta, Zr-Hf, suave em Ti); Grupo 2 mostra padrão similar ao Grupo 1, mas com anomalias mais fortes (Nb-Ta, Ti) e enriquecimento variável em elementos incompatíveis; Grupo 3 é mais enriquecido em elementos incompatíveis do que o Grupo 1, seu padrão sendo mais plano e com depleção em HFSE mais suave (Nb-Ta, Zr-Hf, suave em Ti e Y) e se assemelhando a basalto ligeiramente mais rico do que E-MORB. Análises desses dados sugerem ambiente similar à configuração de arco-retroarco de Ryukyu-Okinawa (Japão) e Kamtchatka (Rússia). Idade de zircão U-Pb LA-ICP-MS obtido em amostra de anfibolito resultou em idade de 743±3 Ma, confirmando as relações geológicas de campo que indicam essa unidade como a mais antiga no domínio. Novos dados petrográficos, geoquímicos e isotópicos dos anfibolitos Novo Gosto levam a reconhecer um antigo sistema de arco-retroarco neoproterozoico, uma configuração rara nas fases iniciais da Orogênese Brasiliana na Província Borborema, que finalizou com o fechamento do mar restrito Canindé e o associado oceano Sergipano em torno de 630 Ma. Também são apresentados estudos de condições metamórficas, geocronologia e estudos isotópicos para essa mesma unidade. As condições metamórficas foram calculadas usando anfibólio, resultando em uma variação principalmente em torno de 600-740 °C e 3,5-10,0 kbars para anfibolitos não-miloníticos, característica de fácies anfibolito. E valores variando principalmente em torno de 636-808 °C e 7,0-12,0 kbars para milonitos. As condições metamórficas mínimas registradas nessas rochas são T: 390 °C e P: 2,5 kbar, características de fácies xisto verde. A idade desse evento metamórfico foi obtida em típicos grãos metamórficos de zircão de amostra de quartzito (U-Pb/LA-ICPMS), resultando em uma idade $^{207}Pb/^{206}Pb$ de 682±3,9 Ma. Grãos detríticos de zircão e idades modelo das rochas

metassedimentares apontam rochas-fonte do cedo-Toniano como fonte primária. Subordinadamente, contribuição de fontes do Mesoproterozoico, Paleoproterozoico e Neoarqueano também são reconhecidas. As fontes primárias são relacionadas a rochas do evento Cariris Velhos (1000-920 Ma), enquanto as fontes secundárias são provavelmente oriundas do Complexo Jirau do Ponciano e rochas do embasamento do superterreno Pernambuco-Alagoas. Pela primeira vez foram reconhecidas idades cedo-Tonianas no domínio Canindé, com idades U-Pb em zircão (LA-ICPMS) de 1005±3 Ma e 989±6 Ma em anfibolito e granito milonítico, expostos no limite sudeste da área. Novas idades foram obtidas também em intrusões vizinhas à unidade Novo Gosto: Intrusão Gabróica Acamadada Canindé (~718 Ma), metagranito Garrote (~715 Ma), metagranito Curralinho-Boa Esperança (~708 Ma) e rocha metavulcânica Gentileza (~700 Ma), que integram o magmatismo pré-colisional da Faixa Sergipana (~740-680 Ma). Finalmente, idades U-Pb em zircão foram obtidas no embasamento adjacente (domínio Poço Redondo), provável área fonte para parte das rochas metassedimentares da unidade Novo Gosto, resultando em idades de 957±11 Ma e 988±15 Ma. Os novos dados obtidos são importantes para compreender a evolução dos estágios iniciais da Faixa Sergipana e traz importante perspectiva para futuras correlações com faixas adjacentes e para o entendimento da estruturação do Gondwana Oeste, durante a Orogenia Brasiliana-Pan-Africana.

Palavras-chave: rochas metavulcanossedimentares; anfibolito; condições metamórficas; Isótopos de Nd; Idades U-Pb; Orogênese Brasiliana inicial; arco-retroarco

ABSTRACT

The Canindé Domain, NW Sergipano Belt, in the southern Borborema Province, Brazil, is an important tract to understand the pre-collisional events in the province, particularly during the late Tonian. The domain comprises an association of metavolcano-sedimentary rocks, gabbroic intrusions, bimodal magmatic rocks and syn- to post-tectonic granitoids. Due to the lithostratigraphic and geochemical complexity of this domain, several controversial interpretations of the tectonic environment were proposed over the years. The Novo Gosto unit is a Neoproterozoic lithotectonic unit composed of metavolcano-sedimentary rocks and comprises the oldest unit of the Canindé domain. The analyzed Novo Gosto amphibolites were classified as high Fe tholeiitic basalt type rocks. Three geochemical groups were identified: Group 1 is dominantly more depleted in incompatible elements and has a pattern similar to IAB with HFSE depletion (Nb-Ta, Zr-Hf, smooth Ti); Group 2 displays a pattern similar to Group 1, but with more evident Nb-Ta, Ti anomalies and a variable enrichment in incompatible elements; Group 3 is more enriched in incompatible elements than Group 1 rocks, their pattern being flatter with milder HFSE depletion (Nb-Ta, Zr-Hf, smooth Ti, Y) and resembling basalt slightly richer than E-MORB. Analysis of these data suggests an environment similar to the Ryukyu-Okinawa (Japan) and Kamchatka (Russia) arc-back-arc setting. LA-ICP-MS U-Pb zircon age obtained from one amphibolite sample yielded ages of 743±3 Ma, confirming the geological field relationships that indicate this unit as the oldest in the domain. The new petrographic, geochemical and isotopic data of the Novo Gosto amphibolites lead to the recognition of an ancient Neoproterozoic arc-back-arc system, a rare setting in the earlier phases of the Brasiliano Orogeny within the Borborema Province, which ended with the closure of the restricted Canindé sea and the associated Sergipano ocean at around 630 Ma. Metamorphic conditions, geochronology, and isotopic studies for this same unit are also presented. The metamorphic conditions were calculated using amphibole, resulting in a ranging mainly around 600-740 ºC and 3.5-10.0 kbars for non-mylonitic amphibolites, characteristic of amphibolite facies. And values ranging mainly around 636-808 ºC and 7.0-12.0 kbars for mylonites. The minimum metamorphic conditions imprint in these rocks is T: 390 °C and P: 2.5 kbar, characteristic of greenschist facies. The age of this metamorphic event was obtained on typical metamorphic zircon grains (U-Pb/LA-ICPMS) of a quartzite sample, resulting in a $^{207}Pb/^{206}Pb$ mean age of 682±3.9 Ma. U-Pb detrital zircon and Nd model ages of the metasedimentary rocks point out Early Tonian source rocks as primary source. Subordinate contributions of

Mesoproterozoic, Paleoproterozoic, and Neoarchean sources were also recognized. The primary sources are related to Cariris Velhos event rocks (1000-920 Ma), whereas the secondary sources are probably the Jirau do Ponciano Complex and basement rocks of the Pernambuco-Alagoas superterrane. For the first time, early Tonian ages were recognized in the Canindé Domain, with U-Pb zircon ages (LA-ICPMS) of 1005±3 Ma and 989±6 Ma on amphibolite and mylonitic granite, exposed in the southeastern limit of the area. New ages were obtained on intrusions surrounding the Novo Gosto unit: Canindé Layered Gabbroic Intrusion (~718 Ma), Garrote metagranite (~715 Ma), Curralinho/Boa Esperança metagranite (~708 Ma) and Gentileza metavolcanic rock (~700 Ma), which integrate the early pre-collisional magmatism of the Sergipano Belt (~740-680 Ma). Finally, U-Pb zircon ages were obtained in the adjacent basement (Poço Redondo Domain), probable source area for part of the Novo Gosto metasedimentary rocks, resulting in ages of 957±11 Ma and 988±15 Ma. The new data are important to understand the evolution of the early stages of the Sergipano Belt and bring an important perspective to future correlations with adjacent belts and to the understanding of the structuration of West Gondwana, during the Brasiliano-Pan-African Orogeny.

Keywords: metavolcanic-sedimentary rocks; amphibolite; metamorphic conditions; Nd isotopes; U-Pb ages; Early Brasiliano Orogeny; Arc-back-arc

LISTA DE FIGURAS

Figuras da Tese:

Figuras dos Artigos:

LISTA DE TABELAS

LISTA DE SIGLAS

ETR	Elementos Terras-Raras
E-MORB	*Enriched Mid-Ocean Ridge Basalt*
HFSE	*High Field Strength Elements*
HREE	*Heavy Rare-Earth Elements*
IAB	*Island Arc Basalts*
LA-MC-ICP-MS	*Laser Ablation - Multi-Collector - Inductively Coupled Plasma - Mass Spectrometry*
LA-SF-ICP-MS	*Laser Ablation - Sector Field - Inductively Coupled Plasma - Mass Spectrometry*
LILE	*Large-Ion Lithophile Elements*
LIP	*Large Igneous Province*
LREE	*Light Rare-Earth Elements*
MORB	*Mid-Ocean Ridge Basalt*
N-MORB	*Normal Mid-Ocean Ridge Basalt*
OIB	*Ocean Island Basalt*
REE	*Rare Earth Elements*
SHRIMP	*Sensitive High-Resolution Ion Microprobe*

SUMÁRIO

CAPÍTULO I - Introdução

1. Apresentação e Justificativa

Este trabalho visa a caracterização petrológica, geoquímica e geocronológica da unidade Novo Gosto e suas implicações para a evolução do domínio Canindé, Faixa Sergipana, Província Borborema. Essa unidade é de particular interesse por ser constituída de rochas metavulcanossedimentares consideradas as mais antigas do domínio e que podem contribuir para o entendimento da formação da Faixa Sergipana durante a fase inicial da Orogênese Brasiliana. Apesar de muitos pesquisadores associarem a formação das rochas deste domínio a ambiente de extensão localizada, inúmeras divergências surgiram ao longo dos anos em relação ao ambiente tectônico, principalmente se houve subducção associada à formação dessas rochas ou não, como discutido abaixo.

As diversas teorias propostas ao longo dos anos favorecem a discussão sobre a origem e evolução deste domínio e de suas unidades. Abaixo segue breve histórico da evolução do conhecimento da área:

- Brito Neves & Cordani (1973) relacionaram as rochas ultramáficas da região à atividade magmática inicial (ofiolítica) do Geossinclinal de Propriá;
- Silva Filho (1976) descreveu as rochas ultramáficas como sendo de uma Suíte Ofiolítica;
- Jardim de Sá et al. (1986) consideraram o Domínio Canindé como gerado em ambiente de arco insular;
- Santos et al. (1988) propuseram que o ambiente seria de arco vulcânico ou margem continental ativa;
- Oliveira & Tarney (1990) consideraram que os gabros e as rochas metavulcânicas da região apresentam semelhança geoquímica com basaltos continentais, e que o Complexo Canindé seria resultante da remobilização do manto listosférico subcontinental durante algum evento termal no Neoproterozoico;
- Bezerra et al. (1991) apud Santos et al. (1998) descreveram o Domínio Canindé como, provavelmente, um arco magmático ou bacia de retro-arco, soldado à Faixa de Dobramentos Sergipana por processo colisional;
- Bezerra (1992) sugeriu a formação em um ambiente anorogênico intracontinental ou sin-orogênico de arco e propôs ambiente sin-orogênico para a Suíte Intrusiva Canindé;

- Silva Filho (1998) propôs que o Domínio Canindé representa um arco intraoceânico. A Suíte Gabróica seria contemporânea aos granitóides cálcio-alcalinos brasilianos;
- Seixas & Moraes (2000) propuseram modelo geotectônico que envolve a formação de rifte, vulcanismo basáltico alcalino, plutonismo gabróico e granítico e deformação compressiva;
- Nascimento (2005) apresenta modelo de evolução tectônica, que corresponde a uma sequência de rifte intracontinental;
- Oliveira et al. (2010) interpretam como sequência de rifte que foi posteriormente deformada e agregada ao Domínio Poço Redondo-Marancó. Esses autores relatam que o rifte provavelmente teria evoluído para uma bacia oceânica por causa da ocorrência de anfibolitos na Unidade Novo Gosto-Mulungu, com pillow-lavas reliquiares e lentes de mármore.
- Liz (2017) continua em conformidade com a hipótese de Oliveira & Tarney (1990), Nascimento (2005) e Oliveira et al. (2010), atribuindo a origem dos ortoanfibolitos a ambiente de rifte continental.

A Unidade Novo Gosto pertence ao Domínio Canindé, que constitui uma faixa de direção NW-SE, norte do Estado de Sergipe, englobada na Faixa de Dobramento Sergipana, também denominada Faixa Sergipana e Cinturão Sergipano (p. ex. D'el-Rey Silva & Mcclay, 1995) e Cinturão Orogênico Sergipano (p. ex. Souza Junior, 2013). Santos et al. (1998) caracterizaram o Domínio Canindé como sendo constituído por rochas metavulcanossedimentares do Complexo Canindé (no qual atualmente encontram-se inseridas as unidades Novo Gosto e Gentileza), polideformadas, frequentemente transpostas e cisalhadas, intrudidas por expressivo corpo gabróico diferenciado, denominado Suíte Intrusiva Canindé. O domínio ainda é afetado por intrusões graníticas sin-, tardi- a pós- e pós-tectônicas.

O Domínio Canindé é formado, de acordo com Nascimento (2005), por uma sequência de rochas metassedimentares e metavulcânicas da Unidade Novo Gosto, e subvulcânicas da Unidade Gentileza, que são intrudidas pelas rochas da Suíte Gabróica de Canindé e diversos granitos neoproterozoicos (Lajedinho, Boa Esperança, Serrota, Sítios Novos, Xingó). A Unidade Novo Gosto, foco deste projeto, é composta essencialmente por metagrauvacas, metapelitos, metassiltitos, metacherts, xistos, grafita xistos, mármores, rochas calciossilicáticas e anfibolitos, truncados por diques máficos e félsicos, assim como corpos gabróicos ricos em Fe-Ti (Nascimento, 2005).

Rochas máficas são encontradas em ambientes geotectônicos variados, tais como riftes, LIPs, MORB, OIB, arco vulcânico, arco de ilhas, frente de arco e retro-arco (Gill, 2010). Por meio de geoquímica de elementos maiores, menores e traços associada com petrologia, a identificação do ambiente tectônico torna-se possível, de acordo com a literatura. Além da identificação e caracterização da fonte do magmatismo máfico, será obtida a idade de cristalização dessas rochas por U-Pb em zircão por espectrometria de massa por plasma indutivamente acoplado (LA-ICP-MS), com o intuíto de localizá-lo temporalmente na evolução da porção meridional da Província Borborema. No presente trabalho dedicou-se os estudos às rochas metavulcânicas da Unidade Novo Gosto, incluindo petrologia, geoquímica e geocronologia.

Por fim, estudou-se de modo complementar as rochas metassedimentares e suas idades de proveniência, considerando também que apenas os trabalhos de Oliveira (2008) e Oliveira et al. (2015) abordam de forma restrita tais aspectos. De forma integrada, esses dados proporcionarão a compreensão de como se desenvolveu essa região entre o final da Orogênese Cariris Velhos e o início da Orogênese Brasiliana no sul da Província Borborema.

2. Objetivos

Os objetivos da tese são compreender a evolução litotectônica das rochas da Unidade Novo Gosto, por meio de estudos petrográficos e de campo, estudo da fonte magmática com auxílio de geoquímica, identificação de ambiente tectônico, idade de metamorfismo, idade e principais fontes de proveniência de rochas metassedimentares, e contextualizar os dados na geologia regional.

3. Localização e vias de acesso

A área de estudo está localizada no extremo noroeste do Estado de Sergipe, abrangendo os municípios de Canindé de São Francisco e Poço Redondo.

Sua principal via de acesso a partir da capital Aracaju se dá pela BR-235 até o encontro com a BR-101 (), seguindo por esta última rumo norte, passando pelas sedes municipais de Maruim e Rosário do Catete. A partir desta cidade, acessa-se a rodovia SE-230 rumo noroeste, passando pelas sedes municipais de Siriri, Nossa Senhora das Dores, Feira Nova, Nossa Senhora da Glória, Monte Alegre de Sergipe, Porto da Folha, até chegar à sede de Poço Redondo. A partir de Poço Redondo, há várias vias de acesso para chegar às áreas do domínio Canindé. A distância percorrida é de aproximadamente 186 km a partir de Aracaju.

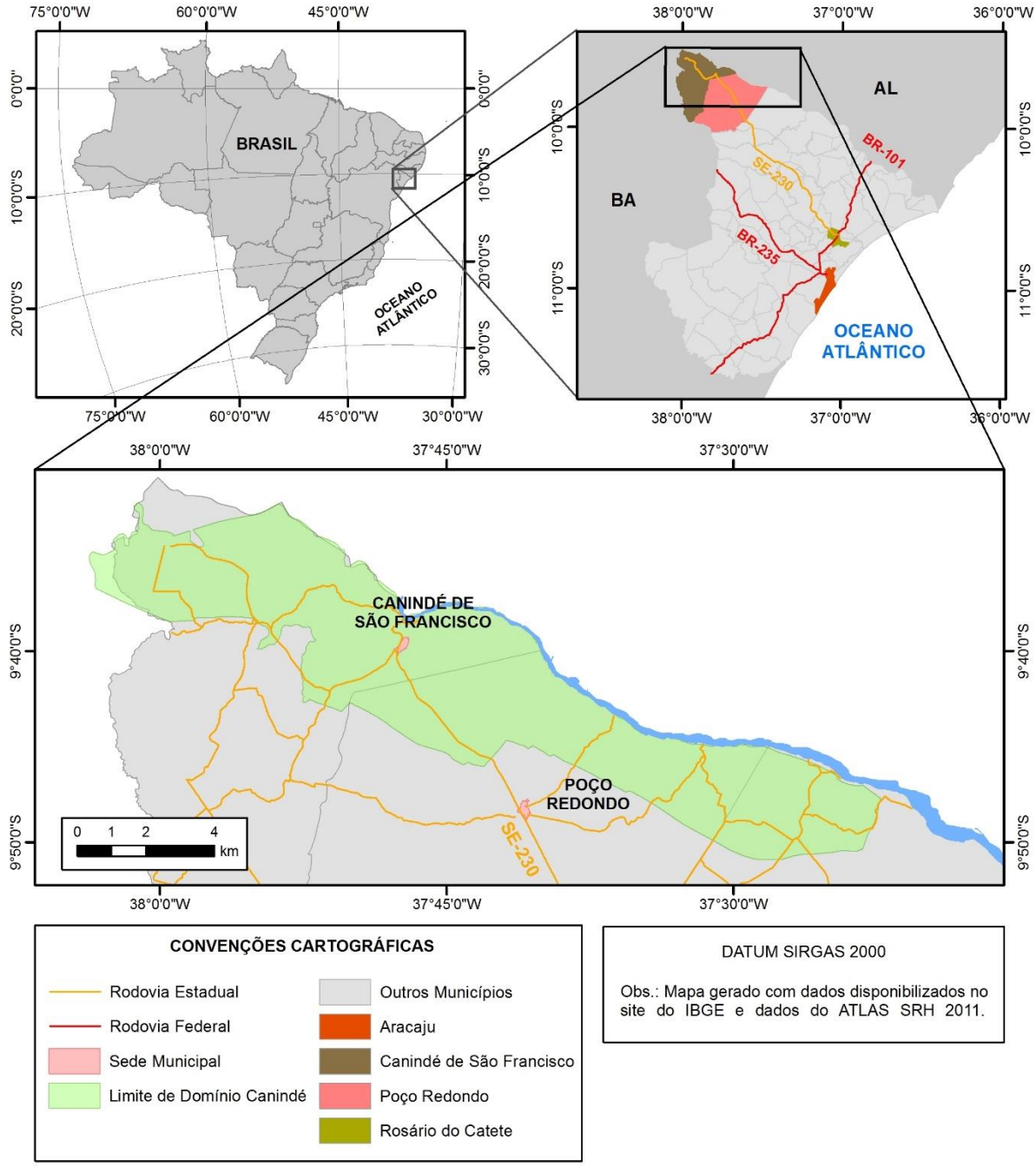

Figura 1: Mapa de localização geográfica do Domínio Canindé

4. Metodologia

- Foi realizado levantamento bibliográfico do tema da tese para servir de embasamento teórico básico para a compreensão dos temas que serão abordados.

- Foram utilizados dados de sensoriamento remoto e geoprocessamento de imagens para mapeamento e localização da unidade na região, além de construção de mapas de localização de dados.

- Foram obtidos dados em campo com coleta de amostras para petrografia, química mineral, geoquímica de rochas e datação.

- Foram descritas lâminas delgadas dos diferentes litotipos da unidade para caracterização das assembleias minerais.

- Foram geradas estimativas das condições de P-T para as rochas.

- Foi analisada a geoquímica de rocha total das rochas máficas, com obtenção de dados de elementos maiores, menores e traços.

- Foi obtida idade de cristalização das rochas máficas, e idades máximas de deposição das rochas metassedimentares, pelo método geocronológico U-Pb em zircão com LA-ICP-MS.

- Foram obtidos dados de geoquímica isotópica Sm-Nd.

- Avaliação e integração dos dados para a publicação de dois artigos científicos a serem submetidos a revistas internacionais indexadas, de acordo com as normas do Programa de Pós-Graduação em Geologia.

- Confecção da Tese de Doutorado.

5. Geologia Regional

5.1 Introdução

Do ponto de vista da geologia regional, será abordada a seguir uma síntese do contexto da área de estudo, partindo do pressuposto de enquadramento em escala decrescente na: Plataforma Sul-Americana > Província Borborema > Faixa Sergipana > Domínio Canindé > Unidade Novo Gosto.

5.2 Plataforma Sul-Americana e Província Borborema

A Plataforma Sul-Americana corresponde à parte continental da placa Sul-Americana e tem em seu embasamento indícios que remontam sua história policíclica do Paleoproterozoico ao Eo-Ordoviciano e de sua participação no supercontinente Gondwana (Schobbenhaus & Brito Neves, 2003). Ele externa, de modo descontinuo, exposições de segmentos de seu embasamento Pré-Cambriano, denominados Escudo das Guianas, Escudo Brasil-Central e Escudo Atlântico, sendo nesse último que a Província Borborema foi consolidada durante a orogênese Brasiliana (Almeida et al., 1976; Schobbenhaus & Brito Neves, 2003; Delgado et al., 2003).

A Província Borborema é uma unidade geotectônica localizada no nordeste do Brasil, limitada a sul pelo Cráton São Francisco, a norte pelo Cráton São Luis, a oeste pela bacia do

Parnaíba e a leste pelas bacias fanerozoicas costeiras (Almeida et al., 1981; Brito Neves et al., 1995). Resultado de aglutinação de cinturões de rochas supracrustais metavulcanossedimentares Paleo- a Neoproterozoicas ao embasamento Paleoproterozoico (Brito Neves et al., 1995), sua configuração final teve envolvimento da convergência entre os crátons São Francisco-Congo, Amazônico e São Luis-Oeste Africano, ocorrido na orogenia Brasiliana/Pan-Africana no fim do Neoproterozoico (Brito Neves & Cordani, 1991; Trompette, 1994). Ela foi dividida primeiramente em três domínios principais, Setentrional, Transversal e Meridional (Van Schmus et al., 1995), e posteriormente em cinco domínios geotectônicos ou subprovíncias, nomeadas Médio Coreaú, Ceará Central, Rio Grande do Norte, Transversal e Meridional (de norte a sul), limitadas entre elas por zonas de cisalhamentos regionais (Figura 2) (Brito Neves et al., 2000; Neves, 2003).

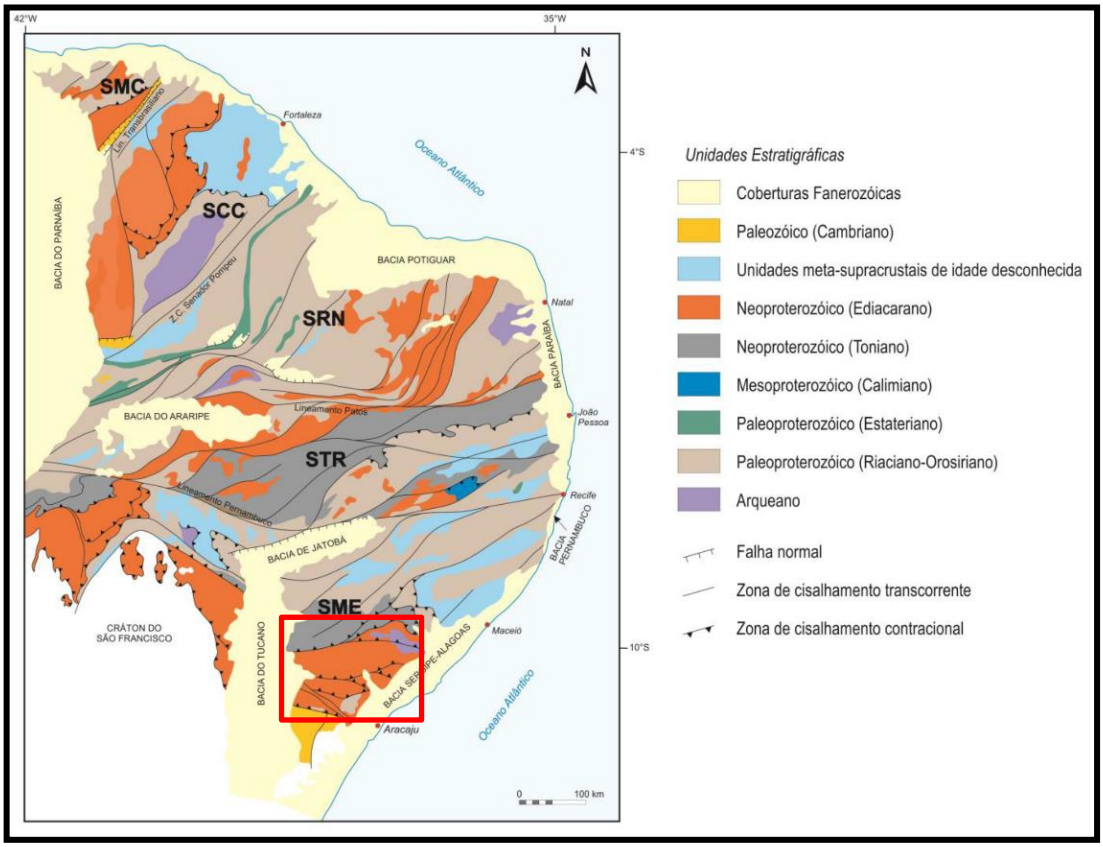

Figura 2: Subdivisão geotectônica da Província Borborema com a idade dos diversos segmentos crustais. Modificado de vários autores (p. ex. Santos, 1996; Brito Neves et al., 2000; Van Schmus et al., 2008). Siglas das subprovíncias: SMC = Médio Coreaú, SCC = Ceará Central; SRN = Rio Grande do Norte; STR = Transversal; SME = Meridional. O retângulo vermelho mostra a localização da Faixa Sergipana. (Santos, 2017)

A história geológica da Província Borborema indica envolvimento nos eventos Cariris Velhos, no Mesoproterozoico, e Brasiliano/Pan-Africano, no Neoproterozoico, sendo esse

último evento responsável pela estruturação final dessa província e responsável pela articulação do supercontinente Gondwana Ocidental (Brito Neves et al., 1995). O evento Cariris Velhos é bem documentado geocronologicamente por U-Pb em zircão com idades em torno de 1,1 a 0,92 Ga (p.ex., Brito Neves et al., 2001; Leite et al., 2000; Kozuch et al., 1997; Van Schmus et al., 1995). Porém, ainda há divergências atuais quanto ao tipo de orogenia que ocorreu no Neoproterozoico. Alguns autores apoiam a existência de uma orogenia intracontinental após o Paleoproterozóico (2.0 Ga), resultado de um evento extensional com formação de bacias e posterior inversão (p.ex., Neves, 2003; Neves et al., 2006, 2015; Neves & Coelho, 2010). Outros autores suportam a ideia da existência de tectônica acrescionária e colisional (p.ex., Santos, 1995; D'el Rey Silva, 1995; Kozuch, 2003; Oliveira et al., 2010; Amaral et al., 2012; Caxito et al., 2014; Santos et al., 2014; Lima et al., 2015; Lages e Dantas, 2016; Padilha et al., 2016; Lima et al., 2017, 2018; Caxito et al., 2020; Caxito et al., 2021)

Ao longo dos limites da província com os crátons adjacentes, encontram-se zonas de extensão nas quais se desenvolveram antigas bacias sedimentares, atualmente dobradas e metamorfisadas, e que foram ativas durante sucessivos períodos tectônicos (Mabessone, 2002). As faixas que as representam e que limitam essa província à sul são as faixas móveis Riacho do Pontal, Rio Preto e Sergipana.

5.3 Subprovíncia Meridional

A Faixa Sergipana está inserida na porção meridional da Província Borborema (Figura 2. Nessa subprovíncia afloram poucas rochas de idade arqueana e paleoproterozóica, predominando rochas do Mesoproterozóico e Neoproterozóico, associadas às orogêneses Cariris Velhos e Brasiliano. As rochas de idade arqueana e paleoproterozóica ocorrem predominantemente na forma de domos ou janelas estruturais, circundadas pelas unidades neoproterozóicas da Faixa Sergipana e do Superterreno Pernambuco-Alagoas (Brito Neves & Silva Filho, 2019; Caxito et al., 2020).

5.4 Faixa Sergipana

A Faixa Sergipana é uma região que foi intensamente deformada durante a Orogenia Brasiliana. Representa a continuação oeste do orógeno Oubanguide que se estende a NW na África (Trompette, 1997) e consiste de um cinturão de forma triangular com trend E-SE a W-NW localizado entre o Cráton do São Francisco-Congo a sul e o Maciço Pernambuco-Alagoas a norte (Oliveira et al., 2010).

A faixa é dividida, conforme Davison & Santos (1989) e Silva Filho (1998), em cinco domínios litotectônicos de N para S: Canindé, Poço Redondo-Marancó, Macururé, Vaza Barris e Estância, os quais são separados por zonas de cisalhamento de idade neoproterozóica nomeadas como Macururé, Belo Monte-Jeremoabo, São Miguel do Aleixo e Itaporanga (Figura 3).

Davison & Santos (1989) afirmam que a faixa, encontrada no sul da Província Borborema, nada mais é que resultado de encurtamento continental, com direção NE-SW a NNE-SSW, entre o Cráton do São Francisco e o Maciço Pernambuco-Alagoas durante o evento Brasiliano há aproximadamente 600 Ma. Segundo esses autores, ocorreram grandes deslocamentos que geraram zonas de cisalhamento *strike-slip* e empurrões que justapuseram diferentes níveis crustais, dividindo a área em domínios com diferentes características litológicas. Acredita-se que a faixa represente o fechamento de extensa bacia intracontinental ao longo da margem norte do Cráton do São Francisco-Congo, não tendo sido, porém, ainda encontrada evidência clara em campo, que prove a subducção ou sutura de placas.

Posteriormente, D'el Rey Silva (1995) interpretou o Faixa Sergipana como sendo formada em orogênese colisional clássica resultante do fechamento do mar Canindé. Oliveira et al. (2010) sugeriram modelo evolutivo para a Faixa Sergipana, apresentado em detalhes em item abaixo.

A seguir, serão abordadas as subdivisões da Faixa Sergipana, com destaque para as unidades Marancó e Poço Redondo, unidades vizinhas ao Domínio Canindé, foco deste trabalho.

5.4.1 Domínio Marancó

O Domínio Marancó caracteriza-se pela presença de rochas de natureza metavulcanossedimentar, imbricadas tectonicamente com granitos tipo Serra Negra, e metamorfisadas em condições de fácies anfibolito. Datações U-Pb de rochas metavulcânicas desse domínio obtiveram valores de idade de 1045±20 Ma e 1007±10 Ma (Van Schmus et al., 1995) e para o granito Serra Negra obteve valor de 951.8±1.5 Ma (Carvalho, 2005). Tanto o complexo, quanto os granitóides tipo Serra Negra estão intensamente cisalhados (Santos et al., 1998). Conforme Oliveira et al. (2010), o granito Serra Negra e os gnaisses Poço Redondo correspondem ao embasamento das rochas metassedimentares do domínio.

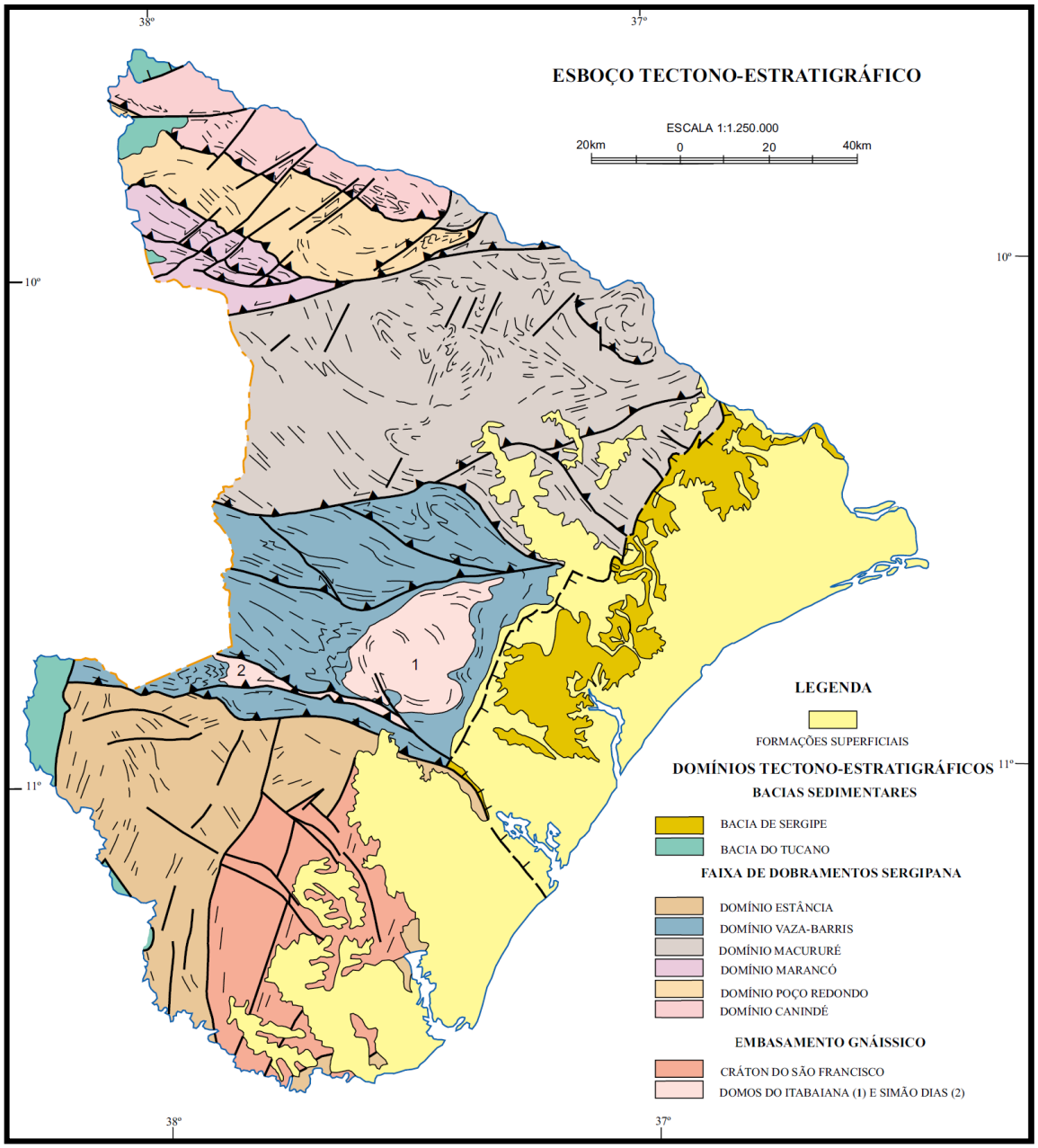

Figura 3: Mapa de esboço tectono-estratigráfico da Faixa de Dobramentos Sergipana (Santos et al., 1998)

5.4.2 Domínio Poço Redondo

O Domínio Poço Redondo é formado por sequência de ortognaisses tonalíticos a granodioríticos e paragnaisses subordinados, frequentemente migmatizados (Complexo Migmatítico de Poço Redondo). São intrudidos por granitoides tardi- a pós-tectônicos do Brasiliano. As rochas gnáissicas alcançam metamorfismo de fácies anfibolito alto. O Domínio Poço Redondo é considerado como terreno exótico e representa nível crustal mais profundo que os demais domínios da faixa (Santos et al., 1998). Carvalho (2005) obteve duas idades U-Pb SHRIMP de 979.8±3.5 e 960±38 Ma para gnaisse migmatítico dessa unidade.

5.4.3 Domínio Canindé

Domínio mais ao norte da faixa, com limite a sul com os domínios Marancó e Poço Redondo por zonas de cisalhamento e a norte, aproximadamente ao longo do Rio São Francisco, com o superterreno Pernambuco-Alagoas. É formado por rochas metavulcanossedimentares do Complexo Canindé, intrudidas por expressivo corpo gabróico diferenciado, denominado Suíte Intrusiva Canindé. Também ocorrem granitoides diversos sin-, tardi- a pós-tectônicos da Orogenia Brasiliana. O conjunto de rochas metamórficas está metamorfisado em fácies xisto-verde a anfibolito (Santos et al., 1998).

Recentemente, Mendes et al. (2017) ampliaram o Domínio Canindé no Estado de Alagoas, incluindo como pertencente a ele o Complexo Araticum. No entanto, Lima (2018) continua a adotar esse complexo como pertencente ao Domínio Macururé.

5.4.4 Modelo geotectônico proposto por Oliveira et al. (2010)

O modelo geotectônico para a Faixa de Dobramentos Sergipana mais atual é o elaborado por Oliveira et. al. (2010), abordando detalhadamente e com base nos dados mais recentes, a evolução da faixa, sintetizada na Figura 4. O modelo inicia com a quebra de um continente paleoproterozóico (Figura 4a), seguida pelo desenvolvimento de um arco continental neoproterozóico (~980-960 Ma) (gnaisses Poço Redondo), possivelmente na margem do Maciço Pernambuco-Alagoas de idade Paleoproterozóica (Figura 4b). A tectônica de extensão desse bloco continental (Figura 4c, d) deu origem a (i) granitos tipo-A Serra Negra e rochas sedimentares associadas à margem estendida do domínio Poço Redondo-Marancó, (ii) entre o Maciço Pernambuco-Alagoas e o domínio Poço Redondo-Marancó a sequência vulcanossedimentar Canindé, (iii) e a margem passiva na borda sul do Maciço Pernambuco-Alagoas. Uma segunda margem passiva se formou no Cráton do São Francisco. A ausência de qualquer rocha ofiolítica sugere que basaltos de fundo oceânico, os quais presumidamente separavam as duas margens passivas opostas, foi removido pela subducção, necessária para a geração de arco magmático continental entre 630 e 620 Ma.

A deposição de sedimentos na margem passiva do Maciço Pernambuco-Alagoas iniciou depois de cerca de 900 Ma, idade dos grãos detríticos de zircão mais jovens em rochas sedimentares do domínio Macururé e subdomínio Marancó. No domínio Canindé a sedimentação provavelmente começou em torno de 715 Ma (idade U-Pb do granito tipo-A, Garrote) e continuou a ao menos 625 Ma – a idade dos grãos detríticos de zircão mais jovens

na unidade Novo Gosto-Mulungu. Deposição das formações Juetê e Itabaiana na margem passiva do Cráton São Francisco poderia ter iniciado qualquer momento após 1975 Ma (idade dos grãos detríticos de zircão mais jovens da Formação Itabaiana).

No domínio Canindé o rifteamento continuou até aproximadamente 640 Ma (Figura 4d) com intrusão das associações ígneas bimodais do granito tipo-A Garrote (715 Ma) e rochas vulcânicas máficas continentais da unidade Novo Gosto-Mulungu, intrusão do complexo gabróico Canindé do tipo continental (cerca de 700 Ma), dos microgabros Gentileza e quartzo-monzodiorito (688 Ma) e granito rapakivi (684 Ma), e dos granitos Boa Esperança com textura rapakivi (641 Ma). Não há evidência conclusiva de abertura de um fundo oceânico incipiente no domínio Canindé, embora alguns anfibolitos com pillow da unidade Novo Gosto-Mulungu se assemelham a basaltos de fundo oceânico.

A convergência do Maciço Pernambuco-Alagoas e do Cráton do São Francisco levou à deformação de sedimentos de plataforma, construindo um arco continental entre 630 Ma e 620 Ma (Figura 4e) nos domínios Macururé, Poço Redondo-Marancó e Canindé, o qual pode ser identificado por: (i) granito Lajedinho no domínio Canindé (621 Ma), granitos no domínio Macururé (628-625 Ma), e granito no domínio Poço Redondo-Marancó (624 Ma; (ii) processo de fragmentação de placas por rasgamento (*slab-tearing*); e (iii) intrusão do monzogranito-sienito Curituba (617 Ma) e de granito sin-colisional (590-570 Ma) nos domínios Macururé, Canindé e Poço Redondo-Marancó (Figura 4e, f). Oliveira et al. (2010) inferiu que uma pequena placa oceânica foi subductada abaixo do domínio Poço Redondo-Marancó para explicar a ocorrência de idade de 603 Ma para rochas de arco vulcânico no subdomínio Marancó (Figura 4f). Subsequente a exumação e erosão do Maciço Pernambuco-Alagoas e dos últimos três domínios, ocorreu a deposição dos sedimentos clásticos de bacia de antepaís nos domínios Estância e Vaza-Barris com grãos detríticos de zircão mais jovens, entre 615 e 570 Ma, bem como a deposição de sedimentos Juá (bacia "*piggy-back*"?) no domínio Macururé (Figura 4f). Nesse momento as rochas supracrustais foram empurradas por sobre a placa inferior, i.e., a margem continental do Cráton do São Francisco, situada ao sul da Faixa de Dobramentos Sergipana (Figura 4g).

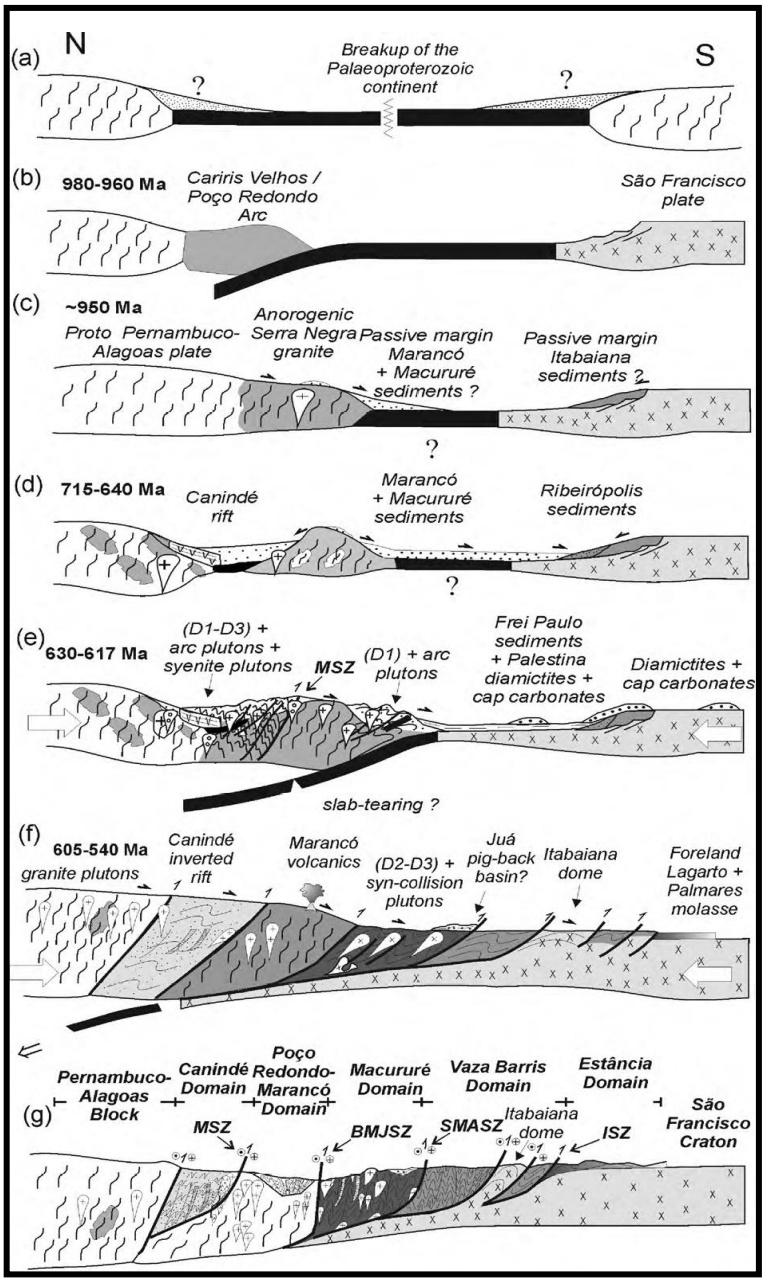

Figura 4: Evolução tectônica proposta para o Cinturão Sergipano do Mesoproterozóico (cerca de 1000 Ma) ao Neoproterozóico (cerca de 570 Ma). As principais zonas de cisalhamento são indicadas por seus acrônimos – MCZ (Zona de Cisalhamento Marancó), BMJSZ (Zona de Cisalhamento Belo Monte-Jeremoabo), SMASZ (Zona de Cisalhamento São Miguel do Aleixo), ISZ (Zona de Cisalhamento Itaporanga) (Oliveira et al., 2010)

5.5 Domínio Canindé

O Domínio Canindé constitui uma faixa de direção NW-SE (Figura 5), paralela ao Rio São Francisco, com cerca de quatro a dez quilômetros de largura e em torno de 50 km de extensão, limitada a sul com o domínio Poço Redondo pela zona de cisalhamento Mulungu-Alto Bonito, a norte com o Maciço Pernambuco-Alagoas, a leste com o domínio Macururé e a oeste pela cobertura sedimentar fanerozóica da Bacia de Tucano-Jatobá. Trata-se de um

domínio composto por complexa litoestratigrafia e com relativa escassez de dados de análises, resultando claramente na falta de consenso entre autores, o que leva a postulação de modelos inconclusivos em relação a origem e evolução do domínio e suas unidades.

Santos et al. (1998) caracterizam o domínio como sendo constituído por rochas metavulcanossedimentares do Complexo Canindé, polideformadas, frequentemente transpostas e cisalhadas, intrudidas por expressivo corpo gabróico diferenciado, denominado Suíte Intrusiva Canindé. O domínio é ainda afetado por intrusões graníticas de colocação sin-, tardi- a pós- e pós-tectônicas.

Como primeira tentativa de individualização do Complexo Canindé, Silva Filho et al. (1979) agruparam suas rochas supracrustais, encaixantes da suíte gabróica, em unidades Mulungu, Garrote, Novo Gosto e Gentileza. Porém, posteriormente, Santos et al. (1998) suprimiram a unidade Garrote, por se tratar apenas de granitoide milonitizado, denominado, a partir de então, como granitóide do tipo Garrote. Em sequência, Seixas & Moraes (2000) reduziram as unidades Mulungu e Novo Gosto a apenas unidade Novo Gosto e a região antes atribuída ao granitóide do tipo Garrote foi contextualizada como faixa de 2 a 5 km de largura, formada por proto-milonitos, milonitos e ultra-milonitos resultantes da deformação das rochas das unidades Novo Gosto e granitos Boa Esperança, Poço Redondo e Xingó, relacionadas à zona de cisalhamento Mulungu-Alto Bonito (Nascimento, 2005).

Com respeito aos granitoides que intrudem a região do Domínio Canindé, também há uma evolução em relação à sua classificação. Santos et al. (1998) distinguiram quatro conjuntos de granitoides no domínio: tipo Garrote, tipo Curralinho, tipo Xingó e tipo Serra do Catu. Seixas & Moraes (2000) e Nascimento (2005) separam os granitoides que intrudem o domínio em Lajedinho, Boa Esperança, Serrota, Sítios Novos, Xingó, Serra do Catu e Curituba.

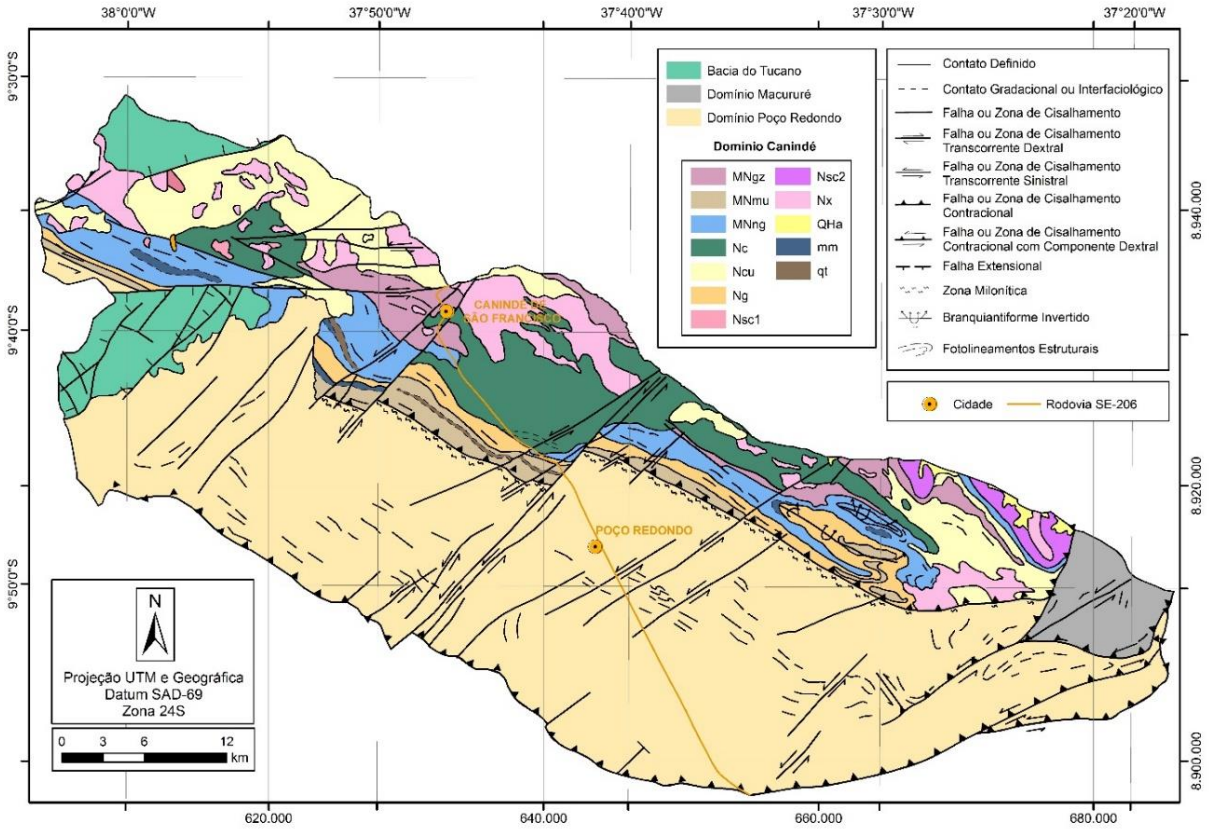

Figura 5: Mapa geológico com detalhe no domínio Canindé. MNgz-Unidade Gentileza, MNmu-Unidade Mulungu, MNng-Unidade Novo Gosto, Nc-Suíte Intrusiva Canindé, Ncu-Granitóides tipo Curralinho, Ng-Granitóides tipo Garrote, Nsc1 e Nsc2-Granitóides tipo Serra do Catu, Nx-Granitóides tipo Xingó, QHa-Depósitos aluvionares, mm-mármores, qt-quartzitos/metachert. (Modificado de Santos et al., 1998)

Recentemente, Souza Júnior (2013) executou trabalhos de mapeamento geológico na porção central do Domínio Canindé. Nesse trabalho foi retomada a denominação anterior de Seixas & Moraes (2000) do granitóide tipo Garrote para a zona deformada nas proximidades da zona de cisalhamento Mulungu-Alto Bonito; além disso, nesse trabalho foi extinta a unidade Mulungu, substituída por Unidade Novo Gosto-Mulungu; o autor continuou utilizando a classificação de granito do tipo Xingó e criou a denominação Suíte Ígnea Bimodal Gentileza-Curralinho, atribuindo a essa suíte a unidade Gentileza e o granitóide tipo Curralinho, usando como base a forte relação de coexistência dos seus litotipos.

A Suíte Intrusiva Canindé teve sua primeira tentativa de diferenciação espacial em mapa geológico em Seixas & Moraes (2000). Estes autores compartimentaram o corpo gabróico em quatro unidades espaciais: Gabro e gabro pegmatítico, posicionados aproximadamente na porção centro-sul do corpo; troctolito e anortosito, posicionados na porção oeste; olivina gabro e gabronorito, ocupando quase todo o resto da suíte; e peridotitos e olivina norito, expostos como lentes na porção oeste da falha Jacaré.

Nota-se que ainda há muito a evoluir em relação a mapeamento geológico no domínio Canindé, já que ao longo das últimas décadas houve mudanças e propostas diversas entre autores em relação a classificação e nomenclatura, tanto das unidades do Complexo Canindé, quanto dos granitóides, assim como em relação a disposição e geometria dos corpos em mapa geológico.

Com relação à organização estrutural, de acordo com Santos et al. (1998), os litotipos do Complexo Canindé encontram-se quase sempre tectonicamente imbricados, principalmente aqueles situados mais na porção sul do domínio. Também é notada menor intensidade na transposição tectônica e maior preservação dos dobramentos em sua porção mais a sudeste, onde se pode visualizar por vezes geometrias de branquiantiformes ou de prováveis seções de megadobras tipo bainha, bem como são observados contatos transicionais entre as unidades. Santos et al. (1998) descrevem o metamorfismo atuante como sendo de fácies anfibolito, com ocorrência de retrometamorfismo para a fácies xisto-verde concentrada nas zonas mais cisalhadas.

Conforme Nascimento (2005), o Domínio Canindé foi atingido por pelo menos quatro fases deformacionais:

- D1: deforma S0 (acamamento) e corresponde ao bandamento composicional das rochas da pilha metavulcanossedimentar;
- D2: caracterizada por dobras do bandamento da fase D1 cujas camadas mostram mergulhos para NE, sendo bem preservadas na unidade Novo Gosto;
- D3: predomina regionalmente, registrada pelas foliações com direções NW-SE, afetando principalmente as unidades Novo Gosto e granitos Boa Esperança e Xingó. A essa fase são atribuídas as zonas de cisalhamento transcorrentes sinistrais de direção NW-SE e mergulhos de alto ângulo para NE e SW, como a zona de cisalhamento Mulungu-Alto Bonito.
- D4: com características rúpteis e direção NE-SE; é associada às zonas rúpteis do Rio Jacaré e Bom Sucesso, com movimento sinistral.

Nascimento (2005) apresenta modelo de evolução tectônica correspondente a uma sequência de rifte intra-continental (Figura 6).

Oliveira et al. (2010) interpretam o domínio como sequência de rifte, posteriormente deformada e agregada ao domínio Poço Redono-Marancó. Esses autores sugerem que o rifte provavelmente teria evoluído para bacia oceânica devido à ocorrência de anfibolitos na unidade Novo Gosto-Mulungu com lentes de mármore e ocorrência de basaltos com pillows.

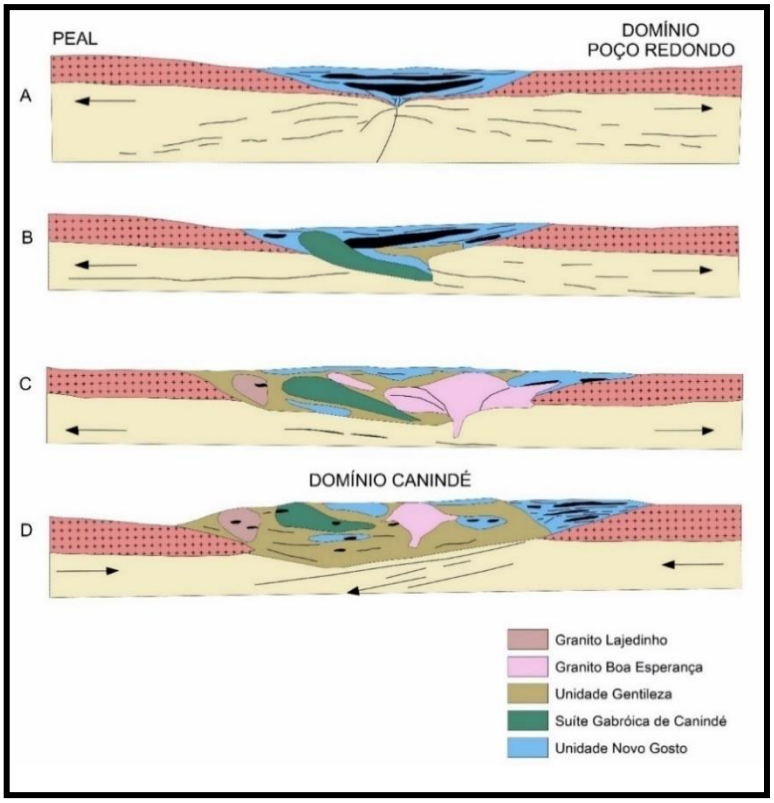

Figura 6: Modelo evolutivo de rifte continental para o Domínio Canindé: (a) colapso da litosfera continental por afastamento das massas continentais PEAL e Domínio Poço Redondo, subsidência, sedimentação, subida da MOHO e consequente magmatismo, primeiros pulsos de sedimentação da unidade Novo Gosto (em torno de 970 Ma) a qual foi invadida pela Suíte Intrusiva Canindé (701) e unidade Gentileza (684 Ma) (b). (c) Intrusão do granito Boa Esperança e posteriormente granito Lajedinho (619 Ma). (d) Fechamento da bacia de Canindé com novos pulsos de sedimentação da unidade Novo Gosto (a partir de 634 Ma) (Modificado de Nascimento, 2005).

5.6.1 Unidade Novo Gosto

Nascimento (2005) descreve a unidade Novo Gosto como formada essencialmente por metagrauvaca, metapelito, metassiltito, metachert, xisto, grafita-xisto, mármore, rochas calciossilicáticas e anfibolito, truncados por diques máficos e félsicos, assim como corpos gabróicos ricos em Fe-Ti. A unidade foi invadida por corpos de quartzo monzodiorito da unidade Gentileza e gabro da Suíte Gabróica Canindé.

Souza Júnior (2013), por sua vez, descreve essa unidade como uma faixa com espessura irregular, descontínua, orientada segundo WNW-ESE. A unidade estaria truncada pela suíte gabróica e em contato tectônico com os granitóides do tipo Garrote e os litotipos da Suíte Ígnea Bimodal Gentileza Curralinho. De acordo com o autor, o bandamento apresentado por seus litotipos, por vezes xistificados, a frequente transposição da foliação em dobras apertadas, configuradas em sinformes e antiformes invertidos, além da forte epidotização, são as principais características das rochas dessa unidade. Souza Júnior (2013) ainda comenta que

a unidade é composta por anfibolitos, anfibolitos xistificados, quartzitos feldspáticos, metarritmitos, mármores e níveis calciossilicáticos.

Segundo Liz (2017), as rochas de filiação ígnea presentes na unidade ocorrem de duas formas principais, a mais comum em corpos tabulares centimétricos a métricos intercalados com metacherts, metamargas, mármores e xistos, a outra em forma de diques. Liz (2017) ainda informa que com relação aos corpos tabulares, não é possível assumir, com clareza, se os protólitos eram rochas efusivas ou intrusivas do tipo soleira, devido ao intenso metamorfismo e às deformações presentes. Com auxílio de dados geoquímicos dos ortoanfibolitos da unidade, Liz (2017) sugere a existência de dois grupos de protólitos ígneos: um caracterizado por teores de TiO_2>2%, acompanhados por concentrações mais elevadas em P_2O_5, HFSE e Σ ETRs, chamados de alto-Ti; e outro caracterizado por baixos terrores de TiO_2 < 1,19%, P_2O_5 < 0,01%, HFSE e ΣETRs chamados de baixo-Ti.

Resultados de análises U-Pb (SHRIMP) executadas em grãos detríticos de zircão de rochas metassedimentares dessa unidade (Nascimento, 2005) evidenciaram ao menos três áreas-fonte, com idades em torno de 977 Ma, 718 Ma e 679 Ma (final do Cariris Velhos até o Brasiliano). A mesma autora concluiu que grande parte das rochas metassedimentares é proveniente de áreas-fonte de caráter químico continental, com composições máficas e félsicas, que podem corresponder às rochas do próprio Domínio Canindé, como anfibolito da Unidade Novo Gosto, rochas da Unidade Gentileza e granitos Boa Esperança e Lajedinho.

Já em relação aos anfibolitos da unidade, Nascimento (2005) determinou, a partir de amostras analisadas, quatro tipos de protólitos diferentes: um grupo considerado de composição basáltica, apresentando estruturas reliquiares preservadas de microamígdalas e cristais euédricos de plagioclásio, sugerindo claramente origem ígnea; outro, também de composição basáltica, mas com maior grau de contaminação crustal, possivelmente contaminação pelos leitos de origem sedimentar nos quais estão intercalados; e ainda os protólitos de origem sedimentar e intermediária.

CAPÍTULO II - Artigo 1: Neoproterozoic (740-680 Ma) Arc-Back-Arc magmatism in the Sergipano belt, Southern Borborema, Brazil

Gmail Luiz Henrique Passos <lhpassos.geologo@gmail.com>

Confirming submission to Journal of South American Earth Sciences
1 mensagem

Journal of South American Earth Sciences <em@editorialmanager.com> 18 de janeiro de 2021 16:49
Responder a: Journal of South American Earth Sciences <sames@elsevier.com>
Para: Luiz Henrique Passos <lhpassos.geologo@gmail.com>

This is an automated message.

Manuscript Number: SAMES_2019_655R2

Neoproterozoic (740-680 Ma) Arc-Back-Arc magmatism in the Sergipano belt, Southern Borborema, Brazil

Dear Dr Passos,

We have received the above referenced manuscript you submitted to Journal of South American Earth Sciences.

To track the status of your manuscript, please log in as an author at https://www.editorialmanager.com/sames/, and navigate to the "Revisions Being Processed" folder.

Thank you for submitting your revision to this journal.

Kind regards,
Journal of South American Earth Sciences

More information and support

You will find information relevant for you as an author on Elsevier's Author Hub: https://www.elsevier.com/authors

FAQ: How can I reset a forgotten password?
https://service.elsevier.com/app/answers/detail/a_id/28452/supporthub/publishing/
For further assistance, please visit our customer service site: https://service.elsevier.com/app/home/supporthub/publishing/
Here you can search for solutions on a range of topics, find answers to frequently asked questions, and learn more about Editorial Manager via interactive tutorials. You can also talk 24/7 to our customer support team by phone and 24/7 by live chat and email

In compliance with data protection regulations, you may request that we remove your personal registration details at any time. (Use the following URL: https://www.editorialmanager.com/sames/login.asp?a=r). Please contact the publication office if you have any questions.

Neoproterozoic (740-680 Ma) Arc-Back-Arc magmatism in the Sergipano belt, Southern Borborema, Brazil

Luiz Henrique Passos[a,*], Reinhardt A. Fuck[a], Farid Chemale Jr.[b], Cristine Lenz[c], Márcio Martins Pimentel[a,**], Adriane Machado[c], Viter Magalhães Pinto[d]

[a] Programa de Pós-Graduação em Geologia, Instituto de Geociências, Universidade de Brasília, Campus Universitário Darcy Ribeiro, Brasília, DF, 70904-970, Brazil

[b] Programa de Pós-Graduação em Geologia, Universidade do Vale do Rio dos Sinos, São Leopoldo, RS, 93.022-750, Brazil

[c] Departamento de Geologia, Universidade Federal de Sergipe, Campus São Cristóvão, São Cristóvão, SE, 49100-000, Brazil

[d] Departamento de Eng. Geológica, Universidade Federal de Pelotas, Pelotas, RS, 96010-440, Brazil

[*] Corresponding author. E-mail address: lhpassos.geologo@gmail.com

[**] *In memoriam*

Abstract

The Novo Gosto amphibolites represent the oldest unit of the Canindé domain, a Neoproterozoic sequence located in the NW Sergipano Belt, southern Borborema Province, Brazil. The domain comprises an association of metavolcano-sedimentary rocks, gabbroic intrusions, bimodal magmatic rocks, and syn- to post-tectonic granitoids. Due to the lithostratigraphic and geochemical complexity of this domain, several controversial interpretations of the tectonic setting have been proposed over the years. The protholits of the

Novo Gosto amphibolites are here classified as high Fe tholeiitic basalt type rocks. Three geochemical groups were identified: Group 1 is more depleted in incompatible elements and has a pattern similar to island arc basalts with HFSE depletion (Nb-Ta, Zr-Hf, smooth Ti); Group 2 displays a pattern similar to Group 1, but with more evident anomalies (Nb-Ta, Ti) and varied enrichment in incompatible elements; Group 3 is more enriched in incompatible elements than Group 1 rocks, with the pattern being flatter with milder HFSE depletion (Nb-Ta, Zr-Hf, smooth Ti, Y) and resembling a geochemical pattern slightly more enriched than E-MORB. Our results suggest an environment similar to the Ryukyu-Okinawa (Japan) and Kamchatka arc-back-arc (Russia) setting. LA-ICP-MS U-Pb zircon dating of one amphibolite sample resulted in a date of 743±3 Ma, confirming the geological field relationships that indicate this unit as the oldest in the domain. The new petrographic, geochemical, and isotopic data for the Novo Gosto amphibolites lead to the recognition of an ancient Neoproterozoic arc-back-arc system, a rare setting in the earlier phases of the Brasiliano Orogeny within the Borborema Province, which ended with the closure of the restricted Canindé sea and the associated Sergipano ocean at around 630 Ma.

Keywords: Arc-back-arc; Amphibolite; Sergipano Belt; Early Brasiliano Orogeny.

1. Introduction

Basaltic magmas occur in several tectonic settings (e.g., MORB, OIB, arc and back-arc, intracontinental flows, etc.), and their geochemistry is considered a useful tool for the discrimination of the environment in which they were introduced (Pearce and Cann, 1973).

The geochemical signature in arc and back-arc settings can be varied, displaying variation from MORB to typically arc-like signatures in a small space. The reason of this

variation can be diverse, like the proximity to a subduction zone (Wilson, 1989; Fretzdorff et al., 2002; Xia et al., 2003, 2016; Xia and Li, 2019) or the subducting plate dip angle (Kearey et al., 2014; Condie, 2016). Besides the classical signatures of continental and island arcs, overlapping of these tectonic signatures can be found, e.g., for continental arcs developed on thinned continental margins, resulting in a mixture of geochemical signatures from the above-mentioned settings (e.g., Ryukyu-Okinawa and Kamchatka arc-back-arc; Shinjo et al., 1999; Volynets et al., 2018).

The Canindé domain is one possible candidate to present overlapping geochemical signatures of arc and back-arc settings. This domain in the NW Sergipano Belt, southern Borborema Province, comprises a Neoproterozoic association of rocks composed of metavolcano-sedimentary rocks (Novo Gosto unit), a gabbroic layered intrusion (Canindé Layered Intrusion), a bimodal association of rocks (Gentileza unit), and syn- to late or post-tectonic granitic suites.

Several hypotheses have been formulated over the years to explain the paleotectonic setting of the Canindé domain rocks, mostly from intraplate to subduction related settings (Brito Neves and Cordani, 1973; Silva Filho, 1976; Jardim de Sá et al., 1986; Santos et al., 1988; Oliveira and Tarney, 1990; Bezerra et al., 1991; Bezerra, 1992; Silva Filho, 1998; Seixas and Moraes, 2000; Nascimento, 2005; Oliveira et al., 2010; Verma and Oliveira, 2015; Passos, 2016; Liz et al., 2018).

We chosed the Novo Gosto metavolcanic rocks, represented by amphibolites, and carried out petrography, lithogeochemistry, Sm-Nd isotope geochemistry, and LA-ICP-MS U-Pb zircon geochronology on representative samples, in order to better understand the paleotectonic setting of this domain. Also, we test the hypothesis of a mixture of geochemical signatures from arc and back-arc settings in an ancient orogenic province, part of Gondwana, whose interpretation of paleotectonic setting is still complex.

2. Geological setting

The Sergipano Belt (Fig. 1A, B), located in the southern part of the Borborema Province, is an E-SE to W-NW trending fold and thrust belt, between the São Francisco-Congo Craton and the Pernambuco-Alagoas superterrane (Oliveira *et al.*, 2010; Brito Neves and Silva Filho, 2019). The Sergipano Belt was formed due to the collision between the craton and the superterrane during the Brasiliano Orogeny (Brito Neves *et al.*, 1977; D'el Rey Silva, 1995; Lima et al., 2017). The Sergipano Belt comprises five lithostratigraphic domains that are named, from north to south, the Canindé, Poço Redondo-Marancó, Macururé, Vaza Barris and Estância domains, which are separated by Neoproterozoic shear zones known as Macururé, Belo Monte-Jeremoabo, São Miguel do Aleixo and Itaporanga (Davison and Santos, 1989; Silva Filho, 1998; Oliveira *et al.*, 2010) (Fig. 1A).

The Canindé domain represents the northwesternmost domain of the Sergipano Belt (Fig. 1A, C). It is separated from the Marancó-Poço Redondo domain by the Mulungu-Alto Bonito Shear Zone (Fig. 1B) and is represented by (i) the Canindé Complex of metavolcano-sedimentary rocks of the Novo Gosto unit and bimodal hypabyssal rocks of the Gentileza unit, (ii) the Canindé layered gabbroic intrusion, and (iii) the syn- to late-tectonic granitic Garrote, Curralinho/Boa Esperança, Sítios Novos, Serra do Catu, Coronel João Sá, Lajedinho, and Xingó suites. The Canindé Complex rocks were metamorphosed under amphibolite facies conditions, with local retrogression to greenschist facies conditions (Santos *et al.*, 1998; Nascimento, 2005; Oliveira *et al.*, 2010, 2017; Souza Júnior, 2013).

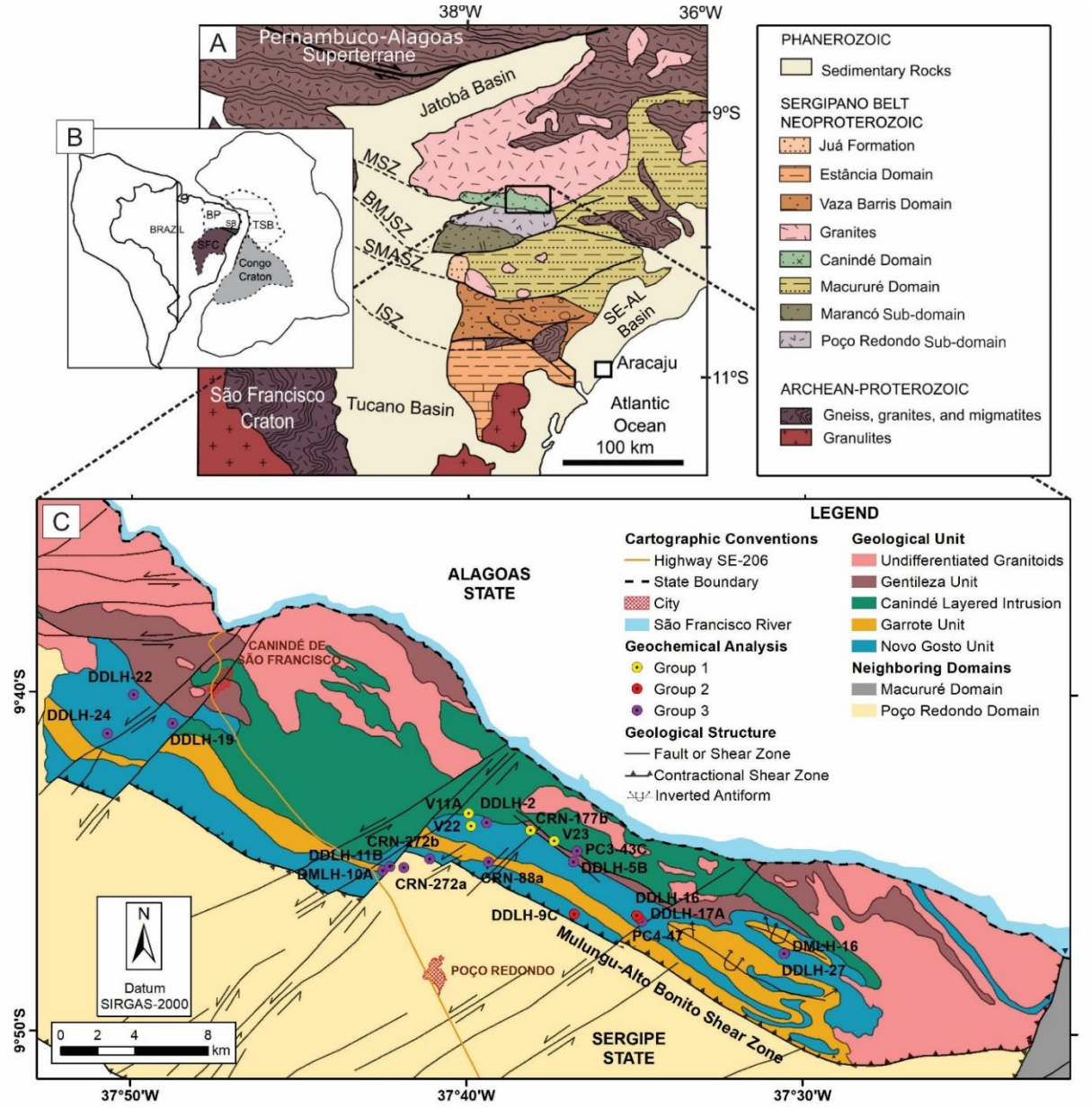

Figure 1: (A) Geological map of the Sergipano Belt. MSZ (Macururé Shear Zone), BMJSZ (Belo Monte-Jeremoabo Shear Zone), SMASZ (São Miguel do Aleixo Shear Zone), ISZ (Itaporanga Shear Zone). (B) Paleogeographic reconstruction showing the Neoproterozoic connection between the Borborema Province (BP, NE Brazil) and the Trans-Saharan belt (TSB, NW Africa). SB (Sergipano Belt) SFC (São Francisco craton). (C) Geological map of the central Canindé domain with location of studied amphibolite samples. Modified from Oliveira et al. (2010) and Santos et al. (1998).

The Novo Gosto unit consists of amphibolites, feldspathic quartzites, metarythmites, schists, marbles, and calc-silicate rock layers. These rocks are mostly fine- to medium-grained, usually banded, and occur as alternate light and dark bands (Souza Júnior, 2013), however massive amphibolites can occur as well. The unit forms an irregular WNW-ESE trending strip

that is intruded by the Canindé layered intrusion. The oldest granites, the Garrote granite and the bimodal Gentileza-Curralinho/Boa Esperança rocks, although intrusive into the Novo Gosto rocks, often occur in tectonic contact with it (Souza Júnior, 2013). Strongly deformed rocks of the Novo Gosto unit were found along the NW-SE shear zones and are marked by frequent transposition of the foliation into tight folds, resulting in inverted synforms and antiforms, accompanied by strong epidotization.

Besides the Novo Gosto amphibolites, another group of quartz-rich amphibolites is exposed in the Canindé domain, belonging to the Gentileza unit. In the field, they are very similar to the Novo Gosto massive amphibolites, especially when they do not have features of mingling with the felsic rapakivi metagranites (Curralinho/Boa Esperança units). According to Nascimento (2005), the Gentileza unit rocks are younger (688±6 Ma, zircon U-Pb in quartz monzodiorite) and contain more biotite than the Novo Gosto amphibolites. Liz et al. (2018) emphasized that besides biotite, hornblende and even visible quartz occur in the Gentileza amphibolites, which thus must be classified as intermediate rocks.

The geochronological data available for the Novo Gosto Unit are restricted to the metasedimentary rocks: a 963±20 Ma Pb-Pb age on a marble sample (Nascimento, 2005) and 650 Ma (youngest U-Pb detrital zircon population) for a meta-greywacke (Oliveira *et al*., 2015). The latter age was interpreted by the authors as the maximum depositional age.

3. Analytical methods

3.1 Zircon U-Pb geochronology

Several amphibolite samples were prepared for zircon concentration. However, only sample DMLH-16 yielded zircon grains for U-Pb isotope analyses. Amphibolite DMLH-16

was crushed and milled using a jaw crusher and swing mill. The heavy minerals were separated by conventional procedures using a magnetic separator and heavy liquids. Zircon was concentrated by handpicking and finally mounted in epoxy resin and polished. Cathodoluminescence images were obtained at the multilayer Leica cathodoluminescence microscope at the State University of Rio de Janeiro (UERJ). The U-Pb isotopic analyses were performed using the Laser Ablation Multi-Collector Inductively Coupled Plasma Mass Spectrometry (LA-MC-ICP-MS) at the Geochronology Laboratory of Universidade de Brasília (UnB). Isotopic data were acquired using static mode with 25 µm spot size. Data acquisition occurred in 40 cycles of 1.048 s of integration time, and the 202, 204, 206, 207, 208, 232, and 238 masses were collected simultaneously, 202, 204, 206, 207, and 208 measured with multiplier ion counting and 232 and 238 with Faraday cups. Laser-induced elemental fractional and instrumental mass discrimination were corrected using the GJ-1 reference zircon (Jackson *et al*., 2004). During the analytical sessions, the zircon standard 91,500 (Wiedenbeck et al., 1995, 2004) was also analyzed as an external standard. U-Th-Pb data reduction was calculated in an Excel spreadsheet (Chemale *et al*., 2012) and details of instrumental operating conditions followed Bühn *et al*. (2009). The Concordia diagram was generated using IsoplotR 2.4 (Vermeesch, 2018).

3.2 Whole-rock geochemistry

Eighteen whole-rock geochemical analyses were performed in the Activation Laboratories Ltd. The analytical treatment employs lithium metaborate/tetraborate fusion and subsequent analysis by inductively coupled plasma-optical emission spectrometry (ICP-OES) for major elements and inductively coupled plasma-mass spectrometer (ICP-MS) for trace elements. Uncertainties in major elements are 0.01%, except for MnO and TiO_2 (0.001%). The

accuracy of ICP–MS analyses has been evaluated from the repeated analyses of the international standards DNC-1, SY-4, W-2a, and BIR-1a. The detection limit for trace elements is in the range of 0.01%-30%. More information in https://actlabs.com/. The concentrations of major and trace elements are given in Tables 1A and 1B.

Table 1 A: Results of geochemical analysis of amphibolites from the Novo Gosto unit. *Ti calculated from TiO2; ** chondrite normalized; (I) New data; (II) Nascimento (2005); n.d. - not determined.

Sample No.	V11A	V22	V23	CRN-177b	DDLH-9C	DDLH-17A	DDLH-16	CRN-272a	CRN-273b	CRN-88a	DMLH-10A	DMLH-16
Group	1	1	1	1	2	2	2	3	3	3	3	3
Reference	(I)	(I)	(I)	(II)	(I)	(I)	(I)	(II)	(II)	(II)	(I)	(I)
Major element [wt. %]												
SiO_2	48.40	48.82	49.10	47.54	54.05	48.92	50.04	46.40	50.68	50.03	53.36	47.96
TiO_2	1.19	1.08	1.10	1.42	0.97	2.05	0.75	2.16	2.37	2.94	3.19	2.07
Al_2O_3	16.91	16.66	17.10	14.43	14.55	12.17	14.51	15.28	14.36	14.12	10.92	14.33
Fe_2O_3	10.98	11.20	10.91	14.29	10.96	13.43	10.93	14.51	13.75	13.94	15.53	12.44
MnO	0.19	0.20	0.20	0.23	0.19	0.24	0.18	0.21	0.21	0.24	0.25	0.18
MgO	6.28	6.41	6.30	7.15	3.97	8.00	6.83	7.90	6.29	5.73	4.08	6.98
CaO	9.07	9.25	8.98	11.77	6.36	9.37	11.11	8.24	5.67	8.55	6.97	11.73
Na_2O	3.08	2.98	2.88	1.93	3.26	2.70	1.96	3.57	4.46	3.65	2.44	2.37
K_2O	1.51	1.60	1.66	0.32	2.16	1.22	1.34	0.18	0.39	0.45	0.52	0.41
P_2O_5	0.18	0.16	0.18	0.15	0.29	0.64	0.38	0.24	0.33	0.35	0.49	0.26
Cr_2O_3	0.011	0.012	0.011	n.d.	n.d.	n.d.	n.d.	n.d.	n.d.	n.d.	n.d.	n.d.
LOI	1.90	1.30	1.60	0.73	2.43	1.62	1.52	1.39	1.35	0.20	1.56	0.71
Total	99.70	99.67	100.02	99.96	99.20	100.36	99.55	100.08	99.86	100.20	99.31	99.45
Trace element [ppm]												
Sc	31	30	31	n.d.	30	38	30	44	23	16	39	38
Ti*	7132	6473	6593	8511	5838	12263	4477	12946	14205	17621	19143	12419
V	296	269	277	n.d.	199	308	289	359	360	406	403	288
Cr	75	82	75	n.d.	160	400	270	218	39	83	50	240
Co	n.d.	n.d.	n.d.	n.d.	30	43	36	n.d.	n.d.	n.d.	44	67
Cu	33	38	36	n.d.	70	130	160	80	72	113	290	60
Ni	19	19	19	n.d.	30	130	90	47	24	42	< 20	90
Ga	18	18	18	n.d.	18	18	17	25	25	24	21	19
Sn	1	1	1	n.d.	2	4	2	<3	<3	<3	2	1

Zn	33	29	32	n.d.	80	120	80	121	92	116	130	90
Rb	42	47	50	23	93	34	31	5	10	5	11	4
Sr	400	395	405	144	299	210	400	250	172	434	236	260
Y	19	18	18	15	34	33	15	37	46	43	52	24
Zr	42	48	44	32	117	190	67	156	210	223	230	114
Nb	3	3	3	3	8	23	3	9	12	15	15	9
Cs	1	1	1	2	2	1	< 0.5	1	1	1	< 0.5	< 0.5
Ba	280	248	288	260	587	293	363	55	150	158	218	225
La	6	6	6	7	19	57	10	12	19	19	23	10
Ce	14	14	14	16	56	122	19	29	43	46	54	24
Nd	11	11	11	9	26	59	14	19	26	31	32	16
Pb	4	3	4	6	5	25	12	5	5	5	8	< 5
Th	1	1	1	1	8	6	3	1	4	3	3	2
U	1	1	1	0	2	2	1	0	1	1	1	1
Hf	1	1	1	1	3	5	2	4	5	5	6	3
Ta	0	0	0	0	1	1	0	1	3	1	1	1
Pr	2	2	2	2	6	15	3	4	6	7	7	3
Sm	3	3	3	2	6	11	4	5	7	8	9	5
Eu	1	1	1	1	2	3	1	2	2	2	3	2
Gd	4	3	4	3	6	9	4	6	7	8	9	5
Tb	1	1	1	0	1	1	1	1	1	1	2	1
Dy	3	3	3	3	7	8	3	6	7	7	10	6
Ho	1	1	1	1	2	2	1	1	1	2	2	1
Er	2	2	2	2	4	4	2	3	4	4	5	3
Yb	2	2	2	2	5	4	2	3	4	4	5	3
Lu	0	0	0	0	1	1	0	0	1	1	1	0
Tm	n.d.	n.d.	n.d.	0	1	1	0	0	1	1	1	0
ΣREE	50	49	50	47	142	298	63	94	129	142	163	81
$(La/Yb)_N$**	2	2	2	3	3	11	4	3	4	4	3	2

Table 1 B: Results of geochemical analysis of amphibolites from the Novo Gosto unit. *Ti calculated from TiO2; ** chondrite normalized; (I) New data; (II) Nascimento (2005); n.d. - not determined.

Sample No.	DDLH-2	DDLH-5B	DDLH-22	DDLH-24	DDLH-27	DDLH-19	PC3-43C	PC4-47	V-20	DDLH-11B
Group	3	3	3	3	3	3	3	3	3	3
Reference	(I)	(I)	(I)	(I)	(I)	(I)	(I)	(I)	(I)	(I)
Major element [wt. %]										
SiO_2	53.30	47.36	47.17	48.66	57.70	53.11	49.96	49.97	49.88	54.81
TiO_2	1.92	2.91	2.54	2.55	1.90	3.08	2.07	2.05	2.10	2.03
Al_2O_3	13.16	15.25	15.58	13.45	11.93	11.95	14.06	13.66	14.98	13.23
Fe_2O_3	12.08	15.18	16.15	14.19	14.32	15.38	13.40	13.26	11.33	13.44
MnO	0.21	0.22	0.25	0.21	0.26	0.24	0.22	0.22	0.21	0.28
MgO	5.45	5.31	3.75	5.28	3.49	3.47	5.58	5.57	5.55	3.37
CaO	8.43	7.68	9.01	10.20	7.06	7.60	9.72	9.59	10.77	7.11
Na_2O	4.21	1.88	3.37	2.66	2.88	3.52	2.49	2.62	2.52	4.07
K_2O	0.15	1.52	1.22	0.47	0.39	0.26	0.77	0.85	0.81	0.30
P_2O_5	0.21	0.54	0.39	0.33	0.39	0.38	0.25	0.24	0.27	0.33
Cr_2O_3	n.d.	n.d.	n.d.	n.d.	n.d.	n.d.	0.014	0.013	0.014	n.d.
LOI	0.67	1.94	0.91	0.98	0.39	0.95	1.20	1.70	1.50	1.73
Total	99.79	99.79	100.34	98.98	100.71	99.95	99.73	99.74	99.93	100.70
Trace element [ppm]										
Sc	38	40	39	44	31	35	41	41	40	32
Ti*	11507	17429	15241	15289	11382	18472	12407	12287	12586	12155
V	270	391	294	387	287	370	340	334	331	330
Cr	230	90	160	180	100	30	96	89	96	60
Co	42	49	47	35	32	36	38	38	38	32
Cu	60	100	50	60	20	80	106	100	101	70
Ni	50	40	60	30	< 20	< 20	16	16	16	< 20
Ga	17	24	24	21	16	22	20	19	19	20
Sn	1	2	3	2	1	3	1	1	1	2

Zn	80	120	140	110	100	150	43	53	45	100
Rb	< 2	54	34	8	4	6	15	19	21	3
Sr	181	543	340	257	214	302	270	248	266	271
Y	25	34	36	36	35	47	31	29	30	42
Zr	117	190	171	151	131	223	143	138	144	155
Nb	8	13	18	11	9	15	8	8	8	9
Cs	< 0.5	11	1	< 0.5	< 0.5	1	0	0	0	1
Ba	44	399	627	176	144	89	195	178	188	132
La	13	20	15	16	12	13	13	12	13	16
Ce	28	48	40	37	30	49	31	28	30	44
Nd	20	30	27	26	18	26	19	18	18	26
Pb	< 5	7	6	7	< 5	19	2	4	3	8
Th	2	2	1	1	1	4	2	2	2	3
U	0	1	0	0	0	1	1	1	1	1
Hf	3	5	5	4	4	6	4	4	4	4
Ta	1	1	2	1	1	1	1	1	1	1
Pr	4	7	6	6	4	5	4	4	4	6
Sm	5	8	7	7	5	8	5	5	5	7
Eu	2	3	3	2	2	3	2	2	2	3
Gd	6	7	8	7	6	9	6	6	6	8
Tb	1	1	1	1	1	2	1	1	1	2
Dy	6	8	8	9	7	10	6	6	6	9
Ho	1	2	2	2	1	2	1	1	1	2
Er	3	4	5	4	4	5	3	3	3	5
Yb	3	3	4	4	4	5	3	3	3	5
Lu	0	1	1	1	1	1	0	0	0	1
Tm	0	1	1	1	1	1	0	0	1	1
ΣREE	94	143	126	124	95	140	96	91	94	133
$(La/Yb)_N$**	3	4	3	3	2	2	3	3	3	3

3.3 Whole-rock Nd isotope analyses

Of the eighteen separate samples for geochemical analyses, thirteen samples were selected for Sm-Nd analyses. These analyses were done in the Geochronology Laboratory of Universidade de Brasília according to the method described by Gioia and Pimentel (2000). About 50 mg of whole-rock powder were mixed with ^{149}Sm-^{150}Nd spike solution and dissolved in Savillex capsules. The extractions of Sm and Nd were carried out on Teflon columns containing LN-Spec resin (HDEHP - Di-(2-ethylhexyl) phosphoric acid supported by polytetrafluorethylene powder). The Sm and Nd fractions were placed into double rhenium filament arrays and the isotopic measurements were done in a Finnigan TRITON multi-collector mass spectrometer in static mode. The uncertainties for Sm/Nd and ^{143}Nd/^{144}Nd are better than ±0.5% (2σ) and ±0.005% (2σ), respectively, based on repeated analyses of the BHVO-2 and BCR-1 rock standards. The ^{143}Nd/^{144}Nd ratios are normalized to ^{146}Nd/^{144}Nd of 0.7219 and the decay constant (λ) used was 6.54×10^{-12}. The final data were processed in the GCDKit 5.0 package used as a complement to the R 3.5.3 software (Janoušek *et al.*, 2006).

4. Results

4.1 Field observations and petrography

The metavolcanic rocks of the Novo Gosto unit comprise fine- to very fine-grained amphibolites forming layers of millimeter to meter width in between layers of fine-grained metasedimentary rock (Fig. 2A, B). The gneisses mostly have a well-marked foliation and compositional banding of amphibolite, calc-silicate and quartz-feldspathic bands, which differ from other mafic rocks of the region. However, there are also massive amphibolites that

resemble sills and that are very similar to the Gentileza unit amphibolites (Fig. 2A). Close to the Mulungu-Alto Bonito shear zone (MABSZ), the Novo Gosto metavolcano-sedimentary rocks display ductile deformation, such as tightly banded mylonitic amphibolites and tight folds transposing foliation (Fig. 2C). Hydrothermal alteration associated with the shear zones resulted in epidotization, carbonate microveins and carbonate replacement of porphyroblasts. Away from the shear zone, the rocks are less deformed (Fig. 2D).

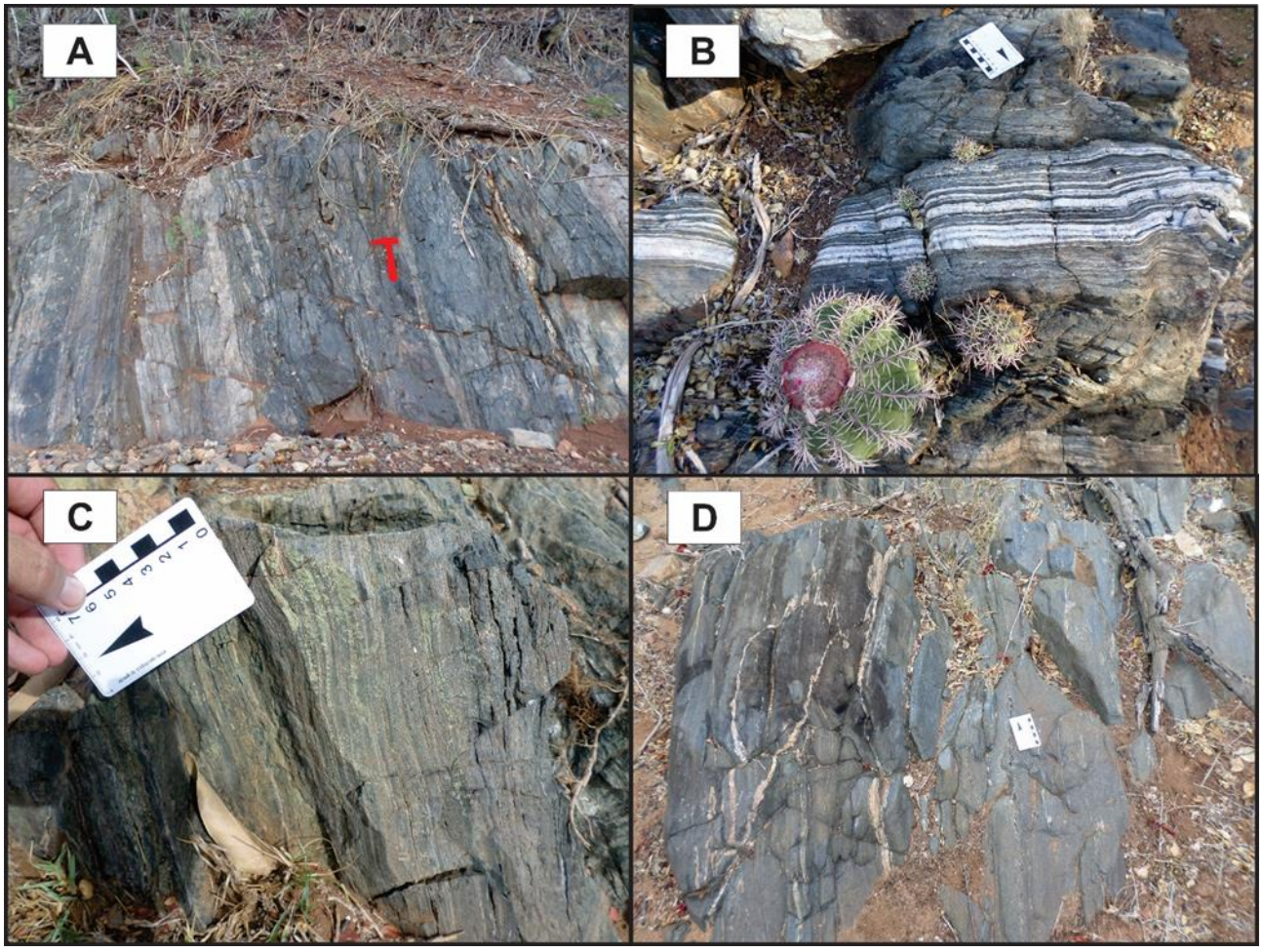

Figure 2: (A, B) Rhythmic intercalation of amphibolites with metasedimentary rock (red geological hammer as scale in A). (C) Mylonitic amphibolite with hydrothermal alteration near the Mulungu-Alto Bonito shear zone. (D) slightly deformed amphibolite less affected by the Mulungu-Alto Bonito shear zone.

The amphibolites contain in their modal composition hornblende (39-67%), plagioclase (21-48%), ilmenite (2-16%), titanite (traces - 13%), epidote (3-8%), quartz (traces - 3%), apatite

(traces), zircon (traces), chlorite (traces - 6%) and carbonate (traces). Chlorite occurs usually in very fine-grained rocks close to the MABSZ (Fig. 3). The hornblende crystals define the foliation, which is sometimes marked by thin elongated plagioclase clusters. Nematoblastic to granoblastic texture is common, mostly in coarser-grained samples, distant from the MABSZ. Some amphibolite samples display vestige of recrystallized microlites immersed in a fine-grained matrix.

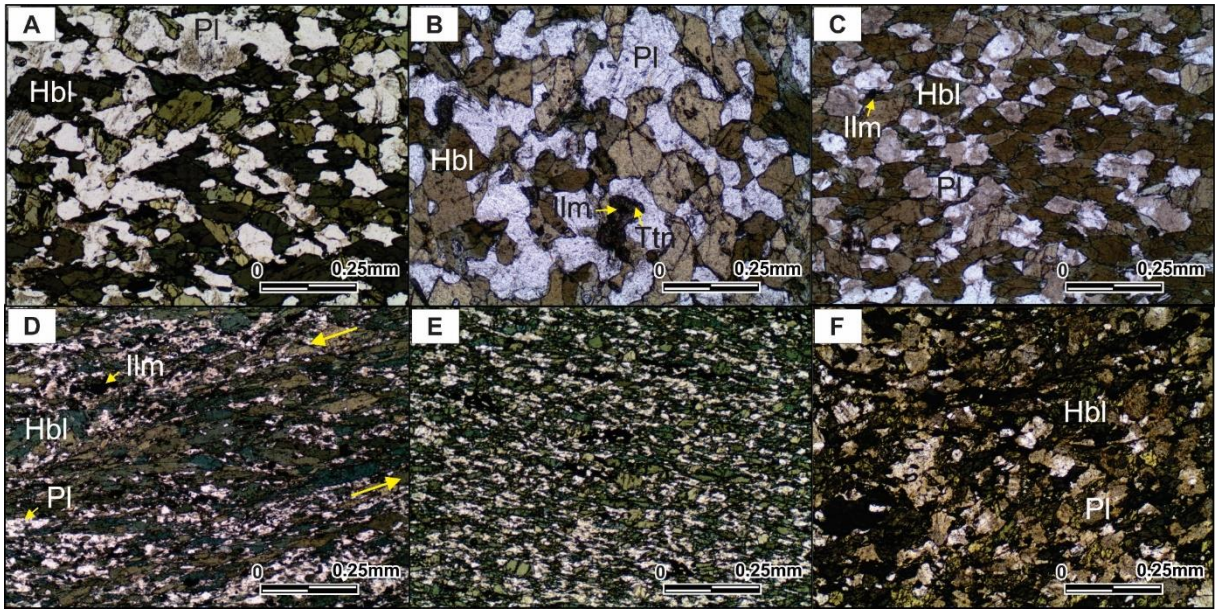

Figure 3: Mineralogical and textural aspects of amphibolites of the Novo Gosto unit. Samples (A) DDLH-27, (B) DMLH-16, and (C) V-11 showing amphibolites with nematoblastic to granoblastic polygonal texture, less foliated and coarser-grained. (D) DMLH-10A is a mylonitic amphibolite with S-C foliation bands. (E) DDLH-11B is a less foliated and very fine-grained amphibolite. (F) DDLH-9C is a foliated amphibolite comparatively with more weathered feldspar crystals.

4.2 Geochemistry

4.2.1 Analysis of element mobility

The selected samples have low LOI values, between 0.2 and 2.43%, and based on LOI, the samples of Liz et al. (2018) were discarded in this work. As in general terms, elements

considered as immobile show little variation in correlation diagrams, whereas mobile elements show low correlation (Cann, 1970; Humphris and Thompson, 1978; Pearce, 2014), and as Zr is an incompatible element considered to be quite immobile and is usually used as a sensitive indicator of immobility (Pearce and Cann, 1973; Pearce, 2014), binary diagrams of variation of incompatible trace elements versus Zr (Fig. 4) were constructed.

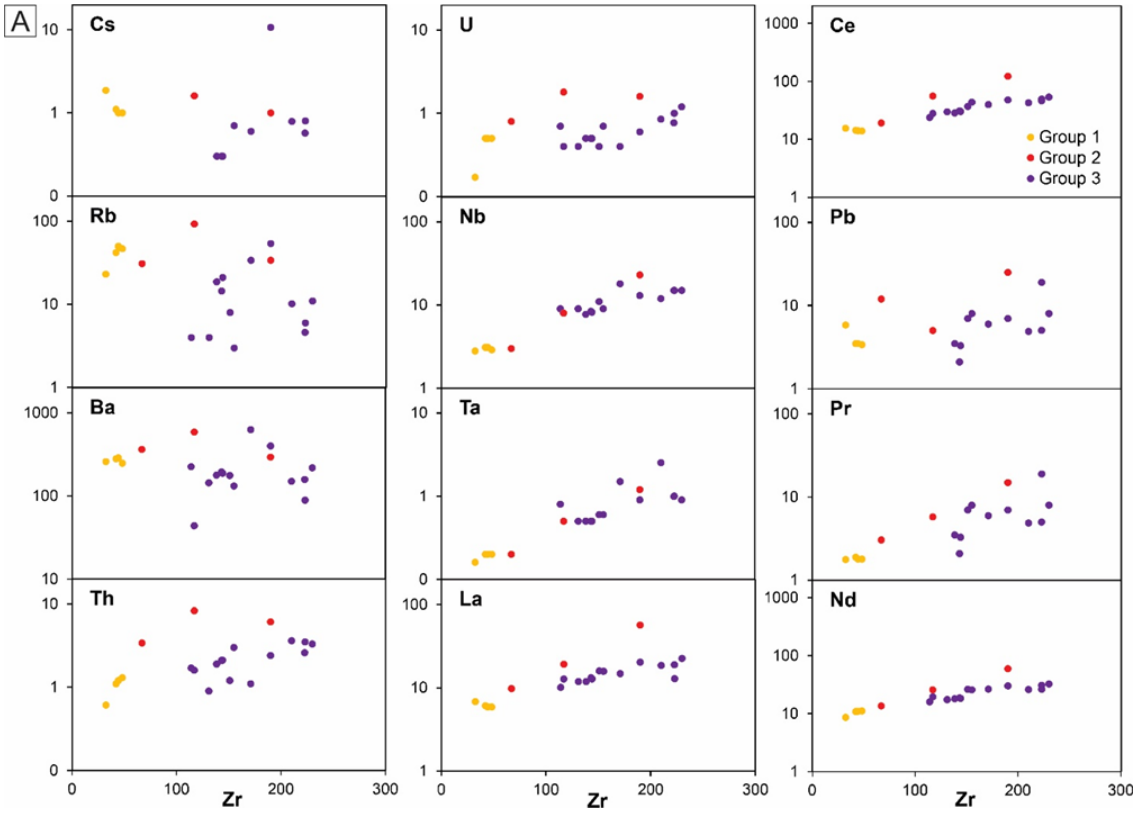

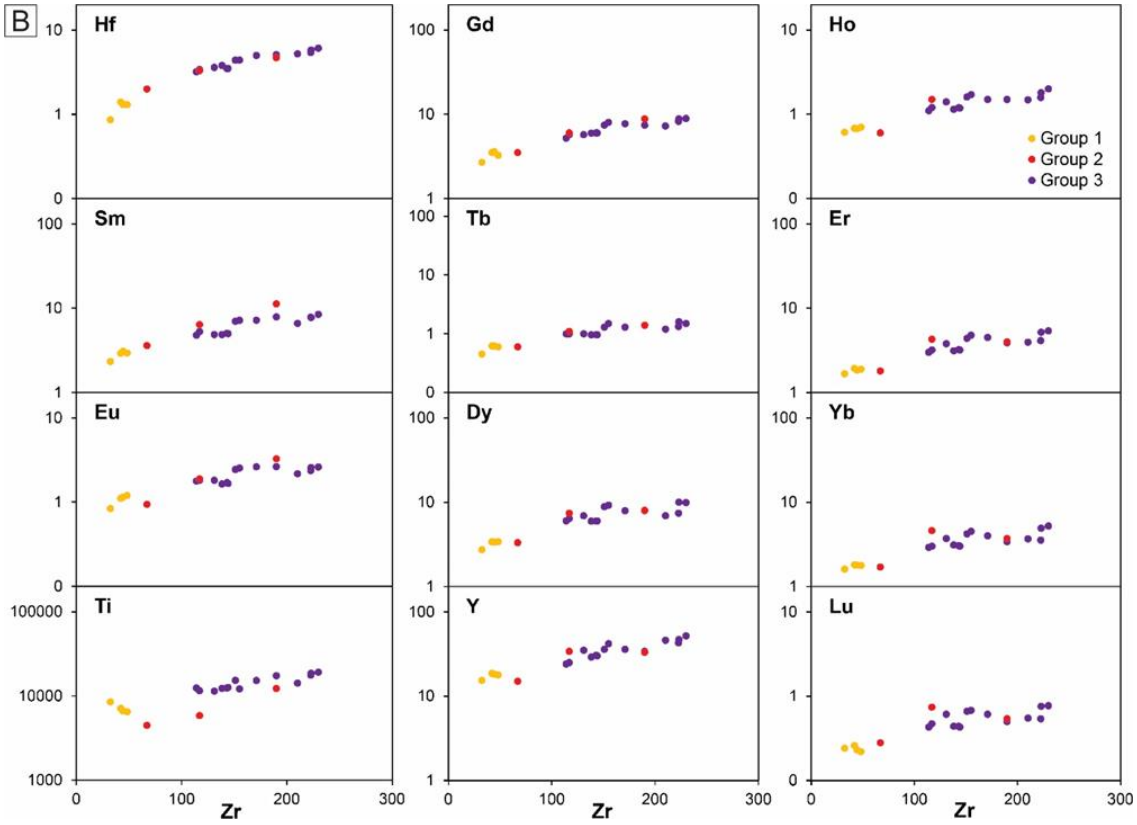

Figure 4: Diagrams with incompatible trace elements (ppm) versus Zr (ppm) for Novo Gosto amphibolites.

LIL elements (Cs, Rb, Ba, Pb), except for Pb that displays a more tapered dispersion, show great dispersion as expected, due to their mobility. Among the HFS elements, Nb, Zr, Hf, and Ti have low dispersion, reflecting their mostly immobile behavior. Ta shows slight dispersion, and Th and U have a more pronounced dispersion like Pb, but much lower than the other LILE. The minimum dispersion observed in the REE is negligible, evidencing that these elements have to be less mobile. Therefore, it is concluded that all diagrams involving the use of LILE should be avoided and that those including Pb, Ta, Th, U, and Pr should be carefully used.

4.2.2 Rock classification and geochemical behavior

The amphibolite samples can be grouped into three distinct chemical groups, without notable distinction of petrography or field relations. The geochemical patterns can be visualized in Figures 5 and 6.

The samples from the three groups are classified as tholeiitic basalts (Fig. 5A, B) with high Fe concentrations (Fig. 5C).

Group 1 has a lower Total REE concentration between 44.95 and 48.25 ppm, is enriched in LREE against HREE (La/Yb_N: 2.39 to 3.05), and lacks a significant Eu anomaly. Most samples of this group are more depleted in REE when compared to the other groups, displaying strong negative Nb-Ta, Zr-Hf anomalies, low Ti and Y negative anomalies and positive Pb anomalies.

Group 2 has variable Total REE concentrations between 44.38 and 136.76 ppm, is enriched in LREE against HREE (La/Yb_N: 2.61 to 4.13), and has a smooth Eu anomaly. This group has similar patterns to Group 1; however, with higher Nb-Ta, and Ti anomalies and with variation in the enrichment of the elements.

Group 3 has higher Total REE concentration between 87.6 and 156.47 ppm, is enriched in LREE against HREE (La/Yb_N: 1.88 to 4.28), and lacks a significant Eu anomaly. This group is more enriched than Group 1 in the entire spectrum of incompatible elements and REE, and displays flatter incompatible element patterns than the previous groups in N-MORB-normalized multi-trace element diagrams. This group has a slightly richer pattern than E-MORB, with positive Pb anomalies, negative Nb-Ta, Zr-Hf and Y anomalies, and smooth Ti anomalies.

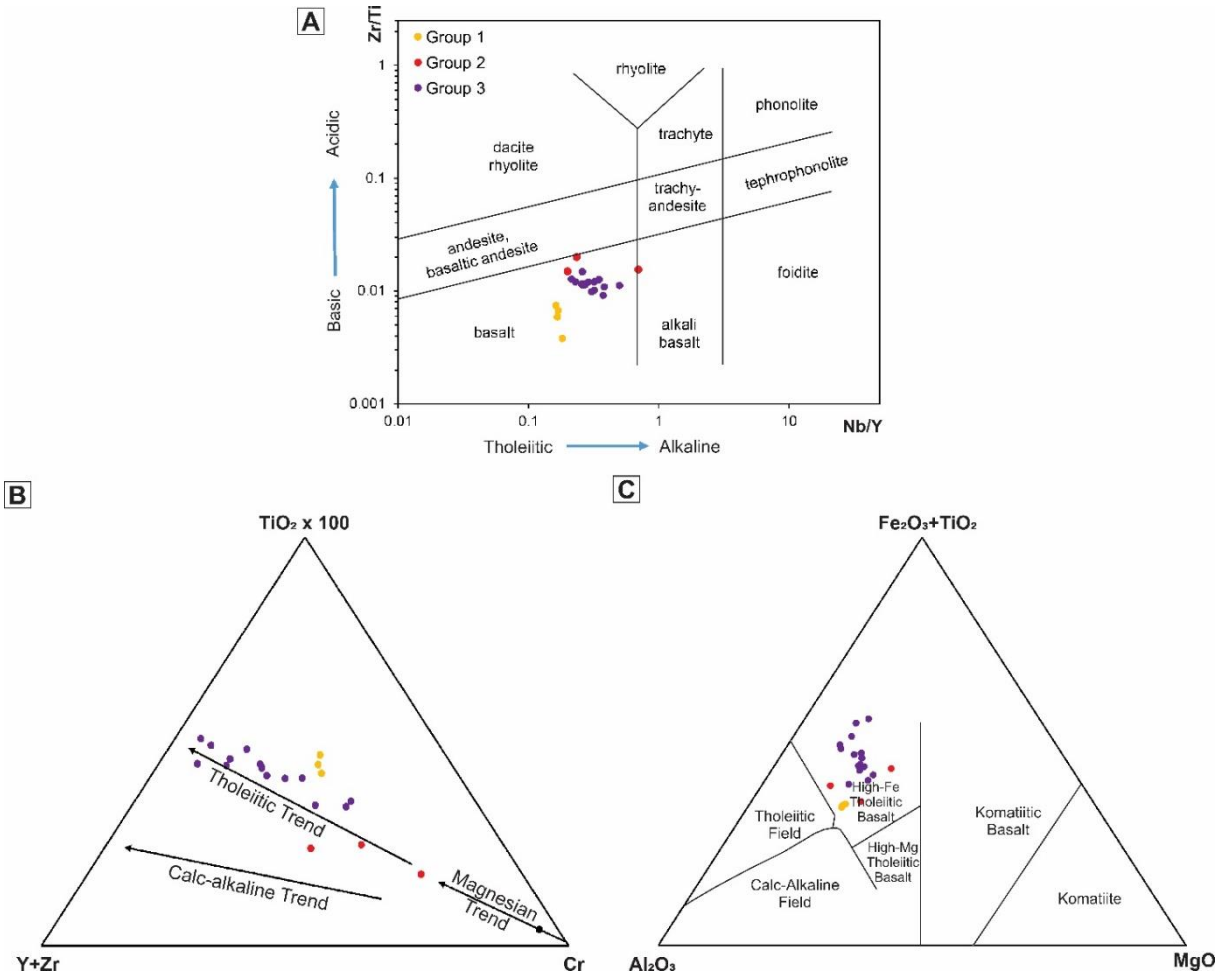

Figure 5: (A) Zr/Ti vs. Nb/Y classification diagram for samples (from Pearce, 1996, after Floyd and Winchester, 1975). (B) (Y+Zr) - (TiO_2 × 100) - (Cr) ternary plot (Davies et al., 1979) showing the tholeiitic affinity of the basic rocks. (C) the same analyses plotted in (Al_2O_3) - (Fe_2O_3+TiO_2) - (MgO) ternary plot (Jensen, 1976).

For a better visualization of the data, minimizing the effects of partial melting, fractional crystallization, and accumulation (e.g., Pearce, 1982, 1983), a multielement diagram with trace elements normalized to N-MORB and later to Yb (Fig. 6B) was made (Pearce, 2008; Keller *et al.*, 2008; Wang *et al.*, 2015).

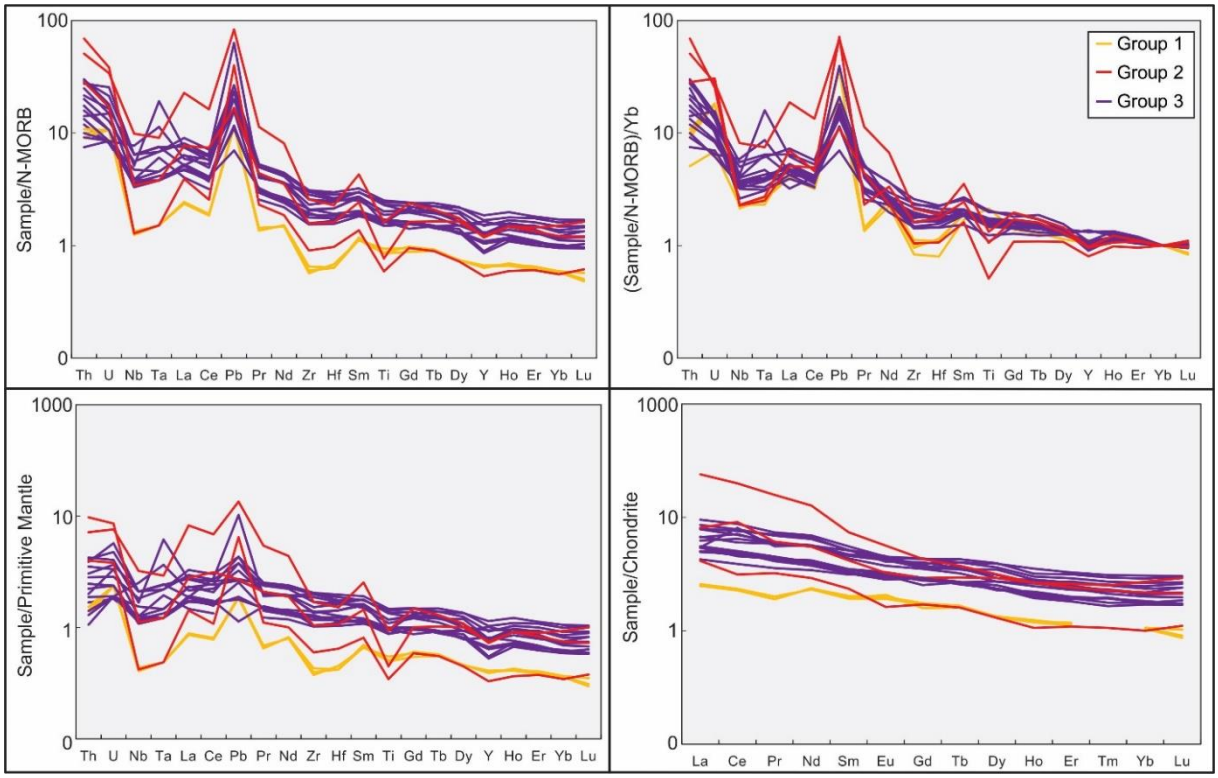

Figure 6: (A) N-MORB-normalized multi-trace element diagrams for the Novo Gosto unit amphibolites. (B) Yb, N-MORB-normalized multi-trace element diagrams. (C) Primitive Mantle-normalized multi-trace element diagrams. (D) Chondrite-normalized REE patterns. Values of N-MORB, Primitive Mantle and Chondrite are from Sun and McDonough (1989).

4.3 U-Pb zircon geochronology

The geochronology data were obtained on sample DMLH-16, which is an amphibolite from Group 3. The sample provided sub-rounded, rarely elongated, subhedral zircon crystals with sizes ranging from 120 to 250 μm. The Th/U ratios range from 0.13 to 0.30, indicating their magmatic origin (Lopez-Sanchez et al., 2016).

A concordant U-Pb age obtained by LA-MC-ICP-MS zircon crystals resulted in 743±3 Ma (2s, MSWD=0.34) for 21 analyses (Table 2, Fig. 7). A similar result for the same amphibolite sample (DMLH-16) was obtained by the LA-SF-ICP-MS method yielding an age of 740±4 Ma (n=27 grains); see supplementary material (SP1). The analyses were placed into cores, grains with common high Pb content were removed, and the last four grains in the table

are discordant (gray in Fig. 7). An older inherited zircon population with Th/U of 2.17 to 2.64 yielded a Concordia age of 938±23 Ma (2s, MSWD=0.27) (Table 2).

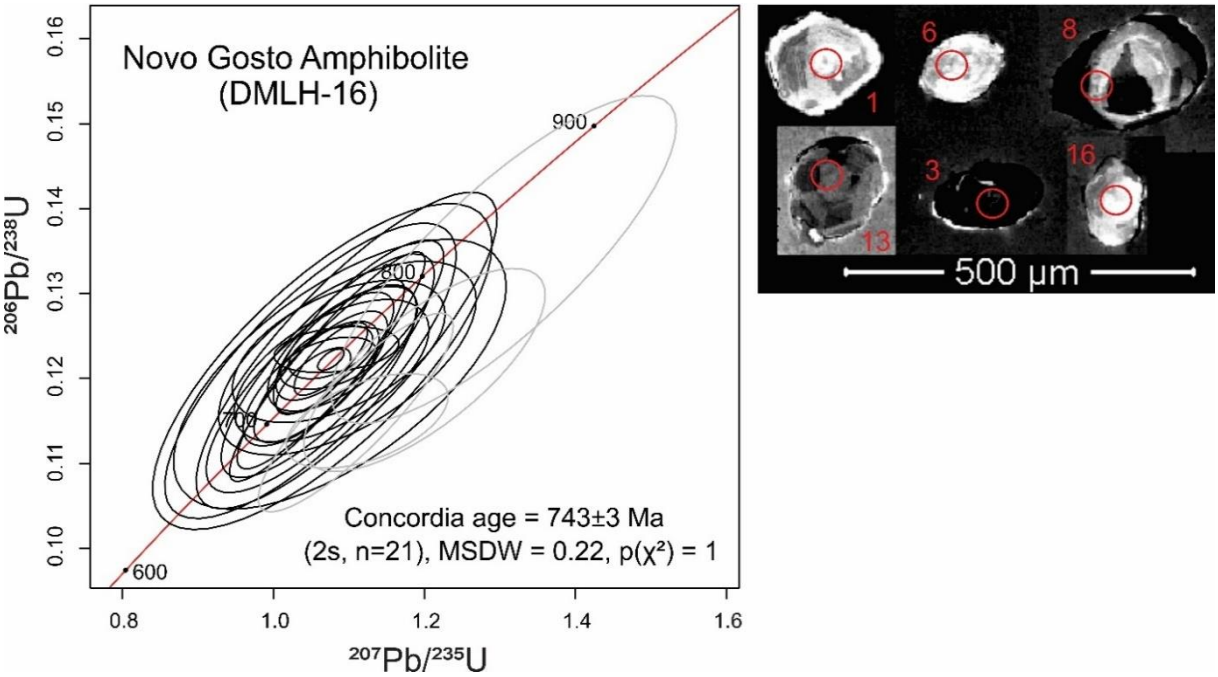

Figure 7: U-Pb concordia diagram for zircon from amphibolite DMLH-16 from the Novo Gosto unit, and representative cathodoluminescence (CL) images for the analyzed zircon grains.

Table 2: U-Pb isotope data for zircon from in situ data amphibolite DMLH-16.

Sample DMLH-16						Isotope ratios[c]							Ages (Ma)						
Spot Number	f_{206}[a]	Pb ppm	Th ppm	U ppm	Th/U[b]	$^{207}Pb/^{235}U$	1 s[g] [%]	$^{206}Pb/^{238}U$	1 s [%]	Rho[d]	$^{207}Pb/^{206}Pb$[e]	1 s [%]	$^{206}Pb/^{238}U$	2 s abs	$^{207}Pb/^{235}U$	2 s abs	$^{207}Pb/^{206}Pb$	2 s abs	% Conc[f]
# 1	0.0024	4	8	24	0.32	1.0769	4.90	0.1209	2.84	0.58	0.0646	4.00	736	41	742	71	761	60	97
# 3	0.0006	18	30	104	0.29	1.0730	2.45	0.1218	1.03	0.42	0.0639	2.22	741	15	740	36	739	32	100
# 4	0.0006	17	25	98	0.26	1.0758	2.12	0.1231	1.04	0.49	0.0634	1.85	749	15	742	31	721	26	104
# 5	0.0013	13	20	80	0.25	1.0499	3.50	0.1194	2.51	0.72	0.0638	2.44	727	36	729	50	735	35	99
# 6	0.0070	4	4	22	0.21	1.0979	6.35	0.1224	3.81	0.60	0.0651	5.07	744	56	752	94	776	77	96
# 7	0.0119	3	5	21	0.22	1.0879	8.28	0.1205	5.39	0.65	0.0655	6.29	734	77	747	121	789	97	93
# 8	0.0004	23	35	135	0.26	1.0761	1.85	0.1223	1.43	0.77	0.0638	1.17	744	21	742	27	736	17	101
# 9	0.0010	11	29	73	0.40	1.0813	2.95	0.1238	2.10	0.71	0.0634	2.07	752	31	744	43	720	29	104
# 12	0.0006	22	31	119	0.26	1.0531	1.92	0.1197	1.34	0.70	0.0638	1.38	729	19	730	28	735	20	99
# 13	0.0020	6	13	37	0.36	1.0915	3.71	0.1235	2.43	0.66	0.0641	2.80	751	36	749	54	745	41	101
# 14	0.0059	7	7	39	0.19	1.0501	5.42	0.1188	4.21	0.78	0.0641	3.42	724	60	729	77	744	50	97
# 16	0.0069	3	6	19	0.31	1.0647	8.63	0.1214	6.46	0.75	0.0636	5.72	738	94	736	125	729	82	101
# 21	0.0020	8	7	40	0.19	1.0834	3.12	0.1234	0.89	0.28	0.0637	2.99	750	13	745	46	732	43	103
# 31	0.0063	3	3	15	0.23	1.0625	4.26	0.1205	3.78	0.89	0.0639	1.97	734	54	735	61	740	29	99
# 36	0.0046	8	6	40	0.16	1.0719	5.38	0.1215	4.43	0.82	0.0640	3.06	739	64	740	78	741	44	100
# 42	0.0028	10	10	48	0.21	1.0712	4.94	0.1214	4.55	0.92	0.0640	1.93	739	66	739	72	741	28	100
# 45	0.0042	8	14	42	0.34	1.0968	7.43	0.1233	6.18	0.83	0.0645	4.13	750	91	752	109	758	61	99
# 46	0.0040	5	6	22	0.25	1.0864	5.30	0.1232	2.78	0.52	0.0639	4.51	749	41	747	78	740	65	101
# 48	0.0014	14	18	66	0.27	1.1126	4.15	0.1261	3.31	0.80	0.0640	2.49	766	50	759	62	741	36	103
# 54	0.0043	6	8	31	0.26	1.0490	7.52	0.1209	5.88	0.78	0.0629	4.69	736	85	728	107	706	65	104
# 56	0.0013	6	5	32	0.15	1.0624	3.41	0.1202	2.63	0.77	0.0641	2.18	732	38	735	49	745	32	98
# 25	0.0057	9	67	26	2.64	1.124	3.90	0.115	1.98	0.51	0.0708	3.36	702	27	765	58	951	63	74

# 34	0.0055	34	288	116	2.49	1.109	4.76	0.116	4.12	0.87	0.0692	2.37	709	57	758	71	904	42	78
# 35	0.0078	19	143	67	2.17	1.200	5.45	0.121	4.04	0.74	0.0720	3.65	735	58	800	85	986	70	75
# 47	0.0072	22	186	67	2.78	1.305	7.16	0.134	5.89	0.82	0.0705	4.08	813	94	848	119	942	75	86

[a] Fraction of the non-radiogenic ^{206}Pb in the analyzed zircon spot, where f_{206}=[$^{206}Pb/^{204}Pb$]c/[$^{206}Pb/^{204}Pb$]s (c=common; s=sample)

[b] Th/U ratios and amount of Pb, Th and U (in pmm) are calculated relative to 91500 reference zircon

[c] Corrected for background and within-run Pb/U fractionation and normalised to reference zircon GJ-1 (ID-TIMS values/measured value); 207Pb/235U calculated using (207Pb/206Pb)/(238U/206Pb * 1/137.88)

[d] Rho is the error correlation defined as the quotient of the propagated errors of the $^{206}Pb/^{238}U$ and the $^{207}/^{235}U$ ratio

[e] Corrected for mass-bias by normalising to GJ-1 reference zircon and common Pb using the model Pb composition of Stacey and Kramers (1975)

[f] Degree of concordance = ($^{206}Pb/^{238}U$ age * 100/$^{207}Pb/^{206}U$ age)

[g] s: sigma standard deviation

4.4 Nd Isotope geochemistry

Ten amphibolite samples were analyzed to obtain Nd ratios and three samples were analyzed by Nascimento (2005) (Table 3, Fig. 8): two samples are from Group 2 and eleven samples are from Group 3.

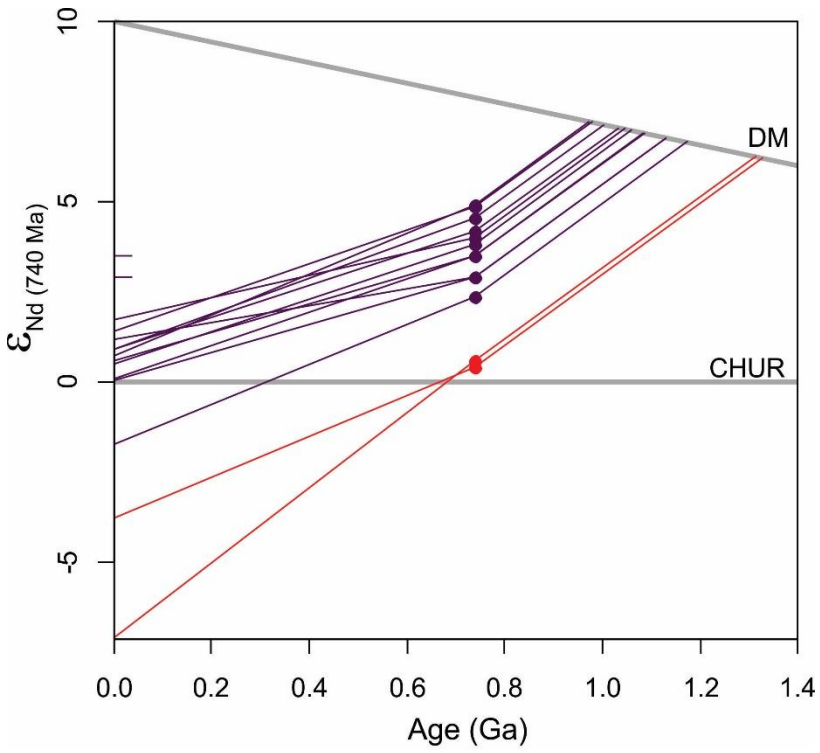

Figure 8: $\varepsilon_{Nd(740)}$ vs. Age diagram showing evolution lines for amphibolites from the Novo Gosto unit. Purple for Group 3 and red for Group 2.

The eleven samples from Group 3 show $^{147}Sm/^{144}Nd$ ratios between 0.1525 and 0.1782 and $^{143}Nd/^{144}Nd$ ratios between 0.512550 and 0.512728. ε_{Nd} (740 Ma) values for Group 3 samples range from +2.37 to +4.93, and the *f*Sm/Nd ratios (fractionation factor) vary between -0.09 and -0.22. These latter values suggest that there is some fractionation of the Sm-Nd ratios, so a 2-stage Nd Model age is recommended to be used (Liew & Hoffmann, 1998). The 2-stage Nd T_{DM} calculated ages are around 1.0 Ga (0.97 to 1.17 Ga). Samples from Group 2 have

$^{147}Sm/^{144}Nd$ ratios between 0.1525 and 0.1155 and the $^{143}Nd/^{144}Nd$ ratios range from 0.512274 to 0.512445. ε_{Nd} (740 Ma) values and fSm/Nd ratios are +0.42 and +0.58 and -0.22 and -0.41, respectively. As there is also evidence for fractionation, the 2-stage Nd T_{DM} values were calculated to 1.31 and 1.33.

Table 3: Sm-Nd isotopic data from Novo Gosto unit. * Nascimento (2005).

Sample	Group	Sm (ppm)	Nd (ppm)	$^{147}Sm/^{144}Nd$	$^{143}Nd/^{144}Nd$ (±2SE)	$\varepsilon_{Nd\ (t=0)}$	$\varepsilon_{Nd(t)}$	*f*Sm/Nd	T_{DM} (Ga)	T_{DM2} (Ga)	t (Ma)
DMLH- 16	3	12.049	42.096	0.1730	0.512728(9)	1.75	4.01	-0.12	1.17	1.04	740
DDLH- 24	3	7.032	26.507	0.1604	0.512711(7)	1.42	4.87	-0.18	1.14	0.98	740
DDLH- 19	3	8.459	28.702	0.1782	0.512698(9)	1.17	2.93	-0.09	1.69	1.13	740
CRN-141d*	3	5.590	21.340	0.1582	0.512684(10)	0.90	4.55	-0.20	1.17	1.00	740
CRN-272A*	3	4.096	15.267	0.1622	0.512684(27)	0.90	4.17	-0.18	1.25	1.03	740
DDLH- 5B	3	8.196	32.484	0.1525	0.512676(10)	0.74	4.93	-0.22	1.09	0.97	740
DDLH- 27	3	5.280	19.218	0.1661	0.512669(17)	0.60	3.51	-0.16	1.39	1.09	740
DDLH- 22	3	7.811	29.158	0.1619	0.512665(5)	0.53	3.82	-0.18	1.30	1.06	740
DDLH- 2	3	5.177	19.496	0.1605	0.512643(4)	0.10	3.53	-0.18	1.32	1.08	740
DDLH- 11B	3	8.158	29.652	0.1663	0.51264(8)	0.04	2.92	-0.15	1.48	1.13	740
CRN-273B*	3	5.124	20.182	0.1535	0.512550(26)	-1.72	2.37	-0.22	1.40	1.17	740
DDLH- 9C	2	6.754	26.779	0.1525	0.512445(9)	-3.76	0.42	-0.22	1.61	1.33	740
DDLH- 17A	2	11.428	59.834	0.1155	0.512274(8)	-7.11	0.58	-0.41	1.19	1.31	740

5. Discussion

5.1 Protoliths, metamorphism and tectonic setting

The textures of the studied rocks are characteristic of metamorphic rocks derived from volcanic and subvolcanic igneous protoliths, as indicated by their fine- to very fine-grained texture and the presence of some amphibolite samples display vestige of recrystallized microlites immersed in a fine-grained matrix. Also, the chemical composition of the rocks plots in the basalt field suggesting a basaltic composition for the protoliths.

The mineral assemblage labradorite/andesine + hornblende + ilmenite is typical of upper amphibolite facies. The assemblage varies to actinolite + albite + titanite + epidote near the shear zones, indicating crystallization under retrograde greenschist facies conditions (Passos, 2016).

In the Th/Yb *versus* Nb/Yb diagram (Fig. 9A), the data plot variably shifted from the MORB-OIB array to higher Th/Yb values. Th and Nb have significantly different properties, which causes them to be decoupled in the metasomatized mantle near subductions (where Nb is immobile and Th is more mobile), and causes an increase in the Th/Nb ratio in magmas from this setting. However, as the continental crust is at least partly derived from subduction, it also has high Th/Nb, so, the magma that assimilated continental crust also has relatively high Th/Nb (Rudnick and Gao, 2003; Wang *et al*., 2013; Pearce, 2014; Dong *et al*., 2018). On the other hand, magma derived from a fluid-modified mantle influenced by subduction is displaced from the MORB-OIB matrix to higher Th/Yb proportions, while continental crust assimilation leads to diagonal alignment, in which Th and Nb are modified together.

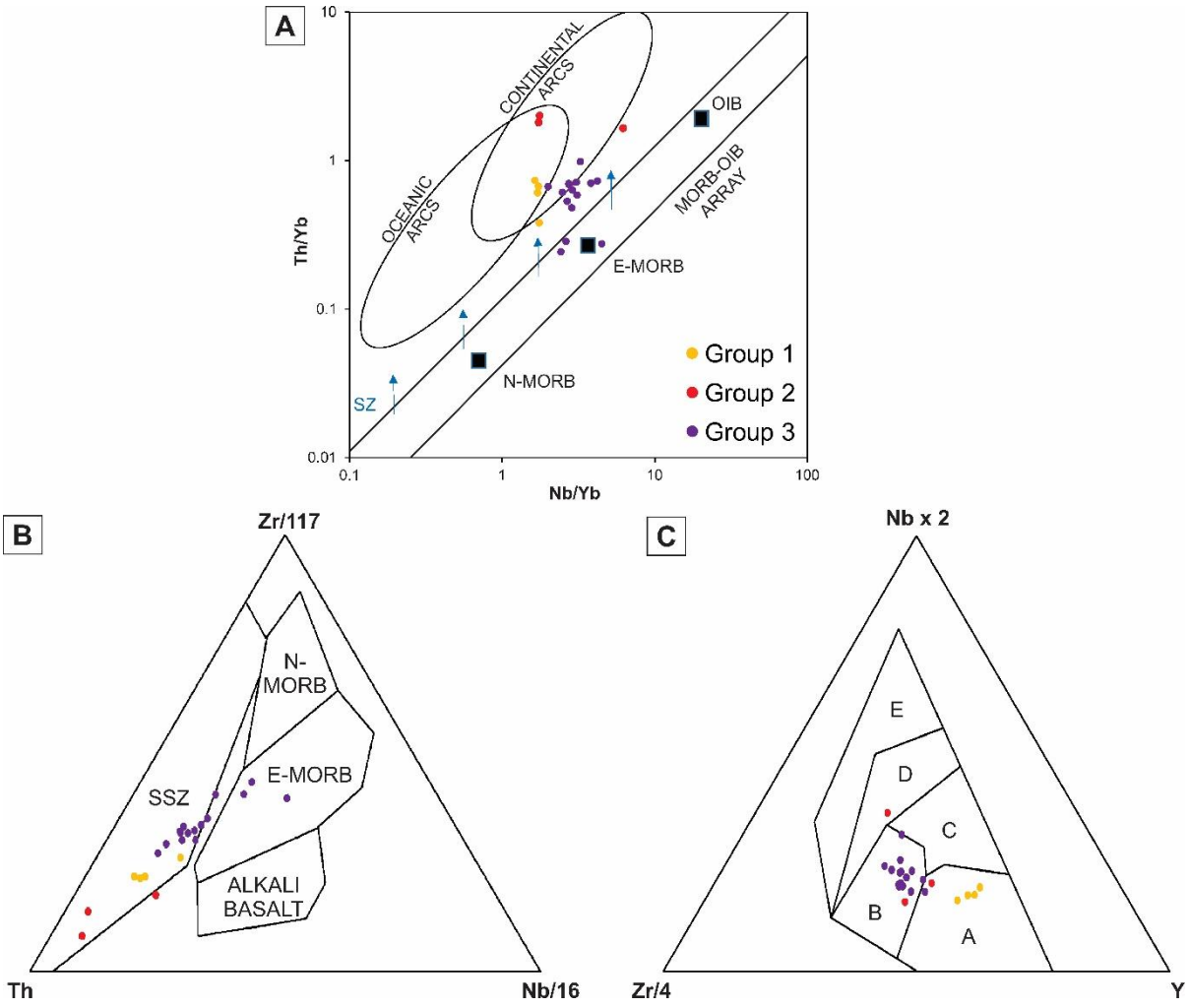

Figure 9: Geological environment discrimination diagrams for amphibolite samples from the Novo Gosto unit: (A) Th/Yb versus Nb/Yb diagram, adapted from Pearce (2008) (SZ - subduction component); (B) Zr/4 - Y - Nbx2 diagram of Meschede (1986). The fields are defined as A - N-MORB and volcanic-arc basalts, B - within-plate tholeiites and volcanic-arc basalts, C - E-MORB, D - within-plate alkali basalts and within-plate tholeiites, E - within-plate alkali basalts; (C) Th - Nb/16 - Zr/117 diagram of Wood (1980), SSZ - Suprasubduction Zone.

All three groups show an increase of Th relative to Nb, indicating a subduction-related metasomatized mantle (Fig. 9A). Samples from groups 1 and 3 show a vertical array, whereas Group 2 samples show dispersion of one sample, in a more discrete vertical array. The samples from the three groups seem to originate from an enriched mantle, as emphasized by three samples from Group 3 that plot in the E-MORB field (DDLH-22, DDLH-24 and DDLH-27). In addition, all three groups display prominent negative HFSE anomalies, suggesting that their mantle source was affected by metasomatism related to subduction zones.

The arc influence can be visualized in other diagrams like figures 9B, C (Meschede, 1986; Wood, 1980), in which the samples plot within the E-MORB and volcanic arc/subduction related basalts fields. Tests performed by Vermeesch (2006) on these two classification diagrams demonstrate that this trend is related to IAB-type.

The characteristics of incompatible trace elements normalized to N-MORB are similar to arc-back-arc volcanic rocks (Fig. 10), showing LILE enrichment (e.g., Th and U), moderate LREE enrichment (e.g., La and Ce) and relative HFSE depletion (e.g., Nb, Ta, Zr, Hf, Y, and Ti-smooth only in Groups 1 and 3), as well as a significant Pb peak. In the chondrite-normalized REE elements diagram (Fig. 6D), the studied rocks show LREE enrichment, with moderate LREE/HREE fractionation and similar La/Yb_N intervals as well as similar fractionation of HREE for all groups.

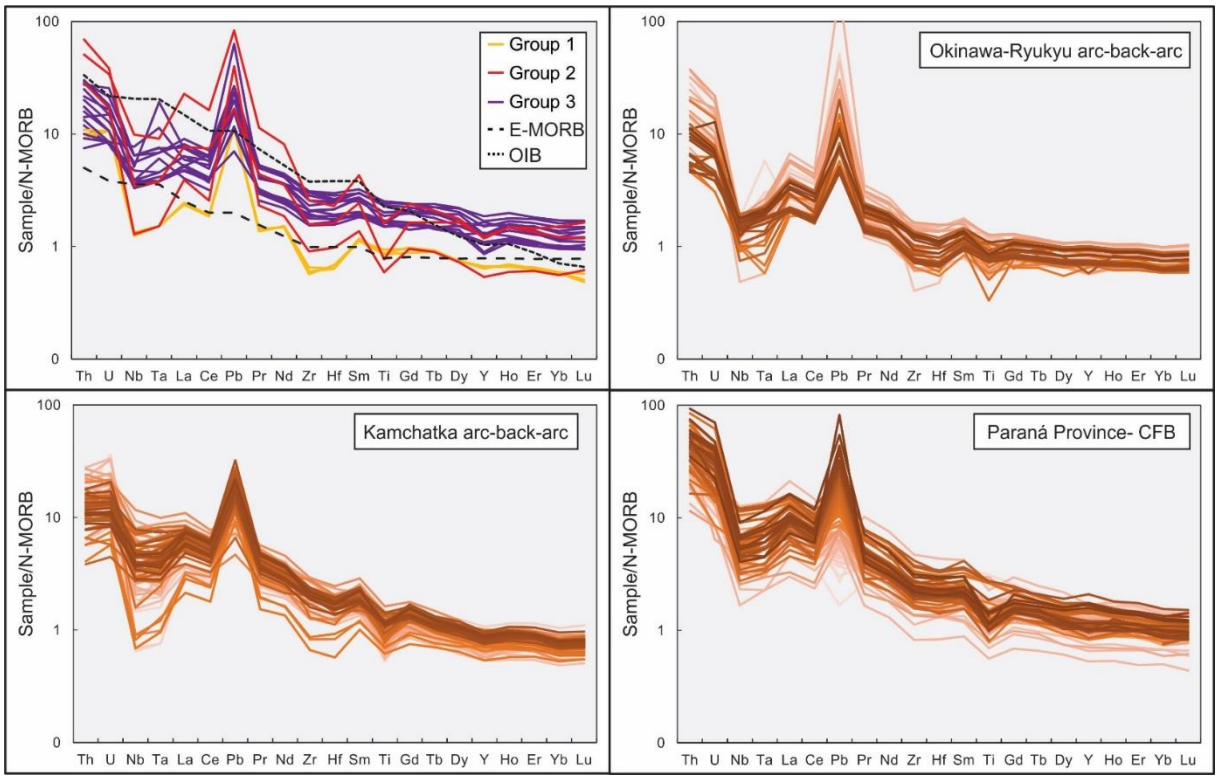

Figure 10: Comparisons between geochemical patterns of the Novo Gosto unit and E-MORB (Sun and McDonough, 1989), OIB (Sun and McDonough, 1989), Okinawa-Ryukyu arc-back-arc (GEOROC database), Kamchatka arc-back-arc (GEOROC database) and Paraná-CFB Province (GEOROC database).

Group 3 samples show lower LILE/HFSE ratio than groups 1 and 2 and slightly higher $^{143}Nd/^{144}Nd$ ratio values (0.51255-051272), which indicate that the group 3 magma source involved less influence of components derived from the subduction zone and are likely juvenile magmas, whereas the rocks from groups 1 and 2 display clear evidence of subduction related components and crustal contamination.

Flatter patterns, although with slightly lower fractionation, similar to Group 3 amphibolites have been reported for back-arc basalts from northern Hokkaido (Fig. 10), Japan, and interpreted as the result of mantle melting affected by the combination of fluid addition by subduction and asthenosphere rise (Hoang *et al.*, 2015). Back-arc basalts have isotopic characteristics or trace elements similar or indistinguishable from those of N-MORB (e.g., Fryer *et al.*, 1982; Hickey-Vargas *et al.*, 1995; Hawkins, 1995). Since the analyzed amphibolites start from an E-MORB-like trend toward a subduction-related trend, it is necessary to discuss two possible sources of magmas: one with an E-MORB-type upper mantle domain and another with a more active subduction component.

In the region between Taiwan and Japan, along the Ryukyu-Okinawa arc-back-arc (Fig. 10), arc-like basalts and E-MORB-like basalts ocurr, respectively. This environment was developed in response to the subduction of the Philippine Sea Plate underneath the east Asian continental margin, generating an arc and back-arc on a submerged thin continental lithosphere, originating magmas with similar characteristics to island arcs (e.g., Gribble *et al.*, 1998; Shinjo *et al.*, 1999; Shinjo and Kato, 2000). Another region with a similar geological context is the Kamchatka arc-back-arc (e.g., Volynets et al., 2018) (Fig. 10). The Kamchatka arc-back-arc has a geochemical pattern of enrichment more similar to the Novo Gosto unit, besides presenting also an Y anomaly.

In continental flood basalt (CFB) environments, basalts with similar characteristics may also occur. Using the case of the Paraná Province as an example (Fig. 10), it is clear that at least

in these rocks, there is a predominance of samples with greater crustal contamination, yielding values of ε_{Nd} (initial) close to the CHUR line or negative ones (e.g., Rocha-Júnior et al., 2013). Also, the patterns of incompatible elements displayed in the multielement diagrams normalized for N-MORB display strong increase in Th and other incompatible elements.

The Sm-Nd isotope signature of group 2 and 3 amphibolites brings some insight into the basaltic magma evolution. The amphibolites of Group 3 display Nd model age close to 1.0 Ga (0.97-1.17 Ga) and positive ε_{Nd} (740Ma) (+2.93 to +4.87) that are compatible with arc-related juvenile rocks. The amphibolites of Group 2 have ε_{Nd} initial values close to the CHUR line (0.42 to 0.58) and Nd T_{DM} values around 1.3 Ga (1.31-1.33 Ga) that can be interpreted as juvenile basalt magmas with contamination of a Mesoproterozoic to early Neoproterozoic source in different proportions, compatible with ages found in the PE-AL superterrane and Poço Redondo domain.

In summary, the amphibolites of the Novo Gosto unit record basaltic magmatism derived from metasomatized mantle that was affected by subduction-related fluids at varying degrees of contamination in a continental arc-back-arc tectonic environment.

5.2 Implications for geological evolution

The obtained age of 743±3 Ma is in agreement with the field relations since the Novo Gosto amphibolites were interpreted in the field as the oldest unit, which is intruded by the other rock units from the Canindé domain.

According to the new data and the above interpretations we suggest that the Canindé domain rocks are related to a Neoproterozoic arc-back-arc system on the Borborema continental margin. The similarity with the geochemical signatures of the Ryukyu-Okinawa and Kamchatka arc-back-arc system leads us to suggest a thinned continental margin at the southern

portion of the Borborema Province, due to previous continental rifting (before 900 Ma) pulling apart the Poço Redondo block (Poço Redondo/Marancó domain) and the Pernambuco-Alagoas Superterrane, both related to the Cariris Velhos Orogeny (~1 Ga). Previous authors have suggested a continental arc or island arc setting for the Canindé domain (Jardim de Sá *et al.*, 1986; Santos *et al.*, 1988; Bezerra *et al.*, 1991; Bezerra, 1992; Silva Filho, 1998; Verma and Oliveira, 2015; Passos, 2016).

The precursor Canindé ocean is here interpreted as a small sea with passive margins of limited lateral extent, possibly opened after the Cariris Velhos Orogeny, or just a branch of the Sergipano ocean that had as its margins the PE-AL superterrane and the São Francisco-Congo Craton. The closure of the Sergipano ocean started with a continental arc probably at around 740 Ma, with accretion of the Poço Redondo Block and continuation of the subduction until continental collision and basin inversion (e.g., Oliveira et al, 2010).

Juvenile rocks crystallized around 740 Ma during an early Brasiliano orogenesis event are rarely evidenced in the Borborema Province (Van Schmus *et al.*, 2008; Caxito *et al.*, 2020). Mafic rocks with a similar range of ages are found in the Oubanguide Orogen interpreted as the extension of the Sergipano Orogen in Africa (Trompette, 1997, 2000; Van Schmus *et al.*, 2008). In the Mayo Kebbi unit, gabbros and metadiorites are exposed, interpreteded as part of a juvenile arc, dated at about 740 Ma (Penaye *et al.*, 2006; Van Schmus *et al.*, 2008). Several metavolcanic rocks in the Poli region, NW Cameroon, yielded ages of 920-730 Ma with Sm-Nd T_{DM} of 0.8 to 1.1 Ga, also indicating a substantial juvenile component (Toteu *et al.*, 2006; Van Schmus *et al.*, 2008). Furthermore, occurrences of mafic rocks along the orogenic belts of the São Francisco-Congo Craton northern margin are related to a Brasiliano paleoceanic crust (Caxito *et al.*, 2014), supporting the existence of an ocean basin between the Pernambuco-Alagoas superterrane and the São Francisco-Congo Craton called Transnordestino-Central African ocean by Caxito et al. (2020).

Recent Sm-Nd results of amphibolites from the Araticum unit (Lima *et al.*, 2018), Sergipano Belt, State of Alagoas, Brazil, are similar to those for the amphibolites of the Novo Gosto unit, and their geochemical pattern is similar to that of the Group 1 that we could relate to island arc basalts. Also, the occurrence of the Araticum unit, connected with the northeast part of the Canindé domain rocks, suggests that the two possibly shared tectonic settings during the Brasiliano Orogeny. Further studies are needed in the Araticum unit, mainly dating the metavolcanic rocks.

5.2.1 Tectonic reconstruction

The evolutionary history of the region started with extensional tectonics that resulted in the opening of the Sergipano ocean between the São Francisco-Congo Craton and the PE-AL superterrane, recorded by the Macururé-Vaza Barris and Canindé basins (Fig. 11A). In the middle of this ocean, a unit related to the Poço Redondo domain occurred as a crustal fragment, possibly a slice from the southern part of the PE-AL superterrane. However, there are no precise data ascertaining that the Poço Redondo domain formed together with the northern PE-AL superterrane, and could be an exotic terrane. On the southern margin of the PE-AL superterrane, in the paleo Canindé basin, continental shelf area was possibly preserved similar to what has been hypothesized for the region to the southeast of the Eurasia Plate (Fig. 11A). Such a terrane may be evidenced by the 963±20 Ma old marble layers (Pb-Pb, Nascimento, 2005). Around 740 Ma, an inversion of the crustal dynamics took place, with converging forces generating subduction and the consequent formation of a continental arc (Fig. 11B). We interpret the configuration recorded by the volcanic rocks of the Novo Gosto unit as similar to the Ryukyu-Okinawa and Kamchatka arc-back-arc systems. The magmatism related to this arc was active at about 680 Ma, with intrusion of the gabbroic bodies from the Canindé layered intrusion and

the Curralinho/Boa Esperança-Gentileza bimodal volcanism (Fig. 11B). The subduction continued until the accretion of the Poço Redondo/Marancó domains and deposition of the deep and shallow oceanic sediments of the Macururé and Vaza Barris domains, with the complete closure of the oceanic basin, regional metamorphism and concomitant intrusions of syn- to late-tectonic granitic intrusive suites (Fig. 11C, 11D). There are still no granite ages for the interval between 680 and 640 Ma. The main granitic intrusions took place over ~20 Ma between 631 and 611 Ma, as evidenced by the Sítios Novos Intrusive Suite with 631±4 Ma (Oliveira et al., 2015), the Coronel João Sá Intrusive Suite with 623±7 Ma (Long et al., 2005), the Lajedinho Suite with 618 Ma (Oliveira et al., 2015) and the Serra do Catu Intrusive Suite with ages of 624±16 Ma - 611±4 Ma (Lima, 2016; Souza et al., 2019). The regional metamorphic age related to the final collision and amalgamation of the Sergipano Belt is still undefined.

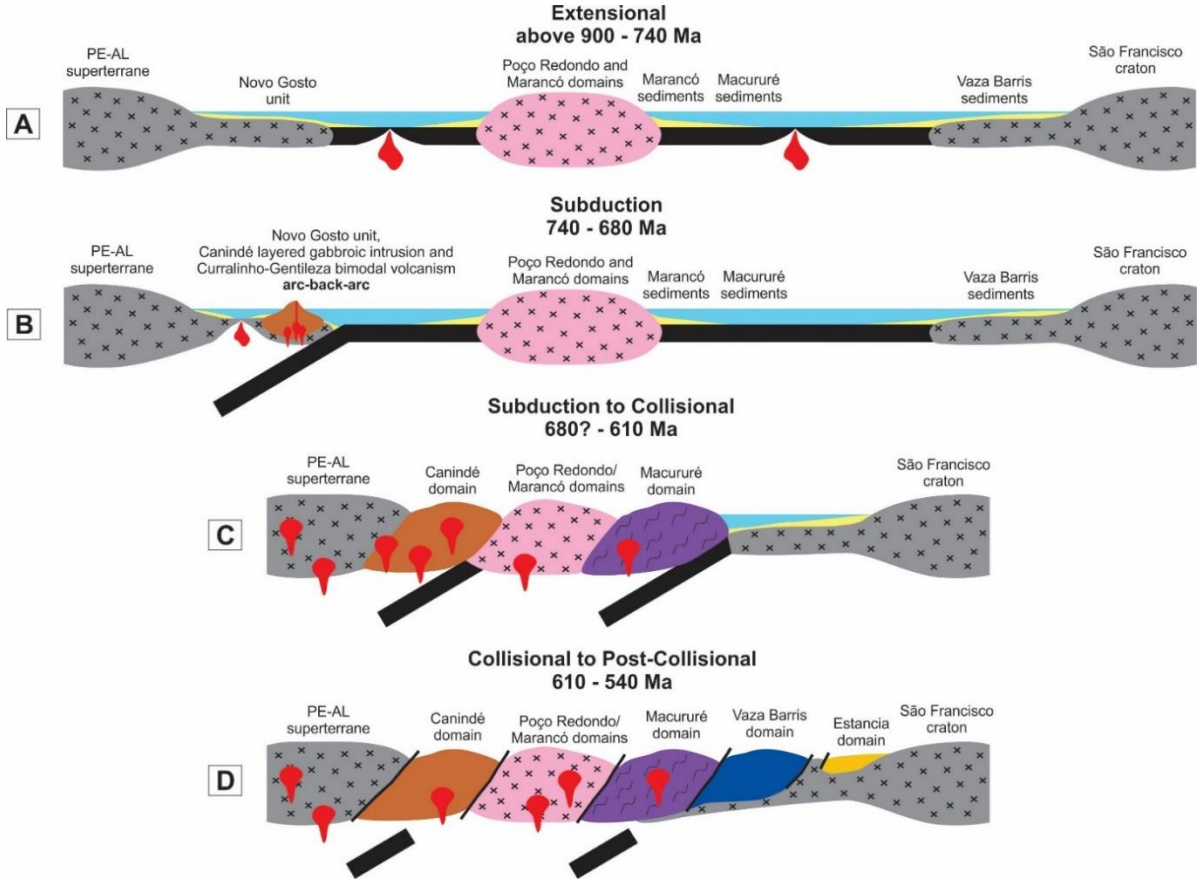

Figure 11: Proposed tectonic evolution model for the Canindé domain, Sergipano Belt. Modified after Oliveira et al. (2010).

6. Conclusions

To bring new constraints to the geological evolution of the Sergipano Belt we investigated the amphibolites of the Novo Gosto unit:

1. Amphibolites are fine- to very fine-grained and generally display well-marked foliation, with the occurrence of foliated amphibolites and banded amphibolites, the latter generated by intercalation with calk-silicate and quartz-feldspathic rocks. The local occurrence of amphibolites with a vestige of recrystallized microlites supports a volcanic to subvolcanic origin for their protoliths. Geochemistry and petrography corroborate the basaltic composition of these rocks and their recrystallization under metamorphic conditions of upper amphibolite facies, with retrogression to greenschist facies conditions near shear zones.

2. The U-Pb zircon age obtained on an amphibolite sample is 743±3 Ma, corroborating field, and literature data that already suggested an older age than the other units of the domain.

3. The Nd isotope data yielded positive values of ε_{Nd} (740 Ma), ranging from + 4.93 to 0.42 and T_{DM} from 0.97 to 1.33 Ga, indicating sources with the dominance of mantle material with no or little crustal contamination of a Mesoproterozoic to Early Neoproterozoic source at different proportions.

4. The analyzed samples are classified as high-Fe tholeiitic basalt type rocks and display a geochemical trend towards the field of acid and alkaline rocks. The geochemical data indicate three different rock groups: Group 1 is generally more depleted in incompatible elements and has a pattern similar to IAB. Group 2 has a pattern similar to group 1, but with more anomalies and variations in the degree of enrichment of incompatible elements. Group 3 has a comparatively enriched pattern of incompatible elements compared to Group 1, being flatter with less HFSE depletion and resembling E-MORB, but more enriched.

5. The amphibolites of the Novo Gosto unit are interpreted as having formed in a continental arc-back-arc tectonic setting, similar to the Ryukyu-Okinawa and Kamchatka arc-back-arc systems. Our results, for the first time, record a convergence event during the Early Brasiliano Orogeny in the Southern Borborema Province. Consequently, the Borborema Province evolved by plate tectonic models and not only intracontinental.

7. Acknowledgments

This study was financed in part by the Coordenação de Aperfeiçoamento de Pessoal de Nível Superior (CAPES), Brasil, Finance Code 001. Support of the CAPES fellowship (grant nº 88882.347179/2019-01) and INCT Estudos Tectônicos research grant were essential for this research and the continuity of future work. This article is dedicated to the memory of Márcio Martins Pimentel, who encouraged the continuity of this research and provided financial support for some analyses. Prof. Uwe Reimold and an anonymous reviewer for their most appreciated and helpful suggestions to improve the manuscript, as well as to Dr. Natalia Hauser, Editor of the special issue. Thanks too are due to Dr. Felipe Torres Figueiredo from the Universidade Federal de Sergipe, Dr. Cristina Maria Burgos de Carvalho, and Dr. Rita Cunha Leal Menezes de Oliveira from the Companhia de Pesquisa de Recursos Minerais - Serviço Geológico do Brasil. RAF and FC acknowledge CNPq research fellowships.

8. References

Bezerra, F. H. R, 1992. Geologia e evolução petrológica do Complexo Gabroico Canindé do São Francisco e rochas adjacentes (Sergipe e Alagoas). Dissertação de Mestrado, Instituto de Geociências, Universidade de Brasília, Brasília, 208p.

Bezerra, F.H.R., Nilson, A.A., Blais, S. *et al*., 1991. Petroquímica de elementos maiores e traços do complexo gabróico Canindé e sequência metavulcano-sedimentar encaixante (SE-AL). Anais III Congresso Brasileiro de Geoquímica, São Paulo, 1, 181-184.

Brito Neves, B.B., Silva Filho, A.F, 2019. Superterreno Pernambuco-Alagoas na Província Borborema: ensaio de regionalização tectônica. Geologia USP, Série Científica, 19(2), 3-28. https://doi.org/10.11606/issn.2316-9095.v19-148257

Brito Neves, B.B., Fuck, R.A., Pimentel, M.M, 2014. The Brasiliano collage in South America: a review. Brazilian Journal of Geology, 44(3), 493-518. https://doi.org/10.5327/Z2317-4889201400030010

Brito Neves, B.B., Sial, A.N., Albuquerque, J.P.T, 1977. Vergência centrífuga residual no Sistema de Dobramentos Sergipano. Revista Brasileira de Geociências, 7(2), 102-114.

Brito Neves, B.B., Cordani, U.G., 1973. Problemas geocronológicos do 'Geossinclinal Sergipano' e de seu embasamento. Anais XXVII Congresso Brasileiro de Geologia, 2, 67-76.

Bühn, B., Pimentel, M. M., Matteini, M., Dantas, E. L., 2009. High spatial resolution analysis of Pb and U isotopes for geochronology by laser ablation multicollector inductively coupled plasma mass spectrometry (LA-MC-ICP-MS). Anais da Academia Brasileira de Ciências, 81(1), 1-16. http://dx.doi.org/10.1590/S0001-37652009000100011

Cann, J.R., 1970. Rb, Sr, Y, Zr and Nb in some ocean floor basaltic rocks. Earth and Planetary Science Letters, 10, 7-11. https://doi.org/10.1016/0012-821X(70)90058-0

Carvalho, M.J., 2005. Evolução tectônica do domínio Marancó - Poço Redondo: Registro das Orogêneses Cariris Velhos e Brasiliana na Faixa Sergipana, NE do Brasil. Tese de Doutorado, Instituto de Geociências, Universidade Estadual de Campinas, Campinas, 202p.

Caxito, F.A., Santos, L.C.M.L., Ganade, C.E., Bendaoud, A., Fettous, E.-H., Bouyo, M.H. 2020. Toward an integrated model of geological evolution for NE Brazil–NW Africa: The Borborema Province and its connections to the Trans-Saharan (Benino-Nigerian and Tuareg shields) and Central African orogens. Brazilian Journal of Geology, 50(2), 1-38. https://doi:10.1590/2317-4889202020190122

Caxito, F.A., Uhlein, A., Stevenson, R., Uhlein, G.J., 2014. Neoproterozoic oceanic crust remnants in northeast Brazil. Geology, 42(5), 387–390. https://doi.org/10.1130/G35479.1

Chemale Jr., F., Kawashita, K., Dussin, I.A., Avila, J.N., Justino, D., Bertotti, A.L., 2012. U-Pb zircon in situ dating with LA-MC-ICP-MS using a mixed detector configuration. Anais da Academia Brasileira de Ciências, 84, 275-295. http://dx.doi.org/10.1590/S0001-37652012005000032

Condie, K.C, 2016. Earth as an evolving planetary system, third ed. Elsevier, London.

D'el-Rey Silva, L.J.H, 1995. Tectonic evolution of the Sergipano Belt, NE Brazil. Geologia, 25(4), 315-332

Davies, J.F., Grant, R.W.E., Whitehead, R.E.S., 1979. Immobile trace elements and Archean volcanic stratigraphy in the Timmins mining area, Ontario. Canadian Journal of Earth Sciences, 16, 305-311. https://doi.org/10.1139/e79-029

Davison, I., Santos, R.S, 1989. Tectonic evolution of the Sergipano belt, NE do Brasil, during the brasiliano orogeny. Precambrian Research, 45, 319-342. https://doi.org/10.1016/0301-9268(89)90068-5

Dobson, P.F., Blank, J.G., Maruyama, S., Liou, J.G., 2006. Petrology and geochemistry of boninite-series volcanic rocks, Chichi-Jima, Bonin Islands, Japan. International Geology Review, 48 (8), 669-701. https://doi.org/10.2747/0020-6814.48.8.669

Dong, Y., Sun, S., Liu, X., He, D., Zhou, X., Zhang, F., Yang, Z., Zhou, D., 2018. Geochronology and geochemistry of the Yazidaban ophiolitic mélange in the Qimantagh:

Constrain on the Early Paleozoic back-arc basin of the East Kunlun Orogen, northern Tibetan Plateau. Journal of the Geological Society, 176, 306-322. https://doi.org/10.1144/jgs2018-145

Fretzdorff, S., Livermore, R.A., Devey, C.W., Leat, P.T., Stoffers, P., 2002. Petrogenesis of the back-arc East Scotia Ridge, South Atlantic Ocean. Journal of Petrology, 43, 1435-1467. https://doi.org/10.1093/petrology/43.8.1435

Fryer, P., Sinton, J., Philpotts, J.A., 1982. Basaltic Glasses from the Mariana Trough. Initial Reports of the Deep Sea Drilling Project, 60, 601-609. https://doi.org/10.2973/dsdp.proc.60.132.1982

Gast, P.W., 1968. Trace element fractionation and the origin of tholeiitic and alkaline magma types. Geochimica et Cosmochimica Acta, 32(10), 1057-1086. https://doi.org/10.1016/0016-7037(68)90108-7

GEOROC. Available online: http://georoc.mpch-mainz.gwdg.de/georoc/ (accessed on sempteber 2019)

Gill, R., 2010. Igneous rocks and processes: a practical guide, first ed. Wiley-Blackwell, Chichester.

Gioia, S.M.C.L., Pimentel, M.M., 2000. The Sm-Nd isotopic method in the Geochronology Laboratory of the University of Brasília. Anais da Academia Brasileira de Ciências, 72(2), 219-245. http://dx.doi.org/10.1590/S0001-37652000000200009

Gribble, R.F., Stern, R.J., Newman, S., Bloomer, S.H., O'Hearn, T., 1998. Chemical and isotopic composition of lavas from the Northern Mariana Trough: implications for magma genesis in back-arc–arc basins. Journal of Petrology, 39, 125-154. https://doi.org/10.1093/petroj/39.1.125

Hawkins, J.W., 1995. Evolution of the Lau Basin: Insights from ODP Leg 135, in: Taylor, B., Natland, J. (Eds.), Active Margins and Marginal Basins of the Western Pacific. Geophysical Monograph Series, 88, 125-173. https://doi.org/10.1029/GM088p0125

Hickey-Vargas, R., Hergt, J.M., Spadea, P., 1995. The Indian ocean-type isotopic signature in western Pacific marginal basins: origin and significance, in: Taylor, B., Natland, J. (Eds.), Active margins and marginal basins of the western Pacific. Geophysical Monograph Series, 88, 175-197. https://doi.org/10.1029/GM088p0175

Hoang, N., Miyagi, I., Itoh, J., 2015. Miocene–Pleistocene magmas in the Monbetsu area, Northeast Hokkaido, tap N-MORB-like sources contaminated by slab-derivedfluids. Journal of Geodynamics, 86, 10-25. http://dx.doi.org/10.1016/j.jog.2015.02.004

Hollocher, K., 2014. A pictorial guide to metamorphic rocks in the field, first ed. Taylor & Francis Group, London, 302p.

Hofmann, A.W., 1988. Chemical differentiation of the Earth: the relationship between mantle, continental crust, and oceanic crust. Earth and Planetary Science Letters, 90(3), 297-314. https://doi.org/10.1016/0012-821X(88)90132-X

Hofmann, A.W., Jochum, K.P., and White, W.M., 1986. Nb and Pb in oceanic basalts: New constraints on mantle evolution. Earth and Planetary Science Letters, 79(1-2), 33-45. https://doi.org/10.1016/0012-821X(86)90038-5

Humphris, S.E., Thompson, G., 1978. Trace element mobility during hydrothermal alteration of oceanic basalts. Geochimica et Cosmochimica Acta, 42(1), 127-136. https://doi.org/10.1016/0016-7037(78)90222-3

Irvine, T.N., Baragar, W.R.A., 1971. A guide to the chemical classification of the common volcanic rocks. Canadian Journal of Earth Sciences, 8, 523-548. https://doi.org/10.1139/e71-055.

Jackson, S.E., Pearson, N.J., Griffin, W.L., Belousova, E.A., 2004. The application of laser ablation inductively coupled plasma-mass spectrometry to in situ U-Pb zircon geochronology. Chemical Geology, 211, 47-69. https://doi.org/10.1016/j.chemgeo.2004.06.017

Jardim de Sá, E.F., Moraes, J.A.C., Silva, L.J.H.D., 1986. Tectônica tangencial na Faixa Sergipana. Anais III Congresso Brasileiro de Geologia, p. 1246.

Janoušek, V., Farrow, C.M., Erban, V., 2006. Interpretation of whole-rock geochemical data in igneous geochemistry: introducing Geochemical Data Toolkit (GCDkit). Journal of Petrology, 47(6), 1255-1259. https://doi.org/10.1093/petrology/egl013

Jensen, L.S., 1976. A new cation plot for classifying subalkalic volcanic rocks. Ontario Division Mines Miscellaneous Paper, 66, 1-21.

Kearey, P., Klepeis, K.A., Vine, F.J., 2014. Tectônica Global, translation: Godoy, D.F., Hackspacher, P.C., third ed. Bookman, Porto Alegre, 436p.

Keller, N.S., Arculus, R.J., Hermann, J., Richards, S., 2008. Submarine back-arc lava with arc signature: Fonualei Spreading Center, northeast Lau Basin, Tonga. Journal of Geophysical Research, 113, 1-28. http://dx.doi.org/10.1029/2007JB005451

Lima, H.M., Pimentel, M.M., Fuck, R.A., Santos, L.C.M.L., Dantas, E.L., 2018. Geochemical and detrital zircon geochronological investigation of the metavolcanosedimentary Araticum complex, Sergipano fold belt: Implications for the evolution of the Borborema Province, NE Brazil. Journal of South American Earth Sciences, 86, 176-192. https://doi.org/10.1016/j.jsames.2018.06.013

Lima, H.M., Pimentel, M.M., Santos, L.C.M.L., Mendes, V.A., 2017. Análise tectônica da porção nordeste da Faixa Sergipana, Província Borborema: dupla vergência em resposta a colisão oblíqua entre o Cráton do São Francisco e o Terreno Pernambuco-Alagoas. Geonomos, 25(2), 20-30.

Lima, D. R., 2016. Caracterização petrológica e geoquímica do Pluton Curituba, Domínio Poço Redondo, Cinturão Sergipano. Dissertação de Mestrado, Pós-Graduação em Geociências, Universidade Federal de Pernambuco, 110p.

Liew, T.C., Hofmann, A.W., 1988. Precambrian crustal components, plutonic associations, plate environment of the Hercynian Fold Belt of Central Europe: indications from a Nd and Sr isotopic study. Contributions to Mineralogy and Petrology, 98, 129-138. https://doi.org/10.1007/BF00402106

Liz, L.C.C., Machado, A., Liz, J.D., Almeida, J.M., 2018. Petrografia e geoquímica dos ortoanfibolitos das unidades Gentileza, Domínio Canindé, Faixa de Dobramentos Sergipana, Nordeste brasileiro. Pesquisas em Geociências, 45, 1-27. https://doi.org/10.22456/1807-9806.88650

Long, L.E., Castellana, C.H., Sial, A.N., 2005. Age, origin and cooling history of the Coronel João Sá Pluton, Bahia, Brazil. Journal of Petrology, 46, 255-273. https://doi.org/10.1093/petrology/egh070

Lopez-Sanchez, M.A., Aleinikoff, J.N., Marcos, A., Martínez, F.J., Llana-Fúnez, S., 2016. An example of low-Th/U zircon overgrowths of magmatic origin in a late orogenic Variscan intrusion: the San Ciprián massif (NW Spain). Journal of the Geological Society, 173, 282-291. http://dx.doi.org/10.1144/jgs2015-071

Meschede, M., 1986. A method of discriminating between different types of mid-ocean ridge basalts and continental tho1eiites with the Nb-Zr-Y diagram. Chemical Geology, 56, 207-218.

Miller, D.M., Goldstein, S.L., Langmuir, C.H., 1994. Cerium/lead and lead isotope ratios in arc magmas and the enrichment of lead in the continents. Nature, 368, 514–520.

Motoki, A., Sichel, S.E., Vargas, T., Melo, D.P., Motoki, K.F., 2015. Geochemical behaviour of trace elements during fractional crystallization and crustal assimilation of the felsic

alkaline magmas of the state of Rio de Janeiro, Brazil. Anais da Academia Brasileira de Ciências, 87(4), 1959-1979. http://dx.doi.org/10.1590/0001-3765201520130385

Nascimento, R.S., 2005. Domínio Canindé, Faixa Sergipana, Nordeste do Brasil: um estudo geoquímico e isotópico de uma sequência de rifte continental Neoproterozóica. Tese de Doutorado, Instituto de Geociências, Universidade de Campinas, 159p.

Oliveira, E.P., Windley, B.F., McNaughton, N.J., Bueno, J.F., Nascimento, R.S., Carvalho, M.J., Araújo, M.N.C., 2017. The Sergipano Belt, in: Heilbron, M., Cordani, U.G., Alkmin, F.F. (Eds.), São Francisco Craton, Eastern Brazil. Regional Geology Reviews, 241-254. https://doi.org/10.1007/978-3-319-01715-0_13

Oliveira, E.P., Windley, B.F., Araújo, M.N.C., 2010. The Neoproterozoic Sergipano orogenic belt, NE Brazil: a complete plate tectonic cycle in western Gondwana. Precambrian Research, 181, 64–84. https://doi.org/10.1016/j.precamres.2010.05.014.

Oliveira, E.P., Tarney, J., 1990. Petrogenesis of the Canindé de São Francisco Complex: a major late Proterozoic gabbroic body in the Sergipe Fold Belt, northeastern Brazil. Journal of South American Earth Sciences, 3, 125-140. https://doi.org/10.1016/0895-9811(90)90025-V

Passos, L.H., 2016. Caraterização petrográfica, química mineral e geotermobarometria de rochas da Unidade Novo Gosto, Domínio Canindé, Faixa de Dobramentos Sergipana. Dissertação de Mestrado, Instituto de Geociências, Universidade de Brasília, 225p.

Pearce, J.A., 1982. Trace element characteristics of lavas from destructive plate boundaries. In: Thorpe, E.S. (Ed.), Orogenic andesites and related rocks. John Wiley and Sons, New York, 525-548.

Pearce, J.A., 1983. Role of the subcontinental lithosphere in magma genesis at active continental margins. In: Hawksworth, C.J., Norry, M.J. (Eds.), Continental Basalts and Mantle Xenoliths. Shiva Publishing, Nantwich, Great Britain, 230-249.

Pearce, J., 1996. A User's Guide to Basalt Discrimination Diagrams. Geological Association of Canada, Short Course Notes, 12, 79-113.

Pearce, J.A., 2008. Geochemical fingerprinting of oceanic basalts with applications to ophiolite classification and the search for Archean oceanic crust. Lithos, 100(1-4), 14-48. https://doi.org/10.1016/j.lithos.2007.06.016

Pearce, J.A., 2014. Immobile element fingerprinting of ophiolites. Elements, 10, 101-108. https://doi.org/10.2113/gselements.10.2.101.

Pearce, J.A., Cann, J.R., 1973. Tectonic setting of basic volcanic rocks determined using trace element analyses. Earth and Planetary Science Letters, 19, 290-300. https://doi.org/10.1016/0012-821X(73)90129-5

Pearce, J.A., Parkinson, I.J., 1993. Trace element models for mantle melting: Application to volcanic arc petrogenesis. Geological Society Special Publications, 76, 373-403. https://doi.org/10.1144/GSL.SP.1993.076.01.19

Penaye, J., Kröner, A., Toteu, S.F., Van Schmus, W.R., Doumnang, J.-C., 2006. Evolution of the Mayo Kebbi region as revealed by zircon dating: An early (ca. 740 Ma) Pan-African magmatic arc in southwestern Chad. Journal of African Earth Sciences, 44, 530-542. https://doi.org/10.1016/j.jafrearsci.2005.11.018

Rocha-Júnior, E.R.V., Marques, L.S., Babinski, M., Nardy A.J.R., Figueiredo, A.M.G., Machado, F.B., 2013. Sr-Nd-Pb isotopic constraints on the nature of the mantle sources involved in the genesis of the high-Ti tholeiites from Northern Paraná Continental Flood Basalts (Brazil). Journal of South American Earth Sciences, 46, 9-25. http://dx.doi.org/10.1016/j.jsames.2013.04.004

Rudnick, R.L., Gao, S., 2003. Composition of the continental crust, in: Holland, H.D., Turekian, K.K. (Eds.), Elsevier Science. Treatise on Geochemistry, 3, 593-659.

Santos, R.A., Martins, A.A.M., Neves, J.P., 1998. Geologia e recursos minerais do estado de Sergipe. CPRM/Codise, 107p.

Santos, R.A., Menezes Filho, N.R., Souza, J.D., 1988. Programa de levantamentos geológicos básicos do Brasil: carta metalogenética/previsional – escala 1:100.000 (Folha CS.24-X-C-VI Piranhas). DNPM/CPRM.

Sato, H., 1977. Nickel content of basaltic magmas: Identification of primary magmas and a measure of the degree of olivine fractionation. Lithos, 10, 113-120. https://doi.org/10.1016/0024-4937(77)90037-8

Seixas, S.R.M., Moraes, L.C., 2000. The Canindé domain: its different gabbroic rocks. Anais 31° International Geological Congress, Rio de Janeiro, p. 6.

Silva, L.C., McNaughton, N.J., Armstrong, R., Hartmann, L.A., Fletcher, I.R., 2005. The Neoproterozoic Mantiqueira Province and its African connections: a zircon-based geochronological subdivision for the Brasiliano/Pan-African system of orogens. Precambrian Research, 136, 203-240. https://doi.org/10.1016/j.precamres.2004.10.004

Silva Filho, M.A., 1976. A suíte ofiolítica da Geossinclinal de Propriá. Anais 29° Congresso Brasileiro de Geologia, Ouro Preto, p. 51.

Silva Filho, M.A., 1998. Arco vulcânico Canindé-Marancó e a Faixa Sul-Alagoana: sequências orogênicas Mesoproterozóicas. Anais 50º Congresso Brasileiro de Geologia, 1998, Belo Horizonte, p.16.

Shinjo, R., Chung, S.-L., Kato, Y., Kimura, M., 1999. Geochemical and Sr-Nd isotopic characteristics of volcanic rocks from the Okinawa Trough and Ryukyu Arc: Implications for the evolution of a young, intracontinental back arc basin. Journal of Geophysical Research, 104, 10,591-10,608. 0148-0227/99/1999JB 900040509.00

Shinjo, R., Kato, Y., 2000. Geochemical constraints on the origin of bimodal magmatism at the Okinawa Trough, an incipient back-arc basin. Lithos, 54, 117-137. 10.1016/S0024-4937(00)00034-7

Sousa, C.S.; Soares, H.S.; Rosa, M.L.S.; Conceição, H., 2018. Petrologia e geocronologia do Batólito Rio Jacaré, Domínio Poço Redondo, Sistema Orogênico Sergipano, NE do Brasil. Geologia USP. Série Científica, 19 (2), 171-194. https://doi.org/10.11606/issn.2316-9095.v19-152494

Souza Júnior, F.D., 2013. Mapeamento geológico da porção central do domínio Canindé, Cinturão Orogênico Sergipano, NE-Brasil. Trabalho de Conclusão de Curso, Geologia Bacharelado, Universidade Federal de Sergipe, 64p.

Sun, S.S., McDonough, W.F., 1989. Chemical and Isotopic systematics of oceanic basalts, implications for mantle composition and processes. Geological Society of London Special Publication, 42, 313-345. https://doi.org/10.1144/GSL.SP.1989.042.01.19

Toteu, S.F., Penaye, J., Deloule, E., Van Schmus, W.R., Tchameni, R., 2006. Diachronous evolution of volcano-sedimentary basins north of the Congo craton: Insights from U–Pb ion microprobe dating of zircons from the Poli, Lom and Yaoundé Groups (Cameroon). Journal of African Earth Sciences, 44, 428-442. https://doi.org/10.1016/j.jafrearsci.2005.11.011

Trompette, R., 1997. Neoproterozoic (~600 Ma) aggregation of Western Gondwana: a tentative scenario. Precambrian Research, 82(1-2), 101-112. https://doi.org/10.1016/S0301-9268(96)00045-9

Trompette, R., 2000. Gondwana evolution; its assembly at around ~600 Ma. Comptes rendus de l'Académie des Sciences, 330, 305-315. https://doi.org/10.1016/S1251-8050(00)00125-7

Van Schmus, W.R, Oliveira, E.P., Silva Filho, A.F., Toteu, S.F., Penaye, J. & Guimarães, I.P., 2008. Proterozoic links between the Borborema Province, NE Brazil, and the Central African Fold Belt. Special Publications, 294, 69-99. https://doi.org/10.1144/SP294.5

Verma, S.K., Oliveira, E.P., 2015. Tectonic setting of basic igneous and metaigneous rocks of Borborema Province, Brazil using multi-dimensional geochemical discrimination diagrams. Journal of South American Earth Sciences, 58, 309-317. http://dx.doi.org/10.1016/j.jsames.2014.08.010

Vermeesch, P., 2006. Tectonic discrimination diagrams revisited. Geochemistry, Geophysics, Geosystems, 7(6). https://doi.org/10.1029/2005GC001092

Vermeesch, P., 2018. IsoplotR: a free and open toolbox for geochronology. Geoscience Frontiers, 9, 1479-1493. https://doi.org/10.1016/j.gsf.2018.04.001

Volynets, A.O., Pevzner, M.M., Tolstykh, M.L., Babansky, A.D., 2018. Volcanism of the southern part of the Sredinny Range of Kamchatka in the Neogene-Quaternary. Russian Geology and Geophysics, 59, 1577-1591. https://doi.org/10.1016/j.rgg.2018.12.004

Wang, X.-S., Gao, J., Klemd, R., Jiang, T., Zhai, Q.-G., Xiao, X.-C., Liang, X.-Q., 2015. Early Neoproterozoic multiple arc–back-arc system formation during subduction–accretion processes between the Yangtze and Cathaysia blocks: New constraints from the supra-subduction zone NE Jiangxi ophiolite (South China). Lithos, 236-237, 90-105. https://doi.org/10.1016/j.lithos.2015.08.007

Wang, H., Wu, Y.B., Qin, Z.W., Zhu, L.Q., Liu, Q., Liu, X.C., Gao, S., Wijbrans, J.R., Zhou, L., Gong, H.J., 2013. Age and geochemistry of Silurian gabbroic rocks in the Tongbai orogen, central China: implications for the geodynamic evolution of the North Qinling arc-back-arc system. Lithos, 179, 1-15. https://doi.org/10.1016/j.lithos.2013.07.021

Wiedenbeck, M., Hanchar, J.M., Peck, W.H., Sylvester, P., Valley, J.W., Whitehouse, M.J., Kronz, A., Morishita, Y., Nasdala, L., Fiebig, J., Franchi, I., Girard, J.P., Greenwood, R.C.,

Hinton, R., Kita, N., Mason, P.R.D., Norman, M., Ogasawara, M., Piccoli, R., Rhede, D., Satoh, H., Schulz-Dobrick, B., Skar, O., Spicuzza, M.J., Terada, K., Tindle, A., Togashi, S., Vennemann, T., Xie, Q., Zheng, Y.F., 2004. Further characterisation of the 91500 zircon crystal. Geostandards and Geoanalytical Research, 28, 9-39. https://doi.org/10.1111/j.1751-908X.2004.tb01041.x

Wiedenbeck, M., Allé, P., Corfu, F., Griffin, W.L., Meier, M., Oberli, F., Von Quadt, A., Roddick, J.C., Spiegel, W., 1995. Three natural zircon standards for U-Th-Pb, Lu-Hf, trace element and REE analyses. Geostandards Newsletter, 19(1), 1-23. https://doi.org/10.1111/j.1751-908X.1995.tb00147.x

Wilson, M., 1989. Igneous petrogenesis, first ed. Chapman & Hall, London, 466p.

Wood, D.A., 1980. The application of a Th-Hf-Ta diagram to problems of tectonomagmatic classification and to establishing the nature of crustal contamination of basaltic lavas of the British Tertiary volcanic province. Earth and Planetary Science Letters, 50, 11-30. https://doi.org/10.1016/0012-821X(80)90116-8

Xia, L., Li, X., 2019. Basalt geochemistry as a diagnostic indicator of tectonic setting. Gondwana Research, 65, 43-67. https://doi.org/10.1016/j.gr.2018.08.006

Xia, L.Q., Li, X.M., Yu, J.Y., Wang, G.Q, 2016. Mid-Late Neoproterozoic to Early Paleozoic volcanism and tectonic evolution of the Qilianshan, NW China. GeoResJ, 9-12, 1-41. https://doi.org/10.1016/j.grj.2016.06.001

Xia, L.Q., Xia, Z.C., Xu, X.Y., 2003. Magma genesis in the Ordovician backarc basins of the Northern Qilian Mountains, China. Geological Society of America Bulletin, 115, 1510-1522. https://doi.org/10.1130/B25269.1

CAPÍTULO III - Artigo 2: Pre-collision events in the Canindé domain as context for the evolution of the Sergipano belt, Southern Borborema Province

Gmail **Luiz Henrique Passos <lhpassos.geologo@gmail.com>**

Confirming submission to Precambrian Research

1 mensagem

Precambrian Research <em@editorialmanager.com> 20 de janeiro de 2021 01:48
Responder a: Precambrian Research <precam-eo@elsevier.com>
Para: Luiz Henrique Passos <lhpassos.geologo@gmail.com>

This is an automated message.

Pre-collision events in the Canindé domain as context for the evolution of the Sergipano belt, Southern Borborema Province

Dear Dr Passos,

We have received the above referenced manuscript you submitted to Precambrian Research.

To track the status of your manuscript, please log in as an author at https://www.editorialmanager.com/precam/, and navigate to the "Submissions Being Processed" folder.

Thank you for submitting your work to this journal.

Kind regards,
Precambrian Research

More information and support

You will find information relevant for you as an author on Elsevier's Author Hub: https://www.elsevier.com/authors

FAQ: How can I reset a forgotten password?
https://service.elsevier.com/app/answers/detail/a_id/28452/supporthub/publishing/kw/editorial+manager/

For further assistance, please visit our customer service site: https://service.elsevier.com/app/home/supporthub/publishing/. Here you can search for solutions on a range of topics, find answers to frequently asked questions, and learn more about Editorial Manager via interactive tutorials. You can also talk 24/7 to our customer support team by phone and 24/7 by live chat and email.

In compliance with data protection regulations, you may request that we remove your personal registration details at any time. (Use the following URL: https://www.editorialmanager.com/precam/login.asp?a=r). Please contact the publication office if you have any questions.

Pre-collision events in the Canindé domain as context for the evolution of the Sergipano belt, Southern Borborema Province

Luiz Henrique Passos[1], Reinhardt A. Fuck[1], Farid Chemale Jr.[2], Cristine Lenz[3], Carla Cristine Porcher[4], Viter Magalhães Pinto[5]

[1] Instituto de Geociências, Universidade de Brasília, Campus Universitário Darcy Ribeiro, Brasília - DF, 70904-970, Brasil

[2] Programa de Pós-Graduação em Geologia, Universidade do Vale do Rio dos Sinos, São Leopoldo - RS, 93.022-750, Brasil

[3] Departamento de Geologia, Universidade Federal de Sergipe, Campus São Cristóvão, São Cristóvão - SE, 49100-000, Brasil

[4] Instituto de Geociências, Universidade Federal do Rio Grande do Sul, Porto Alegre - RS, CEP: 90501-970, Brasil

[5] Centro de Engenharia, Engenharia Geológica, Universidade Federal de Pelotas, Pelotas - RS, CEP: 96010-440, Brasil

Abstract

The Canindé Domain is an important component to understand the pre-collisional events in Sergipano Belt, Borborema Province, especially during the late Tonian/early Cryogenian (740-680 Ma). We present metamorphic conditions, geochronology, and isotopic studies of the metavolcanic-sedimentary rocks of the Novo Gosto unit. The metamorphic conditions were calculated using amphiboles, resulting in a range of T: 600-740 ºC and P: 3.5-10.0 kbars for non-mylonitic amphibolites and values of T: 636-808 ºC and P: 7.0-12.0 kbars for mylonites, both of amphibolite facies. The minimum metamorphic conditions imprint in these rocks are T: 390 °C and P: 2.5 kbar, characteristic of greenschist facies, and possibly related to the uplift of the metamorphic terrane. The probable age of this metamorphic event was obtained in zircon rims (U-Pb/LA-ICPMS) from a quartzite, resulting in a $^{207}Pb/^{206}Pb$ mean age of 682±3.9 Ma. U-Pb detrital zircon and Nd model ages of the metasedimentary rocks point out early Tonian source rocks as a primary source. Subordinate contributions of Mesoproterozoic, Paleoproterozoic, and Neoarchean sources were also recognized. These primary sources are related to Cariris Velhos event rocks, whereas the secondary sources are probably the Jirau do Ponciano Complex and basement rocks of the Pernambuco-Alagoas superterrane. Early Tonian ages for the first time in the Canindé Domain were recognized, with U-Pb zircon ages (LA-

ICPMS) of 1005±3 Ma and 989±6 Ma in amphibolites and mylonitized granites, mostly outcropping at the southwestern limit of the area. New ages were obtained also in the Novo Gosto surrounding intrusions: Canindé Layered Gabbroic Intrusion (~718 Ma), Garrote metagranites (~715 Ma), Curralinho/Boa Esperança rocks (~708 Ma), and Gentileza metavolcanic rock (~700), which integrate the early pre-collisional magmatism of the Sergipano Belt (~740-680 Ma). Finally, U-Pb zircon ages were obtained in the adjacent basement (Poço Redondo Domain), probable source area of the Novo Gosto metasedimentary rocks, resulting in ages of 957±11 Ma and 988±15 Ma. The new data are crucial to understand the evolution of the early stages of the Sergipano Belt, support a collisional and accretional evolution to the Sergipano Belt, already proposed to other sectors of the Borborema Province, and bring an important perspective to future correlations with adjacent belts and the understanding of the structuration of West Gondwana, during the Brasiliano-Pan-African Orogeny.

Keywords: Sergipano Belt, pre-collisional rocks, metamorphic conditions, Nd isotopes, U-Pb ages

1. Introduction

The study of ancient orogenic belts is of fundamental importance to understand the evolutionary history of a paleocontinent. In the Borborema Province, north of the São Francisco-Congo Craton, several orogenic belts arise per crustal addition and structuration of West Gondwana, during the Brasiliano-Pan-African Orogeny, with late Tonian to Ediacaram ages (e.g., Brito Neves et al., 1995; Brito Neves et al., 2001; Van Schmus et al., 2008; Caxito et al., 2020).

The Borborema Province is composed mostly of an Archean to Paleoproterozoic basement and Neoproterozoic rocks. Collisional and accrecional events during the Neoproterozoic are described by several authors (e.g., Santos, 1995; D'el Rey Silva, 1995; Kozuch, 2003; Oliveira et al., 2010; Amaral et al., 2012; Caxito et al., 2014; Santos et al., 2014; Lima et al., 2015; Lages e Dantas, 2016; Padilha et al., 2016; Lima et al., 2017, 2018; Caxito et al., 2020; Caxito et al., 2021) and include subduction zones and closure of some oceans, which is evidenced by rocks with arc association signatures, fragments of preserved oceanic crust and evidence of high-grade metamorphic rocks. The two main collisional events registered in the Neoproterozoic are the Cariris Velhos orogenic cycle (1.1- 0.9 Ga), mostly preserved in the Transversal and Southern sector of the province, and the Brasiliano orogenic cycle. The latter cycle has rare magmatic arc associations, being registered an important association in the northern sector of the Borborema Province, the Santa Quitéria Batholith (635-600 Ma, Caxito et al., 2021 and references therein), and a smaller occurrence in the southern sector, in the Sergipano Belt (743 Ma, Canindé Domain) (Passos et al., 2021). The final amalgamation of West Gondwana led to the production of voluminous granitic rocks (sin to post-collisional) as well as invertion of several paleobasins all along the Borborema Province, mostly during the Cryogenian and Ediacaran period.

According to Oliveira et al. (2010), the Sergipano Belt is one of the best Precambrian examples of a complete plate tectonic cycle, starting with a rift that evolves to a passive margin after the Cariris Velho event (early Tonian orogeny) and ending with a collisional event at the end of the Brasiliano Orogeny. However, recent studies (e.g., Passos et al., 2020) and new data from the present study obtained in the Canindé domain (northernmost Segipano Belt domain), show that the generation of this belt has occurred in a more complex way than previously exposed. The same authors suggest the existence of a continental arc between the Poço Redondo-Marancó domain and the PE-AL super-terrane at ~740 Ma and a younger arc, with

opposite subduction sense during the closure of the Sergipano ocean followed by collision and final configuration of the belt.

In this research, we studied the pre-collisional units (early to late Tonian) of the Canindé domain, with new petrographic characteristics and P-T conditions in the Novo Gosto metavolcanic rocks, combined with Nd isotopic data and U-Pb detrital ages in the Novo Gosto metasedimentary rocks. Additionally, we obtained, for the first time, early Tonian U-Pb zircon ages in rocks from the Canindé domain, and two new ages from the suggested source area of the above-mentioned metasedimentary rocks. Finally, new U-Pb zircon ages were obtained for the late Tonian pre-collisional rocks of the area. The new data provide essential information about the source area, conditions and age of the metamorphic event, and crystallization ages of the basement and pre-collisional intrusive rocks, bringing new and important information about the initial phases of the Sergipano Belt.

2. Geological background

The Sergipano Belt, located in the southern part of the Borborema Province, is an E-SE to W-NW trending fold and thrust belt (fig. 12A, B), cropping out between the São Francisco-Congo Craton and the Pernambuco-Alagoas superterrane (Oliveira et al., 2010; Brito Neves and Silva Filho, 2019). It was formed due to the collision between the cratonic area and the superterrane during the Brasiliano Orogeny (Brito Neves et al., 1977; D'el Rey Silva, 1995). The Sergipano Belt comprises five lithostratigraphic domains, from north to south, named as Canindé, Poço Redondo-Marancó, Macururé, Vaza Barris and Estância, which are separated by Neoproterozoic shear zones known as Macururé, Belo Monte-Jeremoabo, São Miguel do Aleixo and Itaporanga (Davison and Santos, 1989; Silva Filho, 1998; Oliveira et al., 2010) (fig.12A).

The Canindé domain corresponds to the northernmost part of the Sergipano Belt (fig. 12A, C). It is limited with the Poço Redondo-Marancó domain by the Mulungu-Alto Bonito Shear Zone (fig.12A). It is represented by (i) the Canindé Complex rocks: metavolcanic-sedimentary rocks of the Novo Gosto unit and bimodal hypabyssal rocks of the Gentileza unit, (ii) Canindé layered gabbroic intrusion, and (iii) pre-, syn- and late-collisional intrusive granitic suites: Garrote, Curralinho/Boa Esperança, Sítios Novos, Serra do Catu, Coronel João Sá, Lajedinho, and Xingó. The Canindé Complex rocks were metamorphosed under amphibolite facies conditions, with local retrograde metamorphism to greenschist facies conditions (Santos et al., 1998; Nascimento, 2005; Souza Júnior, 2013; Oliveira et al., 2010, 2017).

The Novo Gosto unit consists of amphibolites, feldspathic quartzites, metarythmites, metapelites, marbles, and calc-silicate rock. These rocks are mostly fine- to medium-grained, usually banded, and occur as alternate light and dark bands (Souza Júnior, 2013), with subordinate massive amphibolites. The unit forms an irregular WNW-ESE trending strip intruded by the Canindé layered gabbroic intrusion. The oldest granites, Garrote granite, and the bimodal Gentileza-Curralinho/Boa Esperança rocks, although intrusive in the Novo Gosto rocks, often occur in tectonic contact (Souza Júnior, 2013). Strongly deformed rocks from the Novo Gosto unit were found along the NW-SE shear zones and occur with frequent transposition of the foliation into tight folds, resulting in inverted synforms and antiforms and strong epidotization.

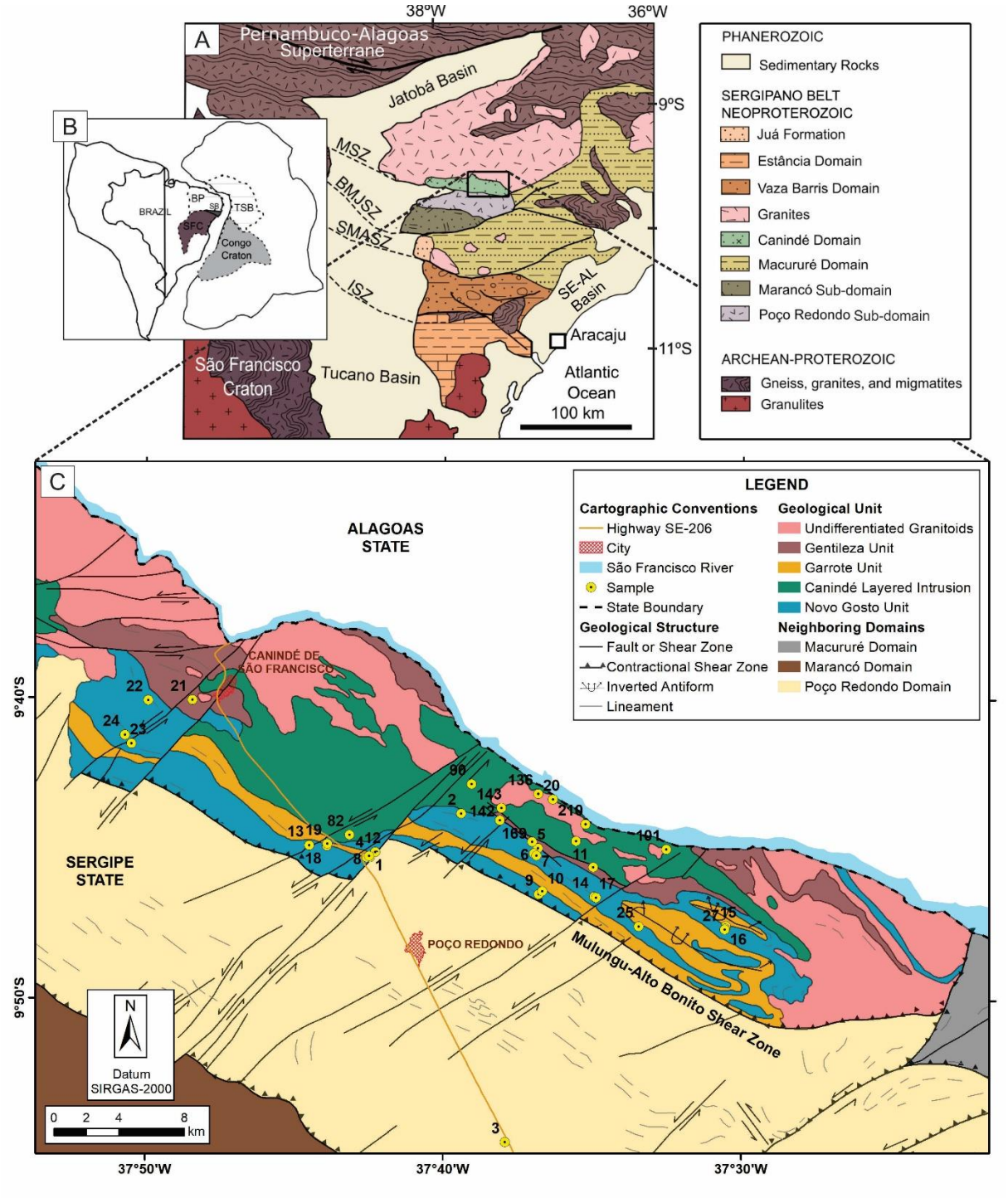

Figure 12: (A) Geological map of the Sergipano Belt. MSZ (Macururé Shear Zone), BMJSZ (Belo Monte-Jeremoabo Shear Zone), SMASZ (São Miguel do Aleixo Shear Zone), ISZ (Itaporanga Shear Zone). (B) Paleogeographic reconstruction showing the Neoproterozoic connection between the Borborema Province (BP, NE Brazil) and the Trans-Saharan belt (TSB, NW Africa). SB (Sergipano Belt) SFC (São Francisco craton). (C) Geological map of the central Canindé domain with the location of studied samples (Table 4). Modified by Passos et al. (2020) from D'el-Rey Silva (1995) and Santos et al. (1998).

Aside from the Novo Gosto amphibolites, another group of quartz-rich amphibolites is exposed in the Canindé domain, belonging to the Gentileza unit. In the field, they are very similar to the Novo Gosto massive amphibolites, mostly when they are not mixed with the felsic rapakivi granites (Curralinho/Boa Esperança units). According to Nascimento (2005), the Gentileza unit rocks are younger (688±6 Ma, U-Pb SHRIMP zircon dating in quartz monzodiorite) and contain mostly more biotite than the Novo Gosto amphibolites. Liz et al. (2018) emphasize that beyond biotite, hornblende and even visible quartz occur in the Gentileza unit amphibolites, being classified as intermediate rocks.

The geochronological data available in the Novo Gosto unit literature were restricted to a marble age of 963±20 Ma ($^{207}Pb/^{206}Pb$) interpreted by Nascimento (2005) as depositional age. Later, Oliveira et al. (2015) published a maximum deposition age of approximately 650 Ma (U-Pb SHRIMP zircon) in a metagraywacke, with peaks of 714 and 995 Ma. Passos et al. (2020) reported a zircon U-Pb age (LA-ICPMS) of 743±3 Ma for a metavolcanic rock sample, interpreted as the crystallization age of the rock.

Table 4: Localization of samples and methodologies.

Number	Sample	X Coordinate	Y Coordinate	Unit	Rock	Petrography	Sm-Nd	U-Pb Zircon
1	DDLH-1	641718	8921412	Novo Gosto	Metasediment		x	
2	DDLH-2	647303	8924082	Novo Gosto	Amphibolite	x		
3	DMLH-1A (PR-1A)	649988	8903941	Poço Redondo	Granite			x
3	DMLH-1B (PR-1B)	649988	8903941	Poço Redondo	Gneiss			x
4	DMLH-10A	641667	8921489	Novo Gosto	Amphibolite	x		
4	DMLH-10B	641667	8921489	Novo Gosto	Amphibolite	x		
4	DMLH-10D	641667	8921489	Novo Gosto	Amphibolite	x		
5	DDLH-5B	652020	8921952	Novo Gosto	Amphibolite	x		
5	DDLH-5A	652020	8921952	Novo Gosto	Metapelite		x	
6	DDLH-6A	651770	8921634	Novo Gosto	Metasediment		x	
6	DDLH-6B	651770	8921634	Novo Gosto	Metasediment		x	
7	DDLH-7B	651921	8921504	Novo Gosto	Metasandstone		x	
7	DDLH-7A	651921	8921504	Novo Gosto	Metapelito		x	
8	DDLH-8	641514	8921414	Novo Gosto	Metasediment		x	
9	DDLH-9C	652059	8919122	Novo Gosto	Amphibolite	x		
9	DDLH-9A	652059	8919122	Novo Gosto	Metasandstone		x	x
9	DDLH-9B	652059	8919122	Novo Gosto	Metasandstone		x	x
10	DDLH-10A	652285	8919314	Basement	Amphibolite	x		x
10	DDLH-10B	652285	8919314	Basement	Mylonitic Granite			x
11	DDLH-11B	655404	8920792	Novo Gosto	Amphibolite	x		
11	DDLH-11A	655404	8920792	Novo Gosto	Phyllite		x	x
12	DMLH-12A	642045	8921719	Gentileza	Metavolcanic			x
12	DMLH-12B	642045	8921719	Basement	Mylonitic Granite			x
13	DMLH-13A	637983	8922132	Garrote	Metasyenogranite			x
14	DDLH-14	655451	8918986	Novo Gosto	Metacarbonate		x	
15	DMLH-15A	663536	8917162	Novo Gosto	Quartz-feldspar paragneiss			x
16	DMLH-16	663492	8917012	Novo Gosto	Amphibolite	x		

17	DDLH-17A	655579	8918926	Novo Gosto	Amphibolite	x		
17	DDLH-17B	655579	8918926	Novo Gosto	Metasandstone		x	
18	DMLH-2	639082	8922094	Canindé layered gabbroic intrusion	Metadolerite			x
19	DMLH-3	639092	8922230	Canindé layered gabbroic intrusion	Fe-Ti oxide gabbro			x
20	DMLH-6	652935	8924945	Canindé layered gabbroic intrusion	Metadolerite			x
21	DDLH-21B	630829	8931070	Curralinho/Boa Esperança	Metasyenogranite			x
22	DDLH-22	628129	8931050	Novo Gosto	Amphibolite	x		
23	DDLH-23	627093	8928392	Novo Gosto	Metasandstone		x	
24	DDLH-24	626698	8928924	Novo Gosto	Amphibolite	x		
25	DDLH-25A	658190	8917160	Novo Gosto	Mica schist		x	
25	DDLH-25B	658190	8917160	Novo Gosto	Metasandstone		x	
27	DDLH-27	663456	8916972	Novo Gosto	Amphibolite	x		
82	CRN-82*	640453	8922772	Novo Gosto	Phyllite		x	
90	CRN-90D*	647949	8925879	Novo Gosto	Metapelite		x	
101	CRN-101C*	659883	8921882	Novo Gosto	Metagreywacke		x	
136	FS-136*	652038	8925283	Novo Gosto	Metasandstone		x	
142	CRN-142A*	649686	8923660	Novo Gosto	Metasediment		x	
143	CRN-143A*	649766	8924425	Novo Gosto	Metapelite		x	
169	CRN-169*	651666	8922357	Novo Gosto	Metasiltite		x	
209	CRN-209*	654349	8922385	Novo Gosto	Phyllite		x	
210	CRN-210A*	654936	8923419	Novo Gosto	Mica schist		x	

** Oliveira et al. (2015)*

3. Methods and materials

3.1 Petrography, Mineral Chemistry and Geothermobarometry

Petrography was investigated on 13 thin sections of amphibolite (Table 4), made at the Lamination Laboratory of the Universidade de Brasília (UnB) Geosciences Institute. Mineral chemistry was carried out in two laboratories: I - In the Laboratory of Electron Microprobe (LASON) of the Universidade de Brasília (DMLH-10A, DMLH-10B, DMLH-10C, DMLH-16), with a JEOL JXA-8230 probe with five WDS spectrometers and an EDS. The analyzer crystals available in the probe (TAPJ, LIF, LIFH, PETJ, PETH, LDE1, and LDE2) allow the measurement of all chemical elements with an atomic number larger than 4. The probe was calibrated with an acceleration voltage of 15 kV and a current of 10 nA. II - The remaining samples were analyzed at the Electron Microprobe Laboratory of the Institute of Geosciences of the Universidade Federal do Rio Grande do Sul (CPGq-IGEO-UFRGS). The laboratory is equipped with a CAMECA SXFive micro-analyzer, which performed the analyses with operation conditions of 15 keV accelerating voltage and 20 nA beam current.

In both laboratories, crystals of feldspar, amphibole, titanite, chlorite, and opaque minerals were analyzed, and the contents of SiO_2, TiO_2, Al_2O_3, FeO, MnO, MgO, CaO, K_2O, Na_2O, V_2O_3, NiO, Cr_2O_3, and OH were determined. The results were processed in the WinAmptb (Yavuz and Döner, 2017), WinCcac (Yavuz et al., 2015), and Microsoft Excel softwares, and were then plotted on classification diagrams for the analyzed minerals.

The amphibole was chosen to calculate the P-T conditions and the data were plotted in the WinAmptb software (Yavuz and Döner, 2017) which is built to perform thermobarometry calculations. The calculation methods are those adopted by Ernst and Liu (1998) (Al-in-amp barometer - kbars; amp-only thermometer - °C) and the results were plotted on a P-T diagram with the metamorphic facies fields.

3.2 Whole-rock Nd isotope analyses

15 metasedimentary rock samples (Table 4) were selected and pulverized for Sm-Nd analyses. These analyses were done in the Geochronology Laboratory of Universidade de Brasília according to the method described by Gioia and Pimentel (2000). About 50 mg of whole-rock powder were mixed with ^{149}Sm-^{150}Nd spike solution and dissolved in Savillex capsules. The extractions of Sm and Nd were carried out on Teflon columns containing LN-Spec resin (HDEHP - Di-(2-Ethylhexyl) phosphoric acid supported by polytetrafluorethylene powder). The Sm and Nd fractions were placed into double rhenium filament arrays and the isotopic measurements were done in a Finnigan TRITON multi-collector mass spectrometer in static mode. The uncertainties for Sm/Nd and $^{143}Nd/^{144}Nd$ are better than ±0.5% (2σ) and ±0.005% (2σ), respectively, based on repeated analyses of the BHVO-2 and BCR-1 rock standards. The $^{143}Nd/^{144}Nd$ ratios are normalized to $^{146}Nd/^{144}Nd$ of 0.7219 and the decay constant (λ) used was $6.54x10^{-12}$. The final data were processed in the GCDKit 5.0 package used as a complement to the R 3.5.3 software (Janoušek *et al.*, 2006). $\varepsilon_{Nd}(t)$ values were calculated using the U-Pb ages defined from zircon grains or estimated ages based on the regional and current results from nearby samples.

3.3 U-Pb zircon geochronology

15 samples were collected, including rocks representative of the units considered as older and rocks of doubtful origin exposed within the limits of the Canindé domain (Tables 4, 5). The samples were crushed and milled using a jaw crusher and swing mill. The heavy minerals were separated by conventional procedures using a magnetic separator and heavy liquids. Zircon was concentrated by handpicking and finally mounted in epoxy resin and polished. The U-Pb isotopic analyses were performed using the Laser Ablation Multi-Collector

Inductively Coupled Plasma Mass Spectrometry (LA-MC-ICP-MS) at Universidade de Brasília (UnB), Laser Ablation Sector Field Inductively Coupled Plasma Mass Spectrometry (LA-SF-ICP-MS) at Universidade Federal de Ouro Preto (UFOP), and Sensitive High-Resolution Ion Microprobe (SHRIMP) at the Australian National University (ANU).

Isotopic data obtained by the LA-MC-ICP-MS were acquired using static mode with 25 μm spot size. Data acquisition occurred in 40 cycles of 1.048s of integration time, and the 202, 204, 206, 207, 208, 232, and 238 masses were collected simultaneously, 202, 204, 206, 207, and 208 measured with multiplier ion counting and 232 and 238 with Faraday cups. Laser-induced elemental fractional and instrumental mass discrimination were corrected using the GJ-1 reference zircon (Jackson et al., 2004). During the analytical sessions, the zircon standard 91,500 (Wiedenbeck et al., 1995, 2004) was also analyzed as an external standard. U-Th-Pb data reduction was calculated in an Excel spreadsheet (Chemale et al., 2012) and details of instrumental operating conditions followed Bühn et al. (2009).

LA-SF-ICP-MS data were acquired in peak jumping mode during 20 s background measurement followed by 20 s sample ablation with a spot size of 20 μm, laser energy of 15%, shot frequency of 10 Hz, and shutter delay of 15 s. To evaluate the accuracy and precision of the laser-ablation results, we analyzed BB-1 zircon (562.58±0.26 Ma; Santos et al., 2017), Plešovice zircon (337±1 Ma; Sláma et al., 2008), GJ-1 zircon (608.5±1.5 Ma; Jackson et al., 2004), The obtained ages were concordant with the experimental errors, where the obtained concordant ages were 562.64±1.20 Ma (n=15, 2s.) for BB-1, 337.30±0.56Ma (n=25, 2s.) for Pleisovice, and 601.44±4.72 Ma (n=60, 95% conf.) for GJ-1. For both methods, raw data were corrected for background signal, and laser-induced elemental fractionation and instrumental mass discrimination were corrected with reference to zircon GJ-1 (Jackson et al., 2004). Common Pb correction was based on the Pb composition model (Stacey and Kramers, 1975). Data were corrected and reduced using software Glitter (Van Achterbergh et al., 2001).

The Poço Redondo domain samples were analyzed by the U-Pb SHRIMP (Sensitive High-Resolution Ion Microprobe) zircon geochronology, at the Research School of Earth Sciences, Australian National University using SHRIMP II equipment. Handpicked zircon grains were mounted in epoxy discs along with zircon standards, ground and polished, microphotographed in transmitted and reflected light, and their internal zoning imaged by cathodoluminescence (CL) using a scanning electron microscope. The mounts were then cleaned and gold-coated in preparation for SHRIMP analysis. Analytical methods and data treatment can be found elsewhere (Compston et al., 1984, Williams, 1998). Zircon grains were analyzed with a 2-3nA, 10kV primary O_2^- beam focused to a ~ 25 to ~20μm diameter spot. At mass resolution ~ 5500 the Pb, Th, and U isotopes were resolved from all significant interferences. Reduction of raw data and age calculation were carried out using Squid 2.02 and Isoplot-Ex (Ludwig, 2003). U and Th concentrations were determined relative to those measured in the RSES standard SL13.

The U-Pb Concordia diagrams and histograms were processed using IsoplotR 2.4 (Vermeesch, 2018). We use the $^{207}Pb/^{206}Pb$ age for the detrital zircon grains with a 100±10% concordance. The U–Pb zircon data are presented in the supplementary material (SP 2).

Table 5: U-Pb ages of the samples collected.

Sample	Rock	Unit	U-Pb Crystallization Age (Ma)	Metamorphic Age (Ma)	Maximum Depositional Age (Ma)	Peak Ages	Main Peak Age
DDLH-9A	Quartzite	Novo Gosto	-	-	886.4 ± 9.7	886 ± 9.7 981 ± 2.7 2100 ± 36	981 ± 2.7 (91%)
DDLH-11A	Phyllite	Novo Gosto	-	-	858 ± 10	858 ± 10 978.2 ± 2.2 1974 ± 7 2624 ± 25	978.2 ± 2.2 (73.8%)
DMLH-15A	Quartz-feldspar paragneiss	Novo Gosto	-	-	712 ± 23	712 ± 23 879 ± 9.2 987 ± 25 1068 ± 5 1132 ± 5.5 1215 ± 5.6 1284 ± 8.7 1612 ± 9	879 ± 9.2 (22%)
DDLH-9B	Quartzite	Novo Gosto	-	682.84 ± 3.91	780.4 ± 6.1	780.4 ± 6.1 962.0 ± 2.2 2174 ± 37	962 ± 2.2 (73%)
DMLH-6	Metadolerite	Canindé layered gabbroic intrusion	717.9 ± 23.2	-	-	-	-
DMLH-2	Metadolerite	Canindé layered gabbroic intrusion	716.03 ± 2.65	-	-	-	-
DMLH-3	Gabbro	Canindé layered gabbroic intrusion	719.30 ± 2.25	-	-	-	-
DMLH-13A	Metasyenogranite	Garrote	720.3 ± 29.1	-	-	-	-
DDLH-21B	Metagranite	Curralinho/Boa Esperança	708.13 ± 8.2	-	-	-	-
DMLH-12A	Metavolcanic	Gentileza	701.27 ± 4.93	-	-	-	-
DDLH-10A	Amphibolite	Canindé Domain Basement	1005.68 ± 3.75	-	-	-	-

DDLH-10B	Milonitic granite	Canindé Domain Basement	989.68 ± 6.36	-	-	-	-
DMLH-12B	Milonitic granite	Canindé Domain Basement	988.58 ± 16.13	-	-	-	-
DMLH-1A (PR-1A)	Granite	Poço Redondo	636 ± 3.76	-	-	-	-
DMLH-1B (PR-1B)	Gneiss	Poço Redondo	956.72 ± 12.08	575.35 ± 14.46	-	-	-

4. Results

4.1 Field relationship and petrography

The Novo Gosto unit metavolcanic rocks are mostly amphibolites and are found in isolated bodies or interleaved with metasedimentary rocks (fig. 13A, B). These rocks occur preferentially and more continuously in the southernmost part of the Canindé domain. Still, they can also be found locally in the northern portions, such as in the vicinity of the Gentileza unit key outcrop, on the SE-303 highway.

They are fine-grained rocks, with mostly greenish-black color or lighter greenish colors with advanced weathering (fig. 13F). Due to deformation and metamorphism, igneous (protolith) textural evidence is rare in field observations. However, punctual porphyroclasts from ancient feldspar phenocrysts can be identified, in addition to sinuous contacts and reaction edges with the neighboring rock, which can be an intrusive feature, like a sill or dike.

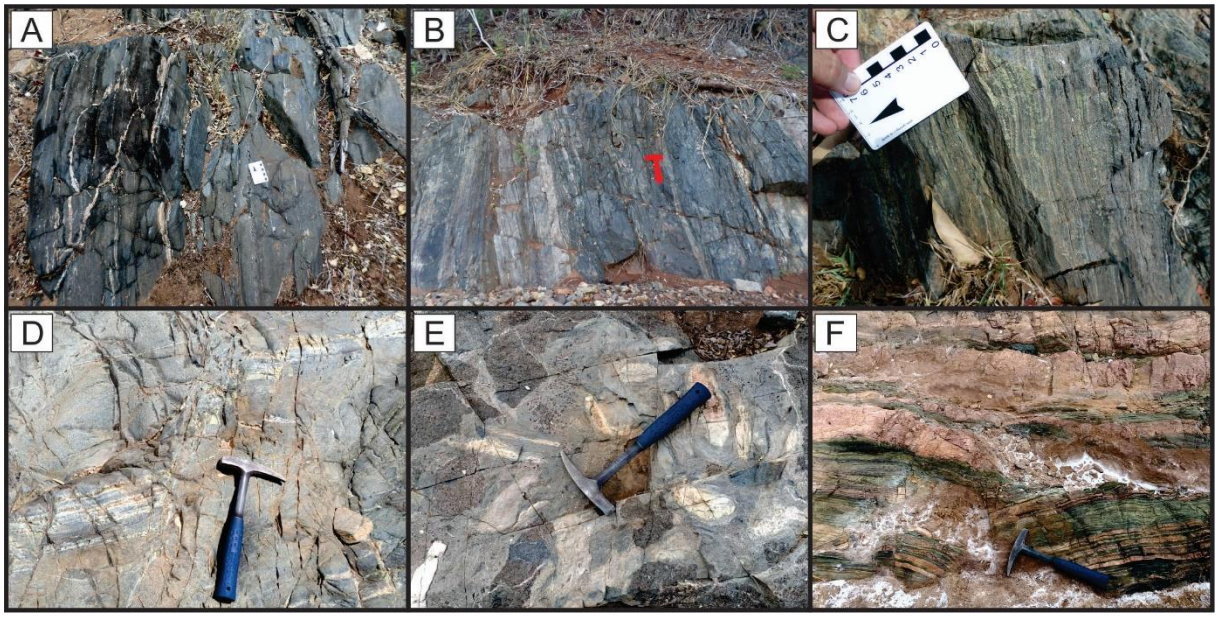

Figure 13: (A) Amphibolite with incipient foliation, far from the Mulungu-Alto Bonito shear zone (red geological hammer as scale; (B) Amphibolite interleaved with metasedimentary rock; (C) Mylonitic amphibolite in the Mulungu-Alto Bonito shear zone; (D) Amphibolite with sinistral NE fault, related to late ruptile deformation that affected the Canindé domain; (E) Xenoliths of the Novo Gosto unit in the Canindé layered gabbroic intrusion; (F) Epidotized amphibolites from the Novo Gosto unit in tectonic contact with the Garrote granite in a shear zone.

Depending on the distance of the shear zones, the rocks vary structurally. In the vicinity of these zones, amphibolites show mylonitic foliation (fig 13C). It is a typical structure at the southern limit of the Canindé domain, where the Mulungu-Alto Bonito ductile shear zone occurs. Mylonitic rhythmic banding occurs in these areas represented by deformed layers from amphibolite, metasedimentary rocks, and metagabbros (Canindé layered gabbroic intrusion) and metasyenogranites (Garrote granite). As the amphibolites occur away from these zones, they tend to have incipient foliation.

The foliation orientation follows the primary trend of the WNW-ESE trending Canindé domain that is similar to the orientation of the Mulungu-Alto Bonito shear zone. Structures, such as anticlines, synclines, closed folds, parasites, in chevron and M, S and Z folds, *boudins*, tension gashes, SC structures, faults (fig. 13D), and pairs of conjugated fractures are identified in the unit, demonstrating that these rocks were affected by ductile, ductile-brittle and brittle deformations. Kinematic indicators point out a left-handed component in tectonic transport.

In the southern region of the domain, contacts with the surrounding rocks are dominantly tectonic due to the shear zones influence (fig. 13F). Xenoliths of the Novo Gosto unit were identified in the Garrote granite and in the Canindé layered gabbroic intrusion (fig. 13E). The contact with the Gentileza unit rocks is not well established since the Canindé layered gabbroic intrusion occurs spatially predominantly between the two. The Gentileza unit has similar rocks (amphibolites), which makes it sometimes difficult to discriminate exclusively through field data and petrography. However, the Gentileza unit striking feature is its bimodal association with the Curralinho/Boa Esperança granite, and because they occur predominantly in the northern portion of the area. All the other rocks of the domain are intrusive in the Novo Gosto unit.

On the microscale, the amphibolites are fine to very fine-grained (fig. 14). They vary structurally, showing mm- to cm mylonitic foliation or bands, alternating amphibole-rich, and

plagioclase-rich bands. Some samples are more isotropic, and others show a granulometric bimodality. The dominant texture is nematoblastic, defined by the preferred orientation of elongated amphibole crystals (fig. 14A, B, C, E).

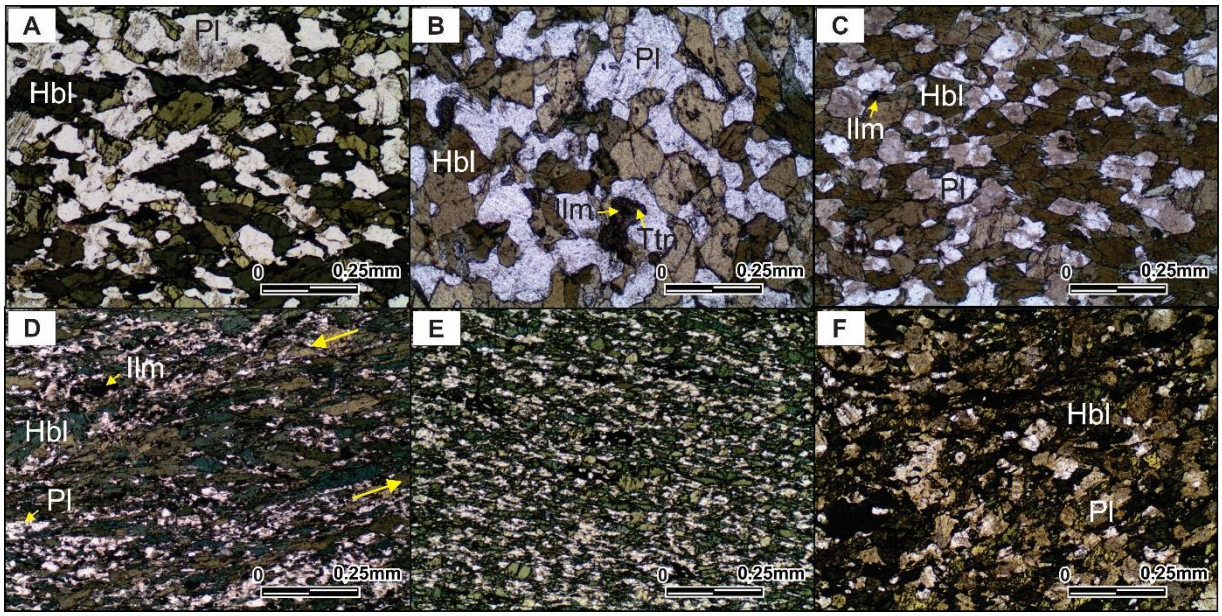

Figure 14: Mineralogical and textural aspects of the amphibolites from the Novo Gosto unit. Samples (A) (DDLH-27), (B) (DMLH-16) and (C) are amphibolites with nematoblastic to polygonal texture, less foliated and coarser-grained ones (V-11); (D) Mylonitic amphibolite with S-C foliation bands (DMLH-10A); (E) Foliated and very fine-grained amphibolite (DDLH-11B); (F) Foliated amphibolite with altered feldspar crystals (DDLH-9C).

The mineralogy is essentially amphibole (30-83%), plagioclase (7-45%) and opaque minerals (trace-15%), and as minor minerals or accessories: titanite (trace-14%), epidote (trace-8%), chlorite (up to 13%), sericite (trace), quartz (up to 3%), K-feldspar (trace), carbonate (trace-2%), apatite (trace) and zircon (trace) (Table 6).

Table 6: Synthesis of petrographic characteristics of the thin section studied.

Petrographic characteristics		**DDLH-22**	**DMLH-16**	**DDLH-9C**	**DDLH-10A**	**DDLH-17A**	**DDLH-2**	**DDLH-24**	**DDLH-27**	**DDLH-5B**	**DDLH-11B**	**DMLH-10A**	**DMLH-10B**	**DMLH-10D**
Colour		greenish black	greenish black	greenish black	greenish black	greenish black	greenish black	greenish black	greenish black	greenish dark gray	greenish black	greenish dark gray	greenish dark gray	greenish dark gray
Structure		Anisotropic; Incipient Gneissic banding	Anisotropic; Gneiss	Anisotropic; Gneiss	Anisotrópico; Bandamento Gnáissico	Anisotropic; Gneiss	Anisotropic; Gneiss	Anisotropic; Milonitic	Anisotropic; Gneiss	Anisotropic; Gneiss	Anisotropic; Gneissic banding	Anisotropic; Milonitic banding	Anisotropic; Milonitic banding	Anisotropic; Milonitic banding
Texture		Grano-nematoblastic equigranular	Grano-nematoblastic equigranular to poligonal	Grano-nematoblástic equigranular	Grano-nematoblastic, inequigranular	Grano-nematoblastic equigranular	Grano-nematoblastic equigranular	Grano-nematoblastic equigranular	Grano-nematoblastic equigranular	Grano-nematoblastic equigranular	Grano-nematoblastic, inequigranular	Grano-nematoblastic, inequigranular	Grano-nematoblastic, inequigranular	Grano-nematoblastic, inequigranular
Grain size		Fine	Fine	Fine	Fine to coarse	Very fine to fine	Very fine to fine	Fine	Fine	Fine	Fine	Fine	Fine	Very fine
Mineralogy (%)	Amphibole	60	61	39	30 - 83	62	62	65 - 56	57	49	66	62	66	68
	Plagioclase	29	39	45	45 - 7	15	22	27 - 30	33	23	24	25	18	17
	Opaque	5	Trace	2	3 - Trace	13	13	8 - Trace	7	15	10	13	14	10
	Titanite	6	Trace	Trace	3 - Trace	5	3	Trace - 14	Trace	Trace	Trace	Trace	Trace	Trace
	Chlorite	-	-	8	11 - 5	Trace	-	-	-	13	Trace	Trace	Trace	5
	Sericite	Trace	Trace	Trace	Trace	Trace	Trace	Trace	Trace	Trace	Trace	Trace	Trace	Trace
	Epidote	-	Trace	3	8 - 5	5	-	-	-	-	-	Trace	Trace	Trace
	Carbonate	Trace	Trace	Trace	Trace	Trace	Trace	Trace	Trace	Trace	Trace	2	2	Trace
	K-Feldspar	-	-	Trace	Trace	-	-	-	-	Trace	-	-	-	-
	Quartz	-	-	3	-	Trace	Trace	-	3	Trace	Trace	Trace	Trace	Trace
	Accessories (Apatite, Zircon)	Trace	Trace	Trace	Trace	Trace	Trace	Trace	Trace	Trace	Trace	Trace	Trace	Trace

Total mafic minerals (%)	66	61	41	30 - 83	75	75	72 - 55	64	64	76	73	80	78
Petrographic classification	Amphibolite with titanite-ilmenite	Amphibolite	Chlorite Amphibolite ±Epidote ±Ilmenite	Epidote-Chlorite Amphibolite with Titanite-Ilmenite	Ilmenite Amphibolite with Titanite-Epidote	Ilmenite Amphibolite with Titanite	Milonitic Ilmenite Amphibolite /Milonitic Titanite Amphibolite	Ilmenite Amphibolite	Chlorite-Ilmenite Amphibolite	Ilmenite Amphibolite	Milonitic Ilmenite Amphibolite	Milonitic Ilmenite Amphibolite	Milonitic Ilmenite Amphibolite ±Chlorite
Metamorphic facies	Upper Amphibolite	Upper Amphibolite with Greenschist retrometamorphism	Upper Amphibolite with Greenschist retrometamorphism	Upper Amphibolite with Greenschist retrometamorphism	Upper Amphibolite with Greenschist retrometamorphism	Upper Amphibolite	Upper Amphibolite	Upper Amphibolite with Greenschist retrometamorphism	Upper Amphibolite with Greenschist retrometamorphism	Upper Amphibolite with Greenschist retrometamorphism	Upper Amphibolite with Greenschist retrometamorphism	Upper Amphibolite with Greenschist retrometamorphism	Upper Amphibolite with Greenschist retrometamorphism
Possible protolith	Basalt	Basalt	Basalt	Basalt	Basalt	Basalt	Basalt	Basalt	Basalt	Basalt	Basalt	Basalt	Basalt
Observation			Relict porphyroclat mineral	Tracks with high and low concentration of amphibole	Thin and ultra thin tracks of amphibole and ilmenite concentration	Oval areas with amphibole and plagioclase concentration, oriented according to the foliation (old recrystallised fenocrystals)	Oval areas with amphibole and plagioclase concentration, oriented according to the foliation, besides S-C foliation and augen structures		Oval areas with amphibole and plagioclase concentration, oriented according to the foliation (old recrystallised fenocrystals)	Trace fenocrystal identified	Presence of S-C foliation, some augen and antique trace porfiroclasts totaly recrystallised	S-C foliation	Intercalated with DMLH-10A and 10B

Amphibole crystals occur with brownish-green, green, and bluish-green colors, anhedral to subhedral, with straight to irregular contacts. They display typical ductile (fig. 14D) and brittle deformation when affected by mylonitization. Deformation structures in amphibole are frequent, for example, the formation of small sub-grains at the edges of larger crystals with some edge migration, SC structures with amphibole crystals folded and stretched in S (fig. 14D), augen-like structure with ilmenite crystals in the pressure shadows, wavy extinction, crystals with fish-like structure, and fragmented crystals.

The kinematics identified in the petrography coincide with the structures identified in the field characterizing sinistral displacement. Out of the shear zone, the amphibole does not present these types of deformation. In some cases, where the granulometry is coarser, and foliation is incipient, polygonal granoblastic texture occurs. Some crystals contain inclusions of opaque minerals, plagioclase, quartz, apatite, and zircon. In some samples, amphibole occurs with bluish-green edges, possibly related to compositional changes due to retrometamorphism. Amphibole minerals are also replaced by chlorite and epidote.

Opaque crystals are anhedral to euhedral, with irregular straight contacts. When they are euhedral, their cubic habit is sometimes rectangular, with a larger axis oriented according to the foliation. They occur homogeneously spread in the rock, but it is also noticed in some samples a relatively higher concentration on the foliation or in bands. Sometimes, opaque minerals are associated with titanite coronae. In some cases, where opaque minerals are absent, small clusters of titanite crystals are noted, suggesting their complete replacement.

Quartz and K-feldspar crystals occur as trace minerals and are generally associated with plagioclase in felsic bands. They occur as anhedral to euhedral crystals, with irregular to straight contacts, with local tendencies towards polygonal texture.

Epidote, chlorite, and sericite are alteration minerals of amphibole and feldspar, respectively. Epidote can also fill fractures, probably associated with hydrothermal

remobilization (fig. 14F). In some samples, reddish chlorite was identified as an alteration of amphibole, most frequently occurring along fractures, indicating a probable hydrothermal effect.

Carbonate is found in mylonitic amphibolites in the vicinity of the Mulungu-Alto Bonito shear zone. In these rocks, there are carbonate venules along or transverse to the foliation. It also appears intergranular, disseminated in the rock. It is also possible to note carbonate concentrations in oval fabrics, possibly representing old calcium plagioclase microlites that have been replaced by metamorphic and or hydrothermal processes. Apatite and zircon crystals are present as accessory, euhedral, intergranular minerals or included in amphibole or feldspar crystals.

4.2 Mineral chemistry and geothermobarometry

Mineral chemistry was acquired in minerals that represent the metamorphic paragenesis of the studied rocks. It was used, at first, to determining the classification and structural formulas in feldspars (n=109), amphiboles (n=99), opaque minerals (n=47), chlorites (n=8) and titanites (n=14) (supplementary materials SP 3, 4, 5, 6, 7).

The data obtained in plagioclase (SP 3) mostly plotted in the fields of albite, oligoclase, and andesine (fig. 15A) and rarely in the labradorite field of the An-Ab-Or diagram of Deer et al. (1992). In 3 samples, K-feldspar was found as an accessory mineral, with anorthoclase, and orthoclase composition (fig. 15A). The compositional variation of calcium-rich plagioclase crystals for more sodium-rich crystals can be related to the variation of P-T conditions in the rock.

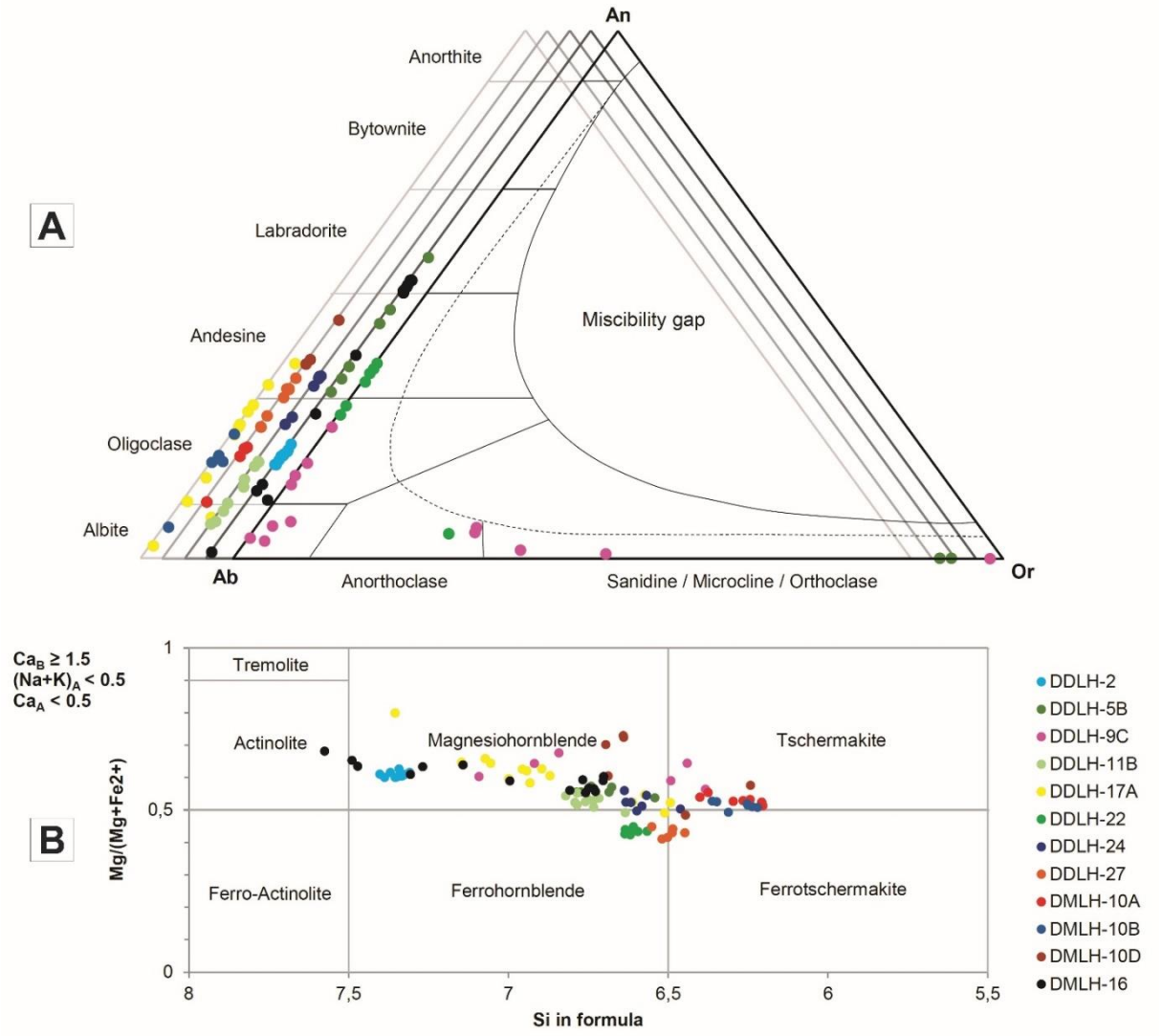

Figure 15: (A) An-Ab-Or feldspar ternary diagram with the feldspar composition of the samples plotted (Deer et al., 1992); (B) Amphibole classification diagram of analyzed amphiboles (Leake et al. (1997); Mg, Fe^{2+}, Si are per formula. Samples DMLH-10A, 10B e 10D are mylonitic.

In general, the analyzed amphibole crystals were classified as calcium amphiboles. The analyses (SP 4) plotted on the Si x Mg/(Mg+Fe^{2+}) diagram of Leake et al. (1997) form an alignment starting from the actinolite field and passing through the magnesiohornblende field, reaching part of the tschermakite, ferrotschermakite, and ferrohornblende fields (fig. 15B). In some samples, the amphibole crystals show zonation, switching to actinolite at the edges, which can be an effect of the retrometamorphism that affected the rock.

Analyses of titanite crystals (SP 5) in the Fe versus Al cations per formula unit diagram (Ling et al., 2015), fall mostly in the metamorphic origin field (fig. 16A). The chlorite crystals (SP 6), were plotted in the Al + vacancy - Mg - Fe ternary diagram (Zane and Weiss, 1998) and fall dominantly in the field of trioctahedral chlorites, with variations between the fields of chamosite and clinochlore (fig. 16B). Only one sample was plotted in the field of dioctahedral aluminous chlorites.

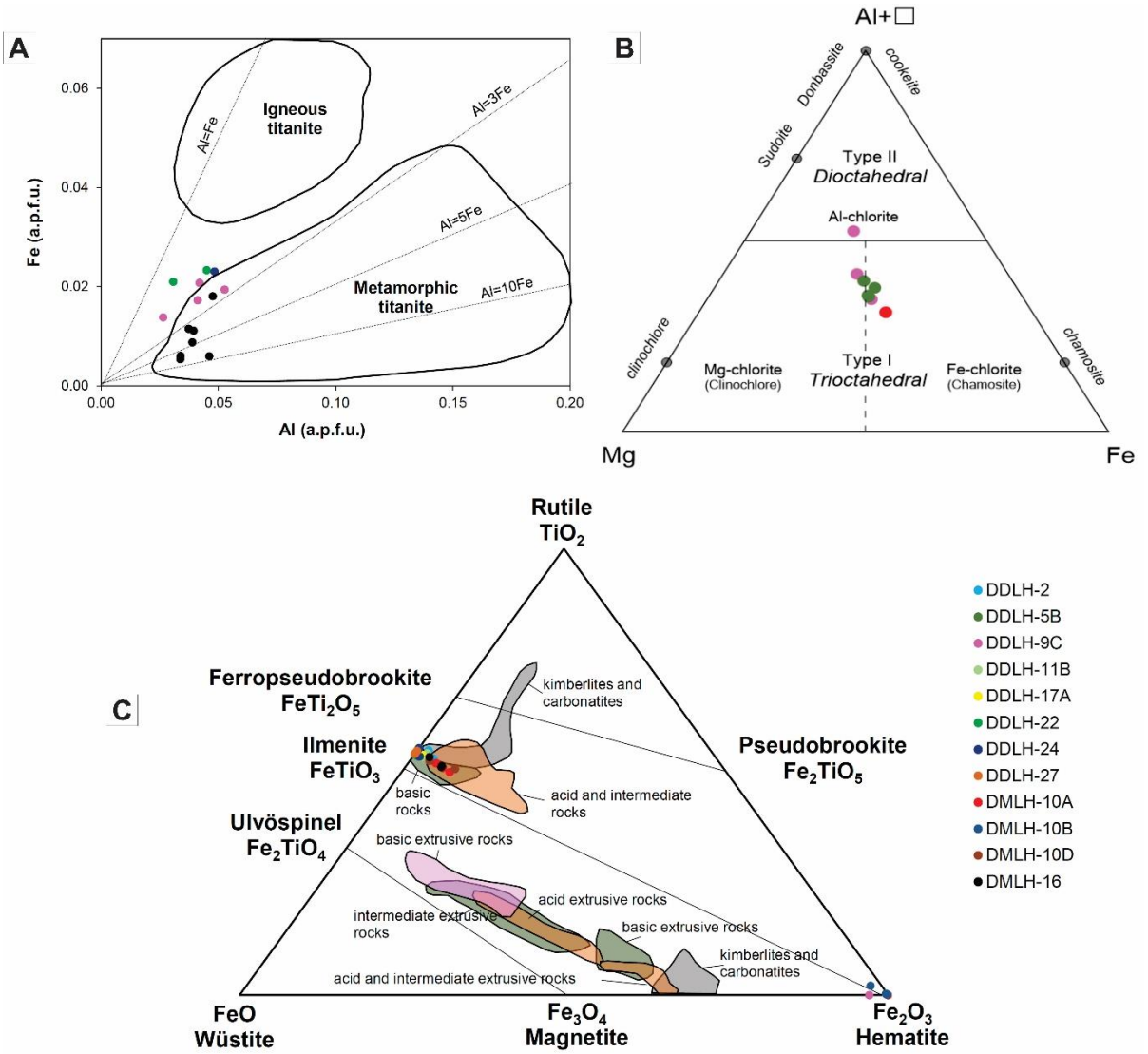

Figure 16: (A) A plot of the analysis in the Fe versus Al cations per formula unit (Ling et al., 2015 after Aleinikoff et al., 2002, and Rasmussen et al., 2013); (B) Chlorite analyses plotted in the Al+□ – Mg – Fe ternary diagram (Zane and Weiss, 1998); (C) Opaque minerals analysis plotted in the composition diagram of titanomagnetite and titanohematite in various types of igneous rocks (Cerný et al., 2016; after Piper, 1987; Cornell and Schwertmann, 2003). Samples DMLH-10A, 10B e 10D are mylonitic.

Analyses of opaque mineral crystals (SP 7), plotted in the TiO_2 - FeO - Fe_2O_3 ternary diagram (Cerný et al., 2016; after Piper, 1987; Cornell and Schwertmann, 2003), show that ilmenite has a typical composition of basic igneous rocks (fig. 16C). Hematite occurs in the mylonitic rocks. It is generated by the breaking of ilmenite, possibly due to the influence of hydrothermal fluids common in the shear zones.

The P and T values were estimated using the method described in section 4. A wide range of P-T conditions was obtained, with a variation in P between 2.5 and 12.0 kbar and in T between 390 and 808 ° C (the complete data can be found in Table 7 and summarized in Table 8). Pressure conditions vary mostly between 4.0 and 10.0. Temperature conditions vary mostly between 550 and 750 °C.

Mylonitic amphibolites show the highest P and T conditions, which is consistent with the textures identified in microscale. In the samples preserved from the mylonitization process, conditions achieve a maximum T of 808 °C and P of 12 kbars, very similar to the mylonitic samples.

Table 7: Geothermobarometry data.

Sample	Hornblend	Method - Ernst and Liu (1998)		Sample	Hornblend	Method - Ernst and Liu (1998)	
		Pressure (Kbars)	Temperature (°C)			Pressure (Kbars)	Temperature (°C)
DDLH-2	DDLH-2_Campo2_Anf1	2.6	460	DDLH-24	DDHL24-Campo2_Anf1	6.8	697
DDLH-2	DDLH-2_Campo2_Anf2	3.5	455	DDLH-24	DDHL24-Campo2_Anf3	7.1	674
DDLH-2	DDLH-2_Campo2_Anf3	3.4	453	DDLH-24	DDHL24-Campo2_Anf4	9.5	697
DDLH-2	DDLH-2_Campo2_Anf4	3.5	438	DDLH-24	DDHL24-Campo2_Anf5	7.4	681
DDLH-2	DDLH-2_Campo2_Anf5	3.6	443	DDLH-24	DDHL24-Campo2_Anf8	7.8	688
DDLH-2	DDLH-2_Campo2_Anf6	2.5	447	DDLH-24	DDHL24-Campo2_Anf9	7.7	700
DDLH-2	DDLH-2_Campo2_Anf7	2.7	453	DDLH-24	DDHL24-Campo2_Anf2	9.1	737
DDLH-2	DDLH-2_Campo2_Anf8	3.2	457	DDLH-27	DDLH-27_Campo1_Anf1	7.1	727
DDLH-2	DDLH-2_Campo2_Anf9	3.3	459	DDLH-27	DDLH-27_Campo1_Anf3	8.3	737
DDLH-2	DDLH-2_Campo2_Anf10	3.9	453	DDLH-27	DDLH-27_Campo1_Anf4	7.7	724
DDLH-2	DDLH-2_Campo2_Anf11	3.3	454	DDLH-27	DDLH-27_Campo1_Anf5	7.9	726
DDLH-5B	DDLH-5B_Campo1_Anf3	10.4	710	DDLH-27	DDLH-27_Campo1_Anf6	8.0	730
DDLH-5B	DDLH-5B_Campo1_Anf5	8.8	662	DDLH-27	DDLH-27_Campo1_Anf7	8.1	705
DDLH-5B	DDLH-5B_Campo2_Anf1	8.2	637	DMLH-10A	10 A_C3_Anf 1	10.0	808
DDLH-5B	DDLH-5B_Campo2_Anf2	8.3	667	DMLH-10A	10 A_C3_Anf 2	9.7	789
DDLH-5B	DDLH-5B_Campo2_Anf3	9.1	648	DMLH-10A	10 A_C1_Anf 3	8.7	804
DDLH-5B	DDLH-5B_Campo2_Anf5	10.1	645	DMLH-10A	10 A_C2_Anf 1	9.0	792
DDLH-9C	DDLH9c_Campo2_Anf-3	5.4	717	DMLH-10A	10 A_C2_Anf 2	9.0	780
DDLH-9C	DDLH9c_Campo2_Anf-1	6.9	751	DMLH-10A	10 A_C1_Anf 1	7.8	751
DDLH-9C	DDLH9c_Campo3_Anf4	5.9	729	DMLH-10A	10 A_C1_Anf 2	7.9	745
DDLH-9C	DDLH9c_Campo3_Anf2	4.7	608	DMLH-10B	10 B_C3_Anf 1	7.7	764
DDLH-9C	DDLH9c_Campo3_Anf3	5.3	544	DMLH-10B	10 B_C3_Anf 2	7.1	780
DDLH-9C	DDLH9c_Campo3_Anf5	4.3	596	DMLH-10B	10 B_C3_Anf 3	9.7	799
DDLH-11B	DDLH-11B_Campo1_Anf1	6.2	638	DMLH-10B	10 B_C1_Anf 1	8.8	792
DDLH-11B	DDLH-11B_Campo1_Anf2	4.6	625	DMLH-10B	10 B_C1_Anf 2	8.6	797
DDLH-11B	DDLH-11B_Campo1_Anf5	5.0	608	DMLH-10B	10 B_C2_Anf 1	9.6	788
DDLH-11B	DDLH-11B_Campo1_Anf8	3.8	634	DMLH-10B	10 B_C2_Anf 2	7.6	744
DDLH-11B	DDLH-11B_Campo1_Anf4	3.9	626	DMLH-10D	10 D_C2_Anf 1	7.9	657
DDLH-11B	DDLH-11B_Campo1_Anf6	4.8	617	DMLH-10D	10 D_C3_Anf 1	7.0	647
DDLH-11B	DDLH-11B_Campo1_Anf7	4.9	614	DMLH-10D	10 D_C3_Anf 2	7.0	636
DDLH-11B	DDLH-11B_Campo1_Anf9	5.3	622	DMLH-10D	10 D_C3_Anf 3	7.1	649
DDLH-17A	DDHL17A-Campo1_Anf5	3.0	459	DMLH-10D	10 D_C3_Anf 4	12.0	797

DDLH-17A	DDHL17A-Campo2_anf3	5.5	520
DDLH-17A	DDHL17A-Campo1_Anf7	6.1	553
DDLH-17A	DDHL17A-Campo1_Anf1	6.4	544
DDLH-17A	DDHL17A-Campo1_anf2	8.5	586
DDLH-17A	DDHL17A-Campo1_anf3	7.4	577
DDLH-17A	DDHL17A-Campo1_anf6	8.2	585
DDLH-17A	DDHL17A-Campo1_anf4	8.8	615
DDLH-17A	DDHL17A-Campo2_anf2	8.6	595
DDLH-17A	DDHL17A-Campo1_anf5	7.1	603
DDLH-17A	DDHL17A-Campo2_anf1	9.9	707
DDLH-17A	DDHL17A-Campo2_anf5	10.6	739
DDLH-17A	DDHL17A-Campo1_Anf6	8.1	688
DDLH-17A	DDHL17A-Campo1_Anf7	9.5	724
DDLH-22	DDHL22-Campo1_Anf1	5.7	686
DDLH-22	DDHL22-Campo1_Anf2	6.5	690
DDLH-22	DDHL22-Campo1_Anf4	5.6	695
DDLH-22	DDHL22-Campo1_Anf5	7.1	692
DDLH-22	DDHL22-Campo1_Anf6	5.6	701
DDLH-22	DDHL22-Campo1_Anf7	5.9	707

DMLH-16	16_C2_Anf 1	5.9	643
DMLH-16	16_C2_Anf 2	6.2	665
DMLH-16	16_C4_Anf 1	6.3	653
DMLH-16	16_C4_Anf 3	6.0	658
DMLH-16	16_C4_Anf 4	5.6	663
DMLH-16	16_C1_Anf 5	5.7	656
DMLH-16	16_C3_Anf 3	5.9	639
DMLH-16	16_C3_Anf 4	6.2	660
DMLH-16	16_C1_Anf 1	6.1	570
DMLH-16	16_C3_Anf 1	5.6	519
DMLH-16	16_C3_Anf 2	6.3	486
DMLH-16	16_C1_Anf 2	4.4	478
DMLH-16	16_C1_Anf 3	3.1	425
DMLH-16	16_C1_Anf 4	3.5	414
DMLH-16	16_C4_Anf 5	2.8	390

Table 8: Summary of the calculated P-T conditions.

	Range P (kbars)	**Range T (°C)**	**N° pairs calc.**
DDLH-2	2.5-3.9	438-460	11
DDLH-5B	8.2-10.4	637-710	6
DDLH-9C	4.3-6.9	544-751	6
DDLH-11B	3.8-6.2	608-638	8
DDLH-17A	3.0-10.6	459-739	14
DDLH-22	5.6-7.1	686-707	6
DDLH-24	7.1-9.5	674-737	7
DDLH-27	7.1-8.3	705-737	6
DMLH-10A	7.8-10.0	745-808	7

DMLH-10B	7.1-9.7	744-799	7
DMLH-10D	7.0-12.0	636-797	5
DMLH-16	2.8-6.3	390-665	15

4.3 U-Pb zircon ages

U-Pb ages were obtained (Table 5, SP2) in zircon grains of four metasedimentary samples from the Novo Gosto unit. Intrusive rocks were investigated, with three samples dated in the Canindé Gabbroic Layered Intrusion and one sample each in the Garrote metagranite, Curralinho/Boa Esperança metagranite, and Gentileza amphibolite. Finally, four samples of the basement (Poço Redondo domain) were also analyzed, of which two are exposed in the Poço Redondo domain and two are exposed as tectonic slices in the Novo Gosto unit.

4.3.1 Novo Gosto unit detrital zircon grains

Detrital zircon grains from metasedimentary rocks of the Novo Gosto unit were investigated to establish their maximum depositional age and provenance (Table 5, SP2).

Sixty-seven zircon analyses of quartzite sample DDLH-9A resulted in three peaks of detrital zircon grains at 886±9.7 Ma (7%), 981±2.7 Ma (91%), 2100±36 Ma (1%) (fig. 17A). The central peak is well established at 981±2.7 Ma (91%) and is interpreted as the age of the main sediment source. The minimum population age of 886±9.7 Ma is the probable maximum sedimentation age of the paleobasin.

Eighty zircon analyses of phyllite sample DDLH-11A resulted in four peaks of detrital zircon grains at 858±10 Ma (3.7 %), 978.2±2.2 Ma (73.8%), 1974±7 Ma (20%), and 2624±25 Ma (2.5%) (fig. 17B). The main peak is well established at 978.2±2.2 Ma and is related to the main source of sediments, while the minor peak of 858±10 Ma is the probable maximum sedimentation age of the paleobasin.

Sixty-one zircon analyses of quartz-feldspar paragneiss sample DMLH-15A resulted in multiple peaks of detrital zircon ages at 712±23 Ma, 879±9.2 Ma, 987±25 Ma, 1068±5 Ma, 1132±5.5 Ma, 1215±5.6 Ma, 1284±8.7 Ma, and 1612±9 Ma (fig. 17C). Around 77 % of the

data fall between Tonian and Steanian ages and a minimum peak at ~700 Ma, with values of 660 Ma as minimum zircon age.

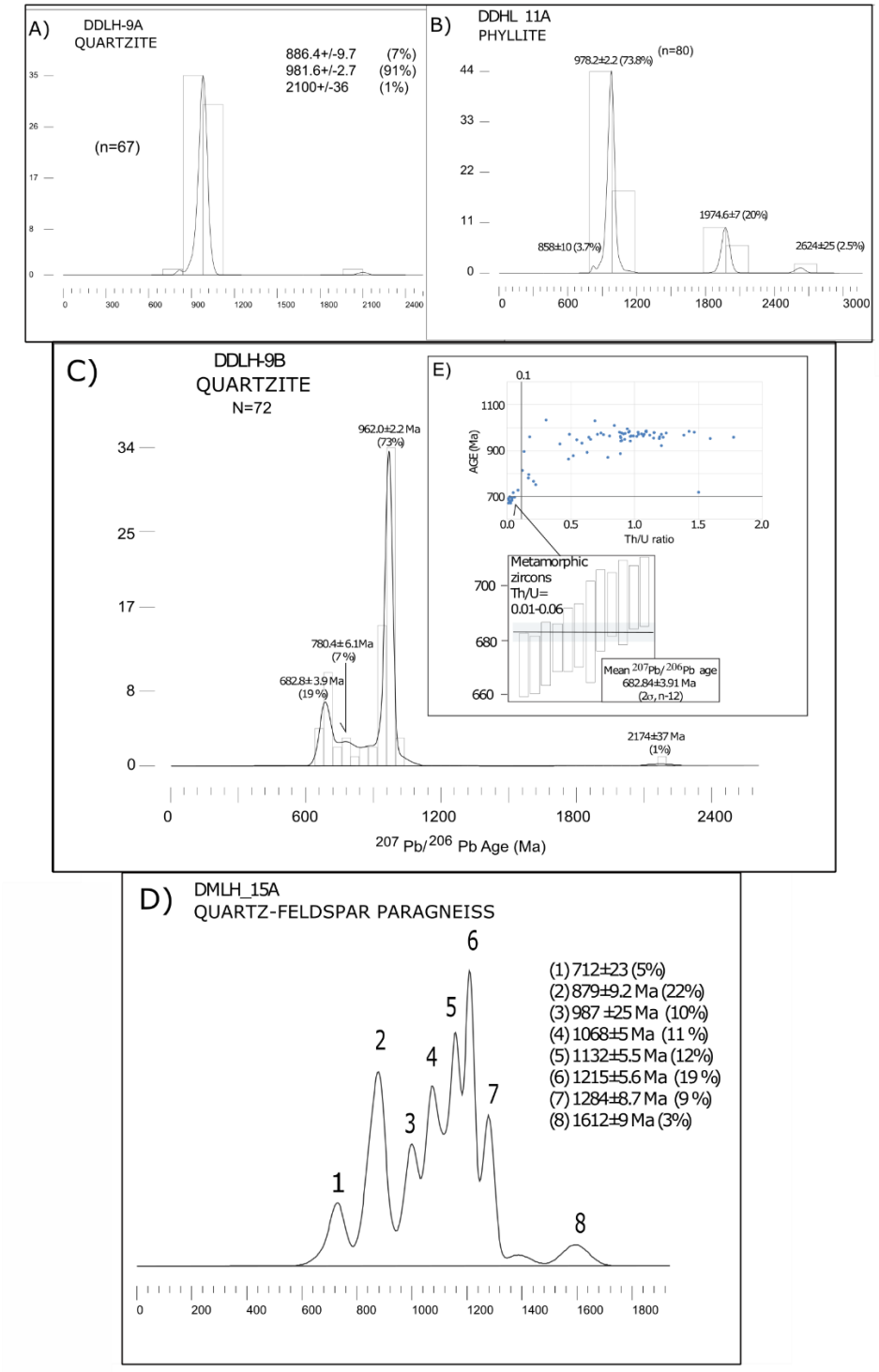

Figure 17: Frequency of occurrence of detrital zircon ages in metasedimentary samples from the Novo Gosto unit; A) Sample DDLH-9A; B) Sample DDLH-11A; C) Sample DMLH-15A; D e E) Sample DDLH-9B.

Seventy-two zircon analyses in quartzite sample DDLH-9B resulted in four peaks of detrital zircon grains at 682.84±3.91 Ma (19%), 780.4±6.1 Ma (7%), 962±2.2 Ma (73%) and 2174±37 Ma (1%), (fig. 17D). The main peak is well established at 962±2.2 Ma (73%) and is interpreted as the main sediment source. In contrast, the younger zircon age population (682.84±3.91 Ma) has a particular characteristic, with low Th/U ratios (between 0.01-0.06), which we interpret as the metamorphic age of the studied metasedimentary rock of the Novo Gosto unit.

4.3.2 Canindé domain Intrusive rocks

a) Canindé layered gabbroic intrusion

Three samples of the Canindé layered gabbroic intrusion were dated: DMLH-2, DMLH-3, and DMLH-6 (SP2). All the fourteen highly concordant U-Pb data obtained for sample DMLH-6 (metadolerite), were used for the construction of the Concordia diagram, resulting in an upper intercept age of 717.9±23.2 Ma (2 sigma, MSWD:0.3, fig. 18A). From the twenty-three analyses obtained in sample DMLH-2 (dolerite), twenty highly concordant U-Pb data were used for the construction of the Concordia diagram, resulting in a Concordia age of 716.03±2.65 Ma (2 sigma, MSWD:1.9, fig. 18B). The three excluded data fall out of the statistical population and/or have extremely high errors (~71 Ma). All the thirty-eight highly concordant U-Pb data obtained for sample DMLH-3 (gabbro) were used for the construction of the Concordia diagram, resulting in a Concordia age of 719.30±2.25 Ma (2 sigma, MSWD:1.1, fig. 19C).

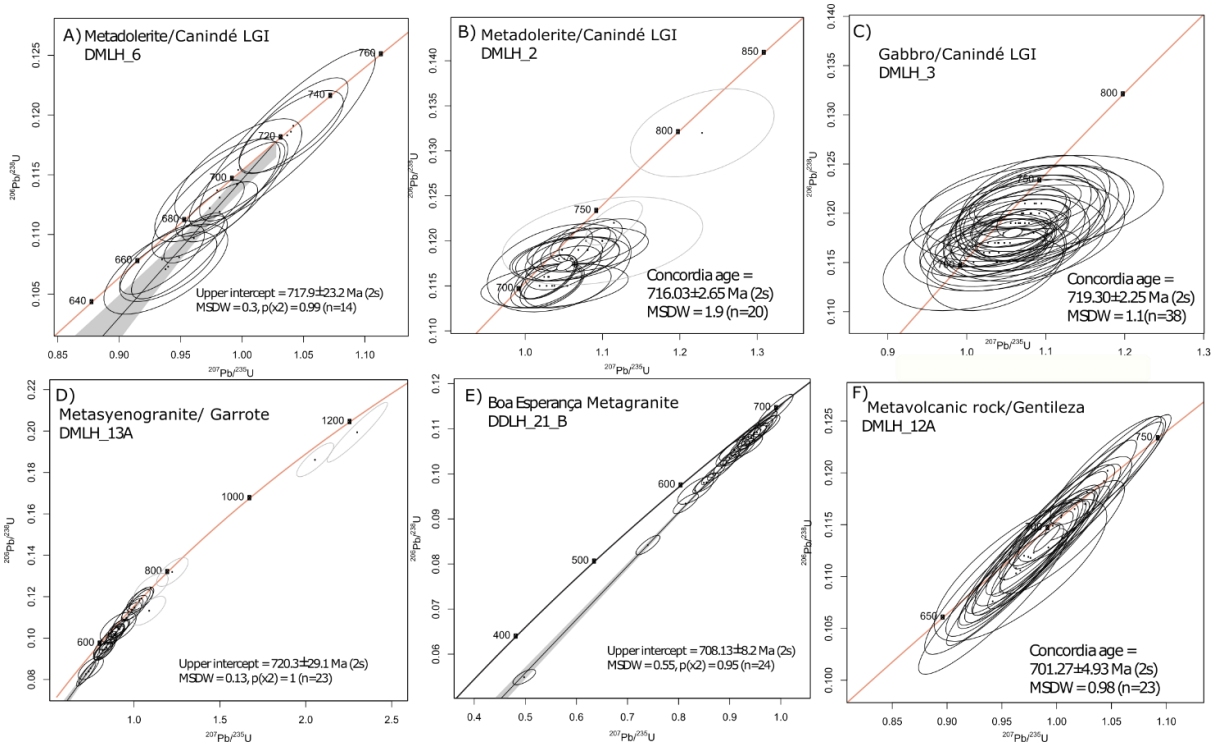

Figure 18: Diagrams with U-Pb ages of Canindé domain intrusive rocks.

b) Garrote metasyenogranite

The sample of mylonitized syenogranite (DMLH-13A), mapped as part of the Garrote metagranite, was collected in an outcrop showing mingling features with a fine-grained amphibolite. Twenty-eight U-Pb zircon data were obtained for these samples (SP2), however, a large dispersion of ages was found, mostly between 750 and 512 Ma. Three older values (~800-1000 Ma) are here interpreted as xenocrystys from the basement, while a group of ages between 512 and 640 show discordance higher than 10%, thus being discarded from the final interpretation. Highly concordant values (±10%) fall between 750 and 640 Ma, although these data still have high errors (~20 Ma). Therefore, we are using for this sample the upper intercept with the Concordia diagram, which resulted in an upper intercept age of 720.3±29.1 Ma (MSWD: 0.13, fig. 18D).

c) Curralinho/Boa Esperança metagranite

From the Curralinho/Boa Esperança metagranite, we collected a metasyenogranite sample (DDLH-21B) with mingling features with fine-grained amphibolite. Twenty-four U-Pb ages were obtained for this sample (SP2) and the data reveal a group of ages between 645 and 345, discordance higher than 10%. Highly concordant values (±10%) fall between 697 and 645 Ma, although with high errors (~35 Ma). Therefore, we are using for this sample the upper intercept with the Concordia diagram, which resulted in an upper intercept age of 708.13±8.2 Ma (2 sigma, MSWD: 0.55, fig. 18E).

d) Gentileza metavolcanic rock

A mafic metavolcanic rock sample (DMLH-12A) of the Gentileza unit, collected in the southern portion of the Canindé domain and intrusive in rocks from the Novo Gosto unit was analyzed. Twenty-five concordant U-Pb ages were obtained for this sample (SP2), resulting in main ages between 732 and 659 Ma. Two early Tonian ages were interpreted as xenocrystys from the basement. Twenty-three data were plotted in the Concordia diagram, resulting in a Concordia age of 701.27±4.93 Ma (2 sigma, MSWD: 0.98, fig. 18F).

4.3.3 Basement Rocks of the Canindé domain

In the Canindé domain, we recognized tectonic slices of basement rocks represented by the samples DDLH-10A, DDLH-10B, and DMLH-12B (SP2). The amphibolite sample DDLH-10A is from an outcrop in tectonic contact with fine-grained mylonitic granite (sample DDLH-10B). Eight highly concordant U-Pb zircon ages were obtained for this amphibolite, resulting in a Concordia age of 1005.68±3.75 Ma (2 sigma, MSWD: 0.29, fig. 19A). From the mylonitic granite sample, fifty-eight zircon ages were obtained, resulting in scattering between 1072 and 816 Ma. A group of younger ages shows discordant values higher than 10%. The upper intercept of the Concordia diagram resulted in an age of 989.68±6.36 Ma (2 sigma, MSWD: 1.2, fig.

19B). The sample DMLH-12B is also a fine-grained mylonitic granite and forty-eight zircon ages were obtained in this sample, resulting in ages between 799 and 978 Ma. All the data were plotted in the Concordia diagram, resulting in an age of 988.58±16.13 Ma (2 sigma, MSWD: 0.91, fig. 19C). This latter sample occurs in an outcrop encompassed by a mafic metavolcanic rock from the Gentileza unit (sample DDLH-12A, see section referring to the Gentileza unit) in the Mulungu-Alto Bonito shear zone.

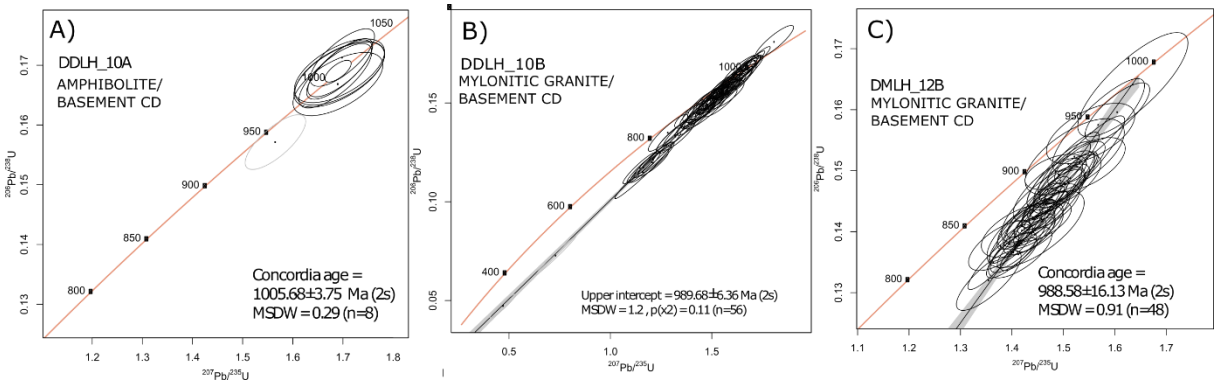

Figure 19: Diagrams with U-Pb ages of basement rocks of the Canindé domain.

4.3.4 Poço Redondo domain

To compare ages and possible sources of metasedimentary rocks from the Novo Gosto unit, we collected two samples in the neighboring domain, the Poço Redondo domain (samples DMLH-1A and DMLH-1B) (SP2). In the gneiss sample DMLH-1B (PR-1B, fig. 20A), we obtained five highly concordant data, which were plotted on the Concordia diagram, resulting in an age of 956.72±12.08 Ma (2 sigma, MSWD:0.81). The DMLH-1A (PR-1A) sample is from granite that intrudes the Poço Redondo gneiss. Thirty-four U-Pb ages were obtained (SP2), however, a big dispersion of ages between 1017 and 569 Ma was found. The group of older ages (~766-1017 Ma) is here interpreted as xenocrystys from the Poço Redondo basement, resulting in a Concordia age of 989.52±7.4 (n = 7) (fig. 20B). A statistical population (10 spots), with highly concordant values (±10%), falls between 670 and 626 Ma and are possibly

the zircon ages related to the granite crystallization. Concordia age of this group resulted in an age of 636±3.76 Ma (fig. 20B). Two younger ages of 569-582 Ma are here interpreted as recrystallized zircon grains, associated with a re-heating event (metamorphism?).

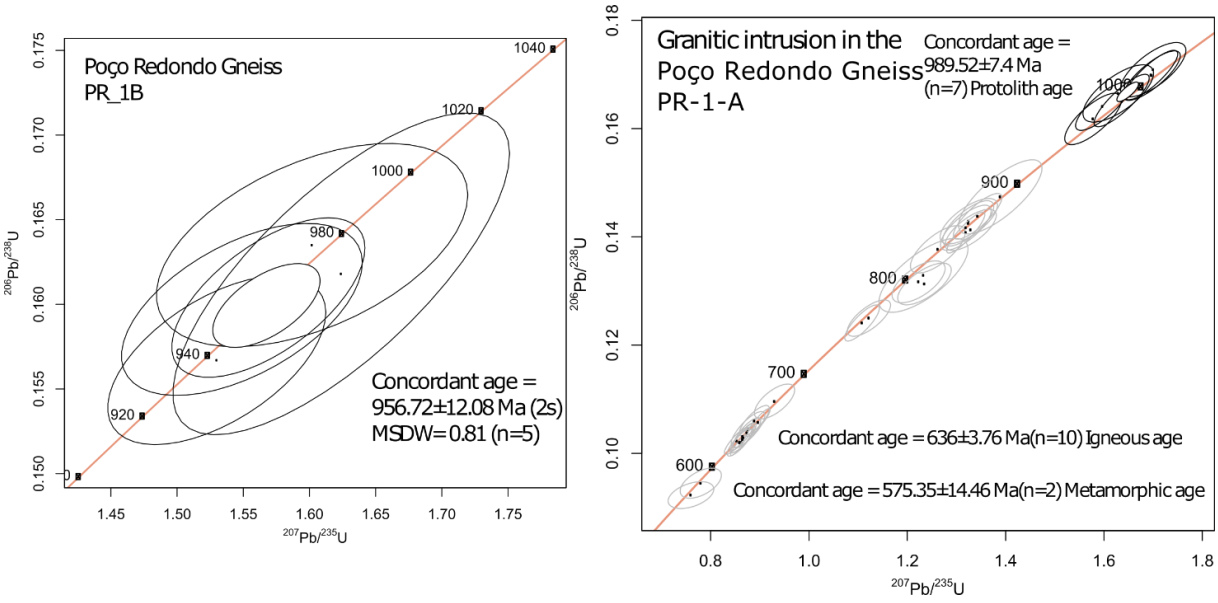

Figure 20: Diagrams with U-Pb ages of Poço Redondo domain rocks.

4.4 Nd Isotopic geochemistry

Whole-rock Sm-Nd isotopes of metasedimentary rocks from the Novo Gosto unit bring important information on the nature of the Novo Gosto basin (Table 9). Among the analyzed rock samples, there are metasandstones, metapelites, phyllites, meta-arkose, and impure metacarbonate. The ratio values of $^{147}Sm/^{144}Nd$ and $^{143}Nd/^{144}Nd$ range from 0.1047 to 0.1553 and 0.511666 to 0.512605, respectively. The values of $\varepsilon_{Nd\ (0)}$ vary from -18.96 to -0.64 and the T_{DM} model ages (single-stage) vary from 1.27 to 2.21 Ga. The values of $\varepsilon_{Nd\ (740\ or\ calculated\ age)}$ vary from -11.25 to 3.28 and the T_{DM} model ages (double-stage) vary from 1.10 to 2.24 Ga (fig. 21A, B). Five samples, mica schist (CRN-210a), metasediment (DDLH-6B), metasediment (DDLH-1), metacarbonate (DDLH-14), metapelite (CRN-143a), have model ages close to 1.3 Ga. Other rocks, meta-arkose, metapelites, phyllite, and metasandstones show Nd model age

between 1.3 and 1.8 Ga. The third group of rocks (metasediment, metasandstone, mica schist) displays Nd model ages in 2.2 Ga.

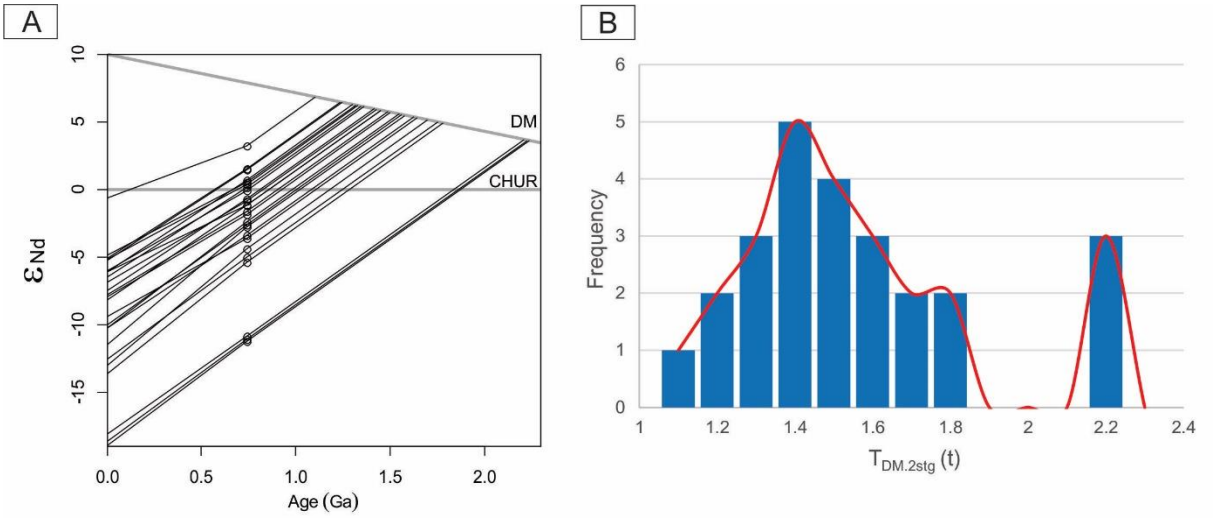

Figure 21: (A) ε_{Nd} vs. Age diagram showing evolution lines for metasedimentary rocks from the Novo Gosto unit. (B) Histogram of frequency of $T_{DM\text{-}2stg}$ ages of the metasedimentary rocks.

Table 9: Sm–Nd isotope data of metasedimentary rocks of the Novo Gosto unit. *Oliveiral et al. (2015)

Sample	Rock	Sm (ppm)	Nd (ppm)	$^{147}Sm/^{144}Nd$	$^{143}Nd/^{144}Nd$ (±2SE)	$f_{Sm/Nd}$	$\varepsilon_{Nd\ (0)}$	$\varepsilon_{Nd\ (t)}$	T_{DM}	$T_{DM.2stg\ (t)}$	t
CRN 143a*	Metapelite	6,24	24,28	0,1553	0,512605(6)	-0,21	-0,64	3,28	1,305	1,104	740
CRN 210a*	Mica schist	5,20	24,89	0,1263	0,512377(25)	-0,36	-5,09	1,57	1,271	1,238	740
DDLH 6B	Metasediment	4,82	23,04	0,1264	0,512372(6)	-0,36	-5,19	1,47	1,281	1,246	740
DDLH 1	Metasediment	2,97	14,41	0,1247	0,512325(6)	-0,37	-6,11	0,71	1,334	1,305	740
DDLH 14	Metacarbonate	0,87	4,16	0,1266	0,512308(9)	-0,36	-6,44	0,2	1,389	1,346	740
DDLH 9 A	Metasandstone	1,36	5,91	0,1387	0,512376(3)	-0,30	-5,11	1,47	1,468	1,359	886
DDLH 9B	Metasandstone	4,48	20,29	0,1334	0,512329(12)	-0,32	-6,03	0,29	1,462	1,369	780
DDLH 5A	Metapelite	4,69	22,53	0,1258	0,512257(6)	-0,36	-7,43	-0,72	1,459	1,418	740
DDLH 17B	Metasandstone	4,81	21,83	0,1333	0,512287(5)	-0,32	-6,85	-0,85	1,534	1,427	740
CRN 101C*	Metagreywacke	5,16	25,50	0,1224	0,51222(7)	-0,38	-8,15	-1,12	1,467	1,449	740
CRN 82*	Phyllite	2,74	11,42	0,1450	0,512328(5)	-0,26	-6,05	-1,16	1,691	1,452	740
FS-136*	Metasandstone	5,30	24,29	0,1319	0,512241(6)	-0,33	-7,74	-1,61	1,589	1,487	740
CRN 169*	Metasiltite	5,66	25,82	0,1326	0,512234(6)	-0,33	-7,88	-1,82	1,614	1,503	740
DDLH 6A	Metasediment	4,54	24,14	0,1138	0,512113(6)	-0,42	-10,24	-2,40	1,501	1,549	740
DDLH 7A	Metapelite	8,08	41,42	0,1179	0,512124(4)	-0,40	-10,03	-2,57	1,546	1,562	740
CRN 90D*	Metapelite	5,74	33,17	0,1047	0,512049(7)	-0,47	-11,49	-2,79	1,467	1,579	740
CRN 209*	Phyllite	5,55	26,95	0,1244	0,512113(6)	-0,37	-10,24	-3,41	1,669	1,627	740
DDLH 11A	Phyllite	4,14	18,46	0,1357	0,512158(4)	-0,31	-9,36	-2,67	1,812	1,661	858
CRN 142A*	Metasediment	7,48	43,06	0,1050	0,511971(6)	-0,47	-13,01	-4,34	1,575	1,701	740
DDLH 7B	Metasandstone	4,29	22,06	0,1174	0,511997(2)	-0,40	-12,5	-5,01	1,728	1,753	740
DDLH 23	Metasandstone	5,19	28,52	0,1100	0,511941(7)	-0,44	-13,6	-5,4	1,688	1,783	740
DDLH 25 A	Mica schist	2,76	13,87	0,1203	0,511712(5)	-0,39	-18,06	-10,85	2,212	2,209	740
DDLH 8	Metasediment	3,71	19,22	0,1167	0,511684(10)	-0,41	-18,61	-11,06	2,177	2,225	740
DDLH 25B	Metasandstone	1,48	7,80	0,1150	0,511666(6)	-0,42	-18,96	-11,25	2,167	2,24	740

5. Discussion

5.1 Basement of the Novo Gosto unit

The field studies and the ages obtained in this research resulted in the identification of rocks that represent basement fragments in the Canindé domain (samples DDLH-10A, 10B, and DMLH-12B, see section 5.3.3). The studied rocks show ages compatible with crystallization during the Cariris Velho event (early Tonian), which in the region are recognized mainly in the Poço Redondo-Marancó domain, to the south (crystallization ages between 1000 and 920 Ma, e.g., Carvalho, 2005; Oliveira et al., 2010; Caxito et al., 2020) and other occurrences to the north of the area (e.g., Brito Neves et al., 1995; Brito et al., 2008; Brito and Freitas, 2011; Cruz and Accioly, 2013; Cruz et al., 2014; Silva Filho et al., 2014; Guimarães et al., 2016; Dáttoli, 2017; Caxito et al., 2020). The samples DDLH-10A and DDLH-10B were collected in the vicinity of the limit with the Poço Redondo domain and the Mulungu-Alto Bonito shear zone, suggesting that these are fragments from the Poço Redondo domain juxtaposed to the Canindé domain units during the collision phase. The mylonitic granite (DMLH-12B) of upper intercept age 988.58±16.13 Ma is intruded by the mafic volcanism of the Gentileza unit (DMLH-12A), which was dated at Concordia age of 701.27±4.93 Ma. Based on the presence of these basement slices, we suggest that the basement of the Novo Gosto unit consists of the same material, which is supported by the new U-Pb detrital zircon ages and Nd model ages.

5.2 Main source area and maximum depositional age

U-Pb ages on detrital zircon grains of the three metasedimentary rocks show a main peak between 962 and 981 Ma, all of them with a high frequency of occurrence (>73%), representing a highly probable source area for the Novo Gosto paleobasin. Besides these source areas, the

same samples show a Paleoproterozoic and Neoarchean source area (1974, 2624 Ma), although with a lower frequency (1-20%). One sample shows a higher range of the main peaks, between 800 and 1200 Ma (77%), being these ages rare in the adjacent areas.

The probable early Tonian source area is well known in the region, occurring even as a rare basement in the Canindé domain, as well as in the adjacent Poço Redondo-Marancó domain and other surrounding areas in the Pernambuco-Alagoas superterrane and Southern Borborema Province (e.g., Brito Neves et al., 1995; Brito et al., 2008; Brito and Freitas, 2011; Cruz and Accioly, 2013; Cruz et al., 2014; Silva Filho et al., 2014; Guimarães et al., 2016; Dáttoli, 2017; Caxito et al., 2020). Adjacent areas with Paleoproterozoic and Neoarchean rocks occur mostly in restricted areas, like the Jirau do Ponciano, Nicolau-Campo Grande, Belém do São Francisco complexes and minor granitic occurrences (Sá et al., 1995; Van Schmus et al., 1995; Accioly et al., 2000; Sá et al., 2002; Silva Filho et al., 2002; Santos et al., 2008b; Hollanda et al., 2011; Santos et al., 2015; Oliveira et. al., 2015; Caxito et al., 2020).

The same source area groups were identified with Nd isotopes, with a positive $\varepsilon_{Nd\ (t:740)}$ and $T_{DM\ 2stage}$: between 1.10 and 1.35 and a highly negative $\varepsilon_{Nd\ (t:740)}$ and $T_{DM\ 2stage}$ of 2.2 Ga. Several samples show values in between these two groups, which can be an effect of sedimentary mixture between the two sources. Oliveira et al. (2015) suggested that the Nd model ages from the Canindé domain (1.0 to 1.6 Ga) were mostly younger than the Marancó domain ages (1.2 to 2.2 Ga), the latter domain being mostly provided by older sources. However, with the new data here obtained, we identified this older source in the Canindé domain as well, being the two domains provided by similar source areas.

The minimum age obtained for the Novo Gosto metasedimentary rocks, commonly interpreted as the maximum depositional age of the paleobasin, is here defined as 712±23 Ma, with possible variations to 780.4±6.1, 858±10, and 886.4±9.7 Ma. The youngest age population at 682±3.91 Ma (2s, n=12) with Th/U ratios from 0.06 to 0.01, determined in sample DMLH-

9B, is interpreted here as metamorphic age, imprinted on the detrital zircon grains. Oliveira et al. (2015) obtained maximum depositional ages for the Novo Gosto unit (metagraywacke) of approximately 650 Ma with two significant peaks at ca. 714 Ma and 995 Ma. These authors also found one zircon grain with an age of 625 Ma, interpreted as a metamorphic zircon.

These maximum depositional ages may reflect a long period of active sedimentation (~170 Ma) or most likely to be influenced by different source areas in the paleobasin. Nascimento (2005) determined the depositional age of carbonate rocks from the Novo Gosto unit at 963±20 Ma, which can suggest, together with the new data, long-term sedimentation for the Novo Gosto paleobasin.

Regarding the source area, we suggest that the source area of the Marancó-Poço Redondo and Canindé domains, in addition to some points of the Macururé domain, have a dominance of an early Tonian source, while in the rest of the Macururé, Vaza-Barris and Estância domains dominate Paleoproterozoic sources, implying a probable source area from the São Francisco Craton (Oliveira et al., 2015; Neves et al., 2016).

5.3 Tectono-metamorphic evolution of the Novo Gosto unit

Petrographic and geothermobarometric data of amphibolites from the Novo Gosto unit demonstrate that the unit was affected by clockwise P-T metamorphic conditions. The metamorphic peak occurred at the Cryogenian age, reaching the sillimanite stability field upper amphibolite facies conditions. Some data evidenced retrometamorphic P-T conditions in greenschist facies (fig. 22). The pressure conditions reached a maximum of 12.0 kbar and the temperature conditions of 808 °C and a minimum of 2.5 kbar and 390 °C. These T and P variations are most probably associated with the tectonic evolution of the metamorphic terrane, the higher P-T values associated with progressive metamorphism until it reached the

metamorphic peak, while the lower P-T conditions are related to the retrogressive metamorphic path, until the complete exposure of the terrane.

The mylonitic amphibolites show the highest P and T conditions (7.0-12.0 kbars and 636-808 °C). It is consistent with the textures identified in the microscale. The samples that were not mylonitized were crystallized under P and T conditions at least lower than those mylonitic rocks, ranging mainly around 600-740 ºC and 3.5-10.0 kbars.

The calculated P-T conditions, plotted in fig. 22 have a distribution compatible with volcanic arc (path 2) evolving to a continental mountain belt path (3).

The age of the metamorphic event was obtained in sample DDLH-9B (Novo Gosto unit/ quartzite), in which a group of zircon grains with very low Th/U ratios (0.01 to 0.06) was found, which are classically associated with metamorphic crystallization. This group of zircon grains provides a $^{207}Pb/^{206}Pb$ age of 682.84±3.91 Ma for the metamorphic peak, during collision and amalgamation of the Sergipano Belt. Younger metamorphic ages for the area were suggested by Oliveira et al. (2015), who reported age of 625 Ma in a metagraywacke from the Novo Gosto Unit and interpreted it as a metamorphic zircon.

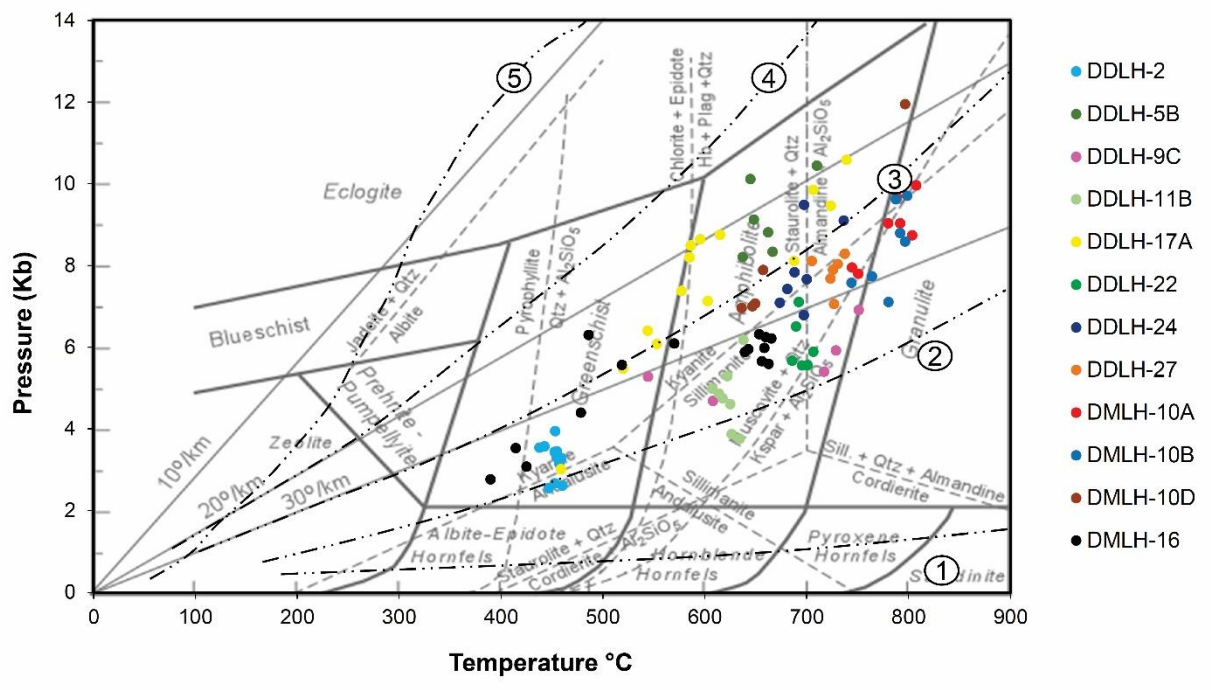

Figure 22: Amphibolite samples are plotted on the metamorphic facies diagram (P-T). (1) Contact (thermal) metamorphism, (2) Volcanic arc, (3) Collisional mountain belt, (4) Stable continent, (5) Accretionary prism (Redrawn from Nelson, 2004 and Marshak, 2019).

Finally, a much younger group of concordant U-Pb zircon ages is recorded in sample DMLH-1A, with ages between 582 and 569 Ma. This sample is from the neighboring Poço Redondo domain, and the younger age can be related to the D3 deformational event of Oliveira et al. (2010), suggested being around 581 Ma (Ar-Ar muscovite age in the Macururé D3 foliation).

5.4 Pre-collisional magmatic intrusions

The ages found for the metavolcanic rocks in the Novo Gosto unit (~743 Ma, Passos et al., 2020), characterize the older magmatism of the Canindé domain, followed by the other magmatic units in order of age: Canindé layered gabbroic intrusion, Garrote unit, Curralinho/Boa Esperança metagranite, and Gentileza unit. New U-Pb ages obtained in the Canindé layered gabbroic intrusion are 717.9±23.2 Ma, 716.03±2.65 Ma, and 719.30±2.25 Ma. These ages are slightly older than the ages reported by Oliveira et al. (2010) of 701±8 Ma and

Pinto et al. (2020) of 703±1.6 Ma. The obtained age for the Garrote metasyenogranite is an upper intercept and has a large error (720.3±29.1 Ma), although it is similar to the age of Van Schmus apud Santos et al. (1998) of 715 Ma. The Curralinho/Boa Esperança metagranite obtained an age of 708.13±8.2 Ma (upper intercept) is older than the age found by Oliveira et al. (2010) of 641±5 Ma (Boa Esperança metagranite) and 684±7 (Curralinho granite). The new Gentileza metavolcanic rock age of 701.27±4.93 Ma is, as well, a little older than the age of 688±6 (quartz-monzodiorite) published by Oliveira et al. (2010).

The metavolcanic rocks of the Novo Gosto unit represent the first records of a convergence event during the early Brasiliano orogeny in the Sergipano Belt (Passos et al., 2020) and together with the other magmatic units mentioned are assumed as the late Tonian (740-680 Ma) pre-collisional magmatism of the Sergipano Belt.

6. Conclusion

With this research, we conclude that:

A) Early Tonian crystallization ages (989.68±6.36, 1005.68±3.75 and 988.58±16.13) were for the first time identified in amphibolite and granitic mylonites of the Canindé domain. The early Tonian rocks outcrop close to the Mulungu-Alto Bonito shear zone, close to the contact with the Poço Redondo-Marancó domain, and possibly represent slices of this unit juxtaposed with the Canindé domain during the collisional event.

B) The main source area was investigated using U-Pb detrital zircon ages and Nd isotopes. The U-Pb ages in the Novo Gosto metasedimentary rocks reveal that the most probable and important source area for the Novo Gosto paleobasin has ages of 962-978 Ma. A minor Paleoproterozoic and Neoarchean source area was identified too (1974 - 2624 Ma). Probable early Tonian source area is well known in the region, occurring even as a rare basement in the Canindé domain, but as the main outcropping area, in the adjacent

Poço Redondo-Marancó domain and other areas of the Pernambuco-Alagoas superterrane and Southern Borborema Province. Paleoproterozoic and Neoachearn rocks occur more restricted in the South Borborema Province, most of them as domes. Nd isotopes confirm the two source areas and an important sedimentary mixture between the two sources.

C) The maximum depositional age obtained for the Novo Gosto paleobasin is 712±23 Ma, occurring in other samples values of 886±9.7, 858±10 Ma, and 780.4±6.1 Ma, which can reflect long-term sedimentation of the paleobasin or only an influence of different source areas in the paleobasin.

D) The tectono-metamorphic evolution of the Novo Gosto unit is here characterized as a clockwise P-T path, with metamorphic conditions ranging mainly around 600-740 ºC and 3.5-10.0 kbars, with peak metamorphic compatible with upper amphibolite facies. And values ranging mainly around 636-808 ºC and 7.0-12.0 kbars for mylonites. The minimum metamorphic conditions imprint in these rocks is T: 390 °C and P: 2.5 kbar, characteristic of greenschist facies, and possibly related to the uplift of the metamorphic terrane. The path distribution of the samples is compatible with a volcanic arc evolving to a continental mountain belt environment. The age of the metamorphic peak was dated at 682.84±3.91 Ma ($^{207}Pb/^{206}Pb$ zircon age/ LA-ICPMS).

E) Ages of 740-680 Ma pre-collisional magmatism are recorded in the Novo Gosto unit, Canindé layered gabbroic intrusion, Garrote, Gentileza and Curralinho/Boa Esperança metagranites.

F) These new results together with those of Passos et al. (2021) support a collisional and accretional evolution to the Sergipano Belt, already proposed to other sectors of the Borborema Province (eg, Santos, 1995; D'el Rey Silva, 1995; Kozuch, 2003; Oliveira et al., 2010; Amaral et al., 2012; Caxito et al., 2014; Santos et al., 2014; Lima et al.,

2015; Lages and Dantas, 2016; Padilha et al., 2016; Lima et al., 2017, 2018; Caxito et al., 2020; Caxito et al., 2021) and contradict the intracontinental evolutionary model for the province (eg, Neves et al., 2003, 2006, 2015).

7. Acknowledgments

This study was financed in part by the Coordenação de Aperfeiçoamento de Pessoal de Nível Superior (CAPES), Brasil, Finance Code 001. Support of the CAPES fellowship (grant nº 88882.347179/2019-01) and INCT Estudos Tectônicos research grant were essential for this research and the continuity of future work. RAF and FC acknowledge CNPq research fellowships. Thanks are due to Márcio Martins Pimentel (in memoriam) for the contribution.

8. References

Accioly, A.C.A., McReath, I., Santos, E.J., Guimarães, I.P., Vannuci, R., and Bottazzi, R., 2000, The Passira meta-anorthositic complex and its tectonic implication, Borborema Province, Brazil, 31st International Geological Congress, Rio de Janeiro: International Union of Geological Sciences, Abstracts.

Amaral, W.S., Santos, T.J.S., Wernick, E., Nogueira Neto, J.A., Dantas, E.L., Matteini, M., 2012. High-pressure granulites from Cariré, Borborema Province, NE Brazil: tectonic setting, metamorphic conditions and U-Pb, Lu-Hf and Sm-Nd geochronology. Gondwana Research, 22, 892-909. https://doi.org/10.1016/j.gr.2012.02.011

Ague, J.J., 1997. Thermodynamic calculation of emplacement pressures for batholithic rocks, California: Implications for the aluminum-in-hornblende barometer. Geology, 25, 563-566. https://doi.org/10.1130/0091-7613(1997)025<0563:TCOEPF>2.3.CO;2

Aleinikoff, J.N., Wintsch, R.P., Tollo, R.P., Unruh, D.M., Fanning, C.M., Schmitz, M.D., 2007. Ages and origins of rocks of Killingworth dome, South-Central Connecticut: implications

for the tectonic evolution of southern New England. American Journal of Science, 307, 63-118.

Anderson, J.L., 2017. Plagioclase-Hornblende Thermobarometry (RiMG069_Ch04_hbld_plag_thermo-jla.xls). http://www.minsocam.org/msa/RIM/RiMG069/RiMG069_Ch04_hbld_plag_thermo-jla.xls (accessed 15.07.17).

Brito, M.F.L., Mendes, V.A., Paiva, I.P., 2008. Metagranitóide Serra das Flores: magmatismo Toniano (tipo-A) no Domínio Pernambuco-Alagoas, Nordeste do Brasil. In: 44º Brazilian Geological Congress, Curitiba. Abstract in CD-ROM.

Brito, M.F.L., Freitas, S., 2011. Caracterização petrológica e geotectônica do ortognaisse Lobo no domínio Pernambuco-Alagoas, Província Borborema; Nordeste do Brasil. In: XIII Brazilian Geochemical Congress. Gramado-RS, Brazil. Extended Abstract e CD-ROM, 796-799

Brito Neves, B.B., Sial, A.N., Albuquerque, J.P.T, 1977. Vergência centrífuga residual no Sistema de Dobramentos Sergipano. Revista Brasileira de Geociências. 7(2), 102-114.

Brito Neves, B.B., Van Schmus, W.R., Santos, E.J., Campos Neto, M.C., Kozuch, M., 1995. O evento Cariris Velhos na Província Borborema: integração de dados, implicações e perspectivas. Brazilian J. Geology, 25, 279–296.

Brito Neves, B.B., Van Schmus, W.R., Fetter, A.H., 2001. Noroeste da África – Nordeste do Brasil (Província Borborema) Ensaio comparativo e problemas de correlação. Revista do Instituto de Geociências-USP. 1, 59-78. http://dx.doi.org/10.5327/S1519-874X2001000100005

Brito Neves, B.B., Silva Filho, A.F., 2019. Superterreno Pernambuco-Alagoas na Província Borborema: ensaio de regionalização tectônica. Geologia USP, Série Científica. 19(2), 3-28. https://doi.org/10.11606/issn.2316-9095.v19-148257.

Bühn, B., Pimentel, M. M., Matteini, M., Dantas, E. L., 2009. High spatial resolution analysis of Pb and U isotopes for geochronology by laser ablation multicollector inductively coupled plasma mass spectrometry (LA-MC-ICP-MS). Anais da Academia Brasileira de Ciências. 81(1), 1-16. http://dx.doi.org/10.1590/S0001-37652009000100011.

Carvalho, M.J.C., 2005. Evolução tectônica do Domínio Marancó-Poço Redondo, margem norte da Faixa Sergipana. Tese de Doutorado. Instituto de Geociências. UNICAMP, 200p.

Caxito, F.A., Uhlein, A., Dantas, E.L., 2014. The Afeição augen-gneiss suíte and the recorf of the Cariris Velhos Orogeny (1000-960 Ma) within the Riacho do Pontal fold belt, NE Brazil. Journal of South American Earth Sciences, 51, 12-27. https://doi.org/10.1016/j.jsames.2013.12.012

Caxito, F.A., Santos, L.C.M.L., Ganade, C.E., Bendaoud, A., Fettous, E.-H., Bouyo, M.H., 2020. Toward an integrated model of geological evolution for NE Brazil–NW Africa: The Borborema Province and its connections to the Trans-Saharan (Benino-Nigerian and Tuareg shields) and Central African orogens. Brazilian Journal of Geology, 50(2), 1-38. https://doi:10.1590/2317-4889202020190122

Caxito, F.A., Basto, C.F., Santos, L.C.M.L., Dantas, E.L., Medeiros, V.C., Dias, T.G., Barrote, V., Hagemann, S., Alkmim, A.R., Lana, C., 2021. Neoproterozoic magmatic arc volcanism in the Borborema Province, NE Brazil: possible flare-ups and lulls and implications for western Gondwana assembly. Gondwana Research, 92, 1-25. https://doi.org/10.1016/j.gr.2020.11.015

Cerny, J., Ramírez-Herrera, M.-T., Bógalo, M.F., Goguitchaichvili, A., Castillo-Aja, R., Morales, J., 2016. Origen, hidrodinámica y variación lateral en sedimentos de tsunami por ams, Costa Mexicana Del Pacífico. Latinmag Letters, 6, 1-7.

Chemale Jr., F., Kawashita, K., Dussin, I.A., Avila, J.N., Justino, D., Bertotti, A.L., 2012. U-Pb zircon in situ dating with LA-MC-ICP-MS using a mixed detector configuration. Anais

da Academia Brasileira de Ciências. 84, 275-295. http://dx.doi.org/10.1590/S0001-37652012005000032.

Compston, W., Williams, I.M., Myer, C., 1984. U-Pb geochronology of zircons from lunar breccia 73217 using a sensitive high mass-resolution ion microprobe. Journal of Geophysical Research, 89B, 525-534. https://doi.org/10.1029/JB089iS02p0B525

Cornell, R.M., Schwertmann, U. 2003. The Iron Oxides, Second edition. Weinheim: Wiley VCH, 664 p.

Cruz, R.F., Acciolly, A.C.A., 2013. Petrografia, geoquímica e idade U/Pb do Ortognaisse Rocinha, no Domínio Pernambuco-Alagoas W da Província Borborema. Estudos Geológicos 23 (2), 3-27.

Cruz, R.F., Pimentel, M.M., Accioly, A.C.A., Rodrigues, J.B., 2014. Geological and isotopic characteristics of granites from the Western Pernambuco-Alagoas Domain: implications for the crustal evolution of the Neoproterozoic Borborema Province. Brazilian Journal of Geology, 44(4), 627-652. https://doi.org/10.5327/Z2317488920140004008.

Dáttoli, L.C., 2017. Geologia, petrologia e geoquímica do ortognaisse Maravilha, domínio Pernambuco-Alagoas. Dissertação de Mestrado. Pós-graduação em geociências, UFPE, 123p.

Davison, I., Santos, R.S, 1989. Tectonic evolution of the Sergipano belt, NE do Brasil, during the brasiliano orogeny. Precambrian Research. 45, 319-342. https://doi.org/10.1016/0301-9268(89)90068-5.

Deer, W.A., Howie, R.A., Zussman, J. 1992. An introduction to the rock forming minerals, 2nd ed. Longman, London. 696 pp.

D'el-Rey Silva, L.J.H, 1995. Tectonic evolution of the Sergipano Belt, NE Brazil. Geologia. 25(4), 315-332.

Gioia, S.M.C.L., Pimentel, M.M., 2000. The Sm-Nd isotopic method in the Geochronology Laboratory of the University of Brasília. Anais da Academia Brasileira de Ciências. 72(2), 219-245. http://dx.doi.org/10.1590/S0001-37652000000200009.

Guimarães, I.P, Brito, M.F.L, Lages, G.A., Silva Filho, A.F., Santos, L., Brasilino, R.G., 2016. Tonian granitic magmatism of the Borborema Province, NE Brazil: A review. Journal of South American Earth Sciences 68, 97-112. https://doi.org/10.1016/j.jsames.2015.10.009

Holland, T., Blundy, J. 1994. Non-ideal interactions in calcic amphiboles and their bearing on amphibole-plagioclase thermometry. Contributions to Mineralogy and Petrology. 116, 433-447.

Hollanda, M.H.B.M., Archanjo, C.J., Souza, L.C., Dunyi, L., and Armstrong, R.A., 2011, Long lived Paleoproterozoic granitic magmatism in the Serido-Jaguaribe domain, Borborema province NE Brazil: Journa of South America Earth Sciences, v. 32, p. 287–300. https://doi:10.1016/j. jsames.2011.02.008.

Jackson, S.E., Pearson, N.J., Griffin, W.L., Belousova, E.A., 2004. The application of laser ablation inductively coupled plasma-mass spectrometry to in situ U-Pb zircon geochronology. Chemical Geology. 211, 47-69. https://doi.org/10.1016/j.chemgeo.2004.06.017

Janoušek, V., Moyen, J.-F., Erban, V. & Hora, J. 2019. GCDkit Goes Platform Independent! Abstracts of the Goldschmidt Conference, Barcelona, Spain.

Kozuch, M., 2003. Isotopic and trace element geochemistry of Early Neoproterozoic gneissic and metavolcanic rocks in the Cariris Velhos Orogen of the Borborema Province, Brazil, and their bearing tectonic setting (PhD thesis). Kansas University, Lawrence, p. 199.

Lages, G.A., Dantas, E.L., 2016. Floresta and Bodocó Mafic-Ultramafic Complexes, western Borborema Province, Brazil: geochemical and isotope constraints for evolution of a

Neoproterozoic arc environment and retro-eclogitic hosted Ti-mineralization. Precambrian Research, 280, 95-119.

Leake, B.E., Woolley, A.R., Arps, C.E.S., Birch, W.D., Gilbert, M.C., Grice, J.D., Hawthorne, F.C., Kato, A., Kisch, H.J., Krivovichev, V.G., Linthout, K., Laird, J., Mandarino, J.A., Maresch, W.V., Nickel, E.H., Rock, N.M.S., Schumacher, J.C., Smith, D.C., Stephenson, N.C.N., Ungaretti, L., Whittaker, E.J.W., Youzhi, G. 1997. Nomenclature of amphiboles: Report of the Subcommittee on Amphiboles of the International Mineralogical Association, Commission on New Minerals and Mineral Names. American Mineralogist. 82, 1019-1037.

Lima, H.M., Pimentel, M.M., Santos, L.C.M.L., Mendes, V.A., 2017. Análise tectônica da porção nordeste da Faixa Sergipana, Província Borborema: dupla vergência em resposta a colisão oblíqua entre o Cráton do São Francisco e o Terreno Pernambuco-Alagoas. Geonomos, 25(2), 20-30.

Lima, H.M., Pimentel, M.M., Fuck, R.A., Santos, L.C.M.L., Dantas, E.L., 2018. Geochemical and detrital zircon geochronological investigation of the metavolcanosedimentary Araticum complex, Sergipano fold belt: Implications for the evolution of the Borborema Province, NE Brazil. Journal of South American Earth Sciences, 86, 176-192. https://doi.org/10.1016/j.jsames.2018.06.013

Lima, M.V.A.G., Berrocal, J., Soares, J.E.P., Fuck, R.A., 2015. Deep seismic refraction experiment in northeast Brazil: New constraints for Borborema province evolution. Journal of South American Earth Sciences, 58, 335-349. https://doi.org/10.1016/j.jsames.2014.10.007

Ling, X.-X., Schmädicke, E., Li, Q.-L., Gose, J., Wu, R.-H., Wang, S.-Q., Li, X.-H. 2015. Age determination of nephrite by in-situ SIMS U–Pb dating syngenetic titanite: A case study of

the nephrite deposit from Luanchuan, Henan, China. Lithos. 220-223, 289-299. https://doi:10.1016/j.lithos.2015.02.019

Liz, L.C.C., Machado, A., Liz, J.D., Almeida, J.M., 2018. Petrografia e geoquímica dos ortoanfibolitos das unidades Gentileza, Domínio Canindé, Faixa de Dobramentos Sergipana, Nordeste brasileiro. Pesquisas em Geociências. 45, 1-27. https://doi.org/10.22456/1807-9806.88650.

Ludwig, K.R., 2003. User's Manual for Isoplot/Ex version 3.00 – A Geochronology Toolkit for Microsoft Excel, No. 4. Berkeley Geochronological Center, Special Publication, 70p.

Marshak, S., 2019. Earth: Portrait of a Planet. 6ed. New York: W. W. Norton & Company, 1008p.

Nascimento, R.S., 2005. Domínio Canindé, Faixa Sergipana, Nordeste do Brasil: um estudo geoquímico e isotópico de uma sequência de rifte continental Neoproterozóica. Tese de Doutorado, Instituto de Geociências, Universidade de Campinas, Campinas, 159p.

Nelson, S. A. 2004. Metamorphic Rocks- Classification, Field Gradients, & Facies. Lecture Note, Earth and Environmental Sciences 2120, Petrology. Available in: http://www.tulane.edu/~sanelson/eens212/metaclassification&facies.htm

Neves, S.P., 2003. Proterozoic history of the Borborema Province (NE Brazil): correlations with neighboring Cratons and Pan-African belts and implications for the evolution of western Gondwana. Tectonics, 22, 1031-1044. https://doi.org/10.1029/2001TC001352

Neves, S.P., Bruguier, O., Vauchez, A., Bosch, D., Silva, J.M.R., Mariano, G., 2006. Timing of crustal formation, deposition of supracrustal sequences and Transamazonian and Brasiliano metamorphism in eastern Borborema Province (NE Brazil): Implications for western Gondwana assembly. Precambrian Research, 149, 197-216. https://doi.org/10.1016/j.precamres.2006.06.005

Neves, S.P., Bruguier, O., Silva, J.M.R., Mariano, G., Da Silva Filho, A.F., Teixeira, C.M.L., 2015. From extension to shortening: dating the onset of the Brasiliano Orogeny in eastern Borborema Province (NE Brazil Journal of South American Earth Sciences, 58, 238-256. https://doi.org/10.1016/j.jsames.2014.06.004

Neves, S.P., Silva, J.M.R., Bruguier, O., 2016. The transition zone between the Pernambuco-Alagoas Domain and the Sergipano Belt (Borborema Province, NE Brazil): geochronological constraints on the ages of deposition, tectonic setting and metamorphism of metasedimentary rocks. Journal of South American Earth Sciences, 72, 266-278. https://doi.org/10.1016/j.jsames.2016.09.010

Oliveira, E.P., Windley, B.F., Araújo, M.N.C., 2010. The Neoproterozoic Sergipano orogenic belt, NE Brazil: a complete plate tectonic cycle in western Gondwana. Precambrian Research. 181, 64–84. https://doi.org/10.1016/j.precamres.2010.05.014

Oliveira, E.P., McNaughton, N.J., Windley, B.F., Carvalho, M.J., Nascimento, R.S., 2015. Detrital zircon U–Pb geochronology and whole-rock Nd-isotope constraints on sediment provenance in the Neoproterozoic Sergipano orogen, Brazil: From early passive margins to late foreland basins. Tectonophysics 662: 183–194. https://doi.org/10.1016/j.tecto.2015.02.017

Oliveira, E.P., Windley, B.F., McNaughton, N.J., Bueno, J.F., Nascimento, R.S., Carvalho, M.J., Araújo, M.N.C, 2017. The Sergipano Belt, in: Heilbron, M., Cordani, U.G., Alkmin, F.F. (Eds.), São Francisco Craton, Eastern Brazil. Regional Geology Reviews, pp. 241–254. https://doi.org/10.1007/978-3-319-01715-0_13.

Owona, S., Mbola-Ndzana, S.P., Mpesse, J.E., Mvondo-Ondoa, J., Schulz, B., Pfänder, J., Jegouzo, P., Affaton, P., Ratschbacher, L., Ekodeck, G.E. 2013. Petrogenesis of amphibolites from the Neoproterozoic Yaounde Group (Cameroon, Central Africa):

Evidence of MORB and implications on their geodynamic evolution. Comunicações Geológicas. 100, 5-13.

Padilha, A.L., Vitorello., Í., Pádua, M.B., Marcelo., Fuck, R.A., 2016. Deep magnetotelluric signatures of the early Neoproterozoic Cariris Velhos tectonic event within the Transversal sub-province of the Borborema Province, NE Brazil. Precambrian Research, 275, 7-83. https://doi.org/10.1016/j.precamres.2015.12.012

Passos, L.H., 2016. Caraterização petrográfica, química mineral e geotermobarometria de rochas da Unidade Novo Gosto, Domínio Canindé, Faixa de Dobramentos Sergipana. Dissertação de Mestrado, Instituto de Geociências, Universidade de Brasília, Brasília. 225p.

Passos, L.H., Fuck, R.A., Chemale Jr., F., Lenz, C., Pimentel, M.M., Machado, A., Pinto, V.M., 2021. Neoproterozoic (740-690 Ma) Arc-Back-Arc Magmatism in the Sergipano belt, Southern Borborema, Brazil. Journal of South American Earth Sciences, Submitted.

Pinto, V.M., Koester, E., Debruyne, D., Chemale Jr., F., Marques, J.C., Passos, L.H., Lenz, C., 2020. Petrogenesis of the mafic-ultramafic Canindé layered intrusion, Sergipano Belt, Brazil: Constraints on the metallogenesis of the associated Fe–Ti oxide ores. Ore Geology Reviews, 122. https://doi.org/10.1016/j.oregeorev.2020.103535

Piper, J. D. A., 1987. Paleomagnetism and the continental crust. Wiley, New York – Toronto, 434p.

Rasmussen, B., Fletcher, I.R., Muhling, J.R. 2013. Dating deposition and low-grade metamorphism by in situ U/Pb geochronology of titanite in the Paleoproterozoic Timeball Hill Formation, southern Africa. Chemical Geology. 351, 29-39.

Sá, J.M., McReath, I., and Leterrier, J., 1995. Petrology, geochemistry and tectonic setting of Proterozoic Igneous suites of the Orós fold belt (Borborema Province, Northeast Brazil):

Journal of South American Earth Sciences, v. 8, p. 299–314. https://doi:10.1016/0895-9811(95)00015-8

Sá, J.M., Bertrand, J.M., Leterrier, J., and Macedo, M.H.F., 2002. Geochemistry and geochronology of pre-Brasiliano rocks from the Transversal Zone, Borborema Province, Northeast Brazil: Journal of South America Earth Sciences, v. 14, p. 851–866. https://doi:10.1016/S0895-9811(01)00081-5.

Santos, E.J., 1995. O complexo granítico Lagoa das Pedras: acresção e colisão na região de Floresta (Pernambuco), Província Borborema (PhD thesis). Instituto de Geociências da Universidade de São Paulo, São Paulo, p. 228.

Santos, A.C.L., Padilha, A. L., Fuck, R. A., Pires, A. C. B., Vitorello, I., Pádua, M. B., 2014. Deep structure of a stretched lithosphere: Magnetotelluric imaging of the southeastern Borborema province, NE Brazil. Tectonophysics, 610, 39-50. https://doi.org/10.1016/j.tecto.2013.10.008

Santos, R.A., Martins, A.A.M., Neves, J.P., 1998. Geologia e recursos minerais do estado de Sergipe. CPRM/Codise. 107p.

Santos, T.J.S., Fetter, A.H., and Nogueira Neto, J.A., 2008. Comparisons between the northwestern Borborema Province, NE Brazil, and the southwestern Pharusian-Dahomey Belt, SW Central Africa: Geological Society of London Spececial Publications, 294, p. 101–119. https://doi:10.1144/SP294.6

Santos, L.C.M.L., Dantas, E.L., Santos, E.J., Santos, R.V., Lima, H.M., 2015. Early to late Paleoproterozoic magmatism in NE Brazil: The Alto Moxoto Terrane and its tectonic implications for the pre-Western Gondwana assembly: Journal of South America Earth Sciences, 58, 188-209. https://doi:10.1016/j.jsames.2014.07.006

Santos, M.M., Lana, C., Scholz, R., Buick, I., Schmitz, M.D., Kamo, S.L., Gerdes, A., Corfu, F., Tapster, S., Lancaster, P., Storey, C.D., Basei, M.A.S., Tohver, E., Alkmim, A., Nalini,

H., Krambrock, K., Fantini, C., Wiedenbeck, M., 2017. A New Appraisal of Sri Lankan BB Zircon as a Reference Material for LA-ICP-MS U-Pb Geochronology and Lu-Hf Isotope Tracing. Geostandards and Geoanalytical Research., 41(3), 335-358.

Silva Filho, M.A., 1998. Arco vulcânico Canindé-Marancó e a Faixa Sul-Alagoana: sequências orogênicas Mesoproterozóicas. Anais 50º Congresso Brasileiro de Geologia, 1998, Belo Horizonte. p.16.

Silva Filho, A.F., Guimarães, I.P., Van Schmus, W.R., 2002. Crustal evolution of the Pernambuco-Alagoas complex, Borborema Province, NE Brasil: Nd isotopic data from Neoproterozoic granitoids. Gondwana Research, 5(2), 409-422. https://doi.org/10.1016/S1342-937X(05)70732-2

Silva Filho, A.F., Guimarães, I.P., Van Schmus, W.R., Armstrong, R.A., Santos, L.S., Concentino, L.M., Lima, D., 2014. Shrimp oxygen, U-Pb, and Hf data of Tonian orthogneiss, evidence of juvenile crust in the Pernambuco e Alagoas domain of the Borborema Province, NE Brazil. In: 9th South American Symposium on Isotope Geology. Program and Abstracts, 95.

Sláma, J., Kosler, J., Condon, D.J., Crowley, J.L., Gerdes, A., Hanchar, J.M., Horstwood, M.S.A., Morris, G.A., Nasdala, L., Norberg, N., Schaltegger, U., Schoene, B., Tubrett, M.N., Whitehouse, M.J., 2008. Plesovice zircon - a newnatural reference material for U-Pb and Hf isotopic microanalysis. Chemical Geology, 249(1-2),1-35. https://doi:10.1016/j.chemgeo.2007.11.005.

Souza Júnior, F.D., 2013. Mapeamento geológico da porção central do domínio Canindé, Cinturão Orogênico Sergipano, NE-Brasil. Trabalho de Conclusão de Curso, Geologia Bacharelado, Universidade Federal de Sergipe, São Cristóvão. 64p.

Stacey, J.S., Kramer, J.D., 1975. Approximation of terrestrial lead isotope evolution by a two-stage model. Earth and Planetary Science Letters, 26, 207-221. https://doi.org/10.1016/0012-821X(75)90088-6

Trompette, R., 1994. Geology of Western Gondwana (2000-500): Pan-African-Brasiliano Aggregation of South America and Africa. 1 ed. Balkema, Rotterdam, 364p.

Van Achterbergh, E., Ryan, C.G., Jackson, S.E., Griffin, W.L., 2001. Data reduction software for LA-ICP-MS: appendix P.J. Sylvester (Ed.), Laser Ablation-ICP-mass spectrometry in the Earth Sciences: principles and applications, MAC Short Courses Series, Ottawa, Ontario, Canada, 239-243.

Van Schmus, W.R., Brito Neves, B.B., Hackspacher, P.C., Babinski, M., 1995. U/Pb and Sm/Nd geochronologic studies of Eastern Borborema Province, northeastern Brazil: Initial conclusions: Journal of South America Earth Sciences, 8, 267-288. https://doi:10.1016/0895-9811(95)00013-6.

Van Schmus W.R., Oliveira E.P., Silva Filho A.F., Toteu F., Penaye J., Guimarães I.P., 2008. Proterozoic Links between the Borborema Province, NE Brazil, and the Central African Fold Belt. Geological Society, London, Special Publication, 294, 69-99. https://doi.org/10.1144/SP294.5

Vermeesch, P., 2018. IsoplotR: a free and open toolbox for geochronology. Geoscience Frontiers, 9, 1479-1493. https://doi.org/10.1016/j.gsf.2018.04.001.

Zane, A., Weiss, Z., 1998. A procedure for classifying rock-forming chlorites based on microprobe data. Rendiconti Lincei Scienze Fisiche e Naturali Serie, 9(1):51-56. http://dx.doi.org/10.1007/BF02904455

Williams, I.S., 1998. U-Th-Pb geochronology by ion microprobe. In: McKibben MA, Shanks III WC and Rydley WI (Eds), Applications of Microanalytical Techniques to Understanding Mineralizing Processes. Reviews in Economic Geology, 7, 1-35.

Yavuz, F., Döner, Z. 2017. WinAmptb: A Windows program for calcic amphibole thermobarometry. Periodico di Mineralogia. 86, 135-167. https://doi.org/10.2451/2017PM710.

Yavuz, F., Kumral, M., Karakaya, N., Karakaya, M.Ç, Yildirim, D.K. 2015. A Windows program for chlorite calculation and classification. Computers & Geosciences, 81, 101-113. https://doi.org/10.1016/j.cageo.2015.04.011

CAPÍTULO IV – Considerações Finais

Muitas controvérsias ainda existem sobre os processos de formação das rochas do domínio Canindé. Nesta tese são apresentadas novas informações investigando as rochas da unidade Novo Gosto, constituinte importante do domínio:

- Os anfibolitos que compõem a unidade são finos a muito finos e geralmente mostram foliação bem marcada, com ocorrência de anfibolitos foliados e anfibolitos bandados, o último gerado por intercalação com rochas calciossilicáticas e quartzo-feldspáticas. A ocorrência local de micrólitos suporta origem vulcânica a sub-vulcânica para seus protólitos. Geoquímica e petrografia corroboram que os protólitos dessas rochas são de composição basáltica e que elas foram recristalizadas sob condições metamórficas de fácies anfibolito, com retrogressão para condições de fácies xisto-verde próximo a zonas de cisalhamento.
- Idade U-Pb em zircão obtida em uma amostra de anfibolito foi definida em 743±3 Ma, corroborando dados de campo e literatura que já sugeriam sua idade como mais antiga que as outras unidades do domínio.
- Dados de isótopos de Nd retornam valores positivos de ε_{Nd} (740 Ma), variando de +4.93 a 0.42 e T_{DM} de 0.97 a 1.33 Ga, indicando fontes com dominância de material mantélico sem ou com pouca contaminação crustal de uma fonte mesoproterozoica a cedo-neoproterozoica em diferentes proporções.
- Amostras analisadas foram classificadas como rochas basálticas toleíticas de alto Fe, mostrando aumento no *trend* geoquímico em direção ao campo das rochas ácidas e alcalinas. Os dados geoquímicos indicam três grupos diferentes: Grupo 1 é dominantemente mais depletado em elementos incompatíveis e mostra padrão similar a IAB; Grupo 2 tem padrão similar ao Grupo 1, mas com anomalias mais evidentes e variações no grau de enriquecimento de elementos incompatíveis; Grupo 3 tem um padrão mais rico em elementos incompatíveis do que o Grupo 1, sendo mais plano e com depleções de HFSE mais suaves e se assemelha a E-MORB, mas mais enriquecido.
- Os anfibolitos da unidade Novo Gosto são interpretados como formados em configuração tectônica de arco-retroarco continental, similar aos arco-retroarcos Ryukyu-Okinawa e Kamtchatka, registrando pela primeira vez, evento convergente no início de Orogênese Brasiliana no sul da Província Borborema.

- Idades de cristalização cedo-Toniana (989.68±6.36, 1005.68±3.75 e 988.58±16.13) foram pela primeira vez identificadas em anfibolito e granito milonítico no domínio Canindé. As rochas de idade cedo-Toniana afloram próximo à zona de cisalhamento Mulungu-Alto Bonito, próximo ao contato com o domínio Poço-Redondo-Marancó, e possivelmente representam fatias desse domínio justapostos ao domínio Canindé durante evento colisional.
- A área-fonte principal para as rochas metassedimentares foi investigada, usando idades U-Pb de zircão detrítico e isótopos de Nd. As idades U-Pb revelaram que a mais provável e importante área-fonte para a paleobacia Novo Gosto tinha idades de 962-978 Ma. Menor quantidade de detritos provinda de área-fonte do Paleoproterozoico e Neoarqueano foi identificada também (1974-2624 Ma). Áreas-fonte de idades cedo-Tonianas são bem conhecidas na região, ocorrendo também como raro embasamento no domínio Canindé, mas como área principal de afloramento no domínio adjacente Poço Redondo-Marancó e em outras áreas do superterreno Pernambuco-Alagoas e Sul da Província Borborema. Rochas paleoproterozoicas e neoarqueanas ocorrem mais restritas no Sul da Borborema, a maior parte em domos. Isótopos de Nd confirmam as duas áreas-fontes e uma importante mistura sedimentar de detritos provenientes das duas fontes.
- A idade máxima deposicional obtida para a paleobacia Novo Gosto é 712±23 Ma, ocorrendo em outras amostras valores de 886±9.7, 858±10 Ma e 780.4±6.1 Ma, que podem ser reflexo de longo tempo de sedimentação da paleobacia ou influência de diferentes áreas-fontes na paleobacia.
- A evolução tectono-metamórfica da unidade Novo Gosto é caracterizada com trajetória P-T no sentido horário, com condições metamórficas variando principalmente em torno de 600-740 ºC e 3.5-10.0 kbars, com pico metamórfico compatível com fácies anfibolito superior. E valores variando principalmente em torno de 636-808 ºC e 7.0-12.0 kbars para milonitos. As condições metamórficas mínimas impressas nessas rochas é T: 390 °C e P: 2.5 kbars, características de fácies xisto verde, e possivelmente relacionado ao soerguimento do terreno metamórfico. O trajeto de distribuição dos dados de P-T das amostras é compatível com um arco vulcânico evoluindo para ambiente de cinturão de montanhas continental. O pico metamórfico foi datado em 682.84±3.91 Ma ($^{207}Pb/^{206}Pb$ idade de zircão/ LA-ICPMS).

- Idades do magmatismo pré-colisional (~740-680 Ma) obtidas na unidade Novo Gosto, Intrusão Gabróica Acamadada Canindé, e nos metagranitos Garrote, Gentileza e Curralinho/Boa Esperança.

Apesar de os novos dados trazerem importantes informações e avanço na compreensão da evolução geológica na região do Domínio Canindé e Faixa Sergipana, é necessário realizar trabalhos exploratórios adicionais na região para consolidar as novas interpretações e melhor contextualizar as relações com as faixas vizinhas.

Devido ao domínio ter grande extensão e poucas vias de acesso, ainda há muito o que se trabalhar, principalmente na região noroeste do domínio, região pouco explorada por estudos de petrografia, geoquímica e de isótopos. E como há poucos trabalhos regionais e específicos na região no geral, é comum ocorrerem conflitos entre nomes de unidades para rochas possivelmente de origem comum, pelas dificuldades de discernir algumas unidades em campo.

REFERÊNCIAS BIBLIOGRÁFICAS

ALMEIDA, F. F., HASUI, Y., BRITO NEVES, B. B., 1976. The Upper Precambrian of South America. Boletim IG, Instituto de Geociências da USP, v. 7, p. 45-80.

ALMEIDA, F.F.M., HASUI, Y., BRITO NEVES, B.B., FUCK, R.A., 1981. Brazilian structural provinces: an introduction. Earth Science Reviews 18, 1-29.

AMARAL, W.S., SANTOS, T.J.S.,WERNICK, E., NOGUEIRA NETO, J.A., DANTAS, E.L., MATTEINI, M. 2012. High-pressure granulites from Cariré, Borborema Province, NE Brazil: tectonic setting, metamorphic conditions and U-Pb, Lu-Hf and Sm-Nd geochronology. Gondwana Research 22, 892-909.

BEZERRA, F. H. R., 1992. Geologia e evolução petrológicado Complexo Gabróico Canindé do São Francisco e rochas adjacentes (Sergipe e Alagoas). Dissertação (Mestrado) – Universidade de Brasília, Instituto de Geociências. Brasília, 208 p.

BRITO NEVES, B. B. de, CORDANI, U. G., 1973. Problemas geocronológicos do "Geossinclinal Sergipano" e do seu embasamento. Anais XXVII Congr. Bras. Geol., v. 2, p. 67-76, Aracaju.

BRITO NEVES, B. B., SIAL, A. N., ALBUQUERQUE, J. P. T., 1977. Vergência centrífuga residual no Sistema de Dobramentos Sergipano. Revista Brasileira de Geociências, Vol.7, pp. 102-114.

BRITO NEVES, B.B., CORDANI U.G., 1991. Tectonic evolution of South America dur-ing the Late Proterozoic. Precambrian Research, v.53, n.1-2, p.23-40.

BRITO NEVES, B. B., VAN SCHMUS, W. R., SANTOS, E. J., CAMPOS NETO, M. C., KOZUCH, M., 1995. O evento Cariris Velho na Província Borborema: integração de dados, implicações e perspectivas. Revista Brasileira de Geociências, v. 25, n. 4, p. 279-296.

BRITO NEVES, B.B., SANTOS, E.J., SCHMUS, W.R.Q., 2000. Tectonic history of the Borborema Province. In: Umberto Cordani; Edson José Milani; Antonio Thomaz Filho; Diogenes de Almeida Campos (Org.). Tectonic Evolution of South America. Rio de Janeiro: 31st International Geological Congress, pp. 151-182. Special Publication.

BRITO NEVES, B.B., CAMPOS NETO, M.C.C., VAN SCHMUS, W.R., FERNANDES, M.G.G., SOIZA, S.L. 2001. O Terreno Alto Moxotó no leste da Paraíba (Maciço Caldas Brandão). Revista Brasileira de Geociências 31, 185-194.

BRITO NEVES, B.B., SILVA FILHO, A.F, 2019. Superterreno Pernambuco-Alagoas na Província Borborema: ensaio de regionalização tectônica. Geologia USP, Série Científica, 19(2), 3-28. https://doi.org/10.11606/issn.2316-9095.v19-148257

BEZERRA, F.H.R., Nilson, A.A., Blais, S. et al., 1991. Petroquímica de elementos maiores e traços do complexo gabróico Canindé e sequência metavulcano-sedimentar encaixante (SE-AL). Anais III Congresso Brasileiro de Geoquímica, São Paulo, v.1, pp. 181-184.

CARVALHO, M. J., 2005. Evolução tectônica do domínio Marancó - Poço Redondo: Registro das orogêneses Cariris Velhos e Brasiliana na Faixa Sergipana, NE do Brasil. Tese de Doutorado em Geociências – Instituto de Geociências, Universidade Estadual de Campinas. Campinas, 202p.

CAXITO, F.A., UHLEIN, A., DANTAS, E.L. 2014. The Afeição augen-gneiss suíte and the recorf of the Cariris Velhos Orogeny (1000-960 Ma) within the Riacho do Pontal fold belt, NE Brazil. Journal of South American Earth Sciences 51, 12-27.

CAXITO, F.A., SANTOS, L.C.M.L., GANADE, C.E., BENDAOUD, A., FETTOUS, E.-H., BOUYO, M.H. 2020. Toward an integrated model of geological evolution for NE Brazil–NW Africa: The Borborema Province and its connections to the Trans-Saharan

(Benino-Nigerian and Tuareg shields) and Central African orogens. Brazilian Journal of Geology. 50(2), 1-38. https://doi:10.1590/2317-4889202020190122

CAXITO, F.A., BASTO, C.F., SANTOS, L.C.M.L., DANTAS, E.L., MEDEIROS, V.C., DIAS, T.G., BARROTE, V., HAGEMANN, S., ALKMIM, A.R., LANA, C., 2021. Neoproterozoic magmatic arc volcanism in the Borborema Province, NE Brazil: possible flare-ups and lulls and implications for western Gondwana assembly. Gondwana Research, 92, 1-25. https://doi.org/10.1016/j.gr.2020.11.015

DAVISON, I., SANTOS, R. A., 1989 Tectonic Evolution of the Sergipano Fold Belt, NE Brazil, during the Brasiliano Orogeny. Precambrian Research, v. 45, p. 319-342.

D'EL-REY SILVA, L. J. H., MCCLAY, K. R., 1995. Stratigraphy of the Southern part of the Sergipano Belt, NE Brazil: tectonic implications. Revista Brasileira de Geociências, São Paulo, v. 25, n. 3, p. 185-202.

D'EL-REY SILVA, L. J. H., 1995. Tectonic evolution of the Sergipano Belt, NE Brazil. Revista Brasileira de Geociências, v. 25, n. 4, p. 119-129.

DELGADO, I. M., SOUZA, J. D., SILVA, L. C., FILHO, N. C. S., SANTOS, R. A., PEDREIRA, A. J., GUIMARÃES, J. T., ANGELIM, L. A. A., VASCONCELOS, A. M., GOMES, I. P., FILHO, J. V. L., VALENTE, C. R., PERROTTA, M. M., HEINECK, C. A., 2003. Geotectônica do Escudo Atlântico. In: BIZZA, L. A., SCHOBBENHAUS, C., VIDOTTI, R. M., GONÇALVES, J. H. (Eds.) Geologia, Tectônica e Recursos Minerais do Brasil. CPRM, Brasília, p. 227-334.

JARDIM DE SÁ, E. F., MORAES, J. A. C., SILVA, L. J. H. D., 1986. Tectônica tangencial na Faixa Sergipana. In: SBG, Congresso Brasileiro de Geologia. Anais (3), p. 1246.

KOZUCH, M., BITTAR, S.M.B., VAN SCHMUS, W.R., BRITO NEVES, B.B., 1997. Magmatismo do Mesoproterozóico Médio e Neoproterozóico médio na Zona

Transversal da província de Borborema, Brasil. XVII Simpósio de Geologia do Nordeste, Soc. Bras. de Geol., Fortaleza, Brasil.

KOZUCH, M., 2003. Isotopic and trace element geochemistry of Early Neoproterozoic gneissic and metavolcanic rocks in the Cariris Velhos Orogen of the Borborema Province, Brazil, and their bearing tectonic setting (PhD thesis). Kansas University, Lawrence, p. 199.

LAGES, G.A., DANTAS, E.L. 2016. Floresta and Bodocó Mafic-Ultramafic Complexes, western Borborema Province, Brazil: geochemical and isotope constraints for evolution of a Neoproterozoic arc environment and retro-eclogitic hosted Ti-mineralization. Precambrian Research 280, 95-119.

LEITE, P.R.B., BERTRAND, J.M., LIMA E.S., LETERRIER, E.J., 2000. Timing of granitic magmatism in the Northern Borborema Province, Brazil: AU - Pb study of granitoids from the Alto Pajeú Land. J. South Am. Earth Sci., 13, 549 - 559.

LIMA, H.M., PIMENTEL, M.M., SANTOS, L.C.M.L., MENDES, V.A., 2017. Análise tectônica da porção nordeste da Faixa Sergipana, Província Borborema: dupla vergência em resposta a colisão oblíqua entre o Cráton do São Francisco e o Terreno Pernambuco-Alagoas. Geonomos, 25(2), 20-30.

LIMA, H. M., 2018. Evolução tectônica da porção nordeste da Faixa Sergipana, Província Borborema, Estado de Alagoas, NE do BRASIL. Tese de doutorado em Geologia Regional – Programa de Pós-Graduação em Geologia, Instituto de Geociências, Universidade de Brasília. Brasília, 161p.

LIMA, H.M., PIMENTEL, M.M., FUCK, R.A., SANTOS, L.C.M.L., DANTAS, E.L., 2018. Geochemical and detrital zircon geochronological investigation of the metavolcanosedimentary Araticum complex, Sergipano fold belt: Implications for the

evolution of the Borborema Province, NE Brazil. Journal of South American Earth Sciences, 86, 176-192. https://doi.org/10.1016/j.jsames.2018.06.013

LIMA, M.V.A.G., BERROCAL, J., SOARES, J.E.P., FUCK, R.A. 2015. Deep seismic refraction experiment in northeast Brazil: New constraints for Borborema province evolution. Journal of South American Earth Sciences 58, 335-349.

LIZ, L.C.C., 2017. Petrografia e geoquímica dos ortoanfibolitos das unidades Novo Gosto e Gentileza, domínio Canindé, Faixa de Dobramentos Sergipana, NE-Brasil. Dissertação de Mestrado em Geociências, Programa de Pós-Graduação de Geociências e Análise de Bacias, Universidade Federal de Sergipe. São Cristóvão, 66p.

MABESSONE, J. M., 2002. História geológica da Província Borborema (NE Brasil). Revista de Geologia, v. 15, p. 119-129.

MENDES, V. A., LIMA, M. A. B., MORAIS, D. M. F., 2017. Programa Geologia do Brasil - PGB. Mapa Geológico do Estado de Alagoas. Escala 1:250.000. Recife: CPRM.

MENDES, V. A., LIMA, M. A. B., MORAIS, D. M. F., 2017. Programa Geologia do Brasil - PGB. Geologia e Recursos Minerais do Estado de Alagoas. Escala 1:250.000. Recife: CPRM.

NASCIMENTO, R. S., 2005. Domínio Canindé, Faixa Sergipana, Nordeste do Brasil: um estudo geoquímico e isotópico de uma sequência de rifte continental Neoproterozóica. Tese de Doutorado em Metalogênese, Instituto de Geociências, Universidade Estadual de Campinas. Campinas, 159p.

NEVES, S.P., 2003. Proterozoic history of the Borborema Province (NE Brazil): correlations with neighboring Cratons and Pan-African belts and implications for the evolution of western Gondwana. Tectonics 22, 1031-1044.

NEVES, S.P., BRUGUIER, O., VAUCHEZ, A., BOSCH, D., SILVA, J.M.R., MARIANO, G., 2006. Timing of crustal formation, deposition of supracrustal sequences and

Transamazonian and Brasiliano metamorphism in eastern Borborema Province (NE Brazil): Implications for western Gondwana assembly. Precambrian Reearch. 149, 197-216.

NEVES, S.P., COELHO, V.A., 2010. Geochemistry of orthogneisses and metasedimentary rocks across a proposed terrane boundary in the Central Domain of Borborema Province, NE Brazil: Geodynamic implications. Journal of South American Earth Sciences. v. 29, p. 498-511.

NEVES, S.P., BRUGUIER, O., SILVA, J.M.R., MARIANO, G., DA SILVA FILHO, A.F., TEIXEIRA, C.M.L., 2015. From extension to shortening: dating the onset of the Brasiliano Orogeny in eastern Borborema Province (NE Brazil Journal of South American Earth Sciences 58, 238-256.

OLIVEIRA, E. P., TARNEY, J., 1990. Petrogenesis of the Canindé de São Francisco Complex: a major late Proterozoic gabbroic body in the Sergipe Fold Belt, northeastern Brazil. Journal of South American Earth Sciences, v. 3, n. 2/3, p. 125-140.

OLIVEIRA, E. P., TOTEU, S. F., ARAÚJO, M. N. C., CARVALHO, M. J., NASCIMENTO, R. S., BUENO, J. F., MCNAUGHTON, N., BASILICI, G., 2006. Geologic correlation between the Neoproterozoic Sergipano belt (NE Brazil) and the Yaoundé schist belt (Cameroon, Africa). Journal of African Earth Sciences, v. 44, p. 470–478.

OLIVEIRA, R. G., 2008. Arcabouço geofísico, isostasia e causas do magmatismo cenozoico da Província Borborema e sua margem continental (nordeste do Brasil). Tese de Doutorado, Instituto de Geociências, Universidade Federal do Rio Grande do Norte, 411 p.

OLIVEIRA, E. P., WINDLEY, B. F., ARAUJO, M. N. C., 2010. The Neoproterozoic Sergipano orogenic belt, NE Brazil: a complete plate tectonic cycle in western Gondwana. Precambrian Research, v.181, p. 64-84.

OLIVEIRA, E. P., MCNAUGHTON, N. J., WINDLEY, B. F., CARVALHO, M. J., NASCIMENTO, R. S., 2015. Detrital zircon U–Pb geochronology and whole-rock Nd-isotope constraints on sediment provenance in the Neoproterozoic Sergipano orogen, Brazil: From early passive margins to late foreland basins. Tectonophysics, v. 662, p 183–194.

OLIVEIRA, E. P., WINDLEY, B. F., MCNAUGHTON, N. J., BUENO, J. F., NASCIMENTO, R. S., CARVALHO, M. J., ARAÚJO, M. N. C., 2017. The Sergipano Belt. In: HEILBRON, M., CORDANI, U.G, ALKMIN, F. F. (Eds.). São Francisco Craton, Eastern Brazil: Tectonic Genealogy of a Miniature Continent. Springer, p. 241-254.

PADILHA, A.L., VITORELLO., Í., PÁDUA, M.B., MARCELO., FUCK, R.A. 2016. Deep magnetotelluric signatures of the early Neoproterozoic Cariris Velhos tectonic event within the Transversal sub-province of the Borborema Province, NE Brazil. Precambrian Research 275, 7-83.

PASSOS, L. H., 2016. Caraterização petrográfica, química mineral e geotermobarometria de rochas da unidade Novo Gosto, domínio Canindé, Faixa de Dobramentos Sergipana. Dissertação (Mestrado em Geologia) - Universidade de Brasília, Brasília, 223 p.

SANTOS, A.C.L., PADILHA, A. L., FUCK, R. A., PIRES, A. C. B., VITORELLO, I.,PÁDUA, M. B. 2014. Deep structure of a stretched lithosphere: Magnetotelluric imaging of the southeastern Borborema province, NE Brazil. Tectonophysics 610, 39-50, 2014.

SANTOS, E.J., 1995. O complexo granítico Lagoa das Pedras: acresção e colisão na região de Floresta (Pernambuco), Província Borborema (PhD thesis). Instituto de Geociências da Universidade de São Paulo, São Paulo, p. 228.

SANTOS, L. C. M. L., 2017. Processos acrescionários na porção central de Gondwana: exemplos de terrenos Alto Moxotó e Alto Pajeú da Província Borborema, NE do

BRASIL. Tese de doutorado em Geologia Regional – Programa de Pós-Graduação em Geologia, Instituto de Geociências, Universidade de Brasília. Brasília, 255p.

SANTOS, R. A., FILHO, N. R. M., SOUZA, J. D., 1988. Programa levantamentos geológicos básicos do Brasil: carta geológica, carta metalogenética/previsional. Folha SC.24-Z-A-III Carira, Estados de Sergipe e Bahia: DNPM/CPRM, 124p.

SANTOS, R. A., MARTINS, A. A. M., NEVES, J. P., 1998 Geologia e recursos minerais do estado de Sergipe. CPRM/Codise. 107p.

SEIXAS, S. R. M., MORAES, L. C., 2000. The Canindé Domain: its different gabbroic rocks. In: Internatinal Geological Congress, Rio de Janeiro, v. 31, Anais, p.6. 64.

SCHOBBENHAUS, C., BRITO NEVES, B. B., 2003. Geologia do Brasil no contexto da Plataforma Sul-Americana In: BIZZI, L. A.; SCHOBBENHAUS, C, VIDOTTI, R.M., GONÇALVES J.H. (eds.) Geologia, tectônica e recursos minerais do Brasil. Texto, mapas e SIG. CPRM-Serviço Geológico do Brasil. p. 5-54.

SILVA FILHO, M. A., 1976. A suite ofiolítica da geossinclinal de Propriá. Anais 29° Congresso Brasileiro de Geologia, v. 4, p. 51-58.

SILVA FILHO, M. A., BONFIM, L. F. C., SANTOS, R. A., LEAL, R. A., BRAZ FILHO, P. A., RODRIGUES, T. L., SANTOS, J. C., BRUNI, D. C., 1979. Projeto Complexo de Canindé do São Francisco. Relatório Final. DNPM/CPRM.

SILVA FILHO, M. A., 1998. Arco vulcânico Canindé-Marancó e a Faixa Sul-Alagoana: sequências orogênicas Mesoproterozóicas. In: XL Congresso Brasileiro de Geologia, Belo horizonte, SBG. p. 16.

SOUZA JUNIOR, F. D., 2013. Mapeamento geológico da porção central do domínio Canindé, Cinturão Orogênico Sergipano, NE - Brasil. Monografia de Graduação, Departamento de Geologia, Universidade Federal de Sergipe. São Cristóvão, 64p.

TROMPETTE, R., 1994. Geology of Western Gondwana. A. Balkema, Amsterdam, 350 p.

TROMPETTE, R., 1997. Neoproterozoic (~600 Ma) aggregation of Western Gondwana: a tentative scenario. Precambrian Research. 82(1-2), 101-112. https://doi.org/10.1016/S0301-9268(96)00045-9.

VAN SCHMUS, W.R., BRITO NEVES, B.B., HACKSPACHER, P.C., BABINSKI, M., 1995. U/Pb and Sm/Nd geochronologic studies of the eastern Borborema Province, Northeast Brazil: initial conclusions. Journal of South American Earth Sciences 8, 267-288.

VAN SCHMUS, W.R, OLIVEIRA, E.P., SILVA FILHO, A.F., TOTEU, S.F., PENAYE, J. & GUIMARÃES, I.P., 2008. Proterozoic links between the Borborema Province, NE Brazil, and the Central African Fold Belt. Special Publications. 294, 69-99. https://doi.org/10.1144/SP294.5.

.

MATERIAIS SUPLEMENTARES (SP)

SP1 (Artigo 1) – Summary of U-Pb zircon data for sample DMLH-16 (amphibolite) obtained by LA-SF-ICP-MS method.

Sample DMHL-16				Isotope ratios[b]							Ages (Ma)						
Spot number	Pb206c (%)	Pb207* cps	Th/U[a]	$^{207}Pb^*/^{206}Pb^*$	± 1s	$^{207}Pb^*/^{235}U$	± 1s	$^{206}Pb^*/^{238}U$	± 1s	RHO	$^{206}Pb/^{238}U$	± 1s	$^{207}Pb/^{235}U$	± 1s	$^{206}Pb/^{207}Pb$	± 1s	Conc
5.sSMPABC008	8660	410	0.22	0.0649	0.0036	1.1086	0.0597	0.1239	0.0023	0.35	753	13	758	29	770	114	99
5.sSMPABC009	3627	118	0.11	0.0639	0.0039	1.0413	0.0620	0.1181	0.0022	0.32	720	13	725	31	738	125	99
5.sSMPABC010	7730	513	0.22	0.0640	0.0019	1.0796	0.0300	0.1222	0.0014	0.40	743	8	743	15	742	60	100
5.sSMPABC011	14865	599	0.17	0.0637	0.0012	1.0583	0.0185	0.1204	0.0012	0.56	733	7	733	9	731	39	100
5.sSMPABC012	4757	311	0.14	0.0633	0.0031	1.0553	0.0499	0.1208	0.0018	0.32	735	10	732	25	718	100	101
5.sSMPABC016	6704	447	0.15	0.0644	0.0029	1.1017	0.0475	0.1241	0.0019	0.35	754	11	754	23	753	92	100
5.sSMPABC017	5567	408	0.17	0.0644	0.0030	1.0898	0.0486	0.1226	0.0019	0.34	746	11	748	24	755	95	100
5.sSMPABC019	6378	425	0.19	0.0639	0.0029	1.0653	0.0470	0.1207	0.0019	0.35	735	11	736	23	740	94	100
5.sSMPABC020	4569	303	0.20	0.0634	0.0040	1.0288	0.0627	0.1175	0.0022	0.31	716	13	718	31	723	128	100
5.sSMPABC028	4916	326	0.14	0.0639	0.0035	1.0586	0.0568	0.1200	0.0020	0.31	731	12	733	28	739	113	100
5.sSMPABC029	6805	328	0.18	0.0641	0.0039	1.0682	0.0619	0.1208	0.0023	0.33	735	13	738	30	746	122	100
5.sSMPABC034	4474	295	0.15	0.0634	0.0034	1.0356	0.0544	0.1184	0.0019	0.31	721	11	722	27	720	111	100
5.sSMPABC035	47623	3139	0.10	0.0637	0.0009	1.0510	0.0142	0.1196	0.0011	0.68	728	6	729	7	730	31	100
5.sSMPABC036	28822	1936	0.09	0.0638	0.0015	1.0559	0.0245	0.1200	0.0014	0.50	730	8	732	12	734	50	100
5.sSMPABC044	6750	447	0.26	0.0645	0.0039	1.0862	0.0639	0.1221	0.0024	0.33	743	14	747	31	758	124	99
5.sSMPABC045	8475	328	0.16	0.0637	0.0020	1.0482	0.0314	0.1193	0.0015	0.41	727	8	728	16	730	65	100
5.sSMPABC047	3686	248	0.15	0.0645	0.0033	1.0931	0.0542	0.1228	0.0019	0.31	747	11	750	26	758	104	100
5.sSMPABC049	7780	502	0.13	0.0635	0.0033	1.0216	0.0509	0.1167	0.0020	0.34	712	11	715	26	723	106	100
5.sSMPABC052	3662	245	0.15	0.0645	0.0031	1.0913	0.0515	0.1227	0.0019	0.32	746	11	749	25	757	100	100
5.sSMPABC053	2965	194	0.16	0.0634	0.0051	1.0592	0.0822	0.1210	0.0027	0.29	736	15	733	41	723	161	100
5.sSMPABC037	10867	736	0.14	0.0646	0.0030	1.1135	0.0492	0.1250	0.0021	0.37	759	12	760	24	760	94	100
5.sSMPABC038	4877	324	0.14	0.0646	0.0031	1.1123	0.0514	0.1249	0.0019	0.33	758	11	759	25	760	98	100
5.sSMPABC030	3913	-166	0.22	0.0646	0.0027	1.1166	0.0448	0.1253	0.0018	0.36	761	10	761	21	761	85	100
5.sSMPABC032	3499	235	0.18	0.0646	0.0069	1.1306	0.1179	0.1270	0.0038	0.29	771	22	768	56	760	211	100
5.sSMPABC033	7192	483	0.20	0.0645	0.0017	1.1196	0.0279	0.1257	0.0014	0.43	764	8	763	13	759	54	100
5.sSMPABC026	5914	395	0.15	0.0644	0.0040	1.1253	0.0679	0.1266	0.0025	0.33	769	14	766	32	756	126	100
5.sSMPABC027	9924	609	0.11	0.0647	0.0030	1.1279	0.0498	0.1263	0.0020	0.36	767	12	767	24	765	94	100
5.sSMPABC015	10304	699	0.21	0.0653	0.0016	1.1608	0.0266	0.1289	0.0014	0.46	781	8	782	12	783	49	100
5.sSMPABC018	6062	412	0.24	0.0658	0.0028	1.1881	0.0493	0.1310	0.0019	0.35	793	11	795	23	798	88	100
5.sSMPABC031	4461	302	0.19	0.0648	0.0040	1.1433	0.0689	0.1278	0.0024	0.31	775	14	774	33	769	126	100
5.sSMPABC046	6741	451	0.13	0.0641	0.0049	1.1310	0.0825	0.1278	0.0031	0.33	775	18	768	39	746	152	101
5.sSMPABC048	9155	615	0.12	0.0658	0.0034	1.1745	0.0579	0.1294	0.0023	0.35	785	13	789	27	800	104	99
5.sSMPABC051	9319	631	0.13	0.0662	0.0034	1.2186	0.0601	0.1335	0.0023	0.35	808	13	809	28	813	104	100
5.sSMPABC050	9172	786	0.11	0.0834	0.0036	1.3637	0.0557	0.1185	0.0020	0.41	722	11	874	24	1278	82	79

[a] *concentration uncertainty ca. 20%*

[b] *data not corrected for common-Pb*

[c] *data corrected/not corrected for common-Pb*

[d] *Concordance calculated as (206Pb-238U age/207Pb-206Pb age)*100*

Decay constants of Jaffey et al. (1971) used

bd = below detection; #N/A = not available

Uncertainties quoted without components related to systematic error unless otherwise stated

SP2 (Artigo 2) – U-Pb - All Data

Table 1: Summary of U-Pb zircon data of the sample DMLH-2 obtained by LA-SF-ICP-MS method.

Sample DMHL-2				Isotope ratios[b]							Ages (Ma)						
Spot number	Pb206* cps	Pb207* cps	Th/U[a]	$^{207}Pb^*/^{206}Pb^*$	± 1s	$^{207}Pb^*/^{235}U$	± 1s	$^{206}Pb^*/^{238}U$	± 1s	RHO	$^{206}Pb/^{238}U$	± 2s	$^{207}Pb/^{235}U$	± 2s	$^{206}Pb/^{207}Pb$	± 2s	Conc
5.sSMPABC012	22750	1537	0,56	0,0640	0,0011	1,048	0,016	0,119	0,001	0,57	723	13	728	22	743	25	99
5.sSMPABC055	26036	1695	0,59	0,0642	0,0011	1,025	0,016	0,116	0,001	0,57	707	13	716	22	748	25	99
5.sSMPABC031	28440	1858	0,57	0,0643	0,0010	1,031	0,015	0,116	0,001	0,60	710	12	720	21	750	24	99
5.sSMPABC017	27160	1775	0,60	0,0643	0,0010	1,030	0,015	0,116	0,001	0,62	709	12	719	20	751	23	99
5.sSMPABC039	13402	874	0,72	0,0643	0,0015	1,044	0,023	0,118	0,001	0,43	717	13	726	32	752	35	99
5.sSMPABC038	21788	1427	0,66	0,0643	0,0015	1,019	0,022	0,115	0,001	0,47	702	14	714	30	752	33	98
5.sSMPABC032	16283	1074	0,63	0,0649	0,0013	1,028	0,019	0,115	0,001	0,51	702	13	718	26	771	29	98
5.sSMPABC042	12503	819	0,60	0,0649	0,0019	1,051	0,029	0,118	0,001	0,38	717	15	730	39	771	44	98
5.sSMPABC053	10439	686	0,54	0,0650	0,0020	1,059	0,031	0,118	0,001	0,36	721	15	733	42	774	46	98
5.sSMPABC054	22045	1426	0,51	0,0650	0,0025	1,044	0,038	0,117	0,002	0,36	711	18	726	52	775	58	98
5.sSMPABC023	14961	988	0,50	0,0650	0,0013	1,049	0,020	0,117	0,001	0,50	713	13	728	27	776	30	98
5.sSMPABC052	12473	828	0,48	0,0651	0,0016	1,061	0,025	0,118	0,001	0,41	721	14	734	34	777	38	98
5.sSMPABC037	22906	1516	0,59	0,0652	0,0012	1,035	0,017	0,115	0,001	0,55	703	12	721	23	780	27	97
5.sSMPABC014	30076	1999	0,44	0,0652	0,0013	1,069	0,020	0,119	0,001	0,51	725	14	738	27	780	31	98
5.sSMPABC036	8363	554	0,56	0,0653	0,0025	1,038	0,039	0,115	0,001	0,32	704	17	723	53	783	59	97
5.sSMPABC013	25605	1706	0,57	0,0655	0,0013	1,079	0,019	0,120	0,001	0,52	728	13	743	26	790	30	98
5.sSMPABC022	59963	4009	0,41	0,0657	0,0008	1,081	0,012	0,119	0,001	0,77	727	12	744	16	797	19	98
5.sSMPABC056	17774	1165	0,59	0,0658	0,0020	1,081	0,032	0,119	0,001	0,38	726	16	744	43	799	48	98
5.sSMPABC058	13217	897	0,41	0,0663	0,0015	1,055	0,023	0,115	0,001	0,44	705	13	731	32	816	37	96
5.sSMPABC044$	39220	2067	0,58	0,0664	0,0010	1,115	0,015	0,122	0,001	0,66	741	13	761	20	818	24	97
5.sSMPABC059&	13725	961	0,69	0,0667	0,0033	1,100	0,053	0,120	0,002	0,33	729	23	753	71	828	81	97
5.sSMPABC062	14576	993	0,58	0,0667	0,0015	1,100	0,023	0,120	0,001	0,46	729	14	754	31	829	36	97
5.sSMPABC020$	15742	1079	0,75	0,0678	0,0022	1,229	0,038	0,132	0,002	0,39	797	18	814	49	863	54	98

[a]data corrected for common-Pb

[b]concentration uncertainty ca. 20%

[c]Concordance calculated as: ((^{206}Pb-^{238}U(age))/(^{207}Pb-^{206}Pb(age)))*100

Decay constants of Jaffey et al. (1971) used

Total systematic uncertainties (σsys): ^{206}Pb/^{238}U = 2.0%, ^{207}Pb/^{206}Pb = 0.55% (2σ)

Uncertainties quoted without components related to systematic error unless otherwise stated

Table 2: Summary of U-Pb zircon data of the sample DMLH-3 obtained by LA-SF-ICP-MS method.

Sample DMHL-3				**Isotope ratios[b]**							**Ages (Ma)**						
Spot number	**Pb206* cps**	**Pb207* cps**	**Th/U[a]**	**^{207}Pb*/ ^{206}Pb***	**± 1s**	**^{207}Pb*/ ^{235}U**	**± 1s**	**^{206}Pb*/ ^{238}U**	**± 1s**	**RHO**	**^{206}Pb/ ^{238}U**	**± 2s**	**^{207}Pb/ ^{235}U**	**± 2s**	**^{206}Pb/ ^{207}Pb**	**± 2s**	**Conc**
11	11385	761	0,53	0,0653	0,0025	1,074	0,039	0,119	0,002	0,38	727	20	**741**	53	785	59	**98**
12	4084	271	0,49	0,0646	0,0027	1,047	0,042	0,118	0,002	0,32	717	18	**727**	57	760	61	**99**
13	12174	768	0,53	0,0652	0,0015	1,055	0,024	0,117	0,001	0,46	716	14	**731**	32	780	36	**98**
14	7286	228	0,55	0,0646	0,0016	1,048	0,024	0,118	0,001	0,46	717	15	**728**	32	761	36	**99**
17	8554	625	0,49	0,0648	0,0017	1,041	0,025	0,117	0,001	0,43	711	14	**725**	34	767	38	**98**
18	9249	623	0,63	0,0648	0,0029	1,062	0,046	0,119	0,002	0,36	724	22	**735**	62	768	68	**99**
19	10766	726	0,47	0,0651	0,0019	1,041	0,028	0,116	0,001	0,42	708	16	**725**	38	776	43	**98**
22	8165	552	0,62	0,0653	0,0017	1,068	0,025	0,119	0,001	0,43	722	15	**738**	35	785	39	**98**
29	9468	625	0,57	0,0637	0,0031	1,009	0,047	0,115	0,002	0,35	702	22	**709**	64	730	69	**99**
30	5391	49	0,38	0,0653	0,0020	1,088	0,032	0,121	0,001	0,40	736	17	**748**	42	784	47	**98**
31	9562	638	0,38	0,0647	0,0036	1,070	0,058	0,120	0,002	0,35	731	27	**739**	78	763	84	**99**
33	11673	790	0,63	0,0647	0,0018	1,040	0,028	0,117	0,001	0,42	712	16	**724**	38	763	42	**98**
37	8963	614	0,65	0,0652	0,0024	1,038	0,036	0,115	0,002	0,37	704	18	**723**	49	782	56	**97**
40	9118	603	0,56	0,0640	0,0022	1,022	0,033	0,116	0,001	0,38	706	17	**715**	45	743	49	**99**
41	9774	648	0,47	0,0643	0,0020	1,036	0,031	0,117	0,001	0,40	713	16	**722**	42	752	46	**99**
42	9228	616	0,52	0,0645	0,0018	1,074	0,029	0,121	0,001	0,40	735	15	**741**	39	758	42	**99**
48	11172	719	0,37	0,0654	0,0014	1,064	0,021	0,118	0,001	0,50	720	14	**736**	28	786	32	**98**
49	9397	418	0,58	0,0646	0,0022	1,072	0,035	0,120	0,002	0,39	733	18	**740**	48	762	52	**99**
50	10012	690	0,53	0,0655	0,0016	1,068	0,025	0,118	0,001	0,44	721	15	**738**	34	789	38	**98**
51	15839	1084	0,44	0,0655	0,0012	1,082	0,018	0,120	0,001	0,57	730	13	**745**	24	791	27	**98**
53	7890	534	0,43	0,0648	0,0016	1,070	0,025	0,120	0,001	0,44	729	15	**739**	34	768	37	**99**
54	12272	826	0,49	0,0643	0,0019	1,029	0,029	0,116	0,001	0,42	708	16	**719**	40	751	44	**99**

55	11403	762	0,48	0,0645	0,0020	1,056	0,031	0,119	0,001	0,41	723	17	**732**	42	759	46	**99**
56	12446	729	0,57	0,0650	0,0016	1,066	0,025	0,119	0,001	0,46	724	15	**737**	34	775	38	**98**
57	12989	859	0,54	0,0651	0,0025	1,086	0,039	0,121	0,002	0,38	737	20	**746**	53	777	58	**99**
58	8855	605	0,51	0,0640	0,0020	1,027	0,030	0,117	0,001	0,40	711	16	**718**	41	742	44	**99**
12	7461	515	0,53	0,0658	0,0027	1,079	0,042	0,119	0,002	0,36	725	20	**743**	57	800	64	**97**
14	6109	423	0,64	0,0658	0,0039	1,095	0,063	0,121	0,002	0,34	735	28	**751**	84	799	93	**98**
15	10848	733	0,51	0,0654	0,0014	1,062	0,021	0,118	0,001	0,51	718	14	**735**	28	787	32	**98**
16	4673	-156	0,58	0,0647	0,0021	1,049	0,032	0,118	0,001	0,40	717	17	**728**	43	764	47	**98**
17	7268	507	0,58	0,0664	0,0027	1,101	0,043	0,120	0,002	0,36	732	20	**754**	58	820	66	**97**
18	5643	386	0,58	0,0651	0,0034	1,048	0,052	0,117	0,002	0,34	712	23	**728**	71	777	79	**98**
20	8286	558	0,43	0,0666	0,0030	1,085	0,047	0,118	0,002	0,36	721	22	**746**	63	824	73	**97**
32	6281	432	0,58	0,0649	0,0029	1,048	0,044	0,117	0,002	0,36	715	21	**728**	60	770	66	**98**
34	11560	714	0,62	0,0668	0,0020	1,067	0,031	0,116	0,001	0,42	707	17	**737**	42	830	50	**96**
36	5682	397	0,44	0,0655	0,0024	1,081	0,039	0,120	0,002	0,37	729	19	**744**	52	792	58	**98**
37	5706	302	0,55	0,0655	0,0022	1,039	0,034	0,115	0,001	0,39	703	18	**723**	46	789	53	**97**
38	5235	130	0,65	0,0663	0,0026	1,092	0,041	0,120	0,002	0,38	728	21	**749**	55	817	63	**97**

[a]data corrected for common-Pb

[b]concentration uncertainty ca. 20%

[c]Concordance calculated as: ((^{206}Pb-^{238}U(age))/(^{207}Pb-^{206}Pb(age)))*100

Decay constants of Jaffey et al. (1971) used

Total systematic uncertainties (σsys): ^{206}Pb/^{238}U = 2.0%, ^{207}Pb/^{206}Pb = 0.55% (2σ)

Uncertainties quoted without components related to systematic error unless otherwise stated

Table 3: Summary of U-Pb zircon data of the sample DMLH-6-A obtained by LA-MC-ICP-MS method.

Sample DMHL-6				**Isotope ratios[b]**							**Ages (Ma)**						
Spot number	**Pb206* cps**	**^{206}Pb/^{204}Pb**	**Th/U[a]**	**^{207}Pb*/^{206}Pb***	**± 1s**	**^{207}Pb*/^{235}U**	**± 1s**	**^{206}Pb*/^{238}U**	**± 1s**	**RHO**	**^{206}Pb/^{238}U**	**± 2s**	**^{207}Pb/^{235}U**	**± 2s**	**^{206}Pb/^{207}Pb**	**± 2s**	**Conc**
031-ZR21	55490851	176123	0,888	0,06365	0,80	0,982	1,28	0,1119	0,92	0,72	684	12	695	13	730	34	94
032-ZR22	37925219	234302	0,607	0,06297	0,70	0,974	1,17	0,1122	0,86	0,73	685	11	691	12	707	30	97
037-ZR27	73205902	81203	1,171	0,06251	1,42	0,980	2,13	0,1137	1,55	0,73	694	20	694	21	692	60	100
040-ZR30	74469099	200553	1,192	0,06358	1,10	1,040	1,67	0,1186	1,19	0,72	722	16	724	17	728	46	99

043-ZR31	77998841	64107	1,248	0,06296	1,33	0,982	2,30	0,1131	1,84	0,80	691	24	695	23	707	56	98
046-ZR34	50797147	92867	0,813	0,06358	1,29	1,037	2,82	0,1183	2,48	0,88	721	34	722	29	728	54	99
049-ZR37	70435583	89724	1,127	0,06282	0,97	0,935	1,51	0,1079	1,10	0,73	660	14	670	15	702	41	94
050-ZR38	89265834	299160	1,428	0,06351	0,60	0,961	1,05	0,1097	0,78	0,74	671	10	684	10	725	25	93
051-ZR39	56897479	125851	0,910	0,06364	0,97	0,949	1,68	0,1081	1,32	0,79	662	17	677	17	730	41	91
055-ZR41	36582842	102748	0,585	0,06354	1,63	0,938	2,20	0,1071	1,44	0,65	656	18	672	22	726	68	90
057-ZR43	44040083	114780	0,705	0,06354	1,27	0,940	1,72	0,1073	1,11	0,64	657	14	673	17	726	53	90
059-ZR45	30232878	40648	0,484	0,06268	1,43	0,997	2,12	0,1154	1,52	0,72	704	20	702	21	697	61	101
061-ZR47	37432061	87988	0,599	0,06342	0,99	1,042	1,74	0,1191	1,38	0,79	725	19	725	18	722	42	100
064-ZR50	72183372	197828	1,155	0,06324	0,91	0,996	1,60	0,1142	1,27	0,79	697	17	702	16	716	38	97

[1] Convertion factor from mV to CPS is 62500

[2] concentration uncertainty c.20%

[3] data not corrected for common-Pb

[4] not corrected for common-Pb

[5] Discordance calculated as (1-(^{206}Pb/^{238}U age/^{207}Pb/^{206}Pb age))*100

Decay constants of Jaffey et al 1971 used

Table 4: Summary of U-Pb zircon data of the sample DDLH_9A obtained by LA-MC-ICP-MS method.

								Isotope ratios[c]							Ages (Ma)						
Spot Number	ƒ206[a]	206Pb cps	207Pb cps	Pb ppm	Th ppm	U ppm	Th/U[b]	207Pb/ 235U	1 s [%]	206Pb/ 238U	1 s [%]	Rho[d]	207Pb/ 206Pbe	1 s [%]	206Pb/ 238U	2s[g] abs	207Pb/ 235U	2s abs	207Pb/ 206Pb	2sg abs	[f]Conc % 6/8-7/6
Zr_1	0,0018	339607	21451	35	87	316	0,28	1,4116	2,38	0,1454	2,25	0,94	0,0704	0,78	875	18	894	25	940	18	93
Zr_2	0,0020	527516	33952	58	257	380	0,68	1,5000	1,87	0,1521	1,71	0,91	0,0715	0,78	913	18	930	25	972	18	94
Zr_3	0,0007	760167	760167	87	362	509	0,72	1,5812	2,10	0,1587	1,98	0,94	0,0723	0,70	949	19	963	25	994	17	96
Zr_4	0,0006	356278	22912	43	222	230	0,97	1,4965	2,27	0,1497	2,16	0,95	0,0725	0,69	899	18	929	25	1000	17	90
Zr_5	0,0004	576033	36843	63	198	372	0,54	1,5356	2,26	0,1535	2,16	0,96	0,0726	0,67	920	18	945	25	1002	17	92
Zr_6	0,0006	356180	22915	43	222	230	0,97	1,4410	2,48	0,1441	2,39	0,96	0,0725	0,69	868	18	906	24	1001	17	87
Zr_7	0,0006	457420	29441	51	187	307	0,61	1,4247	2,64	0,1419	2,55	0,97	0,0728	0,68	856	18	899	24	1009	17	85
Zr_8	0,0033	346664	22405	38	131	244	0,54	1,4644	2,05	0,1488	1,84	0,90	0,0714	0,91	894	18	916	27	969	20	92
Zr_9	0,0010	293666	18618	32	99	221	0,45	1,5494	1,92	0,1589	1,74	0,90	0,0707	0,83	951	19	950	26	949	18	100

Zr_10	0,0009	465884	30058	52	188	381	0,50	1,3269	2,32	0,1323	2,19	0,95	0,0727	0,74	801	17	916	25	1007	18	80
Zr_11	0,0071	610305	40837	80	1991	946	2,12	0,9837	5,09	0,1004	5,01	0,99	0,0710	0,88	617	15	696	23	959	21	64
Zr_12	0,0012	336481	21376	45	132	279	0,48	1,4506	2,42	0,1473	2,25	0,93	0,0714	0,88	886	18	910	26	969	20	91
Zr_13	0,0005	468814	468814	57	85	440	0,20	0,8768	4,38	0,0959	4,29	0,98	0,0663	0,91	590	15	639	21	817	17	72
Zr_14	0,0006	436970	25863	53	83	370	0,23	0,8617	5,16	0,0920	5,05	0,98	0,0679	1,03	568	15	631	22	866	20	66
Zr_15	0,0005	421144	26970	56	153	317	0,49	1,4761	2,50	0,1470	2,38	0,95	0,0728	0,76	884	18	921	25	1008	18	88
Zr_16	0,0054	737671	49428	97	437	780	0,56	1,5328	3,02	0,1545	2,91	0,96	0,0719	0,81	926	18	944	26	984	20	94
Zr_17	0,0015	255834	16469	34	88	220	0,40	1,5785	2,76	0,1575	2,64	0,96	0,0727	0,79	943	19	962	26	1006	19	94
Zr_18	0,0020	255477	15398	32	56	174	0,33	1,4163	2,96	0,1493	2,81	0,95	0,0688	0,93	897	18	896	26	893	19	100
Zr_19	0,0028	394245	25171	53	271	477	0,57	0,9224	3,35	0,0948	3,24	0,97	0,0706	0,85	584	15	664	22	946	19	62
Zr_20	0,0016	334589	21602	45	157	282	0,56	1,4787	2,56	0,1470	2,44	0,96	0,0730	0,75	884	18	896	24	1013	18	87
Zr_21	0,0022	408206	25939	57	182	370	0,50	1,5229	2,53	0,1544	2,38	0,94	0,0715	0,85	926	18	940	26	973	19	95
Zr_22	0,0034	327225	20956	46	131	297	0,44	1,6278	2,82	0,1647	2,63	0,93	0,0717	1,01	983	19	981	29	976	22	101
Zr_23	0,0019	329317	329317	46	119	287	0,42	1,6973	2,82	0,1706	2,65	0,94	0,0721	0,96	1016	19	1008	29	990	22	103
ZR_24	0,0034	343461	22784	49	130	297	0,44	1,2609	3,38	0,1277	3,27	0,97	0,0716	0,88	775	17	828	25	975	20	79
Zr_25	0,0019	622058	40200	100	518	574	0,91	1,6575	2,51	0,1662	2,39	0,95	0,0723	0,79	991	19	992	27	995	19	100
Zr_26	0,0018	291304	18648	43	144	231	0,63	1,6727	2,84	0,1671	2,72	0,96	0,0726	0,83	996	19	998	27	1003	20	99
Zr_27	0,0020	720987	46944	107	458	709	0,65	1,3955	2,98	0,1393	2,86	0,96	0,0727	0,84	841	17	887	25	1005	20	84
Zr_28	0,0007	466825	29367	63	128	456	0,28	1,4724	2,79	0,1510	2,58	0,92	0,0707	1,07	907	18	919	28	949	22	96
Zr_29	0,0020	336740	21695	48	155	291	0,54	1,6317	2,89	0,1637	2,75	0,95	0,0723	0,89	977	19	983	28	994	20	98
Zr_30	0,0063	308946	19963	42	94	323	0,29	1,4368	3,84	0,1420	3,56	0,93	0,0734	1,44	856	18	919	35	1024	32	84
Zr_31	0,0021	617626	39645	100	505	524	0,97	1,5621	2,65	0,1571	2,41	0,91	0,0721	1,11	940	19	955	30	990	24	95
Zr_32	0,0036	266728	17320	38	96	210	0,46	1,5203	2,69	0,1537	2,44	0,91	0,0717	1,12	922	18	939	30	978	24	94
Zr_33	0,0010	310281	310281	46	143	244	0,59	1,5396	2,67	0,1550	2,43	0,91	0,0720	1,10	929	18	946	30	986	24	94
Zr_34	0,0012	684184	44019	106	449	592	0,76	1,5790	2,59	0,1589	2,35	0,91	0,0721	1,10	951	19	962	30	988	24	96
Zr_35	0,0036	655810	42693	98	1405	781	1,81	1,3356	3,42	0,1323	3,22	0,94	0,0732	1,15	801	17	861	29	1020	26	79
Zr_26	0,0011	302765	19366	45	153	241	0,64	1,6087	2,98	0,1628	2,73	0,91	0,0717	1,20	972	19	974	32	977	26	100
Zr_37	0,0007	1186859	134636	175	388	727	0,54	6,3835	1,95	0,3557	1,83	0,94	0,1301	0,69	1962	31	2030	48	2100	36	93
Zr_38	0,0014	214979	13701	32	116	186	0,63	1,4792	2,78	0,1502	2,54	0,91	0,0714	1,14	902	18	922	30	969	24	93
Zr_39	0,0018	389711	25157	60	262	324	0,82	1,6723	2,84	0,1676	2,59	0,91	0,0723	1,19	999	19	998	32	996	26	100
Zr_40	0,0005	414337	26563	61	177	313	0,57	1,5525	2,73	0,1558	2,50	0,92	0,0723	1,10	933	18	922	29	994	24	94
Zr_41	0,0010	552449	35271	83	324	600	0,54	1,3283	3,80	0,1344	3,61	0,95	0,0717	1,18	813	17	858	29	976	25	83
Zr_42	0,0030	263095	17204	39	101	241	0,42	1,6089	3,65	0,1620	3,43	0,94	0,0720	1,23	968	19	974	32	986	26	98
Zr_43	0,0016	323330	323330	50	163	263	0,63	1,5477	3,29	0,1543	3,08	0,93	0,0728	1,18	925	18	950	31	1008	26	92
Zr_44	0,0008	345340	22040	50	122	319	0,38	1,4905	3,57	0,1509	3,36	0,94	0,0716	1,20	906	18	927	30	976	25	93

Zr_45	0,0011	243608	15502	36	95	200	0,48	1,5895	3,39	0,1597	3,17	0,93	0,0722	1,21	955	19	966	32	991	26	96
Zr_46	0,0008	372674	23732	54	128	314	0,41	1,5278	3,42	0,1545	3,18	0,93	0,0717	1,27	926	18	942	32	978	27	95
Zr_47	0,0014	409732	26068	63	248	474	0,53	1,5160	3,68	0,1538	3,49	0,95	0,0715	1,17	922	18	937	30	971	25	95
Zr_48	0,0016	414155	26403	61	178	406	0,44	1,5951	4,02	0,1628	3,81	0,95	0,0710	1,27	972	19	968	32	959	26	101
Zr_49	0,0043	291513	19345	44	213	338	0,63	1,1102	5,03	0,1131	4,88	0,97	0,0712	1,23	690	16	758	27	964	26	72
Zr_50	0,0038	2465781	156881	338	350	2459	0,14	1,0001	4,80	0,1045	4,65	0,97	0,0694	1,19	641	16	968	35	911	24	70
Zr_51	0,0015	260310	16682	42	146	233	0,63	1,6416	2,58	0,1625	2,42	0,94	0,0733	0,90	971	19	986	28	1022	21	95
Zr_52	0,0011	470909	30071	78	280	434	0,65	1,6316	2,31	0,1646	2,14	0,93	0,0719	0,87	982	19	982	27	983	20	100
Zr_53	0,0057	360879	360879	56	126	370	0,34	1,5077	2,68	0,1527	2,24	0,84	0,0716	1,47	916	18	933	35	975	31	94
Zr_54	0,0061	57633	3686	9	19	56	0,34	1,3572	3,41	0,1433	2,95	0,86	0,0687	1,72	863	18	871	37	889	33	97
Zr_55	0,0009	345027	21875	55	170	319	0,54	1,3335	2,98	0,1341	2,86	0,96	0,0721	0,85	811	17	860	25	989	20	82
Zr_56	0,0013	352327	22423	58	261	365	0,72	1,3095	2,65	0,1325	2,51	0,95	0,0717	0,86	802	17	850	25	977	20	82
Zr_57	0,0043	337789	22754	56	672	637	1,06	1,0129	4,32	0,1029	4,20	0,97	0,0714	1,02	632	16	710	24	968	22	65
Zr_58	0,0131	270208	21069	48	154	222	0,70	1,6207	2,47	0,1593	2,29	0,93	0,0738	0,92	953	19	978	31	1036	26	92
Zr_59	0,0011	338819	21689	54	164	306	0,54	1,6129	2,42	0,1618	2,24	0,93	0,0723	0,90	967	19	975	28	995	21	97
Zr_60	0,0007	284867	17730	44	115	310	0,37	1,6411	2,59	0,1620	2,43	0,94	0,0735	0,90	968	19	978	28	1027	21	94
Zr_61	0,0011	345804	22069	60	250	336	0,75	1,6491	2,27	0,1647	2,08	0,91	0,0726	0,92	983	19	989	28	1004	21	98
Zr_62	0,0010	604185	37538	102	322	602	0,54	1,3196	2,45	0,1342	2,17	0,88	0,0713	1,14	812	17	854	28	967	24	84
Zr_63	0,0025	316007	316007	54	168	338	0,50	1,6185	1,96	0,1624	1,74	0,89	0,0723	0,90	970	19	977	28	994	21	98
Zr_64	0,0033	161582	10461	27	60	177	0,34	1,4168	2,59	0,1442	2,09	0,81	0,0713	1,52	868	18	896	34	965	31	90
Zr_65	0,0007	201685	12883	34	98	195	0,50	1,5274	1,94	0,1527	1,73	0,89	0,0726	0,88	916	18	941	27	1001	20	91
Zr_66	0,0009	288665	18360	49	136	279	0,49	1,5560	1,93	0,1573	1,69	0,88	0,0718	0,93	942	19	953	27	979	21	96
Zr_67	0,0017	295452	18920	52	191	297	0,65	1,4179	2,31	0,1427	2,13	0,92	0,0721	0,89	860	18	896	26	987	20	87
Zr_68	0,0017	363770	23282	63	214	393	0,55	1,6061	2,39	0,1623	2,21	0,92	0,0718	0,93	970	19	973	28	979	21	99
Zr_69	0,0018	348575	21047	55	89	444	0,20	1,3257	2,46	0,1358	2,23	0,91	0,0708	1,05	821	17	857	27	951	22	86
Zr_70	0,0010	307987	19522	52	139	345	0,41	1,5403	2,01	0,1557	1,78	0,88	0,0717	0,94	933	18	973	28	978	21	95
Zr_71	0,0005	567806	36355	104	336	582	0,58	1,4468	3,12	0,1449	2,99	0,96	0,0724	0,87	872	18	909	26	998	20	87
Zr_72	0,0014	333941	21184	59	158	346	0,46	1,5357	3,33	0,1564	3,20	0,96	0,0712	0,92	937	18	945	27	963	20	97
Zr_73	0,0021	174258	174258	33	141	212	0,67	1,3990	3,07	0,1430	2,86	0,93	0,0710	1,10	862	18	889	28	956	23	90
Zr_74	0,0032	141632	8997	27	113	181	0,63	1,3866	3,16	0,1419	2,93	0,93	0,0709	1,18	856	18	883	29	953	25	90
Zr_75	0,0010	459754	29344	85	332	538	0,62	1,3724	3,13	0,1380	3,02	0,96	0,0721	0,82	834	17	877	25	989	19	84
Zr_76	0,0017	189310	12041	35	128	188	0,69	1,4336	3,10	0,1455	2,97	0,96	0,0715	0,91	876	18	903	26	971	20	90
Zr_77	0,0015	553873	35691	103	371	596	0,63	1,5153	3,23	0,1524	3,12	0,96	0,0721	0,87	915	18	937	26	989	20	93
Zr_78	0,0027	266699	15936	44	70	393	0,18	1,0600	3,85	0,1157	3,68	0,96	0,0664	1,12	706	16	734	25	820	20	86
Zr_79	0,0012	559334	35484	103	371	667	0,56	1,5842	3,05	0,1603	2,93	0,96	0,0717	0,85	959	19	964	27	976	19	98

Zr_80	0,0006	410009	26144	74	240	462	0,52	1,4862	2,86	0,1493	2,74	0,96	0,0722	0,82	897	18	734	20	991	19	91
Zr_81	0,0011	579161	36509	102	357	684	0,53	1,2393	3,93	0,1265	3,82	0,97	0,0710	0,94	768	17	819	25	959	20	80
Zr_82	0,0010	328083	20829	56	163	413	0,40	1,3903	3,88	0,1410	3,74	0,96	0,0715	1,02	850	18	885	27	972	22	87
Zr_83	0,0008	396334	396334	70	236	426	0,56	1,5635	3,45	0,1552	3,32	0,96	0,0731	0,94	930	18	956	28	1016	22	92
Zr_84	0,0023	128233	8135	25	133	140	0,96	1,1924	4,53	0,1210	4,38	0,97	0,0715	1,14	736	16	797	27	971	24	76
Zr_85	0,0044	296774	19438	49	82	330	0,25	1,2059	4,35	0,1242	4,20	0,97	0,0704	1,13	754	17	803	27	941	24	80
Zr_86	0,0008	323681	20637	57	168	321	0,53	1,3846	3,78	0,1393	3,66	0,97	0,0721	0,94	840	17	882	26	989	21	85
Zr_87	0,0017	325663	20276	55	136	538	0,25	1,4245	4,20	0,1489	4,05	0,96	0,0694	1,14	895	18	899	29	910	23	98
Zr_88	0,0042	348327	23290	61	497	664	0,75	0,8817	6,64	0,0904	6,52	0,98	0,0707	1,24	558	15	642	24	949	26	59
Zr_89	0,0029	378641	24289	68	294	516	0,57	1,4636	3,70	0,1500	3,54	0,96	0,0708	1,07	901	18	916	29	950	23	95
Zr_90	0,0004	419419	26855	73	223	444	0,51	1,4180	3,68	0,1411	3,56	0,97	0,0729	0,94	851	18	642	19	1011	22	84
Zr_91	0,0015	334867	20960	56	199	413	0,48	1,4597	3,69	0,1518	3,57	0,97	0,0697	0,92	911	18	914	26	921	19	99
Zr_92	0,0015	443798	27871	74	264	470	0,57	1,3675	3,85	0,1407	3,76	0,97	0,0705	0,86	849	18	875	25	942	19	90
Zr_93	0,0014	233474	233474	38	90	268	0,34	1,5988	3,43	0,1633	3,30	0,96	0,0710	0,91	975	19	970	28	957	20	102
Zr_94	0,0007	490953	31406	84	277	504	0,55	1,4399	3,49	0,1447	3,41	0,98	0,0722	0,76	871	18	906	25	991	18	88
Zr_95	0,0011	383781	24492	65	199	403	0,50	1,4291	3,59	0,1449	3,50	0,98	0,0715	0,78	872	18	901	25	973	18	90
Zr_96	0,0016	239358	15141	40	123	253	0,49	1,5748	3,54	0,1601	3,45	0,97	0,0714	0,81	957	19	960	26	968	18	99
Zr_97	0,0012	409589	26009	69	231	456	0,51	1,4533	3,52	0,1477	3,41	0,97	0,0714	0,85	888	18	911	26	968	19	92
Zr_98	0,0017	265967	16164	43	104	366	0,29	1,2199	4,04	0,1335	3,86	0,96	0,0663	1,19	808	17	810	27	815	21	99
Zr_99	0,0012	352494	22413	61	229	379	0,61	1,4668	3,35	0,1480	3,26	0,98	0,0719	0,74	890	18	917	25	983	18	91
Zr_100	0,0017	227247	14482	39	134	233	0,58	1,4565	3,42	0,1471	3,32	0,97	0,0718	0,80	885	18	810	22	981	19	90

a Fraction of the non-radiogenic 206Pb in the analyzed zircon spot, where
*f*206=[206Pb/204Pb]c/[206Pb/204Pb]s (c=common; s=sample)
b Th/U ratios and amount of Pb, Th and U (in pmm) are calculated relative
to GJ-1 reference zircon
c Corrected for background and within-run Pb/U fractionation and normalised to reference zircon GJ-1 (ID-TIMS values/measured
value); 207Pb/235U calculated using (207Pb/206Pb)*(206Pb/238U)*(137.88)
d Rho is the error correlation defined as the quotient of the propagated errors of the
206Pb/238U and the 207/235U ratio
e Corrected for mass-bias by normalising to GJ-1 reference zircon and common Pb using the model Pb
composition of Stacey and Kramers (1975)
f Degree of concordance, 6/8-7/6= (206Pb/238U age *
100) / (207Pb/206Pb age)
g Total systematic uncertainties (ssys) 206/238U =2.0%,
207Pb/206Pb = 0.55 % (2s)

Table 5: Summary of U-Pb zircon data of the sample DDLH_9B obtained by LA-MC-ICP-MS method.

								Isotope ratios[c]							Ages (Ma)						
Spot Number	ƒ206[a]	206Pb cps	207Pb cps	Pb ppm	Th ppm	U ppm	Th/U[b]	207Pb/ 235U	1 s [%]	206Pb/ 238U	1 s [%]	Rho[d]	207Pb/ 206Pbe	1 s [%]	206Pb/ 238U	2s[g] abs	207Pb/ 235U	2s abs	207Pb/ 206Pb	2sg abs	[f]Conc % 6/8-7/6
Zr_5	0,0057	695706	92576	55	78	186	0,43	4,97	1,69	0,27	1,55	0,92	0,14	0,67	1517	26	1814	44	2174	37	70
Zr_56	0,0202	192702	16317	22	164	185	0,90	1,08	2,13	0,11	1,91	0,90	0,07	0,95	678	16	979	39	944	30	72
Zr_55	0,0079	586294	40484	58	176	368	0,48	1,12	2,55	0,12	2,45	0,96	0,07	0,72	730	16	764	23	863	17	85
Zr_14	0,0072	281330	20467	22	80	148	0,54	1,32	1,36	0,14	1,06	0,78	0,07	0,84	818	17	854	25	947	20	86
Zr_29	0,0018	517938	34781	48	165	254	0,65	1,33	2,41	0,14	2,32	0,96	0,07	0,64	823	17	858	23	950	15	87
Zr_38	0,0024	687121	45747	71	281	453	0,63	1,21	1,73	0,13	1,48	0,86	0,07	0,90	774	17	805	24	891	18	87
Zr_9N	0,0282	1482766	134092	138	1106	699	1,59	1,39	1,86	0,14	1,74	0,94	0,07	0,64	858	18	885	37	953	35	90
Zr_25	0,0098	683331	683331	57	148	359	0,41	1,36	1,72	0,14	1,56	0,90	0,07	0,74	848	18	871	25	929	19	91
Zr_1	0,0146	363848	28436	30	139	157	0,89	1,43	3,31	0,15	3,24	0,98	0,07	0,70	880	18	902	27	955	21	92
Zr_43	0,0037	439342	29791	39	124	241	0,52	1,26	1,34	0,13	1,08	0,81	0,07	0,79	809	17	827	24	878	17	92
Zr_35	0,0013	727937	48053	64	52	401	0,13	1,30	1,87	0,14	1,64	0,88	0,07	0,90	828	17	847	25	896	19	92
Zr_15B	0,0195	975409	72652	91	1118	751	1,50	0,95	2,32	0,11	1,87	0,81	0,06	1,37	665	16	677	32	718	29	93
Zr_8N	0,0013	718157	49762	61	313	295	1,07	1,52	1,78	0,16	1,66	0,93	0,07	0,64	930	18	940	24	964	16	97
Zr_44B	0,0069	1326013	90207	108	152	894	0,17	1,15	1,29	0,13	1,12	0,87	0,07	0,64	769	17	776	22	795	14	97
Zr_21	0,0022	209123	13864	18	76	97	0,79	1,31	2,03	0,14	1,94	0,96	0,07	0,59	846	18	852	22	870	14	97
Zr_36	0,0018	902165	54983	78	36	754	0,05	1,00	1,76	0,11	1,47	0,84	0,06	0,96	698	16	702	22	717	16	97
Zr_6	0,0041	729011	52452	65	388	314	1,24	1,58	1,69	0,16	1,57	0,93	0,07	0,64	954	19	960	25	976	16	98
Zr_40	0,0020	409451	28564	38	147	200	0,74	1,57	1,61	0,16	1,49	0,93	0,07	0,61	954	19	960	24	975	15	98
Zr_37	0,0028	763732	53097	84	432	447	0,97	1,55	1,39	0,16	1,09	0,78	0,07	0,86	943	19	949	27	963	19	98
Zr_17B	0,0040	894922	57041	64	49	590	0,08	1,02	1,18	0,12	1,12	0,95	0,06	0,39	712	16	715	19	726	9	98
Zr_31B	0,0018	756575	45532	64	9	851	0,01	0,95	1,76	0,11	1,46	0,83	0,06	0,98	677	16	681	22	691	15	98
Zr_3_N	0,0241	329189	329189	27	95	138	0,69	1,72	1,46	0,17	1,07	0,73	0,07	1,00	1009	19	1015	42	1029	38	98
Zr_13N	0,0016	518406	34417	42	201	227	0,89	1,37	2,03	0,14	1,90	0,93	0,07	0,72	872	18	876	24	887	16	98
Zr_8B	0,0118	904748	68209	78	392	384	1,03	1,59	1,63	0,16	1,50	0,92	0,07	0,63	963	19	968	26	979	19	98
Zr_39	0,0019	2896731	197598	258	261	1503	0,17	1,55	1,41	0,16	1,12	0,79	0,07	0,86	944	19	949	27	959	19	98
Zr_18B	0,0029	725982	44399	50	11	453	0,02	0,93	1,25	0,11	1,16	0,93	0,06	0,45	667	16	669	18	677	9	99
Zr_19	0,0017	895633	61854	81	508	458	1,12	1,57	1,09	0,16	1,00	0,92	0,07	0,44	954	19	958	23	968	13	99
Zr_50	0,0007	707734	707734	65	98	481	0,20	1,11	1,45	0,12	1,30	0,89	0,06	0,65	757	17	759	21	765	13	99
Zr_64B	0,0023	701355	43609	63	61	517	0,12	1,22	1,36	0,13	1,15	0,85	0,07	0,72	806	17	808	22	814	14	99
Zr_64B	0,0023	701355	43609	63	61	517	0,12	1,22	1,36	0,13	1,15	0,85	0,07	0,72	806	17	808	22	814	14	99

Zr_45N	0,0022	212694	14659	25	192	109	1,78	1,56	1,29	0,16	1,07	0,84	0,07	0,71	951	19	953	25	958	17	99
Zr_34	0,0050	782943	51485	73	173	573	0,30	1,76	1,56	0,17	1,19	0,76	0,07	1,01	1028	19	1029	31	1033	24	99
Zr_17N	0,0007	736022	736022	65	312	328	0,96	1,62	1,13	0,16	1,09	0,96	0,07	0,31	978	19	979	22	983	12	99
Zr_58	0,0030	575063	40490	64	322	297	1,09	1,62	1,53	0,16	1,38	0,91	0,07	0,65	977	19	979	25	982	16	100
Zr_58	0,0030	575063	40490	64	322	297	1,09	1,62	1,53	0,16	1,38	0,91	0,07	0,65	977	19	979	25	982	16	100
Zr_26B	0,0026	1189332	72997	93	50	883	0,06	0,98	1,23	0,11	1,03	0,84	0,06	0,67	693	16	694	20	696	12	100
Zr_18N	0,0012	315697	21545	29	167	142	1,19	1,55	1,38	0,16	1,28	0,93	0,07	0,52	950	19	951	23	953	14	100
Zr_11_N	0,0017	530084	35806	45	254	212	1,21	1,47	2,10	0,15	1,99	0,95	0,07	0,67	918	18	919	24	921	15	100
Zr_16	0,0005	1049557	72186	95	507	469	1,09	1,64	1,08	0,16	1,03	0,96	0,07	0,31	984	19	985	22	986	12	100
Zr_44N	0,0008	785471	53672	77	373	389	0,97	1,57	1,31	0,16	1,17	0,89	0,07	0,59	960	19	960	24	961	15	100
Zr_33	0,0009	385127	24540	37	100	107	0,94	1,67	1,48	0,17	0,98	0,66	0,07	1,11	996	19	996	31	995	24	100
Zr_41	0,0023	510149	35388	47	160	251	0,64	1,57	1,41	0,16	1,27	0,90	0,07	0,62	960	19	959	24	958	15	100
Zr_4	0,0042	1072449	76383	83	308	530	0,59	1,51	1,15	0,16	0,95	0,83	0,07	0,64	936	18	935	24	932	16	100
Zr_63	0,0006	543068	36777	58	254	304	0,84	1,71	1,16	0,17	0,96	0,83	0,07	0,65	1014	19	1013	26	1010	17	100
Zr_63	0,0006	543068	36777	58	254	304	0,84	1,71	1,16	0,17	0,96	0,83	0,07	0,65	1014	19	1013	26	1010	17	100
Zr_60	0,0013	248913	16845	26	117	133	0,89	1,53	1,66	0,16	1,52	0,92	0,07	0,66	945	19	944	24	941	16	100
Zr_60	0,0013	248913	16845	26	117	133	0,89	1,53	1,66	0,16	1,52	0,92	0,07	0,66	945	19	944	24	941	16	100
Zr_32	0,0042	630285	630285	69	331	367	0,91	1,62	1,47	0,16	1,19	0,81	0,07	0,86	978	19	977	27	973	20	100
Zr_49	0,0010	721812	43414	62	19	528	0,04	0,98	1,84	0,11	1,70	0,92	0,06	0,70	697	16	696	20	693	12	101
Zr_11B	0,0007	634635	39722	43	55	333	0,17	1,16	1,63	0,13	1,44	0,89	0,07	0,75	785	17	783	22	780	14	101
Zr_51B	0,0028	589347	35868	51	6	428	0,01	0,97	1,75	0,11	1,60	0,91	0,06	0,71	688	16	686	20	682	12	101
Zr_51N	0,0087	944089	70276	108	625	547	1,15	1,57	1,22	0,16	1,05	0,86	0,07	0,62	962	19	959	25	954	17	101
Zr_23	0,0006	745573	51129	75	363	336	1,09	1,65	1,53	0,17	1,41	0,92	0,07	0,59	992	19	989	24	984	15	101
Zr_27N	0,0006	681715	46469	64	245	349	0,71	1,62	1,28	0,16	1,13	0,88	0,07	0,61	979	19	976	24	970	15	101
Zr_48	0,0020	724482	44379	64	90	4364	0,02	1,00	1,73	0,12	1,56	0,90	0,06	0,74	705	16	703	20	698	13	101
Zr_28	0,0010	667007	45989	66	305	323	0,95	1,64	1,13	0,17	0,93	0,82	0,07	0,64	990	19	987	25	981	16	101
Zr_53	0,0010	365148	24992	40	204	200	1,03	1,62	1,41	0,16	1,24	0,88	0,07	0,66	979	19	977	25	970	16	101
Zr_54	0,0015	489323	34071	55	302	252	1,21	1,62	1,63	0,16	1,50	0,92	0,07	0,64	982	19	979	25	971	16	101
Zr_7	0,0019	281907	19258	24	120	122	0,99	1,60	1,28	0,16	1,08	0,85	0,07	0,68	975	19	971	25	963	16	101
Zr_24	0,0072	963283	70552	96	456	498	0,92	1,57	0,94	0,16	0,72	0,77	0,07	0,61	961	19	958	25	949	16	101
Zr_31N	0,0022	221766	15096	25	144	119	1,22	1,59	1,36	0,16	0,98	0,72	0,07	0,94	973	19	968	28	958	21	101
Zr_42	0,0026	895397	895397	94	564	475	1,20	1,60	1,10	0,16	0,91	0,83	0,07	0,61	975	19	970	24	960	15	102
Zr_47	0,0022	921051	64196	93	486	482	1,02	1,61	1,19	0,16	0,98	0,83	0,07	0,66	978	19	684	17	961	16	102
Zr_62	0,0009	535041	36662	60	303	284	1,07	1,63	1,24	0,17	1,09	0,88	0,07	0,58	988	19	983	24	971	15	102
Zr_62	0,0009	535041	36662	60	303	284	1,07	1,63	1,24	0,17	1,09	0,88	0,07	0,58	988	19	983	24	971	15	102

Zr_20	0,0003	775790	53027	71	380	333	1,15	1,65	1,13	0,17	1,09	0,96	0,07	0,32	996	19	990	22	978	12	102
Zr_64N	0,0015	751105	52018	91	595	421	1,42	1,67	1,10	0,17	0,94	0,85	0,07	0,57	1004	19	997	24	983	15	102
Zr_64N	0,0015	751105	52018	91	595	421	1,42	1,67	1,10	0,17	0,94	0,85	0,07	0,57	1004	19	997	24	983	15	102
Zr_13B	0,0022	899808	54563	58	17	600	0,03	0,96	1,44	0,11	1,24	0,86	0,06	0,72	685	16	682	20	671	12	102
Zr_3B	0,0179	767819	51048	53	17	451	0,04	0,98	1,50	0,11	1,30	0,86	0,06	0,76	697	16	694	25	683	19	102
Zr_59	0,0005	746440	746440	84	444	388	1,15	1,66	1,37	0,17	1,15	0,84	0,07	0,73	1002	19	994	26	979	17	102
Zr_59	0,0005	746440	746440	84	444	388	1,15	1,66	1,37	0,17	1,15	0,84	0,07	0,73	1002	19	994	26	979	17	102
Zr_45B	0,0006	506445	30119	39	3	365	0,01	0,96	1,42	0,11	1,25	0,88	0,06	0,67	688	16	684	20	671	11	102
Zr_30	0,0026	785439	54325	75	307	351	0,88	1,67	0,97	0,17	0,73	0,75	0,07	0,64	1005	19	987	25	980	16	103
Zr_46	0,0030	849611	52052	66	15	583	0,03	0,97	1,32	0,11	1,10	0,84	0,06	0,72	694	16	689	20	675	12	103
Zr_27B	0,0006	754783	51293	74	327	367	0,90	1,67	0,98	0,17	0,78	0,79	0,07	0,60	1004	19	995	25	977	15	103
Zr_2	0,0035	1155823	73036	78	27	732	0,04	1,01	1,59	0,12	1,22	0,76	0,06	1,03	716	16	940	31	694	16	103
Zr_66N	0,0025	633075	44391	69	333	346	0,97	1,67	1,09	0,17	0,91	0,84	0,07	0,60	1008	19	997	25	974	15	103
Zr_52	0,0005	629417	42688	66	281	353	0,80	1,65	1,26	0,17	1,06	0,84	0,07	0,67	998	19	988	25	964	16	104
Zr_26N	0,0032	260613	17450	23	66	136	0,49	1,67	1,98	0,17	1,71	0,86	0,07	1,01	1009	19	997	30	971	22	104
Zr_61	0,0011	444520	30575	48	219	239	0,92	1,69	1,17	0,17	1,01	0,86	0,07	0,60	1017	19	1004	25	975	15	104
Zr_61	0,0011	444520	30575	48	219	239	0,92	1,69	1,17	0,17	1,01	0,86	0,07	0,60	1017	19	1004	25	975	15	104
Zr_57	0,0011	535843	32244	46	9	417	0,02	1,00	1,62	0,12	1,45	0,90	0,06	0,71	712	16	704	20	680	12	105
Zr_9B	0,0029	1162611	81523	91	353	471	0,76	1,68	1,42	0,17	1,26	0,89	0,07	0,65	1016	19	1001	25	969	16	105
Zr_65	0,0050	3137565	224789	369	2496	1714	1,47	1,72	1,02	0,17	0,86	0,84	0,07	0,55	1030	20	997	24	981	15	105
Zr_65	0,0050	3137565	224789	369	2496	1714	1,47	1,72	1,02	0,17	0,86	0,84	0,07	0,55	1030	20	997	24	981	15	105
Zr_12	0,0008	852219	57328	69	321	335	0,97	1,61	1,73	0,17	1,62	0,94	0,07	0,61	990	19	975	24	942	15	105
Zr_22	0,0009	662645	45362	63	390	284	1,38	1,69	1,24	0,17	1,18	0,95	0,07	0,38	1020	19	990	23	968	12	105
Zr_15	0,0053	1047716	74138	83	411	468	0,89	1,69	1,49	0,17	1,26	0,85	0,07	0,79	1023	19	783	21	962	19	106
Zr_10	0,0434	362712	362712	30	90	171	0,53	1,33	1,38	0,15	0,95	0,69	0,06	1,00	900	18	859	70	756	60	119

a Fraction of the non-radiogenic 206Pb in the analyzed zircon spot, where $f206=[206Pb/204Pb]c/[206Pb/204Pb]s$ (c=common; s=sample)

b Th/U ratios and amount of Pb, Th and U (in pmm) are calculated relative to GJ-1 reference zircon

c Corrected for background and within-run Pb/U fractionation and normalised to reference zircon GJ-1 (ID-TIMS values/measured value); 207Pb/235U calculated using (207Pb/206Pb)*(206Pb/238U)*(137.88)

d Rho is the error correlation defined as the quotient of the propagated errors of the 206Pb/238U and the 207/235U ratio

e Corrected for mass-bias by normalising to GJ-1 reference zircon and common Pb using the model Pb composition of Stacey and Kramers (1975)

f Degree of concordance, 6/8-7/6= (206Pb/238U age * 100) / (207Pb/206Pb age)

g Total systematic uncertainties (ssys) 206/238U =2.0%, 207Pb/206Pb = 0.55 % (2s)

Table 6: Summary of U-Pb zircon data of the sample DDLH_10_A obtained by LA-SF-ICP-MS method.

Sample DMHL-2				Isotope ratios[b]							Ages (Ma)						
Spot number	Pb206* cps	Pb207* cps	Th/U[a]	$^{207}Pb^*/^{206}Pb^*$	± 2s (%)	$^{207}Pb^*/^{235}U$	± 2s (%)	$^{206}Pb^*/^{238}U$	± 2s (%)	RHO	$^{206}Pb/^{238}U$	± 2s	$^{207}Pb/^{235}U$	± 2s	$^{206}Pb/^{207}Pb$	± 2s	Conc
7	1939206	137848	1,41	0,0725	2,03	1,6934	3,18	0,1694	2,45	0,77	1000	41	1009	23	1006	20	102
8	139330	12085	0,21	0,0885	3,27	1,6053	4,21	0,1316	2,64	0,63	1393	63	797	20	972	27	83
9	360822	25694	1,33	0,0726	2,36	1,6849	3,53	0,1682	2,62	0,74	1004	48	1002	25	1003	23	102
11	1284384	91720	1,41	0,0728	3,47	1,6937	4,32	0,1686	2,58	0,60	1009	71	1005	24	1006	28	102
12	639517	45299	1,86	0,0722	2,06	1,5653	3,15	0,1571	2,39	0,76	993	42	941	21	957	20	100
13	1812148	128778	1,92	0,0725	2,06	1,6939	3,09	0,1695	2,30	0,75	1000	42	1009	22	1006	20	102
14	797866	57004	1,63	0,0729	3,47	1,6926	4,36	0,1684	2,65	0,61	1010	71	1004	25	1006	28	102
15	1966604	138681	2,31	0,0719	2,07	1,6987	3,09	0,1713	2,30	0,74	984	42	1019	22	1008	20	103
17	498446	35898	1,11	0,0735	3,47	1,6900	4,34	0,1669	2,60	0,60	1027	71	995	24	1005	28	101
18	2218774	157962	1,82	0,0726	3,49	1,6929	4,35	0,1691	2,58	0,59	1003	71	1007	24	1006	28	102

[a]data corrected for common-Pb

[b]concentration uncertainty ca. 20%

[c]Concordance calculated as: ((^{206}Pb-^{238}U(age))/(^{207}Pb-^{206}Pb(age)))*100

Decay constants of Jaffey et al. (1971) used

Total systematic uncertainties (σsys): $^{206}Pb/^{238}U$ = 2.0%, $^{207}Pb/^{206}Pb$ = 0.55% (2σ)

Uncertainties quoted without components related to systematic error unless otherwise stated

Table 7: Summary of U-Pb zircon data of the sample DMLH-10-B obtained by LA-MC-ICP-MS method.

								Isotope ratios[c]							Ages (Ma)						
Spot Number	f206[a]	206Pb cps	207Pb cps	Pb ppm	Th ppm	U ppm	Th/U[b]	207Pb/ 235U	1 s [%]	206Pb/ 238U	1 s [%]	Rho[d]	207Pb/ 206Pbe	1 s [%]	206Pb/ 238U	2s[g] abs	207Pb/ 235U	2s abs	207Pb/ 206Pb	2sg abs	[f]Conc % 6/8-7/6
Zr_1	0,0017	243838	15927	28	73	168	0,44	1,2431	3,47	0,1247	3,40	0,98	0,0723	0,69	758	17	820	23	994	17	76,2
Zr_2	0,0071	216368	14179	27	123	178	0,70	1,5368	1,27	0,1556	0,93	0,73	0,0716	0,87	932	18	945	27	976	21	95,5
Zr_3	0,0035	207534	207534	26	109	149	0,74	1,5135	1,78	0,1522	1,64	0,92	0,0721	0,70	913	18	936	25	989	17	92,4
Zr_4	0,0007	675270	43238	86	368	472	0,78	1,6757	1,35	0,1694	1,18	0,87	0,0717	0,65	1009	19	999	25	979	16	103,1
Zr_6	0,0016	252416	16389	30	115	196	0,59	1,5770	1,46	0,1580	1,30	0,89	0,0724	0,68	945	19	961	25	997	17	94,8

Zr_6	0,0022	252560	16376	30	115	197	0,59	1,5487	1,45	0,1572	1,24	0,86	0,0714	0,75	941	19	950	25	970	18	97,0
Zr_7	0,0015	313559	20264	38	149	238	0,63	1,5764	1,15	0,1591	0,90	0,79	0,0719	0,71	952	19	961	25	983	17	96,8
Zr_8	0,0041	246750	16765	29	104	247	0,43	1,4916	1,90	0,1524	1,61	0,85	0,0710	1,01	914	18	927	28	957	22	95,5
Zr_9	0,0021	372056	24129	47	247	319	0,78	1,4745	1,15	0,1495	0,83	0,72	0,0715	0,79	898	18	920	25	973	18	92,3
Zr_14	0,0030	190633	12384	26	62	158	0,39	1,5800	2,30	0,1589	1,82	0,79	0,0721	1,40	951	19	962	34	989	30	96,2
Zr_15	0,0365	1861442	172587	277	701	5240	0,13	0,4715	5,47	0,0473	5,26	0,96	0,0722	1,48	298	13	392	32	993	67	30,0
Zr_16	0,0011	570045	36483	80	311	509	0,62	1,5470	2,38	0,1545	1,97	0,83	0,0726	1,33	926	18	949	33	1003	29	92,4
Zr_17	0,0000	204291	11390	28	85	162	0,53	1,4402	2,37	0,1466	1,80	0,76	0,0712	1,55	882	18	906	35	964	31	91,5
Zr_18	0,0000	384390	23215	55	192	325	0,60	1,4260	2,38	0,1449	1,96	0,82	0,0714	1,35	872	18	900	32	969	28	90,0
Zr_19	0,0000	315787	18767	44	141	267	0,53	1,3928	2,23	0,1434	1,76	0,79	0,0705	1,37	864	18	886	32	942	27	91,7
Zr_20	0,0034	508050	34094	73	288	528	0,55	1,4723	3,01	0,1465	2,69	0,89	0,0729	1,35	881	18	900	32	1011	29	87,2
Zr_21	0,0111	644239	49319	109	521	624	0,84	1,5407	2,23	0,1501	1,94	0,87	0,0745	1,11	901	18	947	32	1054	29	85,5
Zr_22	0,0000	365717	21861	57	188	308	0,61	1,6005	2,42	0,1595	2,03	0,84	0,0728	1,31	954	19	970	33	1007	28	94,7
Zr_23	0,0000	397823	397823	62	224	373	0,61	1,5654	2,46	0,1541	1,97	0,80	0,0737	1,48	924	18	957	35	1033	32	89,5
Zr_24	0,0000	259947	15116	39	107	247	0,44	1,4662	2,34	0,1500	1,97	0,84	0,0709	1,27	901	18	917	31	955	26	94,4
Zr_25	0,0000	317315	19046	48	147	315	0,47	1,2839	3,10	0,1349	2,83	0,91	0,0690	1,27	816	17	839	29	900	25	90,6
Zr_26	0,0018	328109	21068	50	162	315	0,52	1,4922	2,34	0,1516	1,95	0,83	0,0714	1,30	910	18	927	32	968	27	94,0
Zr_27	0,0010	328665	21019	48	94	280	0,34	1,4790	2,82	0,1491	2,53	0,90	0,0720	1,24	896	18	922	31	985	26	90,9
Zr_28	0,0222	425155	27827	68	222	502	0,44	1,3215	3,00	0,1330	2,64	0,88	0,0721	1,43	805	17	855	41	988	43	81,4
Zr_29	0,0154	890295	67108	147	821	954	0,87	1,2053	3,70	0,1200	3,48	0,94	0,0729	1,26	731	16	803	32	1010	34	72,3
Zr_30	0,0026	792602	51224	122	374	977	0,39	1,5100	2,44	0,1504	2,13	0,87	0,0728	1,19	903	18	855	28	1009	26	89,6
Zr_31	0,0048	605013	40618	91	276	1005	0,28	1,1637	2,89	0,1173	2,72	0,94	0,0720	0,96	715	16	784	25	985	22	72,5
Zr_32	0,0013	321367	20642	51	154	279	0,55	1,4387	2,49	0,1449	2,26	0,91	0,0720	1,05	872	18	905	28	986	23	88,5
Zr_33	0,0023	166345	166345	27	88	176	0,51	1,4725	2,42	0,1472	2,22	0,92	0,0726	0,97	885	18	919	27	1002	22	88,4
Zr_34	0,0028	375290	24430	64	274	388	0,71	1,3624	3,04	0,1376	2,86	0,94	0,0718	1,03	831	17	873	27	981	23	84,8
Zr_37	0,0052	1145794	76283	174	269	1417	0,19	1,1458	2,98	0,1171	2,80	0,94	0,0709	1,01	714	16	775	25	956	22	74,7
Zr_38	0,0028	293549	19510	49	239	324	0,74	1,2112	3,22	0,1212	3,02	0,94	0,0725	1,11	738	16	806	27	999	24	73,9
Zr_39	0,0020	277918	17932	45	134	259	0,52	1,3186	2,77	0,1338	2,51	0,91	0,0715	1,16	809	17	854	28	971	25	83,3
Zr_40	0,0042	717742	48973	120	366	629	0,59	1,1603	4,87	0,1150	4,77	0,98	0,0732	0,96	702	16	806	26	1019	22	68,9
Zr_41	0,0031	358381	23649	56	175	379	0,47	1,4194	2,60	0,1419	2,39	0,92	0,0725	1,02	856	18	897	28	1001	23	85,5
Zr_42	0,0005	391720	25042	65	229	356	0,65	1,6472	2,62	0,1644	2,41	0,92	0,0727	1,03	981	19	988	30	1004	23	97,7
Zr_43	0,0023	250227	250227	39	99	227	0,44	1,5457	2,43	0,1563	2,11	0,87	0,0717	1,22	936	18	949	31	978	26	95,8
Zr_44	0,0011	336018	21222	51	96	242	0,40	1,8078	2,15	0,1809	1,89	0,88	0,0725	1,02	1072	20	1048	31	999	23	107,2
Zr_48	0,0030	302388	19909	51	191	263	0,73	1,6275	2,33	0,1616	2,09	0,90	0,0730	1,04	966	19	981	30	1015	24	95,2
Zr_49	0,0016	246519	15850	41	162	239	0,68	1,6473	2,28	0,1666	1,93	0,85	0,0717	1,21	993	19	989	32	978	26	101,5

Zr_50	0,0015	237771	15382	37	103	245	0,42	1,5179	2,44	0,1522	2,21	0,91	0,0724	1,02	913	18	981	30	996	23	91,7
Zr_51	0,0024	262257	17045	37	116	274	0,43	1,5652	1,96	0,1577	1,76	0,90	0,0720	0,85	944	19	957	27	985	19	95,8
Zr_52	0,0036	219939	14517	33	137	217	0,64	1,5109	2,12	0,1532	1,93	0,91	0,0715	0,87	919	18	935	27	972	20	94,5
Zr_53	0,0011	412054	412054	62	236	395	0,60	1,6687	1,84	0,1672	1,72	0,94	0,0724	0,64	997	19	997	25	997	16	100,0
Zr_54	0,0079	304570	21340	49	365	345	1,07	1,4378	3,32	0,1456	3,25	0,98	0,0716	0,69	876	18	905	25	975	18	89,8
Zr_55	0,0043	459415	30392	66	331	393	0,85	1,6355	3,14	0,1641	3,06	0,97	0,0723	0,72	980	19	984	26	993	18	98,6
Zr_56	0,0009	960025	61597	151	656	872	0,76	1,5834	1,99	0,1606	1,86	0,93	0,0715	0,71	960	19	964	25	972	17	98,7
Zr_57	0,0031	729522	47532	97	108	562	0,19	1,7119	1,82	0,1714	1,71	0,94	0,0724	0,62	1020	19	1013	25	998	16	102,2
Zr_58	0,0024	1079005	70901	147	218	836	0,26	1,5105	2,20	0,1529	2,11	0,96	0,0717	0,62	917	18	935	24	977	16	93,9
Zr_59	0,0032	547532	36116	79	254	476	0,54	1,6097	2,23	0,1634	2,14	0,96	0,0715	0,64	976	19	974	25	970	16	100,5
Zr_60	0,0090	222908	16064	34	284	336	0,85	0,7308	5,54	0,0728	5,48	0,99	0,0728	0,81	453	14	935	35	1010	21	44,8
Zr_62	0,0135	719322	54637	114	581	736	0,79	1,6274	1,96	0,1614	1,80	0,92	0,0732	0,77	964	19	981	29	1018	23	94,7
Zr_63	0,0029	590276	590276	91	494	584	0,85	1,6372	2,09	0,1639	1,96	0,94	0,0724	0,71	978	19	985	26	998	17	98,0
Zr_64	0,0012	360138	23207	54	202	292	0,70	1,6728	1,66	0,1672	1,50	0,90	0,0726	0,71	997	19	998	26	1002	17	99,5
Zr_65	0,0012	199200	12761	29	86	158	0,55	1,6530	1,73	0,1664	1,56	0,90	0,0720	0,75	992	19	991	26	987	18	100,6
Zr_67	0,0010	339902	21848	51	210	292	0,72	1,5968	1,63	0,1592	1,49	0,91	0,0727	0,67	952	18	969	25	1007	17	94,6
Zr_68	0,0062	174168	11979	25	69	232	0,30	1,2120	2,56	0,1197	2,27	0,88	0,0735	1,19	729	16	806	28	1026	28	71,0
Zr_69	0,0067	1018674	70847	144	297	829	0,36	1,5609	2,56	0,1549	2,46	0,96	0,0731	0,68	928	18	955	25	1017	18	91,3

[1] Convertion factor from mV to CPS is 62500

[2] concentration uncertainty c.20%

[3] data not corrected for common-Pb

[4] not corrected for common-Pb

[5] Discordance calculated as (1-(^{206}Pb/^{238}U age/^{207}Pb/^{206}Pb age))*100

Decay constants of Jaffey et al 1971 used

Table 8: Summary of U-Pb zircon data of the sample DDLH_11A obtained by LA-MC-ICP-MS method.

								Isotope ratios[c]							Ages (Ma)						
Spot		206Pb	207Pb	Pb	Th	U		207Pb/	1 s	206Pb/	1 s		207Pb/	1 s	206Pb/	2s[g]	207Pb/	2s	207Pb/	2sg	[f]Conc %
Number	*f*206[a]	cps	cps	ppm	ppm	ppm	Th/U[b]	235U	[%]	238U	[%]	Rho[d]	206Pbe	[%]	238U	abs	235U	abs	206Pb	abs	6/8-7/6
Zr_1	0,0018	530082	36420	52	229	293	0,79	1,68	2,02	0,16	1,82	0,90	0,08	0,86	960	19	1002	28	1094	22	88
ZR_2	0,0029	262337	17354	25	91	154	0,60	1,45	2,22	0,15	2,07	0,93	0,07	0,81	875	18	911	26	1000	19	88

Zr_3	0,0006	743899	743899	82	537	404	1,34	1,56	2,02	0,16	1,92	0,95	0,07	0,63	933	18	953	24	997	16	94
Zr_4	0,0006	1189932	76040	109	361	682	0,53	1,62	2,32	0,16	2,21	0,96	0,07	0,68	981	19	977	25	969	16	101
Zr_5	0,0015	427741	27899	47	320	248	1,30	1,45	2,20	0,14	2,01	0,91	0,07	0,91	870	18	910	27	1010	21	86
Zr_6	0,0021	321567	21124	32	201	222	0,91	1,21	2,89	0,12	2,73	0,94	0,07	0,96	731	16	805	25	1013	22	72
Zr_7	0,0003	828682	52912	72	152	446	0,34	1,43	2,57	0,14	2,49	0,97	0,07	0,62	865	18	901	23	991	16	87
Zr_8	0,0007	857117	93488	76	60	213	0,28	5,98	1,36	0,35	1,26	0,93	0,12	0,50	1956	31	1973	42	1991	28	98
Zr_9	0,0005	453437	29678	48	298	258	1,16	1,37	2,73	0,13	2,64	0,97	0,07	0,67	813	17	874	24	1034	17	79
Zr+10	0,0009	311758	21455	33	169	159	1,07	1,75	2,23	0,17	2,13	0,96	0,08	0,65	985	19	1973	50	1117	18	88
Zr_11	0,0014	715433	46964	77	342	481	0,72	1,32	2,64	0,13	2,57	0,97	0,07	0,63	805	17	856	23	993	16	81
Zr_12	0,0007	1520506	97353	159	577	1017	0,57	1,52	2,14	0,15	2,06	0,96	0,07	0,57	928	18	940	23	969	15	96
Zr_13	0,0022	243567	243567	25	72	159	0,45	1,68	1,82	0,17	1,62	0,89	0,07	0,84	1000	19	1002	28	1005	20	100
Zr_14	0,0009	431264	27778	45	150	301	0,50	1,43	3,19	0,15	3,14	0,98	0,07	0,55	873	18	903	23	978	15	89
Zr_15	0,0010	703873	75626	80	177	243	0,74	5,54	1,22	0,34	1,03	0,84	0,12	0,66	1870	30	1908	44	1949	32	96
Zr_16	0,0055	373034	25168	40	179	253	0,71	1,49	1,95	0,15	1,84	0,94	0,07	0,64	904	18	928	24	984	17	92
Zr_17	0,0011	1001196	64692	124	1023	819	1,26	1,35	2,16	0,14	2,10	0,97	0,07	0,53	831	17	868	22	964	14	86
Zr_18	0,0013	473533	29806	57	346	347	1,00	1,33	1,88	0,14	1,78	0,95	0,07	0,60	823	17	858	22	948	15	87
Zr_19	0,0010	344968	21944	37	169	234	0,72	1,42	2,23	0,14	2,15	0,97	0,07	0,57	872	18	896	23	955	15	91
Zr_20	0,0010	467977	49590	51	86	155	0,56	5,37	2,03	0,33	1,97	0,97	0,12	0,49	1828	30	858	18	1940	27	94
Zr_21	0,0015	252887	16234	33	141	191	0,74	1,59	1,58	0,16	1,42	0,90	0,07	0,70	953	19	966	25	996	17	96
Zr_22	0,0005	2140135	232126	247	119	788	0,15	5,79	0,91	0,34	0,76	0,84	0,12	0,49	1910	31	1945	42	1983	28	96
Zr_23	0,0006	772201	772201	103	471	567	0,84	1,58	1,58	0,16	1,47	0,93	0,07	0,59	944	19	960	24	999	15	95
Zr_24	0,0059	311826	22058	50	384	241	1,61	1,69	1,76	0,17	1,60	0,91	0,07	0,72	1000	19	1005	27	1016	19	98
Zr_25	0,0028	539370	34085	62	136	392	0,35	1,50	1,42	0,15	1,24	0,87	0,07	0,69	920	18	931	25	956	16	96
Zr_26	0,0012	255901	16508	32	102	181	0,57	1,67	1,99	0,17	1,89	0,95	0,07	0,64	996	19	995	25	993	16	100
Zr_27	0,0007	498140	54387	70	142	141	1,01	6,29	1,48	0,37	1,44	0,97	0,12	0,35	2022	32	2017	41	2013	25	100
Zr_28	0,0028	263793	17297	32	95	219	0,44	1,58	1,60	0,16	1,34	0,84	0,07	0,88	960	19	961	27	966	20	99
Zr_29	0,0014	532803	33835	66	218	408	0,54	1,60	1,46	0,16	1,20	0,82	0,07	0,83	969	19	969	27	967	19	100
Zr_30	0,0027	317892	22466	51	391	256	1,54	1,70	2,13	0,17	2,02	0,95	0,07	0,67	1011	19	961	24	1008	17	100
Zr_31	0,0031	352766	23501	41	53	270	0,20	1,37	3,10	0,14	2,94	0,95	0,07	0,96	824	17	878	27	1018	22	81
Zr_32	0,0067	291600	21236	36	98	289	0,34	1,92	2,91	0,18	2,20	0,76	0,08	1,90	1074	20	1089	49	1118	45	96
Zr_33	0,0002	695317	695317	87	96	227	0,43	5,60	1,71	0,33	1,67	0,98	0,12	0,38	1856	30	1916	39	1982	25	94
Zr_34	0,0019	428717	28164	51	97	337	0,29	1,57	2,05	0,16	1,92	0,94	0,07	0,70	940	19	959	25	1003	17	94
Zr_35	0,0002	912478	96734	117	185	334	0,56	5,20	0,94	0,31	0,87	0,92	0,12	0,36	1760	29	1853	38	1960	24	90
Zr_36	0,0019	181652	11878	23	129	232	0,56	1,33	2,29	0,13	2,13	0,93	0,07	0,86	803	17	858	25	1005	20	80
Zr_27	0,0004	1112212	170232	144	123	287	0,43	10,68	0,90	0,44	0,72	0,81	0,18	0,53	2362	37	2496	53	2606	38	91

Zr_38	0,0003	1087839	170905	147	174	282	0,62	11,59	1,12	0,47	1,05	0,94	0,18	0,38	2488	39	2572	52	2638	33	94
Zr_39	0,0007	999014	63992	114	160	637	0,25	1,59	2,14	0,16	1,88	0,88	0,07	1,03	959	19	967	29	984	22	97
Zr_40	0,0023	610656	39311	78	295	491	0,60	1,55	1,95	0,16	1,82	0,93	0,07	0,71	940	19	2572	68	980	17	96
Zr_41	0,0079	236797	16831	36	169	211	0,81	1,43	3,33	0,14	3,25	0,98	0,07	0,73	856	18	903	25	1020	19	84
Zr_42	0,0005	393582	25186	74	637	327	1,96	1,49	3,16	0,15	3,10	0,98	0,07	0,61	898	18	925	24	990	16	91
Zr_43	0,0008	1028815	1028815	166	1112	1094	1,02	1,66	2,97	0,17	2,90	0,97	0,07	0,68	991	19	995	26	1005	17	99
Zr_44	0,0016	443359	63613	69	159	201	0,80	7,55	2,61	0,34	2,57	0,99	0,16	0,45	1883	30	2179	46	2470	33	76
Zr_45	0,0020	306952	19536	43	266	379	0,71	1,38	3,35	0,14	3,24	0,97	0,07	0,87	854	18	879	25	945	19	90
Zr_46	0,0006	840069	52997	125	620	778	0,80	1,47	3,16	0,15	3,09	0,98	0,07	0,66	906	18	917	24	946	16	96
Zr_47	0,0037	351257	22690	51	270	416	0,65	1,43	3,42	0,14	3,34	0,98	0,07	0,71	861	18	902	24	1002	18	86
Zr_48	0,0018	118194	7519	17	65	102	0,64	1,45	3,29	0,15	3,15	0,96	0,07	0,97	900	18	910	27	932	20	97
Zr_49	0,0017	120189	7415	15	89	122	0,73	1,21	3,71	0,13	3,54	0,96	0,07	1,09	778	17	805	26	883	21	88
Zr_50	0,0021	152800	9702	21	78	132	0,60	1,54	3,06	0,16	2,88	0,94	0,07	1,06	949	19	910	28	947	22	100
Zr_51	0,0029	444307	28599	64	264	347	0,76	1,44	2,24	0,15	2,12	0,95	0,07	0,73	880	18	905	25	967	17	91
Zr_52	0,0004	563377	59845	84	144	223	0,65	5,89	1,69	0,36	1,62	0,96	0,12	0,47	1967	32	1960	41	1953	27	101
Zr_53	0,0007	707002	707002	107	181	268	0,68	5,90	1,45	0,36	1,40	0,97	0,12	0,37	1960	31	1962	40	1964	24	100
Zr_54	0,0012	262397	17474	42	199	209	0,96	1,81	2,11	0,18	1,92	0,91	0,07	0,87	1048	20	1050	29	1052	21	100
Zr_55	0,0016	348224	22149	51	296	355	0,84	1,38	2,18	0,14	2,09	0,96	0,07	0,60	856	18	881	23	943	15	91
Zr_56	0,0013	216185	13793	38	242	183	1,33	1,61	2,11	0,16	2,03	0,96	0,07	0,60	974	19	974	24	974	15	100
Zr_57	0,0016	236929	15116	36	145	197	0,74	1,61	2,12	0,16	2,01	0,95	0,07	0,68	963	19	975	25	1001	17	96
Zr_58	0,0021	218602	14112	33	141	200	0,71	1,58	2,37	0,16	2,18	0,92	0,07	0,93	953	19	961	28	979	21	97
Zr_59	0,0012	542968	34073	79	258	472	0,55	1,46	2,20	0,15	2,13	0,97	0,07	0,56	903	18	912	23	936	14	97
Zr_60	0,0005	674867	43160	99	379	557	0,69	1,56	2,22	0,16	2,16	0,97	0,07	0,52	945	19	961	23	978	14	97
Zr_61	0,0024	218911	14253	31	94	165	0,57	1,55	1,92	0,16	1,78	0,93	0,07	0,73	941	19	951	25	973	17	97
ZR_62	0,0006	1090370	69364	158	548	858	0,64	1,58	1,97	0,16	1,87	0,95	0,07	0,60	962	19	964	24	967	15	99
Zr_63	0,0004	826280	826280	123	195	304	0,65	5,67	0,97	0,34	0,90	0,92	0,12	0,38	1878	30	1926	39	1978	25	95
Zr_74	0,0019	222145	14189	31	94	197	0,48	1,48	3,73	0,15	3,60	0,96	0,07	0,98	915	18	920	27	932	21	98
Zr_65	0,0013	474579	29999	69	275	432	0,64	1,59	1,81	0,16	1,70	0,94	0,07	0,63	954	19	967	25	995	16	96
Zr_66	0,0002	3118443	417906	456	1317	1397	0,95	6,05	1,91	0,29	1,80	0,94	0,15	0,65	1645	27	1983	46	2357	39	70
Zr_67	0,0015	559944	37388	92	556	450	1,25	1,80	1,89	0,18	1,68	0,89	0,07	0,86	1045	20	1046	29	1046	21	100
Zr_68	0,0004	635516	39418	93	438	570	0,77	1,49	2,00	0,15	1,83	0,92	0,07	0,80	925	18	925	25	927	17	100
Zr_69	0,0003	535395	57797	81	140	191	0,74	6,08	1,35	0,36	1,31	0,97	0,12	0,35	1987	32	1987	40	1988	24	100
Zr_70	0,0007	623097	39888	83	168	533	0,32	1,60	1,99	0,16	1,92	0,96	0,07	0,52	963	19	925	22	987	14	98
Zr_71	0,0012	400981	25438	46	109	299	0,37	1,47	2,49	0,15	2,38	0,96	0,07	0,73	904	18	918	25	950	17	95
Zr_72	0,0008	387625	24601	50	245	295	0,84	1,46	2,82	0,15	2,73	0,97	0,07	0,71	897	18	913	24	953	17	94

Zr_73	0,0019	183108	183108	27	187	161	1,17	1,61	2,54	0,16	2,45	0,97	0,07	0,66	966	19	973	25	989	16	98
Zr_74	0,0033	222969	14191	27	88	172	0,52	1,40	2,53	0,15	2,35	0,93	0,07	0,94	888	18	890	26	894	19	99
Zr_75	0,0036	270550	17405	37	360	270	1,34	0,91	5,38	0,10	5,30	0,99	0,07	0,91	587	15	656	22	902	19	65
Zr_76	0,0010	415877	26558	51	180	314	0,58	1,61	2,47	0,16	2,38	0,96	0,07	0,66	975	19	973	25	970	16	101
Zr_77	0,0010	901805	98337	105	92	381	0,24	5,59	1,87	0,33	1,80	0,96	0,12	0,52	1837	30	1915	42	2000	29	92
Zr_78	0,0020	249851	15997	29	68	205	0,33	1,48	2,75	0,15	2,35	0,85	0,07	1,43	905	18	922	34	962	29	94
Zr_79	0,0013	197149	12008	25	126	169	0,75	1,37	2,80	0,15	2,61	0,93	0,07	1,02	877	18	876	27	875	20	100
Zr_80	0,0021	200829	11927	23	51	189	0,27	1,22	2,79	0,13	2,69	0,96	0,07	0,75	804	17	922	26	823	15	98
Zr_81	0,0008	946978	60742	109	448	622	0,72	1,59	2,09	0,16	2,01	0,96	0,07	0,59	963	19	967	24	976	15	99
Zr_82	0,0004	652795	69834	78	157	210	0,75	5,76	1,91	0,35	1,52	0,80	0,12	1,15	1915	31	1940	58	1966	49	97
Zr_83	0,0012	201345	201345	23	94	132	0,71	1,53	2,21	0,16	2,12	0,96	0,07	0,62	930	18	943	24	972	16	96
Zr_84	0,0006	862800	92395	98	152	309	0,50	5,85	1,30	0,35	1,19	0,92	0,12	0,52	1947	31	1954	42	1962	28	99
Zr_85	0,0024	144323	9533	18	111	110	1,02	1,62	2,42	0,16	2,19	0,91	0,07	1,03	979	19	978	29	976	22	100
Zr_86	0,0010	333319	21177	45	309	237	1,31	1,51	2,38	0,15	2,31	0,97	0,07	0,58	920	18	936	23	973	15	95
Zr_87	0,0021	570883	37475	61	159	383	0,42	1,57	1,99	0,16	1,91	0,96	0,07	0,55	934	18	958	24	1015	15	92
Zr_88	0,0013	218225	13707	24	91	160	0,57	1,35	2,42	0,14	2,25	0,93	0,07	0,87	843	17	868	25	934	19	90
Zr_89	0,0007	393115	42399	44	60	108	0,56	5,86	1,81	0,35	1,69	0,94	0,12	0,63	1940	31	1955	45	1972	32	98
Zr_90	0,0017	194533	12642	22	75	123	0,62	1,55	2,25	0,16	2,14	0,95	0,07	0,68	932	18	868	23	987	17	94
Zr_91	0,0005	795786	50841	102	460	498	0,93	1,63	2,07	0,17	2,00	0,97	0,07	0,52	985	19	984	24	981	14	100
Zr_92	0,0015	312021	19789	34	64	201	0,32	1,56	1,99	0,16	1,84	0,93	0,07	0,75	957	19	955	25	951	17	101
Zr_93	0,0012	247712	247712	29	91	172	0,54	1,56	2,16	0,16	2,07	0,96	0,07	0,61	943	19	953	24	978	15	96
Zr_94	0,0003	1650787	175652	179	90	548	0,16	5,46	2,31	0,33	1,50	0,65	0,12	1,75	1829	30	1894	76	1965	72	93
Zr_95	0,0024	104537	6857	15	92	64	1,44	1,59	2,53	0,16	2,29	0,90	0,07	1,09	957	19	968	30	991	24	97
Zr_96	0,0020	405213	25860	50	530	480	1,11	0,96	5,18	0,10	5,12	0,99	0,07	0,80	607	15	684	22	946	18	64
Zr_97	0,0025	905197	58587	98	173	729	0,24	1,63	2,39	0,17	2,31	0,97	0,07	0,62	985	19	982	25	973	16	101
Zr_98	0,0009	292909	18795	35	121	198	0,61	1,46	2,29	0,15	2,21	0,97	0,07	0,60	888	18	914	23	978	15	91
Zr_99	0,0017	466194	30518	61	318	322	0,99	1,54	2,38	0,15	2,32	0,97	0,07	0,54	921	18	946	23	1006	15	92
Zr_100	0,0032	439247	29058	57	278	304	0,92	1,65	1,99	0,17	1,91	0,96	0,07	0,57	990	19	914	23	988	15	100

a Fraction of the non-radiogenic 206Pb in the analyzed zircon spot, where $f206=[206Pb/204Pb]c/[206Pb/204Pb]s$ (c=common; s=sample)

b Th/U ratios and amount of Pb, Th and U (in pmm) are calculated relative to GJ-1 reference zircon

c Corrected for background and within-run Pb/U fractionation and normalised to reference zircon GJ-1 (ID-TIMS values/measured value); 207Pb/235U calculated using (207Pb/206Pb)*(206Pb/238U)*(137.88)

d Rho is the error correlation defined as the quotient of the propagated errors of the 206Pb/238U and the 207/235U ratio

e Corrected for mass-bias by normalising to GJ-1 reference zircon and common Pb using the model Pb composition of Stacey and Kramers (1975)

f Degree of concordance, 6/8-7/6= (206Pb/238U age * 100) / (207Pb/206Pb age)

g Total systematic uncertainties (ssys) 206/238U =2.0%, 207Pb/206Pb = 0.55 % (2s)

Table 9: Summary of U-Pb zircon data of the sample DMLH-12-A obtained by LA-MC-ICP-MS method.

								Isotope ratios[c]							Ages (Ma)						
Spot Number	f206[a]	206Pb cps	207Pb cps	Pb ppm	Th ppm	U ppm	Th/U[b]	207Pb/ 235U	1 s [%]	206Pb/ 238U	1 s [%]	Rho[d]	207Pb/ 206Pbe	1 s [%]	206Pb/ 238U	2s[g] abs	207Pb/ 235U	2s abs	207Pb/ 206Pb	2sg abs	[f]Conc % 6/8-7/6
Zr_1	0,0054	136127	7651	13	54	95	0,58	0,9873	1,94	0,1131	1,81	0,93	0,0633	0,71	691	27	697	30	718	12	96
Zr_2	0,0023	99585	5534	10	51	84	0,61	0,9631	2,21	0,1108	2,03	0,92	0,0631	0,88	677	29	685	33	710	14	95
Zr_4	0,0015	67641	3799	7	34	113	0,30	0,9526	2,31	0,1097	2,04	0,88	0,0630	1,09	671	29	679	34	707	17	95
Zr_5	0,0022	83984	4716	8	42	68	0,63	0,9793	2,33	0,1123	2,20	0,94	0,0633	0,77	686	32	693	35	717	13	96
ZR_6	0,0021	87606	4979	9	46	72	0,64	1,0434	2,12	0,1192	1,96	0,93	0,0635	0,80	726	31	726	33	724	14	100
Zr_7	0,0044	83324	4689	8	37	63	0,59	1,0042	2,80	0,1157	2,64	0,94	0,0629	0,93	706	39	706	42	706	15	100
Zr_08	0,0016	122188	6931	12	47	89	0,53	0,9927	2,29	0,1128	2,15	0,94	0,0638	0,77	689	31	700	34	735	14	94
Zr_9	0,0014	68596	3948	7	31	59	0,53	0,9744	2,72	0,1119	2,53	0,93	0,0632	1,00	684	36	691	40	714	16	96
Zr_10	0,0067	90609	5069	9	43	76	0,57	0,9968	2,02	0,1149	1,86	0,92	0,0629	0,77	701	28	700	31	706	13	99
Zr_13	0,0082	55718	55718	8	56	73	0,77	0,9670	3,33	0,1106	2,53	0,76	0,0634	2,17	676	16	687	36	722	34	94
Zr_14	0,0040	79514	4493	11	63	96	0,66	1,0166	2,09	0,1165	1,78	0,85	0,0633	1,09	711	16	712	24	717	18	99
Zr_15	0,0026	92297	5274	12	50	108	0,46	1,0467	2,06	0,1202	1,78	0,86	0,0632	1,04	732	16	727	23	714	17	102
Zr_16	0,0067	71267	4039	10	42	86	0,49	0,9814	2,32	0,1128	2,04	0,88	0,0631	1,09	689	16	694	24	712	18	97
Zr_17	0,0028	107303	6187	15	65	132	0,50	1,0052	2,31	0,1138	1,96	0,85	0,0641	1,22	695	16	706	25	744	20	93
Zr_18	0,0026	131308	7351	18	75	154	0,49	0,9705	2,26	0,1120	2,03	0,90	0,0629	0,99	684	16	689	22	704	16	97
Zr_19	0,0028	110068	6228	15	65	135	0,48	1,0048	1,96	0,1159	1,72	0,88	0,0629	0,94	707	16	706	22	704	15	100
Zr_20	0,0039	105211	6021	15	67	126	0,53	0,9763	2,25	0,1118	2,03	0,91	0,0633	0,95	683	16	689	22	719	16	95
Zr_21	0,0010	107202	5944	14	76	127	0,60	0,9497	3,02	0,1098	2,72	0,90	0,0628	1,32	671	16	678	25	700	20	96
Zr_22	0,0017	179748	10302	23	82	193	0,43	1,0262	3,12	0,1170	3,01	0,96	0,0636	0,82	713	16	717	21	730	14	98
Zr_23	0,0031	93705	93705	13	62	109	0,57	0,9632	2,71	0,1103	2,58	0,95	0,0633	0,82	675	16	685	21	719	14	94
Zr_24	0,0092	64572	3984	9	41	69	0,60	0,9873	2,95	0,1132	2,76	0,93	0,0633	1,06	691	16	697	24	718	19	96
Zr_15	0,0020	127277	7108	17	76	133	0,57	1,0280	2,68	0,1181	2,55	0,95	0,0631	0,82	720	16	718	21	713	14	101
Zr_26	0,0074	101532	6108	14	57	121	0,47	0,9419	2,95	0,1076	2,67	0,91	0,06	1,25	659	16	674	25	725	21	91
Zr_3	0,0028	384574	384574	42	219	232	0,95	1,5063	1,98	0,1494	1,92	0,97	0,0731	0,51	898	37	933	41	1018	15	88
Zr_11	0,0024	184012	11910	30	172	162	1,07	1,7041	1,55	0,1696	1,33	0,86	0,0729	0,80	1010	19	1010	27	1010	19	100

a Fraction of the non-radiogenic 206Pb in the analyzed zircon spot, where ƒ206=[206Pb/204Pb]c/[206Pb/204Pb]s (c=common; s=sample)

b Th/U ratios and amount of Pb, Th and U (in pmm) are calculated relative to GJ-1 reference zircon

c Corrected for background and within-run Pb/U fractionation and normalised to reference zircon GJ-1 (ID-TIMS values/measured value); 207Pb/235U calculated using (207Pb/206Pb)*(206Pb/238U)*(137.88)

d Rho is the error correlation defined as the quotient of the propagated errors of the 206Pb/238U and the 207/235U ratio

e Corrected for mass-bias by normalising to GJ-1 reference zircon and common Pb using the model Pb composition of Stacey and Kramers (1975)

f Degree of concordance, 6/8-7/6= (206Pb/238U age * 100) / (207Pb/206Pb age)

g Total systematic uncertainties (ssys) 206/238U =2.0%, 207Pb/206Pb = 0.55 % (2s)

241 GJ1 21.static.exp	0,0005	328846	17587	28	6	287	0,02	0,8208	2,07	0,0989	1,96	0,94	0,0602	1,34	608	28	609	33	611	17	109
229 GJ1 20.static.exp	0,0009	250423	13402	30	6	310	0,02	0,8175	2,24	0,0989	2,03	0,91	0,0600	1,86	608	16	607	29	602	23	111

Table 10: Summary of U-Pb zircon data of the sample DMLH-12-B obtained by LA-MC-ICP-MS method.

						Isotope ratios[c]							Ages (Ma)						
Spot Number	ƒ206[a]	206Pb cps	207Pb cps	206Pb/ 204Pb	Th/U[b]	207Pb/ 235U	1 s [%]	206Pb/ 238U	1 s [%]	Rho[d]	207Pb/ 206Pbe	1 s [%]	206Pb/ 238U	2s[g] abs	207Pb/ 235U	2s abs	207Pb/ 206Pb	2sg abs	[f]Conc % 6/8-7/6
006-ZR4	0,0057	429869	31548	273609	0,498	1,468	1,05	0,1451	0,85	0,81	0,07339	0,50	873	14	917	13	1025	20	14,77
008-ZR6	0,0980	304352	22455	15844	0,948	1,514	1,39	0,1488	1,19	0,86	0,07378	0,62	894	20	936	17	1035	25	13,65
011-ZR9	0,0243	381802	28325	63792	0,516	1,545	1,99	0,1510	1,20	0,60	0,07419	1,54	907	20	948	24	1047	62	13,38
015-ZR11	0,0154	372300	27345	100771	0,562	1,420	2,29	0,1402	1,29	0,57	0,07345	1,85	846	21	897	27	1026	74	17,60
016-ZR12	0,0070	500102	37588	223502	0,653	1,416	1,78	0,1366	1,25	0,70	0,07516	1,21	826	19	896	21	1073	48	23,05
018-ZR14	0,0109	642781	47018	141984	0,629	1,408	1,50	0,1396	1,31	0,87	0,07315	0,65	842	21	892	18	1018	26	17,26
019-ZR15	0,0063	383771	28263	246358	0,842	1,448	1,52	0,1426	1,40	0,92	0,07365	0,46	860	23	909	18	1032	18	16,69
021-ZR17	0,0218	294323	21914	71243	0,704	1,355	1,90	0,1320	1,52	0,80	0,07446	1,08	799	23	870	22	1054	43	24,16
022-ZR18	0,0054	403841	29669	290160	0,709	1,527	2,47	0,1507	2,25	0,91	0,07347	0,93	905	38	941	30	1027	38	11,89
023-ZR19	0,0269	144694	10806	57765	0,758	1,446	2,67	0,1404	1,83	0,69	0,07468	1,91	847	29	908	32	1060	76	20,10
024-ZR20	0,0201	429073	31953	77401	0,774	1,417	1,92	0,1380	1,66	0,87	0,07447	0,88	833	26	896	23	1054	35	20,94
027-ZR21	0,0061	500293	36684	256289	0,603	1,364	1,49	0,1349	1,33	0,90	0,07333	0,54	816	20	874	17	1023	22	20,26
028-ZR22	0,0063	421680	31443	247911	0,789	1,419	1,37	0,1380	1,18	0,86	0,07457	0,59	833	18	897	16	1057	24	21,13
029-ZR23	0,0209	195847	14190	74228	0,782	1,522	2,59	0,1523	1,67	0,64	0,07245	1,95	914	28	939	32	999	78	8,48

032-ZR26	0,0142	196131	14489	109636	0,628	1,436	1,81	0,1410	1,14	0,63	0,07387	1,36	850	18	904	22	1038	54	18,09
035-ZR29	0,0197	811511	61034	78871	0,691	1,413	1,04	0,1363	0,80	0,77	0,07521	0,56	823	12	894	12	1074	22	23,33
036-ZR30	0,0095	362446	26292	164013	0,788	1,378	1,85	0,1377	1,21	0,66	0,07254	1,34	832	19	879	22	1001	54	16,92
042-ZR34	0,0062	714422	52601	249428	0,530	1,498	1,70	0,1475	1,54	0,91	0,07363	0,61	887	25	930	21	1031	25	13,98
044-ZR36	0,0070	380905	28607	220598	0,346	1,445	1,09	0,1395	0,84	0,77	0,07510	0,59	842	13	908	13	1071	24	21,42
046-ZR38	0,0047	463603	33993	330808	0,677	1,395	1,15	0,1380	0,95	0,83	0,07332	0,52	833	15	887	14	1023	21	18,52
047-ZR39	0,0134	403135	29600	116230	1,014	1,434	1,35	0,1417	1,07	0,80	0,07342	0,72	854	17	903	16	1026	29	16,72
048-ZR40	0,0062	414119	30934	249003	0,847	1,460	1,55	0,1417	0,94	0,61	0,07470	1,17	855	15	914	19	1060	47	19,41
054-ZR44	0,0066	414715	30792	235331	0,545	1,466	1,19	0,1432	0,97	0,81	0,07425	0,59	863	16	917	14	1048	24	17,69
056-ZR46	0,0215	192496	13895	72135	0,673	1,553	2,26	0,1561	1,30	0,58	0,07218	1,81	935	23	952	28	991	73	5,66
058-ZR48	0,0089	313150	23302	173590	0,782	1,458	1,53	0,1421	1,27	0,83	0,07441	0,77	857	20	913	18	1053	31	18,64
060-ZR50	0,0070	621459	45761	222627	0,577	1,502	1,33	0,1479	0,88	0,66	0,07363	0,93	889	15	931	16	1031	37	13,80
063-ZR51	0,0088	279300	20805	177335	0,726	1,403	1,31	0,1366	0,99	0,75	0,07449	0,78	825	15	890	16	1055	31	21,74
065-ZR53	0,0025	714538	52249	631306	0,510	1,466	1,25	0,1454	1,03	0,83	0,07312	0,59	875	17	916	15	1017	24	13,99
066-ZR54	0,0211	576254	42100	73677	0,693	1,495	1,80	0,1484	1,34	0,74	0,07306	1,14	892	22	928	22	1016	46	12,19
067-ZR55	0,0093	362504	26855	167203	0,764	1,511	1,53	0,1479	1,35	0,89	0,07408	0,60	889	22	935	19	1044	24	14,80
068-ZR56	0,0066	298529	21768	236109	0,815	1,443	1,49	0,1435	1,27	0,85	0,07292	0,69	864	21	907	18	1012	28	14,56
069-ZR57	0,0147	367898	27142	105453	0,982	1,449	1,08	0,1424	0,79	0,74	0,07378	0,63	858	13	909	13	1035	25	17,10
071-ZR59	0,0063	351385	25854	248419	0,755	1,435	1,48	0,1414	1,13	0,76	0,07358	0,89	853	18	904	18	1030	36	17,20
072-ZR60	0,0104	208705	15385	148630	0,952	1,508	1,77	0,1483	1,20	0,68	0,07372	1,25	892	20	933	22	1034	50	13,76
078-ZR64	0,0059	365752	27134	263938	0,863	1,475	1,56	0,1441	1,06	0,68	0,07419	1,08	868	17	920	19	1047	43	17,05
079-ZR65	0,0114	251557	18443	136318	1,221	1,461	2,28	0,1445	1,76	0,77	0,07332	1,40	870	29	914	27	1023	56	14,93
080-ZR66	0,0060	192145	14307	260930	1,048	1,434	1,44	0,1396	0,98	0,68	0,07446	0,99	843	16	903	17	1054	39	20,06
081-ZR67	0,0047	523604	38547	332555	0,764	1,478	1,61	0,1456	1,38	0,86	0,07362	0,75	876	23	921	19	1031	30	15,02
082-ZR68	0,0091	305000	22496	170743	0,599	1,491	1,36	0,1466	1,00	0,73	0,07376	0,85	882	16	927	17	1035	34	14,76
083-ZR69	0,0072	385093	28143	214700	0,570	1,420	1,41	0,1409	1,10	0,78	0,07308	0,80	850	17	897	17	1016	32	16,38
084-ZR70	0,0169	210851	15224	92025	0,935	1,568	2,34	0,1575	1,97	0,85	0,07220	1,19	943	35	958	29	992	48	4,92
087-ZR71	0,0106	224667	16490	146829	0,573	1,532	1,31	0,1513	0,94	0,72	0,07340	0,83	908	16	943	16	1025	33	11,37
088-ZR72	0,0077	669819	48531	201365	0,687	1,510	1,61	0,1511	1,41	0,88	0,07245	0,68	907	24	934	20	999	28	9,17
090-ZR74	0,0064	594167	42718	243765	0,786	1,485	1,64	0,1498	0,79	0,48	0,07189	1,39	900	13	924	20	983	56	8,47
091-ZR75	0,0104	175274	12723	149709	0,723	1,470	1,88	0,1469	1,43	0,76	0,07259	1,16	883	24	918	23	1003	47	11,88
094-ZR78	0,0158	218393	15934	98174	0,763	1,605	1,60	0,1596	1,23	0,77	0,07296	0,96	954	22	972	20	1013	39	5,77
095-ZR79	0,0072	501523	36304	215995	0,823	1,491	1,69	0,1494	1,46	0,86	0,07239	0,78	898	24	927	20	997	31	9,95
096-ZR80	0,0069	430016	31080	225897	0,361	1,635	2,68	0,1641	2,13	0,80	0,07228	1,57	979	39	984	33	994	63	1,45

a Fraction of the non-radiogenic 206Pb in the analyzed zircon spot, where ƒ206=[206Pb/204Pb]c/[206Pb/204Pb]s (c=common; s=sample)

b Th/U ratios and amount of Pb, Th and U (in pmm) are calculated relative to GJ-1 reference zircon

c Corrected for background and within-run Pb/U fractionation and normalised to reference zircon GJ-1 (ID-TIMS values/measured value); 207Pb/235U calculated using (207Pb/206Pb)*(206Pb/238U)*(137.88)

d Rho is the error correlation defined as the quotient of the propagated errors of the 206Pb/238U and the 207/235U ratio

e Corrected for mass-bias by normalising to GJ-1 reference zircon and common Pb using the model Pb composition of Stacey and Kramers (1975)

f Degree of concordance, 6/8-7/6= (206Pb/238U age * 100) / (207Pb/206Pb age)

g Total systematic uncertainties (ssys) 206/238U =2.0%, 207Pb/206Pb = 0.55 % (2s)

Table 11: Summary of U-Pb zircon data of the sample DMLH-13-A obtained by LA-MC-ICP-MS method.

								Isotope ratiosc							Ages (Ma)						
Spot		206Pb	207Pb	Pb	Th	U		207Pb/	1 s	206Pb/	1 s		207Pb/	1 s	206Pb/	2sg	207Pb/	2s	207Pb/	2sg	fConc %
Number	ƒ206a	cps	cps	ppm	ppm	ppm	Th/Ub	235U	[%]	238U	[%]	Rhod	206Pbe	[%]	238U	abs	235U	abs	206Pb	abs	6/8-7/6
Zr_1	0,0335	232817	18452	25	295	163	1,82	0,9172	2,29	0,1043	1,67	0,73	0,0638	1,57	640	23	661	51	734	49	87
Zr-3	0,1832	42744	42744	6	49	28	1,81	0,8498	2,54	0,0972	1,96	0,77	0,0634	1,61	598	25	625	682	721	787	83
Zr_4	0,0053	66605	3902	7	83	46	1,81	0,8304	3,24	0,0971	2,57	0,80	0,0620	1,96	597	32	614	42	675	28	88
Zr_6	0,0061	107214	6690	11	139	76	1,84	0,8726	3,39	0,1006	2,61	0,77	0,0629	2,16	618	34	637	45	704	32	88
Zr_7	0,0158	1240292	88422	92	225	921	0,25	0,8406	2,73	0,0955	2,41	0,88	0,0638	1,29	588	30	619	38	736	26	80
Zr_9	0,0201	1558063	113505	180	10331	1621	6,42	0,7377	3,25	0,0839	2,97	0,91	0,0638	1,32	519	32	561	41	735	30	71
Zr_10	0,0045	4459368	266825	350	2228	2321	0,97	0,8964	2,03	0,1028	1,55	0,76	0,0633	1,31	631	22	676	30	717	20	88
Zr-11	0,0027	2977166	175890	254	1965	1731	1,14	0,8191	2,48	0,0944	2,05	0,83	0,0629	1,40	582	25	608	32	706	21	82
Zr-13	0,0081	69927	4171	6	34	53	0,65	0,9897	2,61	0,1136	1,98	0,76	0,0632	1,70	694	29	699	40	714	27	97
Zr-19	0,0082	2292839	134743	338	9503	2927	3,27	0,7212	3,21	0,0826	2,89	0,90	0,0633	1,41	512	31	551	37	719	23	71
Zr_27	0,0023	962925	55527	96	533	593	0,91	0,8915	2,39	0,1020	1,85	0,78	0,0634	1,51	626	25	647	33	721	23	87
Zr_30	0,0030	162480	9411	17	119	146	0,83	1,0294	2,60	0,1173	2,11	0,81	0,0636	1,51	715	32	811	45	729	23	98
Zr_42	0,0011	370209	21100	42	229	356	0,65	0,8293	3,05	0,0944	2,26	0,74	0,0637	2,04	581	28	613	39	733	31	79
Zr_43	0,0137	31180	31180	4	37	29	1,27	0,9075	4,73	0,1052	2,83	0,60	0,0626	3,78	645	38	656	66	693	57	93
Zr_44	0,0032	212630	12195	30	327	207	1,59	0,9092	2,65	0,1045	1,64	0,62	0,0631	2,08	640	23	657	37	712	31	90
Zr_45	0,0076	35630	2182	5	56	36	1,58	0,9571	3,63	0,1097	2,85	0,79	0,0633	2,24	671	40	682	52	717	34	94
Zr_47	0,0011	205903	11796	36	590	215	2,77	0,8199	2,80	0,0938	1,90	0,68	0,0634	2,06	578	24	608	36	722	31	80
Zr_48	0,0066	1712034	100972	226	2046	1925	1,07	1,0443	2,78	0,1191	1,93	0,69	0,0636	2,00	726	30	726	43	727	31	100
Zr_33	0,0024	70164	70164	10	121	72	1,70	1,0043	3,01	0,1147	2,13	0,71	0,0635	2,12	700	32	706	44	726	32	96
Zr=34	0,0010	164924	9433	23	305	153	2,01	0,8890	2,55	0,1014	1,77	0,70	0,0636	1,83	623	24	646	35	727	28	86
Zr_35	0,0047	200748	11978	21	106	597	0,18	0,9204	2,46	0,1053	1,55	0,63	0,0634	1,90	645	22	663	35	722	29	89

Zr_37	0,0078	32154	1877	4	50	31	1,60	0,7491	4,00	0,0854	2,60	0,65	0,0636	3,04	528	29	568	47	728	46	73
Zr_39	0,0028	43696	2475	5	50	37	1,34	1,0338	3,02	0,1182	1,97	0,65	0,0634	2,29	720	30	721	46	723	34	100
Zr-15$	0,0108	1079402	86789	103	484	509	0,96	2,0550	2,15	0,1861	1,79	0,83	0,0801	1,20	1100	43	1134	55	1199	34	92
Zr_5$	0,0601	792500	93040	84	420	402	1,05	2,3000	3,13	0,1994	2,96	0,95	0,0837	1,01	1172	72	1212	150	1285	138	91
Zr_26$	0,0197	43248	3161	5	48	35	1,40	1,0989	3,72	0,1242	2,33	0,63	0,0642	2,90	754	37	753	65	748	53	101
Zr 28$	0,0206	73171	6751	10	123	58	2,14	1,2235	3,08	0,1319	2,15	0,70	0,0673	2,21	799	36	811	60	846	49	94
Zr-14	0,0214	36812	2734	4	32	28	1,15	1,0895	3,57	0,1132	2,52	0,71	0,0698	2,53	691	36	748	62	923	60	75

a Fraction of the non-radiogenic 206Pb in the analyzed zircon spot, where ƒ206=[206Pb/204Pb]c/[206Pb/204Pb]s (c=common; s=sample)

b Th/U ratios and amount of Pb, Th and U (in pmm) are calculated relative to GJ-1 reference zircon

c Corrected for background and within-run Pb/U fractionation and normalised to reference zircon GJ-1 (ID-TIMS values/measured value); 207Pb/235U calculated using (207Pb/206Pb)*(206Pb/238U)*(137.88)

d Rho is the error correlation defined as the quotient of the propagated errors of the 206Pb/238U and the 207/235U ratio

e Corrected for mass-bias by normalising to GJ-1 reference zircon and common Pb using the model Pb composition of Stacey and Kramers (1975)

f Degree of concordance, 6/8-7/6= (206Pb/238U age * 100) / (207Pb/206Pb age)

g Total systematic uncertainties (ssys) 206/238U =2.0%, 207Pb/206Pb = 0.55 % (2s)

Table 12: Summary of U-Pb zircon data of the sample DMLH-15-A obtained by LA-SF-ICP-MS method.

Sample DMHL-15_A				**Isotope ratios[b]**							**Ages (Ma)**						
Spot number	**Pb206* cps**	**^{206}Pb/ ^{204}Pb**	**Th/U[a]**	**^{207}Pb*/ ^{206}Pb***	**± 1s(%)**	**^{207}Pb*/ ^{235}U**	**± 1s(%)**	**^{206}Pb*/ ^{238}U**	**± 1s(%)**	**RHO**	**^{206}Pb/ ^{238}U**	**± 2s**	**^{207}Pb/ ^{235}U**	**± 2s**	**^{206}Pb/ ^{207}Pb**	**± 2s**	**Conc**
43	498295	0,05	1,12	0,0623	1,67	0,954	1,80	0,1110	0,68	0,38	678,31	8,55	680,06	8,97	685,83	35,66	99
57	340156	0,86	1,94	0,0636	2,31	0,981	2,62	0,1120	1,23	0,47	684,19	15,70	694,22	13,26	726,83	49,02	94
25	127526	0,97	1,12	0,0637	2,15	0,956	2,43	0,1089	1,12	0,46	666,31	13,92	681,28	12,13	731,07	45,65	91
81	406415	0,14	2,94	0,0638	3,22	0,973	3,30	0,1105	0,73	0,22	675,79	9,23	689,84	16,67	735,91	68,17	92
22	285484	0,84	2,23	0,0664	2,86	1,167	3,17	0,1275	1,36	0,43	773,39	19,50	785,07	17,50	818,40	59,85	95
71	417471	0,52	1,35	0,0669	1,65	1,196	1,87	0,1296	0,87	0,47	785,30	12,62	798,63	10,37	835,98	34,38	94
70	845307	0,56	3,36	0,0673	3,83	1,249	6,75	0,1347	5,56	0,82	814,47	42,69	823,15	38,81	846,67	79,64	96
59	199378	0,53	1,76	0,0674	2,17	1,268	2,48	0,1365	1,19	0,48	824,86	18,05	831,59	14,15	849,64	45,14	97
82	802386	0,36	2,76	0,0678	3,98	1,273	6,77	0,1361	5,47	0,81	822,56	42,40	833,52	39,24	862,85	82,64	95
52	276773	1,95	2,76	0,0679	2,87	1,239	3,52	0,1324	2,04	0,58	801,38	30,14	818,56	19,99	865,56	59,57	93
68	794251	0,17	2,81	0,0684	3,22	1,282	6,07	0,1359	5,15	0,85	821,53	39,82	837,73	35,23	880,93	66,54	93
28	579399	1,03	3,17	0,0685	4,09	1,340	6,57	0,1419	5,14	0,78	855,56	41,35	863,26	38,97	883,08	84,67	97
21	237292	0,15	0,00	0,0686	0,58	1,382	1,12	0,1461	0,96	0,86	878,92	15,51	881,11	6,63	886,62	11,91	99

38	543024	0,86	1,74	0,0687	2,64	1,348	3,40	0,1424	2,14	0,63	857,99	33,67	866,79	20,01	889,34	54,64	96
72	398600	0,97	2,22	0,0696	2,63	1,367	2,88	0,1425	1,17	0,40	858,93	18,38	874,83	17,03	915,28	54,17	94
56	596631	0,52	1,74	0,0706	1,91	1,476	2,30	0,1516	1,29	0,56	910,02	21,46	920,45	14,04	945,52	39,12	96
63	807982	0,69	1,12	0,0720	1,35	1,601	1,88	0,1613	1,31	0,70	964,05	23,09	970,49	11,84	985,12	27,48	98
41	479470	1,38	3,37	0,0727	3,40	1,503	3,52	0,1499	0,93	0,26	900,67	15,39	931,60	21,71	1005,52	68,91	90
33	650633	0,14	1,40	0,0730	2,97	1,680	5,24	0,1668	4,32	0,82	994,61	78,24	1001,02	33,92	1015,09	60,19	98
48	399066	0,92	2,28	0,0733	2,33	1,651	2,51	0,1634	0,94	0,38	975,63	16,75	990,02	16,01	1022,04	47,13	95
11	218527	1,21	1,81	0,0747	1,99	1,767	2,11	0,1715	0,69	0,33	1020,58	12,76	1033,30	13,74	1060,31	40,03	96
19	284110	0,77	1,00	0,0748	1,20	1,815	1,55	0,1759	0,99	0,64	1044,73	18,77	1051,01	10,23	1064,08	24,07	98
77	245011	0,80	1,61	0,0750	1,87	1,823	2,03	0,1763	0,81	0,40	1046,91	15,27	1053,85	13,42	1068,26	37,52	98
61	152319	0,78	1,87	0,0755	2,11	1,853	2,41	0,1781	1,18	0,49	1056,59	22,49	1064,62	16,04	1081,13	42,26	98
49	171733	0,67	1,35	0,0755	1,60	1,867	1,95	0,1792	1,12	0,57	1062,65	21,53	1069,31	13,00	1082,91	32,10	98
32	539577	0,98	1,37	0,0756	1,59	1,868	2,15	0,1793	1,45	0,67	1063,15	27,79	1069,99	14,32	1083,96	31,92	98
80	300155	1,24	0,00	0,0766	0,57	1,952	0,95	0,1849	0,75	0,80	1093,85	14,86	1099,26	6,38	1109,99	11,46	99
16	241901	0,86	1,18	0,0767	1,49	1,937	1,69	0,1832	0,81	0,48	1084,50	15,77	1093,80	11,40	1112,37	29,74	97
27	140900	1,16	2,91	0,0769	2,64	1,900	2,83	0,1791	1,01	0,36	1061,86	19,33	1081,03	19,00	1119,89	52,73	95
91	518471	0,75	0,00	0,0771	0,44	1,994	0,95	0,1875	0,84	0,89	1107,61	16,86	1113,34	6,46	1124,56	8,76	98
74	132834	0,91	0,53	0,0784	0,79	2,099	1,02	0,1943	0,65	0,64	1144,49	13,30	1148,49	7,02	1156,04	15,57	99
40	208955	1,01	1,16	0,0784	1,45	2,101	1,58	0,1944	0,65	0,41	1145,11	13,27	1149,01	10,95	1156,39	28,69	99
46	203923	1,03	0,41	0,0784	0,75	2,109	1,00	0,1951	0,67	0,67	1148,99	13,75	1151,90	6,91	1157,36	14,79	99
90	348769	0,83	2,60	0,0785	2,43	2,020	2,55	0,1866	0,75	0,30	1103,19	14,98	1122,20	17,44	1159,20	48,23	95
62	272885	0,62	1,27	0,0786	1,41	2,085	1,55	0,1925	0,66	0,42	1134,94	13,41	1143,98	10,71	1161,17	27,87	98
24	397915	0,27	0,44	0,0787	0,66	2,133	3,09	0,1966	3,02	0,98	1156,83	62,75	1159,71	21,57	1165,08	13,06	99
54	219439	0,88	0,57	0,0804	0,81	2,259	1,07	0,2038	0,70	0,65	1195,51	14,94	1199,54	7,55	1206,81	15,94	99
35	192483	0,96	0,21	0,0804	0,55	2,277	0,96	0,2054	0,79	0,82	1204,25	16,96	1205,22	6,78	1206,96	10,75	100
66	65043	1,78	0,23	0,0804	0,65	2,288	0,94	0,2063	0,68	0,72	1209,07	14,67	1208,56	6,67	1207,64	12,84	100
65	667257	0,36	0,62	0,0806	0,88	2,297	4,30	0,2065	4,21	0,98	1210,40	91,38	1211,30	30,88	1212,91	17,31	100
36	426118	0,38	3,35	0,0808	2,90	2,175	3,00	0,1953	0,77	0,26	1150,03	15,87	1173,08	21,09	1215,86	57,05	95
39	70994	1,16	0,07	0,0816	0,56	2,378	1,08	0,2113	0,92	0,85	1235,65	20,22	1235,91	7,71	1236,37	11,01	100
79	664695	0,72	3,39	0,0830	4,32	2,346	4,38	0,2050	0,69	0,16	1202,00	14,94	1226,28	31,65	1269,25	84,34	95
78	141225	0,88	0,57	0,0831	2,27	2,478	2,43	0,2162	0,87	0,36	1261,95	19,65	1265,62	17,74	1271,84	44,25	99
58	186794	1,00	0,00	0,0835	0,58	2,534	0,88	0,2202	0,66	0,75	1283,04	15,03	1281,87	6,40	1279,90	11,25	100
30	613371	0,41	2,82	0,0835	3,24	2,483	3,37	0,2156	0,90	0,27	1258,47	20,12	1267,05	24,66	1281,64	63,21	98
26	396090	1,02	0,47	0,0837	0,75	2,523	1,32	0,2188	1,08	0,82	1275,31	24,52	1278,75	9,62	1284,54	14,64	99
55	83379	0,70	4,37	0,0974	3,05	3,496	3,14	0,2603	0,78	0,25	1491,57	20,34	1526,26	25,13	1574,67	57,01	95

20	479554	0,54	0,00	0,0994	0,49	4,028	1,07	0,2938	0,96	0,89	1660,52	27,45	1639,86	8,78	1613,48	9,15	103
ZR42	569913	1,01	0,00	0,0808	0,40	2,194	1,12	0,1969	0,98	0,87	1158,45	20,78	1179,19	15,61	1217,31	15,84	95
ZR14B	579284	0,62	0,54	0,0882	1,34	3,101	2,57	0,2550	2,17	0,84	1464,39	56,69	1432,82	39,14	1386,10	50,84	106
ZR66	713335	0,68	0,70	0,0837	1,97	2,573	3,40	0,2228	2,74	0,81	1296,59	64,23	1292,92	49,08	1286,68	75,85	101
ZR90	457480	1,09	0,03	0,0799	1,34	2,016	1,60	0,1831	0,79	0,49	1083,75	15,75	1120,92	21,63	1193,57	52,58	91
ZR20	1331728	0,94	0,20	0,0779	2,41	1,840	2,75	0,1713	1,27	0,46	1019,46	23,94	1059,73	35,85	1143,48	94,33	89
37	70901	0,24	2,12	0,0689	7,09	1,392	7,45	0,1465	2,29	0,31	881,48	37,03	885,47	45,02	895,45	146,38	98
64	689062	1,16	6,68	0,0793	4,94	1,849	5,08	0,1691	1,18	0,23	1007,41	10,99	1062,95	34,01	1178,80	97,64	85
76	617244	0,84	4,15	0,0806	4,75	2,290	7,18	0,2060	5,39	0,75	1207,29	59,57	1209,06	52,05	1212,21	93,42	100
17	514158	0,71	3,77	0,0806	4,30	2,282	7,16	0,2054	5,73	0,80	1204,46	63,26	1206,76	51,86	1210,88	84,55	99
18	686799	0,67	7,43	0,0748	8,44	1,814	10,05	0,1760	5,45	0,54	1044,98	52,82	1050,44	68,00	1061,81	169,83	98
ZR30	1781112	0,79	0,92	0,0722	5,86	1,699	5,98	0,1707	1,13	0,19	1016,09	21,23	1008,17	75,04	990,83	229,62	103
ZR4	534949	0,67	1,08	0,0723	5,21	1,812	5,74	0,1819	2,39	0,42	1077,12	47,41	1049,74	73,81	993,03	204,86	108

[a]data corrected for common-Pb

[b]concentration uncertainty ca. 20%

[c]Concordance calculated as: ((^{206}Pb-^{238}U(age))/(^{207}Pb-^{206}Pb(age)))*100

Decay constants of Jaffey et al. (1971) used

Total systematic uncertainties (σsys): ^{206}Pb/^{238}U = 2.0%, ^{207}Pb/^{206}Pb = 0.55% (2σ)

Uncertainties quoted without components related to systematic error unless otherwise stated

Table 13: Summary of U-Pb zircon data of the sample DDLH-21_B obtained by LA-MC-ICP-MS method.

Sample DDLH_21B				**Isotope ratios[b]**							**Ages (Ma)**						
Spot number	**Pb206* cps**	**^{206}Pb/ ^{204}Pb**	**Th/U[a]**	**^{207}Pb*/ ^{206}Pb***	**± 1s**	**^{207}Pb*/ ^{235}U**	**± 1s**	**^{206}Pb*/ ^{238}U**	**± 1s**	**RHO**	**^{206}Pb/ ^{238}U**	**± 2s**	**^{207}Pb/ ^{235}U**	**± 2s**	**^{206}Pb/ ^{207}Pb**	**± 2s**	**Conc**
003-ZR1	140967	91999	0,557	0,06275	0,85	0,910	1,66	0,1052	1,37	0,83	645	36	657	17	700	16	92
004-ZR2	1143779	214879	0,344	0,06371	0,54	0,972	1,11	0,1106	0,89	0,81	676	37	689	18	732	11	92
006-ZR4	477330	452420	0,411	0,06319	0,68	0,814	1,24	0,0934	0,97	0,78	576	38	605	19	715	11	81
007-ZR5	644917	246417	0,471	0,06303	0,38	0,900	0,84	0,1035	0,65	0,77	635	39	652	20	709	8	90
009-ZR7	707834	4422	1,081	0,06585	1,28	0,498	1,83	0,0549	1,26	0,69	345	40	411	21	801	12	43
012-ZR10	581398	268467	0,470	0,06332	0,51	0,885	1,31	0,1014	1,15	0,88	623	41	644	22	719	12	87
016-ZR12	608003	394456	0,442	0,06314	0,43	0,948	1,93	0,1089	1,85	0,96	666	42	677	23	713	19	93
018-ZR14	416539	150360	0,592	0,06294	0,37	0,850	1,07	0,0980	0,93	0,87	603	43	625	24	706	10	85

022-ZR18	140210	57720	0,780	0,06347	0,65	0,921	1,27	0,1052	1,03	0,81	645	44	663	25	724	12	89
023-ZR19	290143	206193	0,424	0,06371	0,67	0,740	1,30	0,0842	1,05	0,81	521	45	562	26	732	11	71
027-ZR21	318931	204260	0,591	0,06320	0,59	0,855	1,12	0,0981	0,88	0,79	603	46	627	27	715	10	84
031-ZR25	359020	291873	0,408	0,06301	0,43	0,868	1,10	0,0999	0,95	0,86	614	47	635	28	709	10	87
032-ZR26	113952	89767	0,363	0,06278	1,09	0,833	1,73	0,0963	1,29	0,74	593	48	616	29	701	16	85
035-ZR29	562561	174688	0,450	0,06335	0,64	0,947	1,32	0,1084	1,09	0,83	663	49	676	30	720	13	92
036-ZR30	184809	115830	0,617	0,06260	0,86	0,909	1,32	0,1053	0,94	0,71	646	50	657	31	695	13	93
039-ZR31	517551	309943	0,227	0,06323	0,50	0,894	1,15	0,1025	0,96	0,84	629	51	648	32	716	11	88
041-ZR33	365413	115300	0,442	0,06333	0,56	0,943	1,23	0,1080	1,03	0,84	661	52	674	33	719	12	92
042-ZR34	389187	3261448	0,397	0,06333	0,54	0,954	1,31	0,1092	1,14	0,87	668	53	680	34	719	13	93
043-ZR35	407854	41424	0,814	0,06288	0,54	0,990	1,41	0,1142	1,24	0,88	697	54	699	35	704	14	99
044-ZR36	575312	274735	0,431	0,06347	0,49	0,912	1,15	0,1042	0,97	0,85	639	55	658	36	724	11	88
045-ZR37	479633	308858	0,401	0,06349	0,48	0,961	1,34	0,1098	1,19	0,89	671	56	684	37	725	13	93
046-ZR38	211549	120182	0,603	0,06303	0,61	0,949	1,08	0,1092	0,81	0,75	668	57	678	38	709	11	94
047-ZR39	326858	229008	0,411	0,06288	0,57	0,937	1,03	0,1081	0,78	0,75	662	58	672	39	704	10	94
048-ZR40	331325	97293	0,424	0,06369	0,91	0,933	1,37	0,1063	0,95	0,69	651	59	669	40	731	13	89

[1] Convertion factor from mV to CPS is 62500
[2] concentration uncertainty
c.20%
[3] data not corrected for common-Pb
[4] not corrected for common-Pb
[5] Discordance calculated as (1-(^{206}Pb/^{238}U age/^{207}Pb/^{206}Pb age))*100
Decay constants of Jaffey et al 1971 used

Table 14: Summary of SHRIMP U-Pb zircon data for sample PR_1A

Grain.Spot	% $^{206}Pb_c$	ppm U	ppm Th	^{232}Th /^{238}U	ppm $^{206}Pb^*$	(1) ^{206}Pb /^{238}U Age		(1) ^{207}Pb /^{206}Pb Age		% Discordant	(1) $^{207}Pb^*$ /$^{206}Pb^*$	±%	(1) $^{207}Pb^*$ /^{235}U	±%	(1) $^{206}Pb^*$ /^{238}U	±%	err corr
5,2	**0,24**	**125**	**2**	**0,02**	**10,2**	**582**	**± 6.5**	**599**	**± 41**	**3**	**0,0599**	**1,9**	**0,78**	**2,2**	**0,0945**	**1,2**	**,528**
14,3	**1,91**	**1776**	**110**	**0,06**	**144**	**569,1**	**± 6**	**594**	**± 48**	**4**	**0,0597**	**2,2**	**0,76**	**2,5**	**0,0923**	**1,1**	**,442**

7,1	**0,02**	**1073**	**14**	**0,01**	**97,4**	**647,5**	**± 6.4**	**659**	**± 10**	**2**	**0,06157**	**0,48**	**0,897**	**1,1**	**0,1057**	**1**	**,908**
14,2	**0,09**	**119**	**2**	**0,02**	**11,3**	**670,3**	**± 7.5**	**658**	**± 29**	**-2**	**0,06155**	**1,3**	**0,93**	**1,8**	**0,1096**	**1,2**	**,663**
24,1	**0,29**	**1745**	**40**	**0,02**	**155**	**631,6**	**± 6.3**	**643**	**± 13**	**2**	**0,0611**	**0,6**	**0,867**	**1,2**	**0,1029**	**1,1**	**,870**
26,1	**0,10**	**404**	**9**	**0,02**	**36,8**	**649,5**	**± 6.6**	**633**	**± 18**	**-3**	**0,06083**	**0,84**	**0,889**	**1,4**	**0,106**	**1,1**	**,785**
25,1	**0,06**	**264**	**6**	**0,02**	**23,7**	**640,3**	**± 7.6**	**635**	**± 21**	**-1**	**0,06087**	**0,98**	**0,876**	**1,6**	**0,1044**	**1,3**	**,788**
4,1	**0,00**	**1320**	**73**	**0,06**	**116**	**626,6**	**± 6.1**	**652,5**	**± 8.4**	**4**	**0,06138**	**0,39**	**0,8639**	**1,1**	**0,1021**	**1**	**,935**
15,2	**0,10**	**507**	**32**	**0,07**	**45,3**	**636,6**	**± 6.4**	**641**	**± 16**	**1**	**0,06105**	**0,77**	**0,874**	**1,3**	**0,1038**	**1,1**	**,808**
20,1	**0,05**	**633**	**41**	**0,07**	**55,7**	**628**	**± 6.2**	**620**	**± 13**	**-1**	**0,06046**	**0,61**	**0,853**	**1,2**	**0,1023**	**1**	**,865**
27,1	**0,04**	**751**	**111**	**0,15**	**66,2**	**629,5**	**± 6.3**	**645**	**± 13**	**2**	**0,06115**	**0,62**	**0,865**	**1,2**	**0,1026**	**1**	**,860**
19,2	**0,28**	**2433**	**390**	**0,17**	**216**	**632,6**	**± 6.1**	**634**	**± 11**	**0**	**0,06087**	**0,53**	**0,8653**	**1,1**	**0,1031**	**1**	**,886**
31,1	**0,02**	**3003**	**1074**	**0,37**	**263**	**626**	**± 6.1**	**642**	**± 15**	**2**	**0,06107**	**0,69**	**0,859**	**1,2**	**0,102**	**1**	**,830**
1,1	0,06	329	38	0,12	35,1	754,1	± 7.6	766	± 16	2	0,06475	0,75	1,108	1,3	0,1241	1,1	,820
1,2	0,14	193	24	0,13	20,7	759,4	± 8	778	± 23	2	0,06511	1,1	1,122	1,6	0,125	1,1	,714
19,1	0,03	105	81	0,80	12,5	831,4	±10	822	± 27	-1	0,0665	1,3	1,262	1,8	0,1377	1,3	,704
21,1	0,00	86	31	0,37	10,6	861,3	± 9.9	845	± 26	-2	0,06724	1,3	1,325	1,8	0,1429	1,2	,700
20,2	0,30	54	27	0,52	6,14	805	±16	846	± 44	5	0,0673	2,1	1,233	3	0,1329	2,1	,711
22,1	0,17	120	108	0,93	13,6	797,8	± 8.8	848	± 29	6	0,06734	1,4	1,223	1,8	0,1317	1,2	,636
28,1	0,10	178	155	0,90	21,8	858,9	± 9.8	850	± 23	-1	0,06741	1,1	1,324	1,6	0,1425	1,2	,740
13,1	0,04	164	104	0,65	20	854,4	± 9.9	853	± 22	0	0,06748	1,1	1,319	1,6	0,1417	1,2	,755
3,1	0,11	184	94	0,53	22,7	866	±10	861	± 18	-1	0,06775	0,85	1,343	1,5	0,1438	1,2	,824
6,1	0,00	426	305	0,74	51,5	849	± 8.6	867	± 12	2	0,06796	0,57	1,319	1,2	0,1408	1,1	,886
10,1	0,18	98	84	0,88	11	795,1	± 9.1	875	± 28	9	0,06822	1,3	1,235	1,8	0,1313	1,2	,675
29,1	0,05	162	101	0,65	19,7	852,2	± 9	875	± 23	3	0,06821	1,1	1,329	1,6	0,1413	1,1	,717
17,1	0,19	108	40	0,38	13,7	886	±16	880	± 33	-1	0,0684	1,6	1,389	2,5	0,1474	1,9	,771
2,1	0,00	156	98	0,65	22	980	±10	946	± 17	-4	0,07059	0,83	1,597	1,4	0,1641	1,1	,804
9,2	0,18	180	179	1,02	25,1	967	±10	950	± 20	-2	0,07076	0,99	1,578	1,5	0,1618	1,2	,762
12,1	0,00	69	69	1,04	9,84	993	±12	956	± 26	-4	0,07097	1,3	1,629	1,8	0,1665	1,3	,703

18,1	0,00	221	162	0,76	31,4	986	±11	981	± 15	-1	0,07182	0,71	1,636	1,4	0,1652	1,2	,854
23,1	0,10	134	76	0,59	19,7	1017	±11	990	± 23	-3	0,07214	1,1	1,7	1,6	0,1709	1,2	,710
15,1	0,00	220	162	0,76	32,1	1012	±11	997	± 15	-2	0,07238	0,72	1,696	1,3	0,1699	1,1	,848
5,1	0,00	156	92	0,60	22,8	1011	±11	1000	± 17	-1	0,07252	0,84	1,697	1,4	0,1698	1,1	,804

Errors are 1-sigma; Pb_c and Pb^* indicate the common and radiogenic portions, respectively.

Error in Standard calibration was 0.25% (not included in above errors but required when comparing data from different mounts).

(1) Common Pb corrected using measured ^{204}Pb.

Table 15: Summary of SHRIMP U-Pb zircon data for sample PR_1B

Grain.Spot	% $^{206}Pb_c$	ppm U	ppm Th	$^{232}Th/^{238}U$	ppm $^{206}Pb^*$	(1) $^{206}Pb/^{238}U$ Age		(1) $^{207}Pb/^{206}Pb$ Age		% Discordant	(1) $^{207}Pb^*/^{206}Pb^*$	±%	(1) $^{207}Pb^*/^{235}U$	±%	(1) $^{206}Pb^*/^{238}U$	±%	err corr
1,1	0,14	127	140	1,14	17,5	959	±10	955	±30	0	0,0709	1,5	1,569	1,9	0,1604	1,2	,622
1,2	0,42	30	19	0,63	4,3	976	±14	959	±54	-2	0,071	2,6	1,602	3	0,1635	1,5	,493
2,1	0,32	53	45	0,87	7,34	955	±12	939	±42	-2	0,0703	2	1,549	2,4	0,1597	1,3	,543
3,1	0,00	28	31	1,18	3,83	967	±22	1008	±43	4	0,0728	2,1	1,624	3,2	0,1618	2,4	,747
3,2	0,28	72	64	0,91	9,77	938	±11	952	±38	1	0,0708	1,9	1,53	2,2	0,1567	1,3	,565

Errors are 1-sigma; Pb_c and Pb^* indicate the common and radiogenic portions, respectively.

Error in Standard calibration was 0.25% (not included in above errors but required when comparing data from different mounts).

(1) Common Pb corrected using measured ^{204}Pb.

Table 16: Summary of U-Pb zircon data of the standards obtained by LA-SF-ICP-MS method.

Standard GJ-1			Isotope ratios[b]							Ages (Ma)				
Spot number	$^{206}Pb/^{204}Pb$	Th/U[a]	$^{206}Pb/^{207}Pb$	± 2s	$^{207}Pb/^{235}U$	± 2s	$^{206}Pb/^{238}U$	± 2s	Conc	$^{207}Pb^*/^{235}U$	± 2s(%)	$^{206}Pb^*/^{238}U$	± 2s(%)	RHO
1	4884	0,02	574	26	598	6	593	5	101	0,7934	1,03	0,0972	0,82	0,80
2	4199	0,02	611	26	605	6	606	5	100	0,8159	1,02	0,0983	0,82	0,81
3	5003	0,02	576	26	602	6	596	5	101	0,7991	1,02	0,0979	0,82	0,80
4	5080	0,02	605	25	590	6	593	5	99	0,7928	1,01	0,0958	0,82	0,81
5	5073	0,02	631	25	604	6	609	5	99	0,8223	1,02	0,0982	0,82	0,81
6	4561	0,02	622	26	601	6	605	5	99	0,8146	1,06	0,0977	0,84	0,80
7	4517	0,02	634	26	606	6	612	5	99	0,8263	1,06	0,0985	0,83	0,79

8	3598	0,02	623	28	596	7	601	5	99	0,8075	1,16	0,0968	0,86	0,74
9	4068	0,02	624	28	602	7	606	5	99	0,8169	1,16	0,0979	0,86	0,74
10	3622	0,02	617	29	600	7	603	5	99	0,8109	1,23	0,0975	0,87	0,71
11	3880	0,02	589	29	604	7	601	5	101	0,8065	1,22	0,0982	0,88	0,72
12	5170	0,02	625	25	592	6	**599**	5	**99**	0,8030	1,02	0,0962	0,84	0,83
13	5262	0,02	606	25	596	6	**598**	5	**100**	0,8026	1,02	0,0969	0,85	0,83
14	5183	0,02	569	25	605	6	**597**	5	**101**	0,8005	1,02	0,0984	0,85	0,84
15	5277	0,02	613	25	599	6	**602**	5	**100**	0,8086	1,02	0,0974	0,85	0,84
16	5258	0,02	617	25	607	6	**609**	5	**100**	0,8212	1,02	0,0987	0,85	0,83
17	4846	0,02	624	26	599	6	**604**	5	**99**	0,8126	1,05	0,0974	0,86	0,82
18	3781	0,02	608	28	603	7	**604**	5	**100**	0,8124	1,18	0,0980	0,89	0,75
19	4118	0,02	608	28	592	7	**595**	5	**99**	0,7975	1,19	0,0962	0,89	0,75
20	4156	0,02	598	28	603	7	**602**	5	**100**	0,8088	1,19	0,0980	0,90	0,76
21	3838	0,02	608	32	605	8	**605**	6	**100**	0,8149	1,40	0,0983	0,94	0,67
22	3880	0,02	631	32	605	8	**610**	6	**99**	0,8237	1,40	0,0984	0,94	0,67
23	3602	0,02	625	32	606	9	**610**	6	**99**	0,8233	1,41	0,0986	0,94	0,67
24	5573	0,02	617	25	595	6	**599**	5	**99**	0,8046	1,02	0,0967	0,85	0,83
25	5443	0,02	652	25	601	6	**612**	5	**98**	0,8268	1,00	0,0978	0,84	0,84
26	5383	0,02	625	25	595	6	**601**	5	**99**	0,8078	1,00	0,0967	0,84	0,84
27	5302	0,02	603	25	601	6	**602**	5	**100**	0,8083	1,00	0,0978	0,84	0,84
28	5251	0,02	579	25	610	6	**603**	5	**101**	0,8114	1,02	0,0992	0,85	0,83
29	5219	0,02	598	25	600	6	**599**	5	**100**	0,8040	1,02	0,0975	0,85	0,84
30	4848	0,02	649	25	603	6	**612**	5	**98**	0,8274	1,03	0,0980	0,86	0,83
31	5026	0,02	592	25	610	6	**606**	5	**101**	0,8158	1,03	0,0992	0,86	0,83
32	4872	0,02	588	26	611	6	**606**	5	**101**	0,8157	1,04	0,0994	0,86	0,82
33	5218	0,02	617	25	603	6	**606**	5	**100**	0,8163	1,03	0,0981	0,85	0,82
34	5209	0,02	595	26	603	6	**601**	5	**100**	0,8078	1,03	0,0981	0,85	0,82
35	4043	0,02	593	26	604	6	**600**	5	**101**	0,8063	1,07	0,0982	0,85	0,79
36	4761	0,02	620	26	601	6	**604**	5	**100**	0,8134	1,06	0,0978	0,84	0,79
37	4378	0,02	573	27	599	7	**592**	5	**101**	0,7922	1,10	0,0973	0,83	0,76
38	4704	0,02	644	26	604	7	**612**	5	**99**	0,8266	1,08	0,0982	0,83	0,77
39	4558	0,02	636	28	592	7	**600**	5	**99**	0,8064	1,15	0,0962	0,83	0,73
40	4694	0,02	585	27	596	7	**593**	5	**100**	0,7939	1,12	0,0969	0,83	0,74
41	4914	0,02	663	27	602	7	**615**	5	**98**	0,8323	1,10	0,0979	0,83	0,75
42	6248	0,02	576	26	620	6	**611**	5	**102**	0,8248	1,05	0,1010	0,82	0,78

43	6534	0,02	663	26	612	6	**623**	5	**98**	0,8464	1,06	0,0995	0,82	0,78
44	6422	0,02	645	26	612	6	**619**	5	**99**	0,8397	1,06	0,0996	0,82	0,78
45	5676	0,02	589	27	589	6	**590**	5	**100**	0,7877	1,09	0,0957	0,83	0,76
46	5251	0,02	577	27	595	6	**592**	5	**101**	0,7916	1,09	0,0968	0,82	0,75
47	5916	0,02	583	27	591	6	**590**	5	**100**	0,7876	1,09	0,0960	0,82	0,76
48	6373	0,01	598	7	599	8	600	7	100	0,8030	1,33	0,0972	1,21	0,91
49	6942	0,01	601	7	602	8	604	8	100	0,8085	1,39	0,0977	1,26	0,91
50	6875	0,01	601	7	602	9	603	8	100	0,8088	1,47	0,0978	1,29	0,88
51	6597	0,01	602	8	602	9	603	8	100	0,8094	1,47	0,0979	1,33	0,90
52	6555	0,02	604	6	604	8	606	7	100	0,8135	1,24	0,0982	1,10	0,89
53	5979	0,02	605	7	605	8	605	7	100	0,8145	1,34	0,0984	1,18	0,88
54	6286	0,02	599	7	600	9	602	7	100	0,8056	1,49	0,0974	1,19	0,80
55	6239	0,02	600	8	599	11	599	8	100	0,8047	1,80	0,0975	1,32	0,73
56	2539	0,13	594	8	597	11	610	9	97	0,8011	1,86	0,0965	1,41	0,76
57	5898	0,02	598	3	599	5	600	3	100	0,8032	0,86	0,0972	0,54	0,62
58	5769	0,02	600	3	600	7	601	3	100	0,8060	1,12	0,0975	0,57	0,51
59	5972	0,02	597	3	598	6	600	4	100	0,8019	0,92	0,0971	0,59	0,64
60	5895	0,02	599	4	600	6	600	4	100	0,8047	0,94	0,0974	0,71	0,76

Concordia age = 601.44+/-4.72 Ma (n=60, 95% conf.)

Standard BB-9			**Isotope ratios[b]**							**Ages (Ma)**				
Spot number	**$^{206}Pb/^{204}Pb$**	**Th/U[a]**	**$^{206}Pb/^{207}Pb$**	**± 2s**	**$^{207}Pb/^{235}U$**	**± 2s**	**$^{206}Pb/^{238}U$**	**± 2s**	**Conc**	**$^{207}Pb*/^{235}U$**	**± 2s(%)**	**$^{206}Pb*/^{238}U$**	**± 2s(%)**	**RHO**
1	4380	0,19	609	25	555	6	565	4	98	0,7450	1,00	0,0899	0,82	0,83
2	5563	0,19	545	26	563	6	559	5	101	0,7347	1,05	0,0913	0,84	0,81
3	5326	0,19	600	25	553	5	562	4	98	0,7400	0,99	0,0896	0,83	0,83
4	4864	0,18	564	30	556	7	558	5	100	0,7316	1,25	0,0901	0,90	0,72
5	3724	0,20	510	36	565	8	554	6	102	0,7259	1,49	0,0917	0,87	0,58
6	5096	0,18	562	31	561	8	561	6	100	0,7373	1,34	0,0909	0,92	0,69
7	3830	0,20	588	33	560	8	565	6	99	0,7449	1,39	0,0908	0,87	0,63
8	3632	0,20	541	39	570	9	564	7	101	0,7424	1,64	0,0924	0,89	0,54
9	5782	0,18	560	33	562	8	**561**	6	**100**	0,7381	1,39	0,0911	0,91	0,66
10	6406	0,18	588	48	554	12	**560**	9	**99**	0,7361	2,14	0,0898	1,05	0,49

11	4819	0,18	555	28	563	6	**560**	5	**100**	0,7367	1,13	0,0912	0,86	0,75
12	5334	0,18	536	30	568	7	**561**	5	**101**	0,7371	1,25	0,0921	0,89	0,71
13	7021	0,19	494	28	577	7	**561**	5	**103**	0,7371	1,13	0,0937	0,85	0,75
14	6009	0,20	521	29	572	7	**563**	5	**102**	0,7402	1,15	0,0928	0,81	0,71
15	7212	0,19	542	30	565	7	**561**	5	**101**	0,7367	1,21	0,0916	0,86	0,71

Concordia age = 562.64+/-1.20 Ma (n=15, 2s.)

StandardPleisovice			Isotope ratios[b]							Ages (Ma)				
Spot number	$^{206}Pb/^{204}Pb$	Th/U[a]	$^{206}Pb/^{207}Pb$	± 2s	$^{207}Pb/^{235}U$	± 2s	$^{206}Pb/^{238}U$	± 2s	Conc	$^{207}Pb*/^{235}U$	± 2s(%)	$^{206}Pb*/^{238}U$	± 2s(%)	RHO
1	8082	0,08	333	25	338	3	**337**	3	**100**	0,3934	0,941	0,0538	0,84	0,89
2	9057	0,07	310	26	341	4	**337**	3	**101**	0,3939	1,043	0,0544	0,88	0,85
3	8627	0,06	328	30	338	4	**337**	4	**100**	0,3932	1,226	0,0539	0,93	0,76
4	8665	0,09	300	27	342	4	**336**	3	**102**	0,3927	1,087	0,0545	0,90	0,83
5	8733	0,08	348	26	337	3	**338**	3	**100**	0,3955	1,022	0,0537	0,88	0,86
6	8941	0,09	312	26	341	3	**338**	3	**101**	0,3943	1,025	0,0544	0,88	0,86
7	8382	0,08	322	26	343	3	**340**	3	**101**	0,3975	0,986	0,0546	0,84	0,85
8	8829	0,08	328	27	338	4	**337**	3	**100**	0,3932	1,086	0,0539	0,89	0,82
9	8326	0,09	312	26	340	4	**336**	3	**101**	0,3923	1,032	0,0541	0,89	0,86
10	8907	0,09	318	27	340	4	**337**	3	**101**	0,3941	1,086	0,0542	0,90	0,83
11	8788	0,09	345	26	336	3	**337**	3	**100**	0,3937	1,036	0,0535	0,88	0,85
12	8588	0,09	325	27	338	4	**336**	3	**100**	0,3924	1,099	0,0538	0,91	0,83
13	5023	0,10	355	71	337	10	**339**	9	**99**	0,3962	3,107	0,0537	1,23	0,40
14	3532	0,07	337	16	338	5	338	4	100	0,3946	1,391	0,0538	1,21	0,87
15	3576	0,07	338	17	337	5	337	4	100	0,3936	1,482	0,0536	1,27	0,86
16	3123	0,07	338	15	338	5	338	4	100	0,3946	1,396	0,0538	1,23	0,88
17	3183	0,07	339	14	338	5	338	4	100	0,3953	1,442	0,0539	1,30	0,90
18	3451	0,07	342	21	340	6	340	5	99	0,3975	1,669	0,0541	1,38	0,83
19	4533	0,08	338	16	336	3	335	2	99	0,3916	0,957	0,0534	0,63	0,66
20	4565	0,08	339	18	337	4	337	2	99	0,3942	1,066	0,0537	0,73	0,68
21	4608	0,08	336	17	334	3	334	2	99	0,3896	0,944	0,0532	0,59	0,62
22	5125	0,09	339	14	337	3	337	2	100	0,3942	0,892	0,0537	0,63	0,70
23	4964	0,08	338	15	336	4	336	3	99	0,3926	1,146	0,0535	0,94	0,82

24	4968	0,08	336	18	335	4	334	3	99	0,3903	1,241	0,0532	0,94	0,76
25	4954	0,09	338	19	337	4	336	2	99	0,3930	1,094	0,0536	0,69	0,63

Concordia age = 337.30+/-0.56Ma (n=25, 2s.)

SP3 (Artigo 2) – Mineral Chemistry - Feldspar

Sample	DDLH-2	DDLH-2	DDLH-2	DDLH-2	DDLH-2	DDLH-2	DDLH-2	DDLH-2	DDLH-2	DDLH-2	DDLH-2	DDLH-5B	DDLH-5B	DDLH-5B	DDLH-5B
Spot	DDLH-2_Campo2_Pl1	DDLH-2_Campo2_Pl2	DDLH-2_Campo2_Pl3	DDLH-2_Campo2_Pl4	DDLH-2_Campo2_Pl5	DDLH-2_Campo2_Pl6	DDLH-2_Campo2_Pl7	DDLH-2_Campo2_Pl8	DDLH-2_Campo2_Pl9	DDLH-2_Campo2_Pl10	DDLH-2_Campo2_Pl11	DDLH-5B_Campo1_Pl1	DDLH-5B_Campo1_Pl2	DDLH-5B_Campo2_Pl1	DDLH-5B_Campo2_Pl2
Major element															
SiO_2	63,560	63,310	64,540	63,650	63,050	63,850	64,230	63,750	63,550	63,310	63,060	58,620	56,850	53,570	73,350
TiO_2	0,000	0,000	0,040	0,020	0,020	0,000	0,000	0,000	0,020	0,000	0,010	0,020	0,000	0,000	0,000
Al_2O_3	23,000	23,060	22,940	22,640	23,250	23,110	23,030	23,240	23,370	23,290	23,380	25,610	27,410	29,250	22,660
FeO(T)	0,150	0,130	0,240	0,280	0,220	0,160	0,200	0,240	0,220	0,320	0,440	0,280	0,250	0,130	0,090
MnO	0,000	0,040	0,020	0,000	0,000	0,000	0,000	0,030	0,000	0,000	0,000	0,000	0,040	0,000	0,000
MgO	0,000	0,000	0,000	0,020	0,000	0,000	0,000	0,010	0,000	0,000	0,000	0,000	0,010	0,010	0,000
CaO	4,220	4,370	3,870	3,810	4,590	4,290	3,990	4,130	4,410	4,220	4,320	7,580	9,340	11,670	4,340
Na_2O	9,690	9,300	9,890	9,740	9,160	9,610	9,620	9,460	9,450	9,620	9,380	7,290	6,400	4,820	5,170
K_2O	0,020	0,080	0,050	0,020	0,050	0,050	0,040	0,040	0,030	0,060	0,090	0,080	0,060	0,070	0,060
Cations per 32 oxygens															
Si	11,186	11,176	11,244	11,243	11,132	11,187	11,233	11,181	11,141	11,135	11,111	10,537	10,182	9,729	11,943
Ti	0,000	0,000	0,005	0,003	0,003	0,000	0,000	0,000	0,003	0,000	0,001	0,003	0,000	0,000	0,000
Al	4,770	4,798	4,710	4,713	4,838	4,772	4,747	4,804	4,829	4,828	4,855	5,426	5,786	6,261	4,348
Fe(T)	0,022	0,019	0,035	0,041	0,032	0,023	0,029	0,035	0,032	0,047	0,065	0,042	0,037	0,020	0,012
Mn	0,000	0,006	0,003	0,000	0,000	0,000	0,000	0,004	0,000	0,000	0,000	0,000	0,006	0,000	0,000
Mg	0,000	0,000	0,000	0,005	0,000	0,000	0,000	0,003	0,000	0,000	0,000	0,000	0,003	0,003	0,000
Ca	0,796	0,827	0,722	0,721	0,868	0,805	0,748	0,776	0,828	0,795	0,816	1,460	1,792	2,271	0,757
Na	3,306	3,183	3,341	3,336	3,136	3,265	3,262	3,217	3,212	3,280	3,204	2,541	2,222	1,697	1,632
K	0,004	0,018	0,011	0,005	0,011	0,011	0,009	0,009	0,007	0,013	0,020	0,018	0,014	0,016	0,012
%Ab	80,514	79,031	81,997	82,135	78,095	79,993	81,173	80,384	79,367	80,224	79,314	63,219	55,169	42,599	67,957
%Na	19,376	20,521	17,731	17,754	21,625	19,733	18,605	19,393	20,467	19,447	20,186	36,325	44,491	56,994	31,524
%Or	0,109	0,447	0,273	0,111	0,280	0,274	0,222	0,224	0,166	0,329	0,501	0,456	0,340	0,407	0,519

Sample	DDLH-5B	DDLH-5B	DDLH-5B	DDLH-5B	DDLH-5B	DDLH-9C	DDLH-9C	DDLH-9C	DDLH-9C	DDLH-9C	DDLH-9C	DDLH-9C	DDLH-9C	DDLH-9C	DDLH-9C
Spot	DDLH-5B_Campo2_Pl3	DDLH-5B_Campo2_Pl4	DDLH-5B_Campo1_Kf1	DDLH-5B_Campo1_Kf2	DDLH-5B_Campo1_Kf3	DDLH9c_Campo2_Pl-2	DDLH9c_Campo1_Pl3	DDLH9c_Campo1_Pl5	DDLH9c_Campo1_Pl1	DDLH9c_Campo1_Pl4	DDLH9c_Campo1_Pl6	DDLH9c_Campo3_Anf1 (Pl-6)	DDLH9c_Campo2_Pl-1 - KF	DDLH9c_Campo3_Pl2 - KF	DDLH9c_Campo3_Pl3 - KF
Major element															

SiO_2	58,770	55,680	63,34	63,73	64,02	64,890	63,580	63,060	62,160	67,160	66,430	67,280	58,67	64,78	65,75
TiO_2	0,020	0,000	0,02	0	0	0,000	0,060	0,000	0,000	0,000	0,000	0,000	0,01	0,08	0,1
Al_2O_3	25,010	27,220	18,42	18,35	18,31	21,870	22,070	22,410	28,160	20,060	21,100	20,280	24,22	19,35	23,58
FeO(T)	0,150	0,100	0,42	0,41	0,18	0,200	0,020	0,050	1,060	0,000	0,060	0,160	1,03	0,29	0,68
MnO	0,050	0,000	0	0	0	0,020	0,000	0,020	0,020	0,010	0,010	0,000	0	0	0,02
MgO	0,000	0,000	0,01	0,02	0	0,010	0,010	0,000	0,080	0,010	0,040	0,000	0,3	0,03	0,19
CaO	6,940	9,910	0	0	0	3,010	3,240	3,730	1,220	0,810	0,690	1,340	0,89	0,17	0,34
Na_2O	7,370	6,100	0,5	0,5	0,34	10,100	9,540	9,260	8,510	10,930	10,660	10,940	6,55	5,3	7,15
K_2O	0,110	0,070	15,47	15,35	15,58	0,100	0,040	0,110	0,580	0,050	0,420	0,370	4,36	7,56	6,42
Cations per 32 oxygens															
Si	10,649	10,116	11,923	11,958	11,992	11,427	11,363	11,283	10,749	11,854	11,704	11,776	10,943	11,892	11,336
Ti	0,003	0,000	0,003	0,000	0,000	0,000	0,008	0,000	0,000	0,000	0,000	0,000	0,001	0,011	0,013
Al	5,341	5,828	4,087	4,058	4,042	4,539	4,649	4,726	5,739	4,173	4,381	4,184	5,324	4,186	4,792
Fe(T)	0,023	0,015	0,066	0,064	0,028	0,029	0,003	0,007	0,153	0,000	0,009	0,023	0,161	0,045	0,098
Mn	0,008	0,000	0,000	0,000	0,000	0,003	0,000	0,003	0,003	0,001	0,001	0,000	0,000	0,000	0,003
Mg	0,000	0,000	0,003	0,006	0,000	0,003	0,003	0,000	0,021	0,003	0,011	0,000	0,083	0,008	0,049
Ca	1,347	1,929	0,000	0,000	0,000	0,568	0,620	0,715	0,226	0,153	0,130	0,251	0,178	0,033	0,063
Na	2,589	2,149	0,182	0,182	0,123	3,448	3,306	3,213	2,853	3,740	3,642	3,713	2,369	1,886	2,390
K	0,025	0,016	3,715	3,674	3,723	0,022	0,009	0,025	0,128	0,011	0,094	0,083	1,037	1,770	1,412
%Ab	65,352	52,485	4,682	4,717	3,210	85,382	84,003	81,274	88,963	95,789	94,189	91,748	66,091	51,118	61,840
%Na	34,006	47,119	0,000	0,000	0,000	14,061	15,765	18,091	7,048	3,923	3,369	6,210	4,963	0,906	1,625
%Or	0,642	0,396	95,318	95,283	96,790	0,556	0,232	0,635	3,989	0,288	2,442	2,042	28,947	47,976	36,535

Sample	**DDLH-9C**	**DDLH-9C**	**DDLH-11B**	**DDLH-11B**	**DDLH-11B**	**DDLH-11B**	**DDLH-11B**	**DDLH-11B**	**DDLH-11B**	**DDLH-11B**	**DDLH-11B**	**DDLH-17A**	**DDLH-17A**	**DDLH-17A**	**DDLH-17A**
Spot	DDLH9c_Campo3_Pl4 - KF	DDLH9c_Campo3_Pl5 - KF	DDLH-11B_Campo1_Pl1	DDLH-11B_Campo1_Pl2	DDLH-11B_Campo1_Pl5	DDLH-11B_Campo1_Pl8	DDLH-11B_Campo1_Pl3	DDLH-11B_Campo1_Pl4	DDLH-11B_Campo1_Pl6	DDLH-11B_Campo1_Pl7	DDLH-11B_Campo1_Pl9	DDHL17A-Campo1_pl3	DDHL17A-Campo1_pl2	DDHL17A-Campo2_pl4	DDHL17A-Campo1_pl7
Major element															
SiO_2	59,13	64	67,640	67,300	66,600	65,790	64,570	64,450	64,010	64,170	63,920	68,080	65,660	66,410	63,430
TiO_2	0	0	0,000	0,000	0,030	0,300	0,010	0,270	0,000	0,190	0,070	0,000	0,030	0,030	0,040
Al_2O_3	23,58	18,01	20,980	21,060	21,920	21,920	22,650	18,320	22,910	23,150	23,140	19,240	20,760	20,790	21,760
FeO(T)	0,73	0,24	0,060	0,210	0,200	0,860	0,420	3,930	0,220	0,320	0,280	0,240	0,200	0,190	0,160
MnO	0,08	0	0,020	0,000	0,000	0,010	0,000	0,010	0,040	0,030	0,020	0,040	0,040	0,000	0,020
MgO	0,23	0	0,000	0,040	0,000	0,080	0,000	1,950	0,010	0,020	0,000	0,010	0,000	0,000	0,000
CaO	1,06	0	1,430	1,540	2,270	1,870	3,840	2,960	3,940	4,000	3,110	0,490	2,220	1,630	3,080
Na_2O	6,48	0,18	11,320	11,230	10,700	10,440	9,990	10,360	9,690	9,770	9,730	11,250	10,110	10,140	9,380
K_2O	4,32	15,82	0,020	0,090	0,060	0,090	0,060	0,160	0,080	0,060	0,040	0,090	0,130	0,950	0,160
Cations per 32 oxygens															

Si	11,056	12,025	11,703	11,662	11,520	11,453	11,267	11,381	11,229	11,180	11,245	11,976	11,639	11,679	11,401
Ti	0,000	0,000	0,000	0,000	0,004	0,039	0,001	0,036	0,000	0,025	0,009	0,000	0,004	0,004	0,005
Al	5,196	3,988	4,278	4,301	4,468	4,498	4,658	3,813	4,736	4,754	4,798	3,989	4,337	4,309	4,610
Fe(T)	0,114	0,038	0,009	0,030	0,029	0,125	0,061	0,580	0,032	0,047	0,041	0,035	0,030	0,028	0,024
Mn	0,013	0,000	0,003	0,000	0,000	0,001	0,000	0,001	0,006	0,004	0,003	0,006	0,006	0,000	0,003
Mg	0,064	0,000	0,000	0,010	0,000	0,021	0,000	0,513	0,003	0,005	0,000	0,003	0,000	0,000	0,000
Ca	0,212	0,000	0,265	0,286	0,421	0,349	0,718	0,560	0,741	0,747	0,586	0,092	0,422	0,307	0,593
Na	2,349	0,066	3,797	3,773	3,588	3,524	3,380	3,547	3,296	3,300	3,319	3,837	3,475	3,457	3,269
K	1,030	3,792	0,004	0,020	0,013	0,020	0,013	0,036	0,018	0,013	0,009	0,020	0,029	0,213	0,037
%Ab	65,400	1,700	93,373	92,502	89,212	90,526	82,212	85,613	81,293	81,282	84,794	97,150	88,511	86,921	83,845
%Na	5,912	0,000	6,518	7,010	10,459	8,960	17,463	13,517	18,266	18,390	14,977	2,338	10,740	7,721	15,214
%Or	28,688	98,300	0,109	0,488	0,329	0,513	0,325	0,870	0,442	0,328	0,229	0,511	0,749	5,358	0,941

Sample	**DDLH-17A**	**DDLH-17A**	**DDLH-17A**	**DDLH-17A**	**DDLH-17A**	**DDLH-17A**	**DDLH-17A**	**DDLH-17A**	**DDLH-22**	**DDLH-22**	**DDLH-22**	**DDLH-22**	**DDLH-22**	**DDLH-22**	**DDLH-22**
Spot	DDHL17A-Campo2_pl5	DDHL17A-Campo2_pl3	DDHL17A-Campo2_pl1	DDHL17A-Campo2_pl2	DDHL17A-Campo1_pl5	DDHL17A-Campo1_pl1	DDHL17A-Campo1_pl4	DDHL17A-Campo1_pl6	DDHL22-Campo1_Pl1	DDHL22-Campo1_Pl3	DDHL22-Campo1_Pl4	DDHL22-Campo1_Pl5	DDHL22-Campo1_Pl6	DDHL22-Campo1_Pl7	DDHL22-Campo1_Pl2-KF
Major element															
SiO_2	61,840	61,870	61,740	61,330	60,780	60,810	60,040	58,510	60,200	59,600	58,800	60,740	61,530	59,320	59,410
TiO_2	0,040	0,000	0,000	0,000	0,050	0,000	0,000	0,060	0,010	0,000	0,020	0,000	0,000	0,020	0,000
Al_2O_3	23,370	23,920	23,900	23,850	24,100	24,140	24,570	25,850	24,820	24,810	25,620	24,580	23,810	25,410	26,010
FeO(T)	0,290	0,220	0,250	0,310	0,220	0,120	0,070	0,250	0,190	0,260	0,190	0,240	0,050	0,130	0,210
MnO	0,000	0,000	0,000	0,010	0,020	0,000	0,000	0,030	0,030	0,030	0,010	0,010	0,010	0,000	0,020
MgO	0,010	0,010	0,010	0,020	0,000	0,000	0,030	0,000	0,010	0,000	0,000	0,000	0,000	0,000	0,020
CaO	4,970	5,130	5,230	5,300	5,760	5,870	6,640	7,560	7,210	7,090	7,760	6,080	5,680	7,520	0,880
Na_2O	8,960	9,150	8,690	8,600	8,280	7,920	7,490	6,970	7,340	7,730	7,270	8,200	8,340	7,360	7,150
K_2O	0,100	0,090	0,060	0,050	0,020	0,030	0,040	0,290	0,040	0,080	0,040	0,040	0,060	0,050	4,010
Cations per 32 oxygens															
Si	11,031	10,960	10,975	10,954	10,887	10,909	10,792	10,514	10,741	10,688	10,543	10,820	10,975	10,609	10,835
Ti	0,005	0,000	0,000	0,000	0,007	0,000	0,000	0,008	0,001	0,000	0,003	0,000	0,000	0,003	0,000
Al	4,913	4,994	5,007	5,020	5,088	5,104	5,205	5,474	5,219	5,244	5,414	5,161	5,005	5,356	5,591
Fe(T)	0,043	0,033	0,037	0,046	0,033	0,018	0,011	0,038	0,028	0,039	0,028	0,036	0,007	0,019	0,032
Mn	0,000	0,000	0,000	0,002	0,003	0,000	0,000	0,005	0,005	0,005	0,002	0,002	0,002	0,000	0,003
Mg	0,003	0,003	0,003	0,005	0,000	0,000	0,008	0,000	0,003	0,000	0,000	0,000	0,000	0,000	0,005
Ca	0,950	0,974	0,996	1,014	1,105	1,128	1,279	1,455	1,378	1,362	1,491	1,160	1,085	1,441	0,172
Na	3,099	3,143	2,995	2,978	2,876	2,755	2,610	2,428	2,539	2,688	2,527	2,832	2,884	2,552	2,528
K	0,023	0,020	0,014	0,011	0,005	0,007	0,009	0,066	0,009	0,018	0,009	0,009	0,014	0,011	0,933
%Ab	76,111	75,971	74,788	74,384	72,150	70,819	66,961	61,472	64,666	66,065	62,756	70,774	72,407	63,731	69,588

%Na	23,330	23,537	24,873	25,332	27,736	29,005	32,804	36,845	35,102	33,485	37,017	28,999	27,250	35,984	4,733
%Or	0,559	0,492	0,340	0,285	0,115	0,177	0,235	1,683	0,232	0,450	0,227	0,227	0,343	0,285	25,679

Sample	**DDLH-24**	**DDLH-24**	**DDLH-24**	**DDLH-24**	**DDLH-24**	**DDLH-24**	**DDLH-24**	**DDLH-27**	**DDLH-27**	**DDLH-27**	**DDLH-27**	**DDLH-27**	**DDLH-27**	**DMLH-10A**	**DMLH-10A**
Spot	DDHL24-Campo2_Pl1	DDHL24-Campo2_pl4	DDHL24-Campo2_pl5	DDHL24-Campo2_pl6	DDHL24-Campo2_Pl9	DDHL24-Campo2_Pl10	DDHL24-Campo2_pl3	DDLH-27_Campo1_Pl1	DDLH-27_Campo1_Pl3	DDLH-27_Campo1_Pl4	DDLH-27_Campo1_Pl5	DDLH-27_Campo1_Pl6	DDLH-27_Campo1_Pl9	10 A_C1_Pl 2	10 A_C3_Pl 2
Major element															
SiO_2	58,760	59,650	62,060	60,140	61,440	59,590	59,240	60,730	59,440	62,090	61,230	61,990	59,270	62,298	62,905
TiO_2	0,000	0,090	0,020	0,070	0,080	0,020	0,000	0,000	0,170	0,030	0,010	0,010	0,000	0,223	0,000
Al_2O_3	25,380	25,530	23,670	24,850	23,940	25,110	24,810	24,950	25,460	23,720	24,650	24,230	25,380	23,577	23,186
FeO(T)	0,340	0,350	0,330	0,260	0,340	0,170	0,270	0,050	0,390	0,040	0,020	0,140	0,030	0,160	0,123
MnO	0,020	0,040	0,000	0,030	0,000	0,000	0,010	0,000	0,000	0,000	0,000	0,000	0,000	0,020	0,000
MgO	0,000	0,000	0,000	0,010	0,000	0,000	0,000	0,000	0,000	0,000	0,000	0,010	0,000	0,000	0,009
CaO	7,200	7,150	5,350	6,810	5,720	7,170	6,990	6,440	6,860	5,410	5,900	5,370	7,240	4,510	4,280
Na_2O	7,490	7,580	8,650	7,720	8,570	7,510	7,440	8,020	7,960	8,930	8,750	8,840	7,650	9,242	8,920
K_2O	0,070	0,050	0,060	0,070	0,100	0,040	0,060	0,090	0,020	0,070	0,020	0,060	0,050	0,091	0,060
Cations per 32 oxygens															
Si	10,581	10,608	11,007	10,727	10,916	10,669	10,691	10,776	10,594	10,996	10,832	10,940	10,617	11,038	11,172
Ti	0,000	0,012	0,003	0,009	0,011	0,003	0,000	0,000	0,023	0,004	0,001	0,001	0,000	0,030	0,000
Al	5,386	5,351	4,948	5,224	5,013	5,298	5,277	5,218	5,348	4,951	5,139	5,040	5,358	4,923	4,853
Fe(T)	0,051	0,052	0,049	0,039	0,051	0,025	0,041	0,007	0,058	0,006	0,003	0,021	0,004	0,024	0,018
Mn	0,003	0,006	0,000	0,005	0,000	0,000	0,002	0,000	0,000	0,000	0,000	0,000	0,000	0,003	0,000
Mg	0,000	0,000	0,000	0,003	0,000	0,000	0,000	0,000	0,000	0,000	0,000	0,003	0,000	0,000	0,002
Ca	1,389	1,362	1,017	1,301	1,089	1,375	1,352	1,224	1,310	1,027	1,118	1,015	1,390	0,856	0,814
Na	2,615	2,614	2,974	2,670	2,952	2,607	2,603	2,759	2,751	3,066	3,001	3,025	2,657	3,175	3,071
K	0,016	0,011	0,014	0,016	0,023	0,009	0,014	0,020	0,005	0,016	0,005	0,014	0,011	0,021	0,014
%Ab	65,047	65,548	74,275	66,960	72,648	65,313	65,596	68,912	67,664	74,630	72,774	74,618	65,476	78,361	78,767
%Na	34,553	34,167	25,386	32,640	26,795	34,458	34,056	30,579	32,224	24,985	27,116	25,048	34,243	21,131	20,885
%Or	0,400	0,284	0,339	0,399	0,558	0,229	0,348	0,509	0,112	0,385	0,109	0,333	0,282	0,508	0,349

Sample	**DMLH-10A**	**DMLH-10A**	**DMLH-10A**	**DMLH-10A**	**DMLH-10A**	**DMLH-10B**	**DMLH-10B**	**DMLH-10B**	**DMLH-10B**	**DMLH-10B**	**DMLH-10B**	**DMLH-10B**	**DMLH-10D**	**DMLH-10D**	**DMLH-10D**
Spot	10 A_C3_Pl 3	10 A_C1_Pl 1	10 A_C1_Pl 2	10 A_C2_Pl 1	10 A_C3_Pl 1	10 B_C3_Pl 2	10 B_C1_Pl 1	10 B_C1_Pl 2	10 B_C2_Pl 1	10 B_C2_Pl 2	10 B_C2_Pl 3	10 B_C2_Pl 2	10 D_C1_Pl 1	10 D_C1_Pl 2	10 D_C3_Pl 1
Major element															
SiO_2	63,426	62,810	62,298	62,573	65,367	66,720	63,552	63,345	62,707	63,215	63,947	63,215	59,220	57,926	56,152
TiO_2	0,234	0,000	0,223	0,000	0,164	0,000	0,000	0,034	0,219	0,000	0,077	0,000	0,043	0,010	0,000

Al_2O_3	22,976	23,532	23,577	23,029	21,358	20,857	23,122	22,801	23,288	22,694	22,429	22,694	25,047	25,205	27,189
FeO(T)	0,149	0,181	0,160	0,231	0,139	0,309	0,014	0,151	0,186	0,158	0,219	0,158	0,000	0,028	0,085
MnO	0,000	0,009	0,020	0,051	0,066	0,081	0,000	0,000	0,041	0,034	0,049	0,034	0,000	0,087	0,000
MgO	0,021	0,000	0,000	0,000	0,000	0,000	0,000	0,011	0,000	0,000	0,000	0,000	0,004	0,006	0,025
CaO	4,198	4,471	4,510	4,028	2,260	1,247	3,769	4,002	4,838	3,945	3,715	3,945	7,532	7,765	9,150
Na_2O	8,739	9,153	9,242	9,174	10,287	10,954	9,138	9,112	8,651	9,102	9,242	9,102	7,086	7,030	6,080
K_2O	0,043	0,081	0,091	0,073	0,079	0,130	0,275	0,083	0,079	0,092	0,041	0,092	0,042	0,068	0,061
Cations per 32 oxygens															
Si	11,215	11,099	11,038	11,164	11,534	11,687	11,232	11,238	11,103	11,249	11,315	11,249	10,661	10,549	10,197
Ti	0,031	0,000	0,030	0,000	0,022	0,000	0,000	0,005	0,029	0,000	0,010	0,000	0,006	0,001	0,000
Al	4,788	4,901	4,923	4,843	4,442	4,306	4,816	4,768	4,860	4,760	4,677	4,760	5,314	5,410	5,819
Fe(T)	0,022	0,027	0,024	0,034	0,021	0,045	0,002	0,022	0,028	0,024	0,032	0,024	0,000	0,004	0,013
Mn	0,000	0,001	0,003	0,008	0,010	0,012	0,000	0,000	0,006	0,005	0,007	0,005	0,000	0,013	0,000
Mg	0,006	0,000	0,000	0,000	0,000	0,000	0,000	0,003	0,000	0,000	0,000	0,000	0,001	0,002	0,007
Ca	0,795	0,846	0,856	0,770	0,427	0,234	0,714	0,761	0,918	0,752	0,704	0,752	1,453	1,515	1,780
Na	2,996	3,136	3,175	3,174	3,519	3,720	3,131	3,134	2,970	3,140	3,171	3,140	2,473	2,482	2,141
K	0,010	0,018	0,021	0,017	0,018	0,029	0,062	0,019	0,018	0,021	0,009	0,021	0,010	0,016	0,014
%Ab	78,821	78,385	78,361	80,137	88,774	93,395	80,146	80,084	76,043	80,247	81,630	80,247	62,842	61,853	54,400
%Na	20,924	21,159	21,131	19,443	10,777	5,875	18,267	19,436	23,500	19,220	18,132	19,220	36,912	37,753	45,241
%Or	0,255	0,456	0,508	0,420	0,449	0,729	1,587	0,480	0,457	0,534	0,238	0,534	0,245	0,394	0,359

Sample	**DMLH-10D**	**DMLH-10D**	**DMLH-10D**	**DMLH-16**	**DMLH-16**	**DMLH-16**	**DMLH-16**	**DMLH-16**	**DMLH-16**	**DMLH-16**	**DMLH-16**	**DMLH-16**	**DMLH-16**	**DMLH-16**	**DMLH-16**
Spot	10 D_C1_Pl 1	10 D_C1_Pl 2	10 D_C3_Pl 1	16_C3_Pl 1	16_C4_Pl 3	16_C2_Pl 2	16_C4_Pl 1	16_C2_Pl 3	16_C3_Pl 4	16_C4_Pl 2	16_C2_Pl 3	16_C1_Pl 3	16_C2_Pl 1	16_C2_Pl 5	16_C1_Pl 1
Major element															
SiO_2	59,220	57,926	56,152	55,165	54,921	54,073	54,617	54,483	54,653	54,871	54,483	55,219	54,495	58,117	60,297
TiO_2	0,043	0,010	0,000	0,049	0,000	0,000	0,000	0,000	0,040	0,267	0,000	0,000	0,040	0,005	0,000
Al_2O_3	25,047	25,205	27,189	28,172	28,598	28,829	28,474	28,560	28,372	28,395	28,560	27,888	28,162	26,500	24,242
FeO(T)	0,000	0,028	0,085	0,061	0,050	0,029	0,082	0,036	0,103	0,183	0,036	0,049	0,143	0,145	0,042
MnO	0,000	0,087	0,000	0,000	0,063	0,050	0,000	0,000	0,000	0,057	0,000	0,038	0,016	0,000	0,060
MgO	0,004	0,006	0,025	0,006	0,000	0,000	0,000	0,011	0,024	0,000	0,011	0,000	0,000	0,027	0,029
CaO	7,532	7,765	9,150	10,395	10,680	10,785	10,604	10,401	10,254	10,499	10,401	10,446	10,275	7,970	5,727
Na_2O	7,086	7,030	6,080	5,118	5,298	5,322	5,408	5,517	5,330	5,422	5,517	5,651	5,493	7,009	8,329
K_2O	0,042	0,068	0,061	0,072	0,051	0,036	0,056	0,059	0,063	0,068	0,059	0,094	0,052	0,043	0,105
Cations per 32 oxygens															
Si	10,661	10,549	10,197	10,007	9,923	9,836	9,915	9,904	9,946	9,915	9,904	10,009	9,946	10,412	10,849
Ti	0,006	0,001	0,000	0,007	0,000	0,000	0,000	0,000	0,005	0,036	0,000	0,000	0,005	0,001	0,000
Al	5,314	5,410	5,819	6,023	6,090	6,181	6,092	6,119	6,085	6,047	6,119	5,958	6,058	5,596	5,140

Fe(T)	0,000	0,004	0,013	0,009	0,008	0,004	0,012	0,005	0,016	0,028	0,005	0,007	0,022	0,022	0,006
Mn	0,000	0,013	0,000	0,000	0,010	0,008	0,000	0,000	0,000	0,009	0,000	0,006	0,002	0,000	0,009
Mg	0,001	0,002	0,007	0,002	0,000	0,000	0,000	0,003	0,007	0,000	0,003	0,000	0,000	0,007	0,008
Ca	1,453	1,515	1,780	2,020	2,068	2,102	2,062	2,026	1,999	2,033	2,026	2,029	2,009	1,530	1,104
Na	2,473	2,482	2,141	1,800	1,856	1,877	1,903	1,944	1,881	1,900	1,944	1,986	1,944	2,435	2,905
K	0,010	0,016	0,014	0,017	0,012	0,008	0,013	0,014	0,015	0,016	0,014	0,022	0,012	0,010	0,024
%Ab	62,842	61,853	54,400	46,913	47,163	47,075	47,839	48,808	48,289	48,116	48,808	49,202	49,022	61,259	72,033
%Na	36,912	37,753	45,241	52,653	52,538	52,716	51,835	50,848	51,336	51,486	50,848	50,259	50,673	38,493	27,370
%Or	0,245	0,394	0,359	0,434	0,299	0,210	0,326	0,343	0,376	0,397	0,343	0,539	0,305	0,247	0,597

Sample	**DMLH-16**	**DMLH-16**	**DMLH-16**	**DMLH-16**
Spot	16_C1_Pl 2	16_C3_Pl 3	16_C3_Pl 2	16_C2_Pl 4
Major element				
SiO_2	64,174	56,648	67,989	52,829
TiO_2	0,016	0,000	0,000	0,055
Al_2O_3	21,686	24,673	19,517	26,782
FeO(T)	0,000	0,000	0,095	0,172
MnO	0,031	0,051	0,000	0,000
MgO	0,000	0,000	0,002	0,003
CaO	2,305	3,116	0,239	2,872
Na_2O	9,977	10,516	11,266	10,829
K_2O	0,439	0,065	0,037	0,048
Cations per 32 oxygens				
Si	11,462	10,630	11,970	10,133
Ti	0,002	0,000	0,000	0,008
Al	4,565	5,457	4,050	6,054
Fe(T)	0,000	0,000	0,014	0,028
Mn	0,005	0,008	0,000	0,000
Mg	0,000	0,000	0,001	0,001
Ca	0,441	0,626	0,045	0,590
Na	3,455	3,826	3,846	4,027
K	0,100	0,016	0,008	0,012
%Ab	86,459	85,631	98,631	86,996
%Na	11,038	14,021	1,156	12,750
%Or	2,503	0,348	0,213	0,254

SP4 (Artigo 2) – Mineral Chemistry - Amphibole

Sample	DDLH-2	DDLH-2	DDLH-2	DDLH-2	DDLH-2	DDLH-2	DDLH-2	DDLH-2	DDLH-2	DDLH-2	DDLH-2	DDLH-5B	DDLH-5B	DDLH-5B	DDLH-5B
Spot	DDLH-2_Campo2_Anf1	DDLH-2_Campo2_Anf2	DDLH-2_Campo2_Anf3	DDLH-2_Campo2_Anf4	DDLH-2_Campo2_Anf5	DDLH-2_Campo2_Anf6	DDLH-2_Campo2_Anf7	DDLH-2_Campo2_Anf8	DDLH-2_Campo2_Anf9	DDLH-2_Campo2_Anf10	DDLH-2_Campo2_Anf11	DDLH-5B_Campo1_Anf3	DDLH-5B_Campo1_Anf5	DDLH-5B_Campo2_Anf1	DDLH-5B_Campo2_Anf2
Major element															
SiO_2	50,500	50,200	50,660	50,500	50,520	50,260	50,380	49,980	49,99	50,16	50,47	44,22	45,2	45,63	45,33
TiO_2	0,860	0,660	0,430	0,410	0,600	0,710	0,720	0,680	0,58	0,65	0,58	0,81	0,83	0,83	0,97
Al_2O_3	4,590	4,720	4,850	4,510	4,580	4,340	4,480	4,730	4,86	4,87	4,79	12,15	10,58	9,91	10,52
Cr_2O_3	0,000	0,080	0,010	0,080	0,000	0,050	0,040	0,060	0,06	0,11	0,15	0	0,11	0,06	0,17
FeO(T)	18,330	18,340	17,590	17,480	17,940	17,600	18,450	17,930	17,85	17,63	17,89	18,38	18,32	17,6	18,06
MnO	0,380	0,350	0,320	0,340	0,410	0,250	0,390	0,330	0,3	0,34	0,31	0,34	0,29	0,37	0,27
MgO	11,920	11,740	12,230	12,020	11,910	12,190	11,910	11,700	11,76	11,64	11,78	8,76	9,43	9,65	9,54
CaO	11,350	10,940	11,460	11,320	11,070	11,310	11,070	11,340	11,41	11,33	11,57	11,27	11,05	11,49	11,39
Na_2O	0,770	0,780	0,670	0,610	0,640	0,580	0,690	0,640	0,64	0,67	0,6	1,06	1,05	0,88	1,06
K_2O	0,060	0,070	0,110	0,090	0,080	0,070	0,070	0,060	0,08	0,06	0,1	0,66	0,57	0,55	0,61
Cations per 23 oxygens															
Si	7,409	7,426	7,433	7,480	7,464	7,451	7,433	7,419	7,412	7,431	7,428	6,631	6,780	6,858	6,766
Ti	0,095	0,073	0,047	0,046	0,067	0,079	0,080	0,076	0,065	0,072	0,064	0,091	0,094	0,094	0,109
Al	0,794	0,823	0,839	0,787	0,797	0,758	0,779	0,828	0,849	0,850	0,831	2,147	1,870	1,755	1,851
Cr	0,000	0,009	0,001	0,009	0,000	0,006	0,005	0,007	0,007	0,013	0,017	0,000	0,013	0,007	0,020
Fe2+	2,251	2,274	2,159	2,168	2,221	2,182	2,278	2,227	2,214	2,190	2,203	2,307	2,302	2,214	2,258
Mn	0,047	0,044	0,040	0,043	0,051	0,031	0,049	0,041	0,038	0,043	0,039	0,043	0,037	0,047	0,034
Mg	2,607	2,589	2,675	2,654	2,623	2,694	2,619	2,589	2,599	2,571	2,584	1,958	2,109	2,162	2,123
Ca	1,784	1,734	1,801	1,796	1,752	1,796	1,750	1,804	1,813	1,798	1,824	1,811	1,776	1,850	1,821
Na	0,219	0,224	0,191	0,175	0,183	0,167	0,197	0,184	0,184	0,192	0,171	0,308	0,305	0,256	0,307
K	0,011	0,013	0,021	0,017	0,015	0,013	0,013	0,011	0,015	0,011	0,019	0,126	0,109	0,105	0,116

Sample	DDLH-5B	DDLH-5B	DDLH-9C	DDLH-9C	DDLH-9C	DDLH-9C	DDLH-9C	DDLH-9C	DDLH-9C	DDLH-11B	DDLH-11B	DDLH-11B	DDLH-11B	DDLH-11B	DDLH-11B
Spot	DDLH-5B_Campo2_Anf3	DDLH-5B_Campo2_Anf5	DDLH9c_Campo2_Anf-3	DDLH9c_Campo2_Anf-1	DDLH9c_Campo3_Anf4	DDLH9c_Campo1_Pl2 (Anf-3)	DDLH9c_Campo3_Anf2	DDLH9c_Campo3_Anf3	DDLH9c_Campo3_Anf5	DDLH-11B_Campo1_Anf1	DDLH-11B_Campo1_Anf2	DDLH-11B_Campo1_Anf5	DDLH-11B_Campo1_Anf8	DDLH-11B_Campo1_Anf3	DDLH-11B_Campo1_Anf4
Major element															
SiO_2	45,45	45,89	43,54	42,61	43,29	42,38	46,4	46,21	46,11	45,26	45,39	45,62	45,08	45,19	45,2
TiO_2	0,83	0,71	0,64	0,55	0,7	0,61	0,42	0,38	0,38	0,76	1,27	1,15	1,18	1,29	1,25
Al_2O_3	10,4	10,73	10,12	11,27	10,54	11,96	8,04	6,93	7,59	9,08	8,08	7,86	7,98	7,89	7,88
Cr_2O_3	0,08	0,21	0,19	0,05	0,11	0,11	0,2	0,05	0,11	0,08	0,1	0	0,01	0,08	0,02
FeO(T)	17,36	17,05	18,94	19,48	17,8	18,63	16,07	15,73	15,44	21,22	21,55	21,64	21,76	23,98	22,12
MnO	0,25	0,27	0,39	0,41	0,45	0,34	0,34	0,46	0,36	0,44	0,42	0,46	0,49	0,42	0,47
MgO	9,74	9,63	10,01	9,25	10,59	8,75	12,13	11,04	12,07	8,5	8,78	8,91	8,89	9,06	8,66
CaO	11,24	11,45	11,61	11,67	11,38	10,86	11,69	11,5	11,83	10,88	10,42	10	10,66	10,75	10,53
Na_2O	0,96	0,96	1,3	1,24	1,31	1,5	1,02	0,81	1,24	1,36	1,38	1,35	1,32	1,51	1,25
K_2O	0,55	0,52	0,89	0,84	0,92	0,96	0,6	0,45	0,58	0,42	0,51	0,48	0,57	0,52	0,49
Cations per 23 oxygens															
Si	6,823	6,834	6,609	6,503	6,572	6,517	6,948	7,148	6,986	6,856	6,896	6,950	6,867	6,767	6,892
Ti	0,094	0,080	0,073	0,063	0,080	0,071	0,047	0,044	0,043	0,087	0,145	0,132	0,135	0,145	0,143
Al	1,840	1,883	1,811	2,027	1,886	2,168	1,419	1,263	1,355	1,621	1,447	1,411	1,433	1,392	1,416
Cr	0,009	0,025	0,023	0,006	0,013	0,013	0,024	0,006	0,013	0,010	0,012	0,000	0,001	0,009	0,002
Fe2+	2,185	2,131	2,404	2,486	2,260	2,396	2,013	2,035	1,956	2,688	2,742	2,763	2,772	3,003	2,821
Mn	0,032	0,034	0,050	0,053	0,058	0,044	0,043	0,060	0,046	0,056	0,054	0,059	0,063	0,053	0,061
Mg	2,180	2,138	2,265	2,105	2,397	2,006	2,708	2,546	2,726	1,919	1,989	2,024	2,019	2,023	1,968
Ca	1,808	1,827	1,888	1,908	1,851	1,789	1,876	1,906	1,920	1,766	1,696	1,632	1,740	1,725	1,720
Na	0,279	0,277	0,383	0,367	0,386	0,447	0,296	0,243	0,364	0,399	0,407	0,399	0,390	0,438	0,370
K	0,105	0,099	0,172	0,164	0,178	0,188	0,115	0,089	0,112	0,081	0,099	0,093	0,111	0,099	0,095

Sample	DDLH-11B	DDLH-11B	DDLH-11B	DDLH-17A	DDLH-17A	DDLH-17A	DDLH-17A	DDLH-17A	DDLH-17A	DDLH-17A	DDLH-17A	DDLH-17A	DDLH-17A	DDLH-17A	DDLH-17A
Spot	DDLH-11B_Campo1_Anf6	DDLH-11B_Campo1_Anf7	DDLH-11B_Campo1_Anf9	DDHL17A-Campo1_Anf5	DDHL17A-Campo2_anf3	DDHL17A-Campo1_Anf7	DDHL17A-Campo1_Anf1	DDHL17A-Campo1_anf2	DDHL17A-Campo1_anf3	DDHL17A-Campo1_anf6	DDHL17A-Campo1_anf4	DDHL17A-Campo2_anf2	DDHL17A-Campo1_anf5	DDHL17A-Campo2_anf1	DDHL17A-Campo2_anf5
Major element															
SiO_2	45,32	45,78	44,88	51,59	49,1	48,01	48,5	47,38	47,3	47,53	46,46	46,77	46,96	44,16	43,29
TiO_2	1,14	0,9	1,26	0,33	0,3	0,45	0,57	0,46	0,44	0,57	0,68	0,32	0,56	0,46	0,71
Al_2O_3	8,04	8,13	8,22	4,91	6,93	7,72	7,62	9,15	8,58	9,03	9,65	9,42	9,05	11,87	12,69
Cr_2O_3	0,04	0,02	0,07	0,13	0,12	0	0,06	0,11	0,11	0,17	0,04	0	0,02	0,09	0,04

FeO(T)	21,5	21,64	21,42	10,43	15,91	15,27	15,24	15,99	15,82	15,45	15,66	16,32	15,78	17,55	17,12
MnO	0,4	0,41	0,6	0,24	0,24	0,29	0,24	0,25	0,26	0,32	0,24	0,27	0,34	0,25	0,28
MgO	8,6	8,8	8,55	16,46	12,22	12,07	12,23	11,09	11,12	11,33	10,89	10,54	11,39	9,31	8,92
CaO	10,61	10,74	9,92	12,45	11,93	11,93	11,64	11,5	11,9	11,65	11,54	11,77	11,81	11,71	11,81
Na_2O	1,24	1,31	1,15	0,62	0,69	0,77	0,83	0,96	0,95	0,83	1,06	0,9	0,97	1,21	1,24
K_2O	0,48	0,45	0,51	0,22	0,17	0,31	0,31	0,29	0,26	0,41	0,44	0,3	0,37	0,52	0,63
Cations per 23 oxygens															
Si	6,920	6,930	6,904	7,414	7,224	7,120	7,148	7,016	7,045	7,021	6,927	6,988	6,965	6,642	6,540
Ti	0,131	0,102	0,146	0,036	0,033	0,050	0,063	0,051	0,049	0,063	0,076	0,036	0,062	0,052	0,081
Al	1,447	1,450	1,490	0,832	1,202	1,349	1,324	1,597	1,506	1,572	1,696	1,659	1,582	2,104	2,260
Cr	0,005	0,002	0,009	0,015	0,014	0,000	0,007	0,013	0,013	0,020	0,005	0,000	0,002	0,011	0,005
Fe2+	2,747	2,740	2,760	1,253	1,958	1,894	1,881	1,985	1,973	1,913	1,959	2,041	1,957	2,207	2,163
Mn	0,052	0,053	0,078	0,029	0,030	0,036	0,030	0,031	0,033	0,040	0,030	0,034	0,043	0,032	0,036
Mg	1,958	1,986	1,961	3,526	2,680	2,669	2,687	2,448	2,469	2,495	2,421	2,348	2,518	2,087	2,009
Ca	1,736	1,742	1,635	1,917	1,881	1,896	1,838	1,825	1,899	1,844	1,844	1,884	1,877	1,887	1,912
Na	0,367	0,384	0,343	0,173	0,197	0,221	0,237	0,276	0,274	0,238	0,306	0,261	0,279	0,353	0,363
K	0,094	0,087	0,100	0,040	0,032	0,059	0,058	0,055	0,049	0,077	0,084	0,057	0,070	0,100	0,121

Sample	**DDLH-17A**	**DDLH-17A**	**DDLH-22**	**DDLH-22**	**DDLH-22**	**DDLH-22**	**DDLH-22**	**DDLH-22**	**DDLH-24**	**DDLH-24**	**DDLH-24**	**DDLH-24**	**DDLH-24**	**DDLH-24**	**DDLH-24**
Spot	DDHL17A-Campo1_Anf6	DDHL17A-Campo1_Anf7	DDHL22-Campo1_Anf1	DDHL22-Campo1_Anf2	DDHL22-Campo1_Anf4	DDHL22-Campo1_Anf5	DDHL22-Campo1_Anf6	DDHL22-Campo1_Anf7	DDHL24-Campo2_Anf1	DDHL24-Campo2_Anf3	DDHL24-Campo2_Anf4	DDHL24-Campo2_Anf5	DDHL24-Campo2_Anf8	DDHL24-Campo2_Anf9	DDHL24-Campo2_Anf2
Major element															
SiO_2	44,24	43,15	43,53	43,61	43,81	43,48	43,54	43,29	43,89	44,52	44,19	44,36	44,32	43,62	43,12
TiO_2	0,82	0,68	1,56	1,43	1,69	1,2	1,52	1,28	0,99	0,82	0,65	0,83	0,85	0,92	0,66
Al_2O_3	10,73	11,83	9,39	9,83	9,61	10,13	9,77	10,03	10,33	10,08	11,51	10,34	10,66	10,69	11,97
Cr_2O_3	0,04	0,09	0,06	0,05	0,07	0,03	0,06	0	0,1	0,05	0	0,08	0,03	0	0,16
FeO(T)	19,15	19,25	21,25	21,15	21,49	21,32	21,33	21,61	19,22	18,98	19,16	19,3	19,03	19,13	19,43
MnO	0,32	0,3	0,34	0,34	0,39	0,33	0,38	0,42	0,37	0,32	0,27	0,33	0,32	0,32	0,34
MgO	8,83	8,13	7,66	7,48	7,57	7,34	7,66	7,52	9,12	9,39	8,43	8,92	8,95	8,7	8,29
CaO	11,23	11,38	11,05	11,25	11,34	11,17	11,35	11,32	11,29	11,23	11,48	11,4	11,46	11,43	11,44
Na_2O	1,21	1,3	1,32	1,24	1,4	1,26	1,36	1,33	1,2	1,12	1,25	1,13	1,18	1,21	1,31
K_2O	0,73	0,57	0,95	0,99	0,93	0,97	0,96	0,96	0,68	0,66	0,53	0,66	0,65	0,66	0,69
Cations per 23 oxygens															
Si	6,701	6,589	6,707	6,695	6,677	6,686	6,659	6,642	6,671	6,744	6,670	6,722	6,699	6,662	6,549
Ti	0,093	0,078	0,181	0,165	0,194	0,139	0,175	0,148	0,113	0,093	0,074	0,095	0,097	0,106	0,075
Al	1,915	2,129	1,705	1,779	1,726	1,836	1,761	1,814	1,850	1,800	2,048	1,847	1,899	1,924	2,142
Cr	0,005	0,011	0,007	0,006	0,008	0,004	0,007	0,000	0,012	0,006	0,000	0,010	0,004	0,000	0,019

Fe2+	2,426	2,458	2,744	2,721	2,745	2,747	2,731	2,773	2,443	2,404	2,419	2,446	2,406	2,443	2,468
Mn	0,041	0,039	0,044	0,044	0,050	0,043	0,049	0,055	0,048	0,041	0,035	0,042	0,041	0,041	0,044
Mg	1,994	1,851	1,759	1,712	1,720	1,683	1,747	1,720	2,066	2,120	1,897	2,015	2,017	1,981	1,877
Ca	1,822	1,862	1,824	1,850	1,852	1,840	1,860	1,861	1,839	1,823	1,857	1,851	1,856	1,870	1,861
Na	0,355	0,385	0,394	0,369	0,414	0,376	0,403	0,396	0,354	0,329	0,366	0,332	0,346	0,358	0,386
K	0,141	0,111	0,187	0,194	0,181	0,190	0,187	0,188	0,132	0,128	0,102	0,128	0,125	0,129	0,134

Sample	**DDLH-27**	**DDLH-27**	**DDLH-27**	**DDLH-27**	**DDLH-27**	**DDLH-27**	**DMLH-10A**	**DMLH-10A**	**DMLH-10A**	**DMLH-10A**	**DMLH-10A**	**DMLH-10A**	**DMLH-10A**	**DMLH-10B**	**DMLH-10B**
Spot	DDLH-27_Campo1_Anf1	DDLH-27_Campo1_Anf3	DDLH-27_Campo1_Anf4	DDLH-27_Campo1_Anf5	DDLH-27_Campo1_Anf6	DDLH-27_Campo1_Anf7	10 A_C3_Anf 1	10 A_C3_Anf 2	10 A_C1_Anf 3	10 A_C2_Anf 1	10 A_C2_Anf 2	10 A_C1_Anf 1	10 A_C1_Anf 2	10 B_C3_Anf 1	10 B_C3_Anf 2
Major element															
SiO_2	42,94	42,65	43,06	42,97	42,87	43,34	41,639	41,846	41,551	41,731	41,949	42,854	42,698	42,484	42,088
TiO_2	1,5	1,2	1,28	1,5	0,98	0,65	0,776	0,659	0,797	0,659	0,776	0,671	0,55	0,645	0,725
Al_2O_3	10,82	11,53	11,08	11,04	11,33	10,91	13,553	13,044	12,931	12,828	12,613	11,691	11,569	11,873	11,876
Cr_2O_3	0,07	0,11	0,04	0,05	0,07	0	0	0	0	0	0	0	0	0	0
FeO(T)	21,38	21,78	21,8	21,69	21,37	21,47	20,565	20,001	20,796	20,626	20,104	20,288	20,258	20,544	21,063
MnO	0,35	0,29	0,36	0,38	0,36	0,31	0,378	0,387	0,287	0,337	0,258	0,27	0,244	0,282	0,41
MgO	7,09	6,91	7,15	6,91	7,18	7,44	7,736	8,084	8,041	8,052	8,169	8,754	8,602	8,467	8,111
CaO	11,4	11,01	10,96	11,01	11,27	11,2	11,155	11,111	11,201	11,194	11,124	11,231	11,238	11,498	11,63
Na_2O	1,33	1,23	1,29	1,32	1,4	1,37	1,543	1,56	1,486	1,328	1,374	1,366	1,293	1,377	1,499
K_2O	0,82	0,77	0,69	0,87	0,78	0,62	0,503	0,536	0,734	0,652	0,718	0,586	0,754	0,648	0,852
Cations per 23 oxygens															
Si	6,579	6,546	6,589	6,581	6,567	6,646	6,327	6,386	6,339	6,376	6,413	6,504	6,523	6,463	6,412
Ti	0,173	0,138	0,147	0,173	0,113	0,075	0,089	0,076	0,091	0,076	0,089	0,077	0,063	0,074	0,083
Al	1,954	2,086	1,998	1,993	2,046	1,972	2,427	2,346	2,325	2,310	2,273	2,091	2,083	2,129	2,132
Cr	0,008	0,013	0,005	0,006	0,008	0,000	0,000	0,000	0,000	0,000	0,000	0,000	0,000	0,000	0,000
Fe2+	2,741	2,795	2,790	2,785	2,738	2,754	2,613	2,553	2,653	2,636	2,570	2,575	2,588	2,613	2,684
Mn	0,045	0,038	0,047	0,049	0,047	0,040	0,049	0,050	0,037	0,044	0,033	0,035	0,032	0,036	0,053
Mg	1,619	1,581	1,631	1,578	1,640	1,701	1,752	1,839	1,829	1,834	1,862	1,981	1,959	1,920	1,842
Ca	1,871	1,810	1,797	1,807	1,850	1,840	1,816	1,817	1,831	1,833	1,822	1,826	1,840	1,874	1,898
Na	0,395	0,366	0,383	0,392	0,416	0,407	0,455	0,462	0,440	0,393	0,407	0,402	0,383	0,406	0,443
K	0,160	0,151	0,135	0,170	0,152	0,121	0,098	0,104	0,143	0,127	0,140	0,113	0,147	0,126	0,166

Sample	DMLH-10B	DMLH-10B	DMLH-10B	DMLH-10B	DMLH-10B	DMLH-10D	DMLH-10D	DMLH-10D	DMLH-10D	DMLH-10D	DMLH-10D	DMLH-16	DMLH-16	DMLH-16	DMLH-16
Spot	10 B_C3_Anf 3	10 B_C1_Anf 1	10 B_C1_Anf 2	10 B_C2_Anf 1	10 B_C2_Anf 2	10 D_C2_Anf 1	10 D_C2_Anf 2	10 D_C3_Anf 1	10 D_C3_Anf 2	10 D_C3_Anf 3	10 D_C3_Anf 4	16_C4_Anf 3	16_C4_Anf 4	16_C1_Anf 5	16_C3_Anf 3
Major element															
SiO_2	41,603	41,989	41,464	41,742	42,222	45,073	43,475	45,612	46,274	45,506	41,962	45,267	45,006	45,269	45,387
TiO_2	0,517	0,929	0,57	0,408	0,524	0,568	0,26	0,505	0,57	0,408	0,408	1,295	1,322	1,33	1,244
Al_2O_3	13,222	12,812	12,68	12,973	11,28	10,17	14,335	9,686	9,572	9,749	14,21	9,448	9,324	9,261	8,986
Cr_2O_3	0	0	0	0	0	0	0	0	0	0	0	0,107	0,074	0,057	0,122
FeO(T)	21,21	20,556	20,774	21,289	21,887	17,77	18,854	18,008	17,847	17,643	18,24	17,482	17,202	17,182	16,978
MnO	0,299	0,424	0,464	0,203	0,204	0,366	0,226	0,605	0,591	0,358	0,388	0,187	0,408	0,19	0,28
MgO	7,632	8,014	7,929	7,713	7,967	10,03	7,479	11,006	11,171	11,341	8,575	10,493	10,435	10,305	10,274
CaO	11,13	11,223	11,444	11,065	10,633	11,225	11,136	10,344	10,647	10,535	11,231	11,392	11,674	11,95	11,73
Na_2O	1,393	1,391	1,431	1,275	1,458	1,2	1,237	1,328	1,134	1,152	1,436	1,028	1,021	1,104	1,043
K_2O	0,722	0,725	0,721	0,805	0,701	0,228	0,37	0,209	0,18	0,212	0,348	0,561	0,548	0,609	0,564
Cations per 23 oxygens															
Si	6,355	6,376	6,361	6,389	6,525	6,795	6,520	6,828	6,861	6,820	6,361	6,792	6,779	6,799	6,851
Ti	0,059	0,106	0,066	0,047	0,061	0,064	0,029	0,057	0,064	0,046	0,047	0,146	0,150	0,150	0,141
Al	2,380	2,293	2,293	2,340	2,054	1,807	2,534	1,709	1,673	1,722	2,539	1,671	1,655	1,639	1,599
Cr	0,000	0,000	0,000	0,000	0,000	0,000	0,000	0,000	0,000	0,000	0,000	0,013	0,009	0,007	0,015
Fe2+	2,709	2,610	2,665	2,725	2,829	2,240	2,371	2,255	2,213	2,211	2,312	2,194	2,167	2,158	2,144
Mn	0,039	0,055	0,060	0,026	0,027	0,047	0,029	0,077	0,074	0,045	0,050	0,024	0,052	0,024	0,036
Mg	1,738	1,814	1,813	1,760	1,835	2,254	1,672	2,456	2,469	2,534	1,938	2,347	2,343	2,307	2,312
Ca	1,822	1,826	1,881	1,815	1,761	1,813	1,789	1,659	1,691	1,692	1,824	1,831	1,884	1,923	1,897
Na	0,413	0,410	0,426	0,378	0,437	0,351	0,360	0,385	0,326	0,335	0,422	0,299	0,298	0,321	0,305
K	0,141	0,140	0,141	0,157	0,138	0,044	0,071	0,040	0,034	0,041	0,067	0,107	0,105	0,117	0,109

Sample	DMLH-16	DMLH-16	DMLH-16	DMLH-16	DMLH-16	DMLH-16	DMLH-16	DMLH-16	DMLH-16
Spot	16_C3_Anf 4	16_C1_Anf 1	16_C3_Anf 1	16_C3_Anf 2	16_C1_Anf 2	16_C1_Anf 3	16_C1_Anf 4	16_C4_Anf 5	16_C4_Anf 2
Major element									
SiO_2	45,315	47,746	48,916	49,063	49,403	51,238	51,242	52,727	53,069
TiO_2	1,259	0,414	0,356	0,009	0,113	0,211	0,029	0,107	0,133
Al_2O_3	9,597	8,045	6,876	6,468	5,667	4,223	4,207	3,507	2,491
Cr_2O_3	0,138	0	0,022	0,003	0,038	0,037	0,002	0	0,035
FeO(T)	17,336	17,371	16,495	15,463	16,191	15,778	15,519	14,596	14,091
MnO	0,224	0,335	0,124	0,253	0,158	0,278	0,207	0,299	0,206
MgO	10,222	10,982	11,969	12,019	12,11	12,975	13,13	14,309	15,131

CaO	11,703	11,994	11,592	11,686	12,081	12,278	12,046	12,1	12,071
Na_2O	1,16	0,803	0,796	0,678	0,671	0,402	0,395	0,367	0,278
K_2O	0,518	0,378	0,299	0,243	0,282	0,165	0,119	0,07	0,051
Cations per 23 oxygens									
Si	6,787	7,067	7,227	7,329	7,353	7,519	7,552	7,629	7,699
Ti	0,142	0,046	0,040	0,001	0,013	0,023	0,003	0,012	0,015
Al	1,694	1,403	1,197	1,139	0,994	0,730	0,731	0,598	0,426
Cr	0,016	0,000	0,003	0,000	0,004	0,004	0,000	0,000	0,004
Fe2+	2,172	2,150	2,039	1,934	2,015	1,936	1,913	1,766	1,710
Mn	0,028	0,042	0,016	0,032	0,020	0,035	0,026	0,037	0,025
Mg	2,282	2,423	2,636	2,676	2,687	2,839	2,885	3,086	3,273
Ca	1,878	1,902	1,835	1,870	1,926	1,931	1,902	1,876	1,876
Na	0,337	0,230	0,228	0,196	0,194	0,114	0,113	0,103	0,078
K	0,099	0,071	0,056	0,046	0,054	0,031	0,022	0,013	0,009

SP5 (Artigo 2) – Mineral Chemistry - Titanite

Sample	DDLH-10A	DDLH-10A	DDLH-10A	DDLH-10A	DDLH-22	DDLH-22	DDLH-24	DMLH-16	DMLH-16	DMLH-16	DMLH-16	DMLH-16	DMLH-16	DMLH-16
Spot	DDHL10A-Campo1_tn1	DDHL10A-Campo1_tn2	DDHL10A-Campo1_tn3	DDHL10A-Campo2_tn1	DDHL22-Campo1_Tn1	DDHL22-Campo1_Tn2	DDHL24-Campo2_tn1	16_C2_Ttn 1	16_C2_Ttn 2	16_C4_Ttn 1	16_C4_Ttn 2	16_C4_Ttn 3	16_C1_Ttn 1	16_C3_Ttn 1
Major element														
SiO_2	30,280	30,370	30,320	29,870	30,520	30,110	30,140	30,860	30,499	30,237	30,509	30,711	30,632	30,468
TiO_2	38,260	39,180	37,780	37,770	37,890	37,900	37,450	36,964	38,989	38,231	35,564	37,638	37,210	39,002
Al_2O_3	1,050	0,680	1,350	1,060	1,150	0,780	1,220	0,986	0,869	1,177	1,185	0,859	1,004	0,961
FeO(T)	0,620	0,500	0,700	0,740	0,840	0,750	0,820	0,313	0,218	0,215	0,634	0,192	0,398	0,417
MnO	0,040	0,090	0,120	0,000	0,070	0,080	0,050	0,000	0,212	0,076	0,152	0,052	0,030	0,016
MgO	0,000	0,000	0,000	0,030	0,000	0,000	0,000	0,044	0,000	0,000	0,001	0,020	0,110	0,025
CaO	27,980	28,290	28,440	27,960	27,760	28,200	27,350	28,162	27,750	28,154	27,610	28,233	28,431	28,192
Na_2O	0,000	0,000	0,000	0,010	0,000	0,000	0,000	0,000	0,031	0,007	0,015	0,008	0,039	0,022
K_2O	0,000	0,000	0,000	0,000	0,000	0,010	0,000	0,001	0,000	0,012	0,000	0,010	0,054	0,028
Cations per 5 oxygens														
Si	1,006	1,001	1,004	1,002	1,013	1,007	1,013	1,032	1,008	1,005	1,039	1,023	1,021	1,002
Ti	0,956	0,972	0,941	0,953	0,946	0,953	0,947	0,930	0,969	0,956	0,911	0,943	0,933	0,965
Al	0,041	0,026	0,053	0,042	0,045	0,031	0,048	0,039	0,034	0,046	0,048	0,034	0,039	0,037
Fe^{+2}	0,017	0,014	0,019	0,021	0,023	0,021	0,023	0,009	0,006	0,006	0,018	0,005	0,011	0,011
Mn	0,001	0,003	0,003	0,000	0,002	0,002	0,001	0,000	0,006	0,002	0,004	0,001	0,001	0,000
Mg	0,000	0,000	0,000	0,002	0,000	0,000	0,000	0,002	0,000	0,000	0,000	0,001	0,005	0,001
Ca	0,996	0,999	1,009	1,005	0,988	1,010	0,985	1,009	0,982	1,002	1,007	1,008	1,015	0,994
Na	0,000	0,000	0,000	0,001	0,000	0,000	0,000	0,000	0,002	0,000	0,001	0,001	0,003	0,001
K	0,000	0,000	0,000	0,000	0,000	0,000	0,000	0,000	0,000	0,001	0,000	0,000	0,002	0,001

SP6 (Artigo 2) – Mineral Chemistry - Chlorite

Sample	DDLH-5B	DDLH-5B	DDLH-5B	DDLH-5B	DDLH-9C	DDLH-9C	DDLH-9C	DMLH-10A
Spot	DDLH-5B_Campo1_Clor1	DDLH-5B_Campo1_Clor2	DDLH-5B_Campo1_Clor3	DDLH-5B_Campo1_Clor4	DDLH9c_Campo2_Cl1	DDLH9c_Campo3_Cl1	DDLH9c_Campo3_Cl2	10A_C1_Chl1
Major element								
SiO_2	26,6	26,51	28,45	28,04	29,36	34,79	39,11	26,105
TiO_2	0,07	0,11	0,13	0,08	0,07	0	0,16	0,306
Al_2O_3	19,84	19,79	20,19	19,69	16,59	15,98	17,97	17,644
Cr_2O_3	0	0,02	0,05	0,12	0,35	0,09	0,39	0
FeO(T)	26,8	26,24	23,86	26,46	25,84	20,53	15,77	30,688
MnO	0,16	0,14	0,11	0,18	0,38	0,16	0,08	0,187
MgO	14,4	14,32	13,7	13,09	13,51	12,95	10,85	13,473
CaO	0,06	0,05	0,1	0,14	0,38	0,68	1	0,143
Na_2O	0,01	0,07	0,09	0,07	0,14	0,18	0,21	0,198
K_2O	0,04	0,08	0,39	0,38	0,58	1	1,14	0,097
H_2O(c)	11,350	11,289	11,459	11,429	11,270	11,658	12,175	11,149
Cations per 14 oxygens								
Si	2,8107	2,8164	2,9777	2,9426	3,1245	3,579	3,8525	2,8059
Ti	0,0056	0,0088	0,0102	0,0063	0,0056	0	0,0119	0,0247
Al	2,4708	2,4779	2,4905	2,4353	2,0808	1,9375	2,0862	2,2351
Cr	0	0,0017	0,0041	0,01	0,0294	0,0073	0,0304	0
Fe^{2+}	2,3682	2,3313	2,0884	2,3222	2,2997	1,7663	1,2991	2,7423
Mn	0,0143	0,0126	0,0098	0,016	0,0343	0,0139	0,0067	0,017
Mg	2,2683	2,268	2,1376	2,0479	2,1433	1,986	1,5933	2,1588
Ca	0,0068	0,0057	0,0112	0,0157	0,0433	0,075	0,1055	0,0165
Na	0,002	0,0144	0,0183	0,0142	0,0289	0,0359	0,0401	0,0413
K	0,0054	0,0108	0,0521	0,0509	0,0787	0,1312	0,1433	0,0133
OH	8	8	8	8	8	8	8	7,9932

SP7 (Artigo 2) – Mineral Chemistry - Ilmenite-Hematite

Sample	DDLH-2	DDLH-2	DDLH-2	DDLH-2	DDLH-5B	DDLH-5B	DDLH-5B	DDLH-5B	DDLH-9C	DDLH-11B	DDLH-11B	DDLH-11B	DDLH-11B	DDLH-11B	DDLH-11B
Spot	DDLH-2_Campo2_Op1	DDLH-2_Campo2_Op2	DDLH-2_Campo2_Op3	DDLH-2_Campo2_Op4	DDLH-5B_Campo1_Op1	DDLH-5B_Campo1_Op2	DDLH-5B_Campo1_Op3	DDLH-5B_Campo2_Op1	DDLH9c_Campo2_Op1	DDLH-11B_Campo1_Op1	DDLH-11B_Campo1_Op2	DDLH-11B_Campo1_Op3	DDLH-11B_Campo1_Op4	DDLH-11B_Campo1_Op5	DDLH-11B_Campo1_Op6
Mineral	Ilmenite	Ilmenite	Ilmenite	Ilmenite	Ilmenite	Ilmenite	Ilmenite	Ilmenite	Hematite	Ilmenite	Ilmenite	Ilmenite	Ilmenite	Ilmenite	Ilmenite
Major element															
SiO_2	0,26	0,01	0,00	0,05	0,04	0,00	0,00	0,05	2,86	0,00	0,02	0,00	0,04	0,00	0,04
TiO_2	49,06	52,70	53,38	53,80	53,60	52,97	53,42	53,51	0,00	52,14	51,99	52,79	51,71	52,77	51,67
Al_2O_3	0,00	0,00	0,00	0,00	0,22	0,00	0,00	0,00	0,00	0,00	0,00	0,01	0,00	0,00	0,00
FeO(T)	43,21	43,83	43,74	43,42	43,42	43,48	43,56	44,19	76,11	44,73	45,04	45,12	45,25	44,47	44,37
MnO	1,90	1,96	1,71	1,82	1,89	2,03	1,96	1,96	0,00	2,46	2,27	2,29	2,35	2,19	2,53
MgO	0,11	0,12	0,15	0,11	0,13	0,10	0,05	0,05	0,50	0,01	0,10	0,03	0,05	0,05	0,06
CaO	1,54	0,24	2,92	0,14	0,04	0,02	0,01	0,08	0,06	0,05	0,19	0,03	0,04	1,79	0,12
Cations per 3 oxygens															
Si	0,007	0,000	0,000	0,001	0,001	0,000	0,000	0,001	0,122	0,000	0,001	0,000	0,001	0,000	0,001
Ti	0,972	1,007	0,990	1,018	1,014	1,014	1,017	1,012	0,000	0,997	0,993	1,000	0,990	0,989	0,994
Al	0,000	0,000	0,000	0,000	0,007	0,000	0,000	0,000	0,000	0,000	0,000	0,000	0,000	0,000	0,000
Fe(ii)	0,952	0,931	0,902	0,914	0,913	0,925	0,922	0,929	2,721	0,951	0,956	0,950	0,964	0,926	0,949
Mn	0,042	0,042	0,036	0,039	0,040	0,044	0,042	0,042	0,000	0,053	0,049	0,049	0,051	0,046	0,055
Mg	0,004	0,005	0,006	0,004	0,005	0,004	0,002	0,002	0,032	0,000	0,004	0,001	0,002	0,002	0,002
Ca	0,043	0,007	0,077	0,004	0,001	0,001	0,000	0,002	0,003	0,001	0,005	0,001	0,001	0,048	0,003

Sample	DDLH-17A	DDLH-17A	DDLH-17A	DDLH-17A	DDLH-22	DDLH-22	DDLH-22	DDLH-22	DDLH-24	DDLH-24	DDLH-24	DDLH-27	DDLH-27	DDLH-27	DMLH-10A
Spot	DDHL17A-Campo2_op1	DDHL17A-Campo2_op1	DDHL17A-Campo1_op1	DDHL17A-Campo2_op2	DDHL22-Campo1_Op1	DDHL22-Campo1_Op2	DDHL22-Campo1_Op3	DDHL22-Campo1_Op4	DDHL24-Campo2_Op1	DDHL24-Campo2_Op2	DDHL24-Campo2_Op3	DDLH-27_Campo1_Op1	DDLH-27_Campo1_Op2	DDLH-27_Campo1_Op3	10 A_C3_Op 1
Mineral	Ilmenite	Ilmenite	Ilmenite	Ilmenite	Ilmenite	Ilmenite	Ilmenite	Ilmenite	Ilmenite	Ilmenite	Ilmenite	Ilmenite	Ilmenite	Ilmenite	Hematite
Major element															
SiO_2	0,00	0,04	0,07	0,07	0,00	0,00	0,00	0,01	0,00	0,03	0,14	0,00	0,02	0,03	0,00
TiO_2	52,42	51,42	51,53	52,25	51,47	52,34	52,02	51,34	52,12	51,63	53,28	52,93	53,09	52,70	0,00
Al_2O_3	0,00	0,00	0,00	0,00	0,03	0,00	0,02	0,00	0,00	0,00	0,00	0,00	0,00	0,00	0,00

FeO(T)	43,41	43,98	43,01	43,00	44,56	44,67	44,41	44,72	44,30	44,84	43,11	44,94	44,79	43,61	96,96
MnO	2,86	3,05	3,23	2,95	1,99	2,03	1,84	2,10	2,08	2,14	2,26	1,80	1,90	1,97	0,07
MgO	0,07	0,03	0,05	0,03	0,13	0,17	0,21	0,12	0,23	0,09	0,14	0,00	0,00	0,06	0,01
CaO	0,10	0,24	0,19	0,08	0,03	0,06	0,18	0,07	0,11	0,12	0,26	0,04	0,05	0,00	0,06
Cations per 3 oxygens															
Si	0,000	0,001	0,002	0,002	0,000	0,000	0,000	0,000	0,000	0,001	0,004	0,000	0,001	0,001	0,000
Ti	1,004	0,991	0,997	1,005	0,996	1,000	0,999	0,993	0,999	0,993	1,011	1,006	1,007	1,012	0,000
Al	0,000	0,000	0,000	0,000	0,001	0,000	0,001	0,000	0,000	0,000	0,000	0,000	0,000	0,000	0,000
Fe(ii)	0,925	0,942	0,925	0,919	0,958	0,949	0,948	0,961	0,944	0,959	0,910	0,949	0,944	0,931	2,995
Mn	0,062	0,066	0,070	0,064	0,043	0,044	0,040	0,046	0,045	0,046	0,048	0,039	0,041	0,043	0,002
Mg	0,003	0,001	0,002	0,001	0,005	0,006	0,008	0,005	0,009	0,003	0,005	0,000	0,000	0,002	0,001
Ca	0,003	0,007	0,005	0,002	0,001	0,002	0,005	0,002	0,003	0,003	0,007	0,001	0,001	0,000	0,002

Sample	**DMLH-10A**	**DMLH-10A**	**DMLH-10A**	**DMLH-10A**	**DMLH-10A**	**DMLH-10A**	**DMLH-10B**	**DMLH-10B**	**DMLH-10B**	**DMLH-10B**	**DMLH-10B**	**DMLH-10B**	**DMLH-10D**	**DMLH-10D**	**DMLH-16**	**DMLH-16**	**DMLH-16**
Spot	10 A_C1_Op 1	10 A_C1_Op 2	10 A_C1_Op 3	10 A_C2_Op 1	10 A_C2_Op 2	10 A_C3_Op 2	10 B_C3_Op 1	10 B_C3_Op 2	10 B_C1_Op 1	10 B_C1_Op 2	10 B_C1_Op 3	10 B_C2_Op 1	10 D_C2_Op 1	10 D_C1_Op 1	16_C2_Op 1	16_C3_Op 1	16_C1_Op 1
Mineral	Hematite	Hematite	Hematite	Ilmenite	Ilmenite	Ilmenite	Hematite	Hematite	Hematite	Hematite	Hematite	Hematite	Ilmenite	Ilmenite	Ilmenite	Ilmenite	Ilmenite
Major element																	
SiO_2	0,03	0,03	0,05	0,03	0,00	0,04	0,03	0,06	1,42	0,00	0,02	0,02	0,06	0,01	0,03	0,02	0,03
TiO_2	0,00	0,00	0,19	48,74	51,16	50,27	0,14	0,18	2,16	0,14	0,00	0,34	48,28	50,66	48,78	49,40	51,17
Al_2O_3	0,03	0,01	0,04	0,03	0,01	0,04	0,02	0,05	0,16	0,02	0,02	0,04	0,01	0,00	0,00	0,04	0,05
FeO(T)	96,30	96,28	95,84	48,19	46,89	47,88	96,39	96,28	90,87	95,90	96,76	96,54	46,30	45,61	45,81	46,75	44,53
MnO	0,00	0,00	0,00	2,09	2,61	2,51	0,00	0,00	0,05	0,00	0,03	0,06	3,69	1,88	2,12	2,11	3,36
MgO	0,00	0,00	0,04	0,05	0,07	0,00	0,00	0,00	0,04	0,00	0,02	0,00	0,03	0,04	0,28	0,23	0,19
CaO	0,01	0,03	0,05	0,03	0,17	0,06	0,02	0,03	1,40	0,04	0,20	0,06	0,14	0,49	0,13	0,00	0,03
Cations per 3 oxygens																	
Si	0,001	0,001	0,002	0,001	0,000	0,001	0,001	0,002	0,051	0,000	0,001	0,001	0,002	0,000	0,001	0,001	0,001
Ti	0,000	0,000	0,005	0,952	0,973	0,961	0,004	0,005	0,058	0,004	0,000	0,009	0,949	0,981	0,965	0,964	0,982
Al	0,001	0,001	0,002	0,001	0,000	0,001	0,001	0,002	0,007	0,001	0,001	0,002	0,000	0,000	0,000	0,001	0,002
Fe(ii)	2,995	2,996	2,979	1,046	0,991	1,018	2,987	2,981	2,716	2,989	2,988	2,973	1,012	0,982	1,007	1,014	0,951
Mn	0,000	0,000	0,000	0,046	0,056	0,054	0,000	0,000	0,002	0,000	0,001	0,002	0,082	0,041	0,047	0,046	0,073
Mg	0,000	0,000	0,002	0,002	0,003	0,000	0,000	0,000	0,002	0,000	0,001	0,000	0,001	0,002	0,011	0,009	0,007
Ca	0,000	0,001	0,002	0,001	0,004	0,002	0,001	0,001	0,053	0,002	0,008	0,003	0,004	0,014	0,004	0,000	0,001